BIOMIMETIC CALCIUM PHOSPHATE COATINGS:

PHYSICOCHEMISTRY AND BIOLOGICAL ACTIVITY

DISSERTATION

to obtain

the doctor's degree at the University of Twente,

on the authority of the rector magnificus,

prof. dr F.A. van Vught,

on account of the decision of the graduation committee,

to be publicly defended

on Friday May 3rd, 2002 at 13:15

by

Florence Barrère

born on June 25th, 1973

in Saint-Gaudens (France)

Promotor: Prof. C.A. van Blitterswijk

Promotor: Prof. K. de Groot

Assitant Promotor: Dr. P. Layrolle

A Maman,
Papy, Mamy et Memée.

This thesis is based on the following publications:

1-**F. Barrère**, P. Layrolle, C.A. van Blitterswijk, K. de Groot. "Biomimetic Calcium phosphate Coatings on Ti6Al4V: a Crystal Growth Study of Octacalcium Phosphate and Inhibition by Mg^{2+} and HCO_3^-." Bone 25 (1999): 107S-111S.

2-**F. Barrère**, P. Layrolle, C.A. van Blitterswijk, K. de Groot. "Physical and chemical characteristics of plasma-sprayed and biomimetic apatite coating." Bioceramics 12 (1999): 125-128.

3-**F. Barrère**, P. Layrolle, C.A. van Blitterswijk, K de Groot. "Fast formation of biomimetic Ca-P coating on Ti6Al4V." Mat Res Soc Symp Proc (2000): 135-140.

4-**K. de Groot**, HB Wen, Y Liu, P. Layrolle, **F. Barrère**. "Biomimetic coatings on orthopedic implants." Mat Res Soc Symp Proc (2000): 109-116.

5-**F. Barrère**, M. Stigter, P. Layrolle, C.A van Blitterswijk, K. de Groot. "*In vitro* dissolution of various calcium phosphate coatings on Ti6Al4V." Bioceramics (2000): 67-70.

6-**F. Barrère**, P. Layrolle, C.A. van Blitterswijk, K. de Groot. "Biomimetic Calcium Phosphate coatings on Ti6Al4V: growth study of OCP." J Mat Sci Mat Med 12 (2001): 529-534.

7-S. Leeuwenburgh, P. Layrolle, **F. Barrère**, J. de Bruijn, J. Schoonman, C.A. van Blitterswijk, K. de Groot. "Osteoclastic resorption of biomimetic calcium phosphate coatings *in vitro.*" J Biomed Mater Res 56 (2001): 208-215.

8-**F. Barrère**, C.A. van Blitterswijk, K. de Groot, P. Layrolle. "Influence of ionic strength and carbonate on the Ca-P coating formation from SBFx5 solution." Biomaterials, in press.

9-**F. Barrère**, C.A. van Blitterswijk, K. de Groot, P. Layrolle. "Nucleation mechanism of Ca-P coating formed from SBFx5 solution: influence of magnesium." Biomaterials 23 (2002):2211-2220.

10-P. Habibovic, **F. Barrère**, C.A. van Blitterswijk, K. de Groot, P. Layrolle. "Biomimetic Hydroxyapatite coating on metal implants." J Am Ceram Soc 85 (2002);

11-**F. Barrère**, C.M. van der Valk, R.A.J. Dalmeijer, C.A. van Blitterswijk, K. de Groot and P. Layrolle. "*In vitro* and *in vivo* dissolution study of biomimetic calcium phosphate coatings on Ti6Al4V". J Biomed Mater Res, in press.

12-**F. Barrère**, C.M. van der Valk, R.A.J Dalmeijer, G. Meijer, C.A. van Blitterswijk, K. de Groot, P. Layrolle. "Osteogenicity of octacalcium phosphate coatings applied on porous metallic implants". J Biomed Mater Res (submitted for publication)

13-**F. Barrère**, M. Snel, C.A. van Blitterswijk, K. de Groot, P. Layrolle. Nanoscale study of the nucleation and growth of a biomimetic Ca-P coating. Chem Mater (submitted for publication).

14-**F. Barrère**, C.A. van Blitterswijk, K. de Groot, C. Rey, P. Layrolle. "Calcium Phosphate interactions with titanium oxide and aluminum oxide substrate: an XPS study". J Mat Sci Mat Med (submitted for publication)

BIOMIMETIC CALCIUM PHOSPHATE COATINGS:
Physicochemistry and Biological Activity

CONTENTS   **Page**

CHAPTER 1

GENERAL INTRODUCTION

I-Generalities

From Icarus in the Greek mythology, via Leonardo da Vinci, to the NASA engineers, mankind has always intended to copy nature, because of its enviable properties. With the increase of environmental pollution concerns since the 70s, copying nature became attractive because biological materials are produced under mild energetic conditions. Learning from nature, in order to synthesize its "products" has become a challenge in research. Biomimetics is the generic name to define such investigations. Biomimetics originates from ancient Greek "Bios" (life, nature) and "Mimesis" (imitation, copy), and can be defined as "the investigation of the structures and functions of biological materials that allows possible future design and synthesis of engineered composites based on the principles obtained from the biological materials" [1]. Biomineralization is one of the challenges of biomimetics because biominerals like shells, nacre or bone exhibit enviable excellent mechanical properties. Their composite structure has been processed in aqueous environment at ambient temperature. The products result from a direct chemical reaction rather than from thermally-induced changes. Biomineralization processes fall into two groups: intracellular precipitation such as sponge spicules or magnetic particles in magnetotatic bacteria, and extracellular precipitation such as bone, tooth and shells minerals [2] (figure 1). The principal regulatory factors controlling nucleation and crystal growth by intracellular and extracellular processes are: (1) spatial delineation by supramolecular assemblies, (2) chemical regulation by transport processes, and (3) molecular recognition at inorganic-organic interfaces [3].
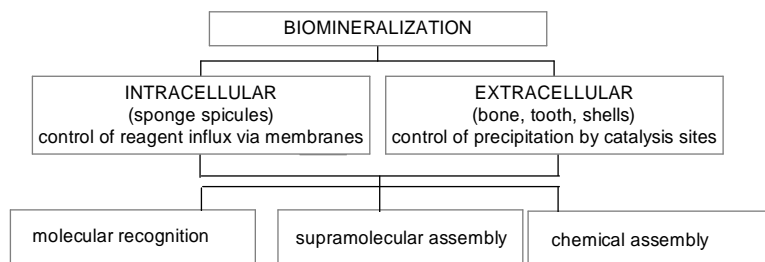
Figure 1: Biomineralization control

Replacing body parts goes back at least 2,500 years, when the Etruscans learned to substitute missing teeth with bridges made from artificial teeth carved from the bones of oxen. Evidence of crude dental implants dates back to Roman populations of the first or second century AD and to pre-Columbian cultures of Central and South America. The first use of dental amalgam to repair decayed teeth was recorded in the Chinese literature in the year 659 AD. In 1920, Albee showed that calcium phosphate could induce osteogenesis, and he proposed therefore their use in bone repair. Since the 60s, extensive research has been performed on calcium phosphates and led within few years to the first calcium phosphate product on the market. However, the use of calcium phosphate ceramics in skeletal repair was limited due to their weak mechanical properties. In 1980, in order to overcome the weak mechanical properties of calcium phosphate ceramics, de Groot used plasma-spraying technique to apply calcium phosphate coating onto metal prosthesis for load bearing applications, such as hip or teeth implants. The deposition of such coatings led to major improvements in prosthesis fixation and in the implant longevity. Nowadays, the use of ceramics substitute, the controlled porosity of the implant surface, or the introduction of bone-stimulating biological agents aim at stimulating bone contact with the implant, by the exploit of "tricks" such as bone-like mineral (calcium phosphate), bone-like porous surfaces, or bone-like proteins… Moreover, the increasing knowledge in bone biology, bone mineralization, and - last but not least – the preceding experience in bone repair raise always the challenge to get closer to synthetic bone. In this perspective, Kokubo developed in the 90s, mineralizing solutions inspired from body fluids. These so-called Simulated Body Fluids (SBF) are able to reproduce *in vitro* bone-like mineral. In the field of bone repair, this method, mimicking bone mineralization, opens large perspective related mainly to the mild conditions under which the calcium phosphate coating is produced. The biomimetic approach to coat biomaterials does require few energy because of the physiological conditions of the process. In addition, biological active agents can be incorporated homogeneously into the

calcium phosphate coating, and porous and heat-sensitive materials can be coated. The present thesis aims at investigating the feasibility of biomimetic calcium phosphate coatings and their evaluation *in vitro* and *in vivo*.

II-Bone

II.1-Bone function

Bone is the component of the skeletal system, which is involved in the protection, the support and the motion of the body. Bone is a protection and production site for specialized tissues such as blood-forming system, i.e. bone marrow. Hart, lungs and other organs and structures in the chests are protected by the rib cage. The function of these organs involving motion, expansion and contraction requires flexibility and elasticity of the protective rib cage. Bone supports structurally the mechanical action of soft tissues, like the contraction of muscles or expansion of lung. Finally, it is a mineral reservoir, whereby endocrine systems regulate the level of calcium and phosphate ions in the circulating body fluids [4].

II.2-Macro and microstructure of mature bone

In shape and macroscopic structure, bones are affected by genetic, metabolic, and mechanical factors. Intrinsic factors result into a macro-structural diversity of bone. Broad, flat plates, such as scapula, anchor large muscle masses, whereas hollow and thick-walled tubes, such as femur or radius, support weight. All bone consists in a basic double structure, for which their importance varies with the function. An external layer, or cortex, covers the bone; it is smooth, dense and continuous. In the interior, cancellous bone is arranged in a network of intersecting plates and spicules varying in amount and enclosing spaces. These cavities are filled with blood vessels and marrow, either red, haemapoietic or yellow, adipose, its character varying with age and site.

Microscopically, bone is a highly complex and specialized form of connective tissue. It is a mineralized tissue, which is composed of an organic matrix strengthened by deposits of calcium phosphate crystals, in other words a natural composite material. Collagen type I, based on fibers constitute approximately 95% of the organic matrix; the remaining 5% are composed of proteoglycans and numerous non-collagenous proteins. This calcified matrix embeds bone cells, which participate to the maintenance and organization of bone, namely osteoprogenitor cells, osteoblasts, osteocytes, and osteoclasts. Osteoprogenitor cells can be defined as persistent, migratory stem cells, which can proliferate and differentiate into osteoblasts prior to bone formation. Osteoblasts are responsible for the synthesis, deposition and mineralization of bone matrix and, on becoming embedded in this matrix, they finally transform

into osteocytes. The function of osteoclasts is the removal of bone, although how is not known. Clearly, they cause demineralization, and there is also structural evidence of organic matrix destruction. In addition to bone cells, cells related to vascular and nervous system and other components of the perisosteum, endosteum and marrow participate to bone microstructure. However, these last mentioned compounds have an external origin to the one of bone [5].

II.3-Mechanical properties of bone

The intimate blend of hard inorganic and resilient organic components results in excellent mechanical properties. For example, compact bone specimens have been found to have tensile strength in the range of 700 to 1400 kg/cm^2, and compressive strength in the range of 1400 to 2100kg/cm^2. These values are within the same magnitude as for aluminum or mild steel, but bone is much lighter. The great strength of bone exists principally along its axis and hence roughly parallel both to the collagen fiber axis and to the long axis of mineral crystals. Although apparently stiff, bones exhibit a considerable degree of elasticity, which is important in the skeleton's ability to withstand impact. Estimates of modulus of elasticity of bone samples are of the order of 420 to 700 kg/cm^2, values very much less than steel, for example, indicating much greater elasticity of bone [4].

II-4-The mineral of bone

II.4.1-Bone mineral structure

Bone mineral, or enamel (biological apatite) have structure close to a type AB carbonated calcium phosphate apatitic structure more or less deficient, which can be tentatively represented by the formula [6].

$$Ca_{8.3}\square_{1.7}(PO_4)_{4.3}(CO_3)_1(HPO_4)_{0.7}(OH,CO_3)_{0.3}\square_{1.7}$$
$$\square = lacuna$$
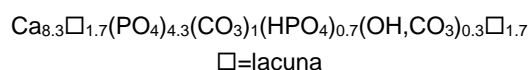
However, bone mineral apatite contains non-apatitic carbonate and phosphate groups, which are, from a structural and physical point of view, unstable and very reactive [7,8]. This high reactivity provides certain physicochemical, biological, functional and chemical features important in the formation and dissolution of the crystals in biological tissues [6]. Furthermore, bone contains minor or trace elements, which are not indicated in the above formula, and which are difficult to attribute to either the mineral phase or the organic matrix [6]. In bone and other mineralized tissues, the mineral crystals are formed of thin plates of irregular shapes. Their sizes range in length from 20 Å for the smallest particles, to 1100 Å for the largest particles [9,10]. This

results in their having a very large surface area to present to the extracellular fluids, which is critically important for the rapid exchange of ions with these fluids.

II.4.2-Bone biomineralization

Bone mineral starts to nucleate into the holes and pores present in the collagen fibrils [11-14]. This heterogeneous nucleation is catalyzed by the presence of phosphated esters groups [15] and carboxylate groups [16] present in the collagen fibrils. Thereafter, the growth, or mineralization, takes place along the collagen fibrils, and finally interconnecting all of the collagen fibrils (figure 3).

The nature of the primary mineral phase formed prior to mature bone mineral apatite remains controversial. According to Posner, bone mineral apatite derives from calcium phosphate clusters ($Ca_9(PO_4)_6$) packing randomly with interfacial water to form amorphous calcium phosphate precursor [17]. This theory is supported by the presence of several calcium phosphate growth inhibitors such as magnesium that stabilize amorphous state [18]. However, dicalcium phosphate (DCPD) [19-21] and octacalcium phosphate (OCP) phases have been also proposed as bone mineral precursors because of the partial similarities between apatite and OCP [22-24]. DCDP and OCP are kinetically favored as compared to apatitic phases, supporting their role as precursors in bone apatite formation [25]. However, a recent study has shown that apatitic phase seems to be largely dominant as compared to other possible transient phases even at the earliest stages of mineralization [26].
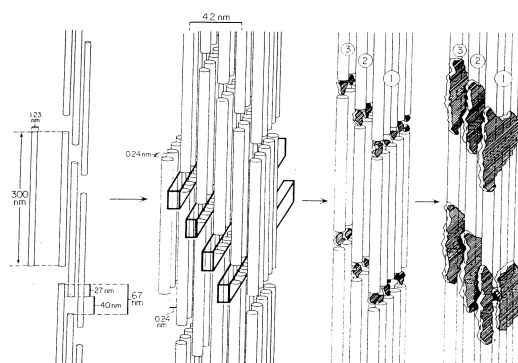
Figure 3: Bone mineralization along collagen fibrils.

III-Bone repair by biomaterials

The increase of life expectancy goes along with partial or dramatic degradation of tissues or organs. The needs and advances in repair are therefore in continuous expansion. Natural materials sources are mainly utilized for bone repair. The source of these materials is from the own patient (autografting),

from a donor (allografting) or from animal (xenografting). Autografts are obviously the most favorable repairing procedure. However, solely small volumes can be transferred and two surgical operations are required. Allografting and xenografting are restricted by facts of limited supply, and a decrease of potential disease transmission and host rejection. In addition, grafting can alter the initial properties of the implant, decreasing the potential of a graft. Replacements of defectuous tissues are achieved by implantation of numerous materials, so-called biomaterials, which are dedicated to be temporarily or permanently in contact with living tissues or organs. The development of synthetic bone substitute is in regular increase [27,28].

III.1-Biomaterials in general

Bone repairing material must meet both biofunctionality and biocompatibility. The biofunctionality concerns the ability of the implant to perform the purpose for which it was designated. These requirements are:

(i) mechanical such as tensile strength, fracture toughness, elongation at fracture, fatigue strength, young's modulus;

(ii) physical such as density in the case of orthopedic implants, or thermal expansion in the case of bone cement;

(iii) surface chemistry such as degradation resistance, oxidation and corrosion [29].

The biocompatibility can be defined as the biological acceptance of the implant. Osborn and Newesely [30] classified biocompatibility into three categories based on their reactions on the surrounding bone tissue. Biotolerent materials are characterized by a distant osteogenesis with the formation of fibrous tissue layer between implant and bone. Bioinert implants are encapsulated with a thin fibrous tissue layer. Bioactive implants are able to enhance the bonding with bone.

Various types of synthetic bone substitutes have been developed in order to comply with biofunctionality and biocompatibility, such as:

(i) metallic materials including titanium, titanium alloys, stainless steel, cobalt-chromium alloys;

(ii) ceramics such as aluminum oxide, carbon, calcium phosphate, bioglass®, glass-ceramics;

(iii) polymers: silicon rubber, poly(methyl methacrylate) (PMMA), polylactide, Polyactive®;

(iv) composites of the above materials, for example hydroxyapatite coating on metal implants, or hydroxyapatite-reinforced Polyactive®.

Depending on the type of repair, and therefore the type of function that needs to be replaced, one or the other material will be chosen. Among the afromentionned biomaterials, calcium phosphate ceramics have demonstrated

unique bioactive properties for bone repair. However, in the case of load bearing applications (dental or hip implants), solely metals can comply as yet for such strong mechanical requirements. In addition to the mandatory high mechanical properties, these metal implants must be properly fixed into bone.

III.2-Calcium phosphates as biomaterials

Sintered calcium phosphate ceramics have been produced under the form of hydroxylapatite (HA), tricalcium phosphate (TCP), or a mixture of these two phases because of their thermal stability. They have been extensively used in bone repair because of their remarkable biological activity [31]. The physico-chemical dissolution of these calcium phosphate ceramics is one of the first events occurring when they are in contact with body fluid. The release of calcium ions is believed to be at the origin of the bioactivity of calcium phosphates [32-35], although a too intense release of these ions can destabilize bone cells [36,37], and subsequently inhibiting bone formation. The role of released phosphate ions from calcium phosphates remains unclear: on one hand, they were found to promote bone formation [35]; on the other hand, they were found to inhibit bone formation [38,39]. This dissolution is followed by the precipitation of a biological calcium phosphate layer with the partial contribution of the calcium ions released from the implanted calcium phosphate ceramic [40]. Experimentally, a poorly crystallized carbonated apatite layer of few micrometers in thickness is formed on the calcium phosphate substrate [41-44]. In addition, organic compounds are incorporated into this newly formed layer, and cells like osteoprogenitor cells, osteoclasts and osteoblasts colonize the biomaterial [45,46]. The degree of crystallinity, the crystal structure, the microporosity, the chemical composition, and the lattice defects of the calcium phosphate ceramics affect the physico-chemical dissolution *in vitro* [46-50], and the cellular activity *in vitro* [36, 51-54]. *In vivo* identical factors affect the osteogenicity of the calcium phosphate implant [55-60].

Recently, calcium phosphate ceramics with specific porosity and microporosity have been found to induce bone in ectopic sites [61-65]. These osteoinductive properties of calcium phosphates have been attributed possibly to

(i) the ability of adsorbing Bone Morphogenetic Proteins (BMPs),

(ii) the surface charge of the substrate triggering cell differentiation,

(iii) the bone-like apatite layer formed *in vivo* that recognize mesenchymal cells,

(iv) the local high level of free calcium provided by the calcium phosphate material that triggers cell differentiation and bone formation [66].

III.2.1-Generalities

Calcium phosphates, or more accurately calcium orthophosphates, are salts of the orthophosphoric acid (H_3PO_4), and thus can form compounds that contain $H_2PO_4^-$, HPO_3^{2-} or PO_4^{3-}. The calcium phosphate salts constitute a wide group of compounds [67]. Table 1 summarizes the chemical name, the formula, the abbreviation and the calcium to phosphorus ratio (Ca/P) of some calcium phosphate compounds.

Name	Formula	Abbreviation	Ca/P
Dicalcium phosphate anhydrate or Monetite	$CaHPO_4$	DCPA	1.00
Dicalcium phosphate dihydrate or Brushite	$CaHPO_4.2H_2O$	DCPD	1.00
Octacalcium Phosphate	$Ca_8(PO_4)_4(HPO_4)_2.5H_2O$	OCP	1.33
Tricalcium Phosphate	$Ca_3(PO_4)_2$	TCP	1.50
Hydroxyapatite	$Ca_{10}(PO_4)_6(OH)_2$	HA	1.67

Table 1: Some calcium phosphate salts

Calcium phosphate salts vary by their composition and their crystal structures, leading to specific physicochemical properties. Most of calcium phosphates are sparingly soluble in water, and some are very insoluble, but all dissolve in acids.
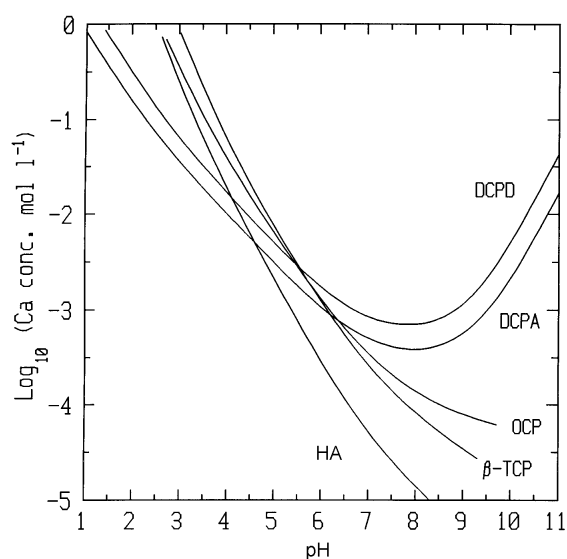
Figure 2: Solubility isotherms of calcium phosphate phases in the system $Ca(OH)_2$-H_3PO_4-H_2O at 37ºC and 1 atm (after Elliot, 1994**)**

Figure 2 indicates the thermodynamical stability at 37ºC of various calcium phosphate phases, although kinetics dictate more the formation of one or the other phase under any given conditions. The solubility of calcium phosphates decreases with the increase of temperature and pH [67]. The diagram displayed in figure 2 shows that HA is the most thermodynamically stable phase.

III.2.2-Calcium phosphates of biological interest

Apatites

Stoichiometric HA belongs to the general and wide apatitic group, represented by the formula:

$$Me_{10}(XO_4)_6Y_2$$
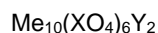
Where Me is a divalent metal (Ca, Sr, Ba, Pb…), XO_4 is a trivalent anion (PO_4, AsO_4, VO_4…), and Y is a monovalent anion (F, Cl, Br, I, OH…). Apatitic crystal structure has usually a hexagonal lattice, having a strong ability to form solid solutions, and to accept numerous substitutions. For example, Me can be partially substituted by monovalent ions (Na, K…), trivalent ions (La, Eu, Ga…), or by lacunae. Similarly, XO_4 groups can be substituted by bivalent ions (CO_3, SO_4, HPO_4…), or tetravalent ions (SiO_4). The second anionic site can be also replaced by divalent ions (CO_3, O, O_2, S…) or by lacunae.

In the case of stoichiometric HA, the substitution of XO_4 by divalent ions such as HPO_4 induces lacunas in the lattice, decreasing the apatitic crystallinity. In this case, these apatites are called deficient apatite. The carbonate (CO_3) substitution can occur in two different sites, the substitution of: 1) XO_4 groups leading the so-called type B-carbonated apatite; 2) Y_2 groups leading to the so-called type A-carbonated apatite; 3) or both XO_4 and Y_2 sites so-called type AB-carbonated apatite [68]. With regard to the stoichiometry, the substitution by carbonates creates lacuna in the crystals and affects the lattice parameters. The crystal size is decreased, and thereby the surface area is increased. In addition, apatitic chemical bonds are weaker with carbonate groups, leading to a higher dissolution than stoichiometric HA [69].

Octacalcium Phosphate

Octacalcium phosphate (OCP, $Ca_8H_2(PO_4)_6.5H_2O$) crystals are triclinic and they consist of alternating "apatite layers" (arrangement of calcium and phosphate groups similar to that of apatite) and "hydrated layers" [69]. These two layers are linked to each other's by Van der Walls and hydrogen bonds. OCP often occurs as a transient intermediate in the precipitation of the thermodynamically more stable HA and biological apatites. The close relationship between OCP and HA has been used to explain the incorporation

(via hydrolysis) of impurities, particularly carbonate, magnesium and sodium ions, and hence the nonstoichiometry of precipitated apatites [67].

Tricalcium Phosphate

Two major distinct phases of anhydrous tricalcium phosphate crystals exist: α-TCP and β-TCP phases. The α-TCP crystallizes in the monoclinic space group, and β-TCP crystallizes in the rhombohedral space group. TCP is more soluble than HA, and it has been used as an additional compound to HA biomaterials in order to increase their solubility.

Dicalcium Phosphate Dihydrate

Dicalcium phosphate dehydrate crystals (DCPD, $CaHPO_4.2H_2O$) are monoclinic. There are four formulas per unit cell with an asymmetric unit $CaHPO_4.2H_2O$. DCPD is one of the most soluble of the calcium phosphate salts, and it is the most stable at pH=5.0.

Amorphous Calcium Phosphates

Amorphous calcium phosphates vary widely in composition because of the possible insertion of several secondary ions. They are characterized by the broad X-Ray diffraction bumps, and by infrared monocomponents PO_4 bands. The basic structure unit of amorphous calcium phosphates is a cluster of ions comprising $Ca_9(PO_4)_6$ packed with interfacial water to form bigger entities [17].

Thermal behavior of calcium phosphates

The calcium phosphate salts do not behave equally towards thermal treatments. The water-containing phases such as DCPD or OCP dehydrate at approximately $180°C$. In addition, the calcium phosphate compounds containing hydrogenophosphate groups in their lattice, such as non-stoichiometric apatite, OCP or DCPD sustain a condensation resulting in the formation of pyrophosphates ions ($P_2O_7^{4-}$) at approximately $300°C$ according to the reaction (1):

$$2HPO_4^{2-} \quad P_2O_7^{4-} + H_2O \quad (1)$$
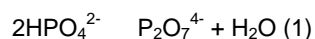
Depending on the substitution mode, the thermal treatment of carbonated apatite leads to the possible release of CO_2 gas with subsequent rearrangements [67].

Therefore, non-stoichiometric apatite, OCP and DCPD are unstable at high temperature. Depending on the thermal treatment, they can degrade in a mixture of sub-products: pyrophosphate, HA and TCP.

On the contrary, TCP and HA phases remain stable up to $1000°C$. The β-TCP phase is stable up to $1125°C$, whereas above this and up to

1430ºC, the α-TCP phase is stable. With regard to stoichiometric HA, above 1000ºC, some hydroxyl groups may condensate to produce water following the reaction (2) [67]:

$$Ca_{10}(PO_4)_6(OH)_2 \leftrightarrow Ca_{10}(PO_4)_6O\square + H_2O \quad (2)$$
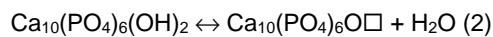
$$\square: lacuna$$

IV-Hip arthroplasty

For the fixation of hip stems, there are basically two different techniques that can be utilized cemented and cementless fixation. Cemented fixation is based upon the use of an acrylic cement to fill the space between the prosthesis and the surrounding bone, resulting in mechanical fixation of the prosthesis [70,71]. On the other hand, cementless fixation is based upon retention of the prosthesis itself, without an intermediate substance. In cementless devices, a long lasting fixation has to be achieved by functional integration of the prosthesis with the surrounding bone [72-74]. The functional integration will depend on the physicochemical and biological performances of the implant. Titanium and certain of its alloys combined with calcium phosphate coating confer the most effective osseointegration to date [75].

IV.1-Titanium and its alloys
Among metals used for hip stems, titanium and certain titanium alloys have shown excellent biocompatibility and osseointegration compared to other metals [76].

Titanium exhibits a strong tendency towards passivation and rapidly forms an oxide film in the presence of oxygen. Within less than a millisecond of exposure to air or aqueous solution, an oxide layer of 1 nm in thickness will be formed on the surface; and within one minute, the oxide film is about 5 nm. The oxide film is very adherent and stable, and should not break down under normal physiological conditions. Since an oxide film is formed so rapidly, there is no contact between the titanium and the host tissue; instead, the surface oxide of the implant is in contact with the tissue [77]. The biocompatibility of metal implants is closely related to their corrosion behavior in biological environments. The corrosion resistance of titanium is provided by the protective oxide film spontaneously formed on the surface [78]. Therefore, the oxide film on titanium is of the utmost importance to the tissue acceptance and the biocompatibility of titanium implants.

Although some *in vivo* studies reported the presence of fibrous tissues [55,57,79,80], direct contact between titanium and bone has been often observed [79-83]. From that perspective, it appears that the initial surface roughness of the titanium implant influences greatly tissues reaction promoting

either fibrous tissues [84-86] or bone apposition [80,87]. A smooth surface induces rather fibrous tissues than bone apposition. The strong relation between bone formation and roughness could suggest that surface morphology can stimulate bone cells to colonize the substrate, since it has been already reported that bone marrow cells can lie directly onto titanium substrate [88,89]. The excellent bone-bonding ability and osseointegration of titanium implants are attributed to the growth of the oxide layer *in vivo* within incorporation of mineral ions presents in the body fluids [77]. Bone fixation can be also improved by roughening the titanium surface or by creating a porous surface [73, 90-94]. In addition to its excellent bone-bonding and bone-fixation properties, the bone-like elasticity of titanium justifies its increasing use for biomaterials and in particular as hip stem prosthesis [29].

IV.2-Hydroxyapatite plasma-sprayed coatings
Calcium phosphate ceramics cannot be used as unique material for load-bearing applications due to their poor mechanical properties [95,96]. Nevertheless, they can be applied as coating by plasma-spraying technique [97] so that the strong mechanical properties of titanium and the bioactivity of calcium phosphates are combined. Plasma-spraying technique consists at producing an ionized gas (plasma), in which HA powder is injected, molten and transported. A substrate placed at distance of the spraying torche is coated by a layer having a close composition as the powder. Due to the very high temperature of the plasma, the thermodynamical instability of calcium phosphate at such temperatures plays an important role in the final properties of the deposited coating. Ideally, only a thin outer layer of each powder particle gets into the molten plastic state, which undergoes phase transitions. This plastic state is necessary to ensure dense and adhesive coatings. By plasma spraying, solely thermally stable calcium phosphate phases can be produced, i.e. HA, TCP or amorphous phases. With regard to plasma spraying, the molten HA powder withstands a heterogeneous thermal history. When the molten particles reach the substrate, their outer layer suddenly cools down. This leads to the solidification of an amorphous envelope, whereas in the center of the particle, a milder cooling-down leads to a crystalline structure. Depending on the setting of the flame and the initial powder granulometry, the amorphous-to-crystalline ratio of the coating can vary [98].

HA plasma-sprayed coatings have shown an increase of the clinical success in hip arthroplasty [75, 99-101]. These coatings applied on metallic implants accelerate significantly bone growth onto the implant [57, 102] and lead to a better fixation of the implants [103,104]. Moreover, HA plasma-sprayed coatings facilitate the healing of gaps up to 2mm between implants and hosting bone [105-107].

Besides the excellent performance of these bioactive HA plasma sprayed coatings, their longevity, i.e. their degradation or solubility, remains debated. Changes in the coating solubility were performed by changes in the coating composition. The solubility of the coating could be increased by increasing the amorphous phase content, or by adding the more soluble TCP phase. On the other hand, the solubility of the plasma-sprayed coating could be decreased by implementation of fluorohydroxyapatite. At the early stage of implantation, the fast dissolution of soluble coatings enhanced bone formation [51,55], whereas non-soluble calcium phosphate led to a better fixation between the implant and the hosting bone [55,57].

On the other hand, publications concerning clinical failure cases of hydroxyapatite coated reported stresses and weakening of the coating-implant interface [108-110], and loosening of crystalline hydroxyapatite particles that creates foreign body response [111] and osteolysis [112]. Despite the large variability in crystallinity and composition of the reported studies, all of these plasma sprayed coatings have common morphological heterogeneities induced by the thermal history as illustrated in figure 4. Calcium phosphate plasma sprayed coatings exhibit distinct phases, which dissolve in their proper way. Therefore, when the amount of highly soluble phase is too high, the loosening of the implants occurs consequently to the "unsealing" of the less soluble phase, provoking the coating fragmentation, and inhibiting bone fixation.
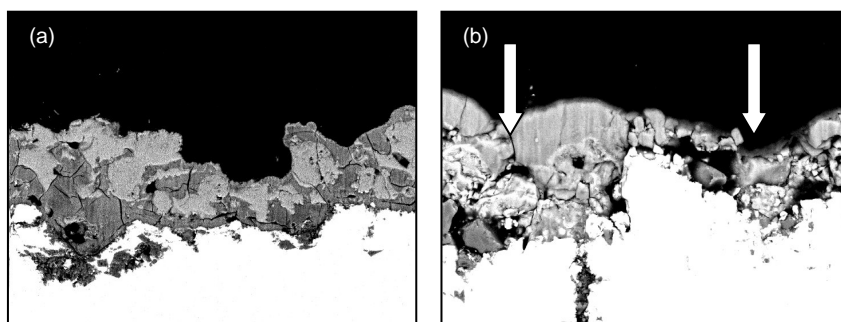
Figure 4: Back-scattering micrographs of cross-sections of: (a) a typical hydroxyapatite-plasma sprayed coating 70% crystalline, and (b) immersed for 4 weeks in a physiological medium (alpha-MEM). Titanium is white, the amorphous Ca-P phase is in dark gray, and mild gray represents crystalline hydroxyapatite. The white arrows point out the fragmentation of the hydroxyapatite coating. Note the decrease in coating thickness after immersion (magnification x75).

However, when the complete dissolution of HA plasma sprayed coating was achieved, bone reaction was found similar for titanium or hydroxyapatite coated titanium implants in terms of bone bonding and bone fixation [80, 102, 113-115]. Therefore, an optimized complete dissolution of the calcium phosphate coating would enhance bone apposition and bone ingrowth

23

for a fast osseointegration of the implant, and it would avoid interfacial consequences of a partial remain of the coating for a more stable bone-bonding on the implant.

V-Biomimetic calcium phosphate coatings

Advantages and drawbacks of calcium phosphate coatings applied on implants are intrinsic to the plasma-spraying process. Other pathways have been developed to process coatings, intending to overcome plasma-spraying drawbacks. These other techniques can be divided in two groups: 1) processes which require energy such as High Velocity Oxygen-Fuel spraying, electrophoretic deposition, sol-gel deposition, hot isostatic pressing, frit enamelling, sputter deposition, ion-assisted deposition, or electrochemical deposition (for review see 98, 114); 2) the biomimetic process [117,118], which is low-energy consuming. This technique is based upon the biomineralization of bone. Biomimetic calcium phosphate coatings are formed from simulated physiological fluids such as Hank's Balanced Salt Solution or Simulated Body Fluids [117,118] under physiological pH and temperature. These simulated solutions have a closely similar composition in inorganic salts as human blood plasma (table 2).

Ions	Concentration (mM)	
	SBF	Blood Plasma
Na^+	142.0	142.0
K^+	5.0	5.0
Mg^{2+}	1.5	1.5
Ca^{2+}	2.5	2.5
Cl^-	147.8	103.8
HCO_3^-	4.2	27.0
HPO_4^{2-}	1.0	1.0
SO_4^{2-}	0.5	0.5
pH	7.4	7.2-7.4

Table 2. Ionic concentrations and pH of simulated body fluids in comparison with those in human blood plasma (after Kokubo 1990)

These simulated body fluids are buffered at pH=7.4 with a mixture of trishydroxymethylaminomethane $(CH_2OH)_3CNH_2)$ and hydrochlorhydric acid in order to maintain the system under physiological pH. Under these physiological conditions of pH and temperature, these solutions are supersaturated towards apatite. The immersion of a chosen substrate leads to the nucleation of apatite

onto the surface, which grows overtime and covers homogeneously the substrate.

V.1-Chemistry of the calcium phosphate mineralizing solutions

A solution can be categorized in three different states, for a given temperature. These states depend on the pH and on the concentrations (figure 5).

- Stable (undersaturated) zone, where crystallization is impossible;
- Metastable zone (supersaturated), where spontaneous crystallization is improbable, although the concentrations are higher than the ones corresponding to the salt solubility. If a crystal seed were placed in such a metastable solution, growth would occur on the seed;
- Unstable or labile (supersaturated) zone, where spontaneous crystallization is probable, but not inevitable [Mullin 119].
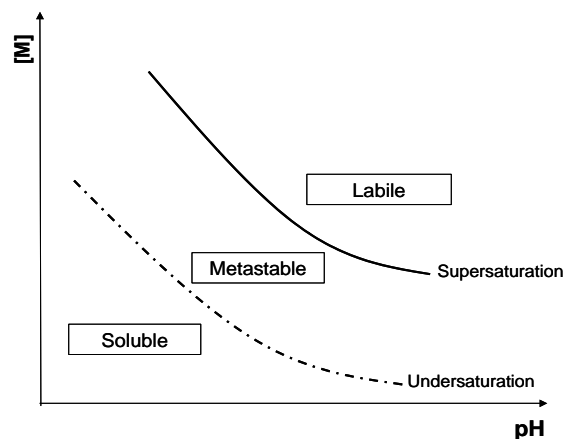
Figure 5: Solubility isotherm of salts in solutions versus pH

The condition of supersaturation alone is not sufficient cause for a system to begin to crystallize. Before crystals can develop there must exist in the solution a number of minute solid bodies, embryos, nuclei or seeds that act as center of crystallization. Nucleation of crystals may occur spontaneously or it may be induced artificially. Mullin has defined the distinct possible nucleation paths (figure 6) [119].

Nucleation can occur spontaneously (homogeneous nucleation), induced by seeds of nature similar to the salt (secondary nucleation), or by a foreign substrate (heterogeneous nucleation). Homogeneous nucleation is rarely achieved since it is quasi impossible to eliminate totally solid particles in the solution, and heterogeneous nucleation is energetically favored as compared to homogenous nucleation [119].

```
                    ┌─────────────────────────┐
                    │       NUCLEATION        │
                    └─────────────────────────┘
                                 │
                 ┌───────────────┴────────────────┐
        ┌────────────────┐              ┌─────────────────────┐
        │    PRIMARY     │              │     SECONDARY       │
        │                │              │ (induced by crystals)│
        └────────────────┘              └─────────────────────┘
                 │
         ┌───────┴────────┐
  ┌────────────────┐ ┌──────────────────────────┐
  │  HOMOGENEOUS   │ │     HETEROGENEOUS        │
  │ (spontaneous)  │ │(induced by foreign particles)│
  └────────────────┘ └──────────────────────────┘
```
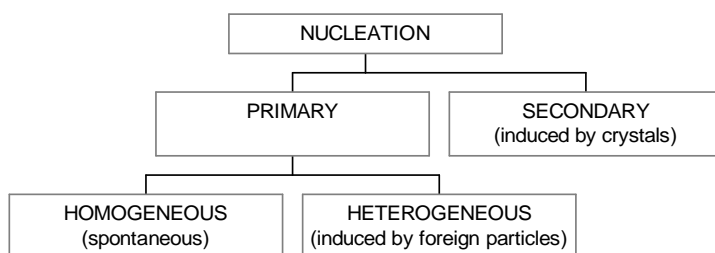
Figure 6: mechanisms of the different nucleation processes

Regarding metastable calcium phosphate solutions, the degree of saturation and the pH influence the nucleated calcium phosphate phase. The secondary nucleation markedly depends on the nature of the calcium phosphate seeds [120-122], on the degree of supersaturation [122, 123-125], on calcium to phosphorus ratio [125-127], on the pH of the solution [127-129], and on the temperature [130]. The closer the relationship is between the lattices of the seed and the nuclei, the more favored the nucleation is [121,122]. In the case of heterogeneous nucleation, calcium phosphate nucleation kinetics is relatively slower than secondary nucleation [122,131]. The supersaturation degree required to induce heterogeneous calcium phosphate nucleation is higher than the one that can induce secondary nucleation [131]. Moreover, the physicochemistry of the heterogeneous surface can affect markedly the calcium phosphate nucleation ability [78, 122, 132-134].

With regard to their composition, simulated body fluids are highly complex solutions. Besides calcium ions and phosphate ions, which are obviously necessary for the formation of calcium phosphates, simulated body fluids contain also magnesium ions and carbonate ions. Magnesium slows down apatite nucleation [18, 135-140], and favors amorphous state [18,135,136,141]. Magnesium poisons the calcium phosphate nucleus surface by complexing phosphate ions. Consequently, defects are created in the crystal lattice, generating stable amorphous calcium phosphates [18,140, 142]. On the other hand, carbonate groups enter the apatitic lattice, substituting anionic groups, either phosphate groups or hydroxyl groups, leading to the formation of lacuna in the apatitic lattice, and thereby a decrease of crystallinity [69].

Recently, possible nucleation precursors attributed to Posner's clusters ($Ca_9(PO_4)_6$, [17]) have been detected by dynamic light scattering spectrophotometer in simulated body fluids [143,144]. These clusters were 0.7 to 1nm of diameter. Their size was not affected by the presence of magnesium or carbonate ions [144], neither by a decrease of pH leading to lower degree of supersaturation. On the contrary, their size slightly augmented in a SBF

concentrated by 1.5 compared to a regular SBF solution. Posner's clusters are believed to aggregate randomly with water to form amorphous calcium phosphate entities, which evolve with the time into crystalline calcium phosphate phases such as DCPD, OCP or apatite depending on the experimental *in vitro* conditions of pH, temperature and crystal growth inhibitors [145-148].

V.2-Chemistry of the substrate

The deposition of calcium phosphate coating on heterogeneous substrates, i.e. non-calcium phosphate substrates does not occur systematically [122,132]. On one hand, hydrophobicity and hydrophilicity of the substrate affect calcification. For example, the highly hydrophobic teflon does not induce calcium phosphate nucleation, whereas the water-permeable Polyactive® does [149].

Regarding inorganic substrates, their surface charge influences the heterogeneous nucleation of calcium phosphate from simulated body fluids. At pH=7.2-7.4, the negatively charged silica glass and titanium oxides substrates can induce calcium phosphate formation [132], whereas the positively charged alumina substrates do not induce the deposition under similar conditions [122,132]. In addition, the oxide gels exhibiting hydroxyl groups, such as tantalum oxide, niobium oxide and zirconium oxide are favorable to the nucleation of calcium phosphates [150-152].

Numerous studies have attempted to investigate the physicochemistry behind the mineralization mechanism of titanium [133,153-159]. Both physical and chemical parameters seem to favor calcification. On one hand, Leitao [153] has shown that specific surface morphology affects the nucleation *in vitro* of bone-like apatite. On the other hand, bone-like apatite nucleation is attributed to the specific properties of the passive titanium dioxide layer that covers any titanium and alloys. This passive layer is hydrated in aqueous solutions, exhibiting hydroxyl groups and physiosorbed water [133,154,155]. These hydroxylated surfaces can then show acidic and basic properties depending on the environmental pH. Quantitative and qualitative studies have shown that titanium dioxide can interact with calcium and/or phosphate [78,155-159]. Despite this negatively charged surface, the majority of the studies have reported that phosphate groups are firstly present on titanium dioxide, followed by calcium ions [133,155,156]. However, Li has shown that calcium ion was deeper present at the calcium phosphate/titanium dioxide interface [158].

V.3-Biomimetic calcium phosphate coating processes on titanium

The formation of a uniform layer requires approximately 7 days, requiring a refreshing of the SBF solutions every 2 days [117,160,161]. The resulting coating is a poorly crystallized carbonated apatite with an approximate

thickness of 1-5μm [117,160,161]. Titanium surface treatment, either physical or chemical, can enhance apatitic nucleation. The modification of the surface morphology by grid blasting is effective for enhancing apatitic nucleation and growth onto titanium substrate [153]. Titanium surface can be also chemically modified with an alkaline treatment by augmenting the pH of the oxide layer in order to favor the calcium phosphate formation [162]. The alkaline and precalcification of titanium substrate can also enhance the formation of calcium phosphate by the grafting and release of calcium ions at the vicinity of a basic surface [163,164]. These chemical treatments accelerate the calcium phosphate growth on titanium, and create a specific roughness that might also stimulate the formation of the calcium phosphate coating. However, this drastic chemical treatment can weaken the calcium-phosphate/substrate interface.

Knowing that heterogeneous nucleation can be enhanced by increasing the degree of supersaturation [122,131,165], the acceleration of the biomimetic process could be enhanced by an increase of the concentration in simulated body fluids. However, simulated body fluids are metastable solutions. Doubled concentrated simulated body fluids are labile, and a calcium phosphate precipitation occurs in the solution rather than on the substrate.

V.4-Future of biomimetic calcium phosphate coatings

Because the biomimetic process is an aqueous process under physiological conditions of pH and temperature, two obvious advantages can be highlighted. Calcium phosphate coating can be applied on complex shaped implants, and on heat-sensitive materials such as PolyActive® [166]. In addition, biological agents can be incorporated within the coating process, such as bovine serum albumin [167,168], antibiotics [169], and bone morphogenetic proteins (Habibovic and Marin, internal communication 2001). In relation to the low temperature required for the biomimetic process, several calcium phosphate phases, which are solely stable at low temperature, can be now deposited as coating, for example OCP or carbonated apatites. Based on previous works, these two calcium phosphates applied as coating could be susceptible to show diverse *in vivo* behavior and positive bone response.

V.4.1-An Octacalcium phosphate coating?

The biological evaluation of OCP has been subjected to few studies compared to HA and TCP ceramics. *In vitro* and *in vivo*, octacalcium phosphate transforms into a carbonated apatitic structure [43,44,170,171]. As a rough or flat substrate, octacalcium phosphate was less resorbed by osteoclasts compared to hydroxyapatite and carbonated apatite [53,54], whereas it was more resorbed compared to DCPD and TCP *in vitro* [53]. On the other hand, OCP stimulates osteogenesis by osteoblatic cells *in vivo* [172], and it appears to resorb faster than HA and TCP, leading to an earlier bone formation [59] in

rat cranial defects. Recently, it has been reported that biomimetic OCP coating with cultured rat bone marrow cells induced bone formation under the skin of nude mice, and the presence of OCP coating applied on porous implants induced bone in dog muscles whereas identical non-coated porous implants did not induce bone [63,173].

V.4.2-A bonelike carbonated apatite coating?

Carbonated apatites are tremendously various in their composition and structure. Many publications have attributed bone mineral structure as HA because of an identical calcium to phosphorus ratio of 1.67. Bone mineral shall be better described as a type AB-carbonated apatite, although carbonate groups can be also located in non-apatitic environment in bone mineral [8]. The biological evaluations of carbonated apatite are as much various as their structures. Nowadays the tendency to study carbonated apatites as bone substitutes increases because of their close nature to that of bone mineral. However this close relationship has not been proven yet to have a marked influence on the osteogenicity and osseointegration of carbonated apatites compared to other calcium phosphate ceramics. *In vitro* osteoclastic assays indicated that sintered carbonated apatite resorbs faster than sintered hydroxyapatite [53,174], and than octacalcium phosphate [53,54]. Likewise, when subcutaneously implanted, sintered carbonated apatite dissolved significantly more than sintered HA, but less than TCP [175]. The role of the carbonate group seems to affect significantly the biological response towards carbonated apatite. On one hand, the presence of carbonate groups seems to stimulate the osteoclastic resorption [54,176]. On the other hand the presence of carbonate groups reduces the surface energy of apatite, reducing the early osteoblasts growth compared to HA substrate. However, this effect was solely noticeable at the early culturing time. In the final stage of culture, osteoblasts growth was identical for HA and type A-carbonated apatite at the end of the experiments [52]. Like OCP coating, cultured rat bone marrow cells on biomimetic carbonated apatite coatings induced bone formation under the skin of nude mice [173].

VI-Objectives of the present thesis

The objective of the present thesis was 1) to develop a novel biomimetic process for producing calcium phosphate coatings on titanium alloy (Ti6Al4V), and 2) to evaluate the biological response towards these biomimetic coatings. The chemistry behind the process will be studied from the simulated body fluids point of view and from the substrate point of view, in order to answer the following questions:

1) Is there other pathway to accelerate the formation of biomimetic calcium phosphate coatings?

2) Why and how does titanium calcify from simulated body fluids?

In view of clinical applications, several questions will be addressed:

3) What are the advantages offered by the biomimetic technique?

4) What is the biological response towards biomimetic calcium phosphate coatings?

The first part of this thesis was dedicated to the physicochemical processes involved on the development of calcium phosphate coatings. The development of a novel biomimetic process derived from the regular simulated body fluids was studied in chapter 2. Chapter 3 and 4 describe the physicochemical interactions during the calcium phosphate formation from a simulated body fluids point of view and from the substrate point of view. After considering the chemistry of interactions, chapter 5 aimed at studying the nucleation and growth kinetics of the calcium phosphate formation at a nanoscale range. Chapter 6 was dedicated to evaluate the flexibility of the biomimetic method to produce calcium phosphate coatings.

In the second part, the developed biomimetic calcium phosphate coatings were tested *in vitro* and *in vivo* in order to evaluate their potential in clinics. Chapter 7 was dedicated to the comparison between different biomimetic calcium phosphate and hydroxyapatite plasma sprayed coatings, while in chapter 8 parallel *in vitro* and *in vivo* investigations were performed between biomimetic octacalcium phosphate and carbonated apatite coatings. Finally in chapter 9, the *in vivo* osteogenic potential was evaluated on similar biomimetic coatings.

References

1-Wainwright SA. "What we can learn from soft biomaterials and structures." Biomimetics. Design and processing of materials Ed. Sarikaya M, Aksay IA. Woodbury, US: AIP press, 1995. 1-12.

2-Calvert P. "Biomimetic ceramics and hard composites." Biomimetics. Design ans processing materials Ed. Sarikaya M, Aksay IA. Woodbury, US, 1995. 145-161.

3-Mann S. "Biomineralization, the inorganic-organic interface, and crystal engineering." Biomimetics. Design and processing of materials Ed. Sarikaya M, Aksay IA. Woodbury, US: AIP Press, 1995. 91-115.

4-"Encyclopedia Britannica, 15th edition." Ed. Encyclopaedia Britannica, Inc 1998, vol 28.

5-Gray' Anatomy. Williams PL, Warwick R, Dyson M, Bannister LH editors.Churchill Livingstone, London UK 37th Edition.

6-Rey C. "Calcium phosphate biomaterials and bone mineral. Differences in composition, structure and properties." Biomaterials 11 (1990): 13-15

7-Rey C, Collins B, Goehl T, Dickson IR, Glimcher MJ. "The carbonate environment in bone mineral: a resolution-enhanced fourier transform infrared spectroscopy study." Calcif Tissue Int 45 (1989): 157-164.

8-Rey C, Lian J, Grynpas M, Shapiro F, Zylberberg L, Glimcher MJ. "Non-apatitic environments in bone mineral: FT-IR detection, biological properties and changes in several disease states." Connect Tissue Res 21 (1989): 267-273.

9-Morodian-Oldak J, Weiner S, Addadi L, Landis WJ, Traub W. "Electron imaging and diffraction study of individual crystals of bone, mineralized tendon and synthetic carbonate apatite." Connective Tissue Research 25 (1991): 219-228.

10-Kim HM, Rey C, Glimcher MJ. "Isolation of calcium phosphate crystals of bone by non aqueous methods at low temperature." J Bone and Min Res 1995; 10:1589-1601.

11-Green M, Isaac DH, Jenkins GM. "Bone microstructure by collagenase etching." Biomaterials 6 (1985): 150-152.

12-Glimcher MJ. "The nature of the mineral component of bone and the mechanism of calcification." Instr Course Lect 36 (1987): 49-69.

13-Lee DD, Glimcher MJ. "Three-dimensional spatial relationship between the collagen fibrils and the inorganic calcium phosphate crystals of pickerel (Americanus americanus) and herring (Clupea harengus) bone." J Mol Biol 217 (1991): 487-501.

14-Bonucci E. "Role of collagen fibrils in calcification." Calcification in biological systems Ed. Bonucci E Boca Raton, USA: CRC Press, 1992. 19-40.

15-Glimcher MJ, Kossiva D, Brickley-Parsons D. "Phosphoproteins of chicken bone matrix. Proof of synthesis in bone tissue." J Biol Chem 259 (1984): 290-293.

16-Rhee SH, Lee JD. "Nucleation of hydroxyapatite crystal through chemical interaction with collagen." J Am Ceram Soc 83 (2000): 2890-2892.

17-Posner AS. "The mineral of bone." Clin Orthop 200 (1985): 291-305

18-Boskey AL, Posner AS. "Magnesium stabilization of amorphous calcium phosphate: a kinetic study." Mat Res Bull 9 (1974): 907-916.

19-Glimcher MJ, Bonar LC, Grynpas MD, Landis WJ, Roufosse AH. "Recent studies of bone mineral: is the amorphous calcium phosphate theory valid?" J Crystal Growth 53 (1981): 100-119

20-Grynpas MD, Bonar LC, Glimcher MJ. "Failure to detect an amorphous calcium phosphate solid phase in bone mineral: a radial distribution function study." Calcif Tissue Int 36 (1984): 291-301.

21-Roberts JE, Bonar LC, Griffin RG, Glimcher MJ. "Characterization of very young mineral phases of bone by solid state 31phosphorus magic angle sample spinning nuclear magnetic resonance and X-ray diffraction." Calcif Tissue Int 50 (1992): 42-48.

22-Brown WE. "Crystal structure of octacalcium phosphate." Nature 1962: 1048

23-Brown WE, Chow LC. "Thermodynamics of apatite crystal growth and dissolution." J Crystal Growth 53 (1981): 31-41.

24-Brown WE, Eidelman N, Tomazic B. "Octacalcium phosphate as a precursor in biomineral formation." Adv Dent Res 1 (1987): 306-313.

25-Nancollas GH, Wu W. "Biomineralization mechanism: a kinetics and interfacial energy approach." J Crystal Growth 211 (2000): 137-142.

26-Kuhn LT, Wu Y, Rey C, Gerstenfeld, Grynpas MD, Ackerman JL, Kim HM, Glimcher MJ. "Structure, composition, and maturation of newly deposited calcium phosphate crystals in chicken osteoblast cell culture." J Bone Miner Res 15 (2000): 1301-1309.

27-Mendenhall S. "Commentary: The bone-graft in the United States." Bone Engineering Ed. Davies JE Toronto, Canada: em squared incorporated, 2000. 585-590.

28-Wright S. "Commentary: The bone-graft market in Europe." Bone Engineering Ed. Davies JE Toronto, Canada: em squarem incorporated, 2000. 591-596.

29-Breme HJ, Biehl V, Helsen JA. "Metals and implants." Metals as biomaterials Ed. Helsen JA, Breme HJ Chichester, UK: John Wiley & Sons, 1998. 37-71

30-Osborn JF, Newesely H. "Dynamic aspects of the implant bone interface." Dental implants Ed. Heimke G, Munchen Germany: Carl Hansen Verlag, 1980. 111-123

31-Manley MT. "Calcium phosphate biomaterials: a review of the literature." Hydroxyapatite coatings in orthopaedic surgery (1993): 1-19.

32-Geesink RG, de Groot K, Klein CP. "Bonding of bone to apatite-coated implants." J Bone Joint Surg Br. 70B (1988): 17-22.

33-Hanawa T, Kamira Y, Yamamoto S, Kohgo T, Amemyia A, Ukai H, Murakami K, Asaoka K. "Early bone formation around calcium-ion-implanted titanium inserted into rat tibia." J Biomed Mater Res, 36 (1997) 131

34-Kay JF, Cook SD. "Biological profile of calcium phosphate coatings." Hydroxylapatite coatings in orthopaedic surgery Ed. Geesink RGT, Manley MT New-York, USA: Raven Press, Ltd, 1993. 89-106.

35-Chang YL, Stanford CM, Keller JC. "Calcium and phosphate supplementation promotes bone cell mineralization: implication for hydroxyapatite (HA)-enhanced bone formation." J Biomed Mater Res 52 (2000): 270-278.

36-Yamada S, Heymann D, Bouler JM, Daculsi G. "Osteoclastic resorption of calcium phosphate ceramics with different hydroxyapatite/b-tricalcium phosphate ratios." Biomaterials 18 (1997): 1037-1041.

37-Suzuki T, Yamamoto T, Toriyama M, Nishizawa K, Yokogawa Y, Mucalo MR, Kawamoto Y, Nagata F, Kameyama T. "Surface instability of calcium phosphate ceramics in tissue culture medium and the effect on adhesion and growth of anchorage-dependent animal cells." J Biomed Mater Res 34 (1997): 507-517.

38-Knabe C, Gildenhaar R, Berger G, Ostapowicz W, Fitzner R, Radlanski RJ, Gross U. "Morphological evaluation of osteoblasts cultured on different calcium phosphate ceramics." Biomaterials 18 (1997): 1339-1347.

39-Knabe C, Driessens FCM, Planell JA, Gildenhaar R, Berger G, Reif D, Fritzner R, Radlanski RJ, Gross U. "Evaluation of calcium phosphates and experimental calcium phosphate bone cements using osteogenic cultures." J Biomed Mater Res 52 (2000): 498-508.

40-Le Huec JC, Clement D, Brouillaud B, Barthe N, Dupuy B, Foliguet B, Basse-Cathalinat B. "Evolution of the local calcium content around irradiated b-tricalcium phosphate ceramic implant: *in vivo* study in the rabbit." Biomaterials 19 (1998): 733-738.

41-Heughebaert M, LeGeros RZ, Gineste M, Guihlem A, Bonel G. "Physicochemical characterization of deposits associated with HA ceramics implanted in nonosseous sites." J Biomed Mater Res Appl Biomat 1988;A3:257-268

42-Daculsi G, LeGeros RZ, Nery E, Lynch K, Kerebel B. "Transformation of biphasic calcium phosphate ceramics *in vivo*: ultrastructural and physicochemical characterization." J Biomed Mater Res 23 (1989): 883-894

43-Suzuki O, Nakamura M, Miyasak Y, Kagamay M, Sakurai M. "Bone formation on synthetic precursors of hydroxyapatite." Tohoku J Exp Med 164 (1991): 37-50.

44-Suzuki O, Nakamura M, Miyasaka Y, Kagayama M, Sakurai M. "Maclura pomifera agglutin-binding glycoconjugates on converted apatite from synthetic Octacalcium phosphate implanted subperiosteal region of mouse calvaria." Bone and Mineral 20 (1993):151-166

45-Ducheyne P, Bianco P, Radin S, Schepers E. "Bioactive materials: mechanism and bioengineering considerations." Bone-bonding materials Ed. Ducheyne P, Kokubo T, van Blitterswijk CA Leiderdorp, The Netherlands: Reed Healthcare Communications, 1993. 1-12.

46-LeGeros RZ, Orly I, Gregoire M, Daculsi G. "Substrate surface dissolution and interfacial biological mineralization." The Bone-Biomaterial interface Ed. Davies JE Toronto, Canada: University of Toronto Press, 1991. 76-87.

47-Radin S, Ducheyne P. "The effect of calcium phosphate ceramic composition and structure on *in vitro* behavior. I Dissolution." J Biomed Mater Res 27 (1993): 25-34.

48-Radin S, Ducheyne P. "The effect of calcium phosphate ceramic composition and structure on *in vitro* behavior. II Precipitation." J Biomed Mater Res 27 (1993): 35-46.

49-Radin S, Ducheyne P. "The effect of calcium phosphate ceramic composition and structure on *in vitro* behavior. III Porous versus dense ceramics." J Biomed Mater Res 28 (1994): 471-488.

50-Klein CPAT, Wolke JGC, de Blieck-Hogervorst JMA, de Groot K. "Features of calcium phosphate plasma-sprayed coatings: an *in vitro* study." J Biomed Mater Res 28 (1994): 961-967.

51-de Bruijn, Bovell YP, Klein CPAT, de Groot K, van Blitterswijk CA. "Structural arrangements at the interface between plasma-sprayed calcium phosphates and bone tissue *in vivo*." Biomaterials 15 (1994): 543-550.

52-Redey SA, Nardin M, Bernache-Assolant D, Rey C, Delannoy P, Sedel L, Marie PJ. "Behavior of human osteoblastic cells on stoichiometric hydroxyapatite and type A carbonate apatite: role of surface energy." J Biomed Mater Res 50 (2000): 353-364.

53-Doi Y, Iwanaga H, Shibutani T, Moriwaki Y, Iwayama Y. "Osteoclastic responses to various calcium phosphates in cell cultures." J Biomed Mater Res 47 (1999): 424-433.

54-Leeuwenburgh S, Layrolle P, Barrere F, de Bruijn J, Schoonman J, van Blitterswijk CA, de Groot K. "Osteoclastic resorption of biomimetic calcium phosphate coatings *in vitro*. 2001;56:208-215." J Biomed Mater Res 56 (2001): 208-215.

55-Klein CPAT, Wolke JGC, de Blieck-Hogervorts JMA, de Groot K. "Calcium Phosphate plasma-sprayed coatings and their stability: an *in vivo* study." J Biomed Mater Res 28 (1994): 909-917.

56-Frayssinet P, Hardy D, Hanker JS, Giammara BL. "Natural history of bone response to hydroxylapatite-coated hip prostheses implanted in humans." Cells and Mater 5 (1995): 125-138.

57-Dhert WJA, Klein CPAT, Jansen JA, van der Velde EA, Vriesde RC, de Groot K, Rozing PM. "A histological and histomorphometrical investigation of fluoroaptite, magnesium-whitlockite and hydroxyapatite plasma-sprayed coatings in goats." J Biomed Mater Res 27 (1993): 127-138.

58-Nagano M, Nakamura T, Kokubo T, Tanahashi M, Ogawa M. "Differences of bone bonding ability and degradation behaviour *in vivo* between amorphous calcium phosphate and highly crystalline hydroxyapatite coating." Biomaterials 17 (1996): 1771-1777.

59-Kamakura S, Sasano Y, Shimizu T, Hatori K, Suzuki O, Kagayama, Motegi K. "Implanted octacalcium phosphate is more resorbable than beta-tricalcium phosphate and hydroxyapatite." J Biomed Mater Res 59 (2002): 29-34.

60-de Bruijn JD, Flach JS, Leenders H, van den Brink J, van Blitterswijk CA. " Degradation and interface characteristics of plasma sprayed hydroxyapatite coatings with different crystallinities." Bioceramics 1992. 291-298.

61-Ripamonti U. "The morphogenesis of bone in replicas of porous hydroxyapatite obtained from conversion of calcium carbonate exoskeletons of coral." J Bone and Joint Surg 73A (1991): 692-703.

62-Yuan H, de Bruijn JD, Yang Z, de Groot K, Zhang X. "Osteoinduction by calcium phosphates." J Mat Sci Mat Med 9 (1998): 717-721.

63-Yuan H, Kurashina K, de Bruijn JD, Li Y, de Groot K, Zhang X. "A preliminary study on osteoinduction of two kind of calcium phosphate ceramics." Biomaterials 20 (2000): 1283-1290

64-Yuan H, de Bruijn JD, Li Y, Feng Z, Yang K, de Groot K, Zhang X. "Bone formation induced by Calcium phosphate ceramics in soft tissue of dogs: a comparative study between α-TCP and β-TCP." J Mat Sci Mat Med 12 (2001):7-13

65-Magan A, Ripamonti U. "Geometry of porous hydroxyapatite implants influences osteogenesis in baboons (Papio ursinus)." J Craniofac Surg 7 (1996): 71-78.

66-Yuan H, Osteoinduction by Calcium Phosphates, PhD thesis, Leiden University, The Netherlands 2001

67-Elliot JC. "Structure and chemistry of the apatites and other calcium orthophosphates." Studies in inorganic chemistry Amsterdam, The Netherlands: Elsevier Science BV, 1994.

68-Heughebaert JC. "Contribution a l'etude de l'evolution des orthophosphates de calcium precipites amorphes en orthophosphates apatitiques ." These d'Etat INP Toulouse, France: 1977.

69-LeGeros RZ, Calcium phosphates in oral biology and medicine, Krager Ed, Basel 1991

70-Charnley J. "The nine and ten years results of low-friction arthroplasty of the hip." Clin Orthop 95 (1973): 9-25.

71-Harris WH. "The first 32 years of total hip arthroplasty - One surgeon's perspective." Clin Orthop 274 (1992): 6-11.

72-Cook SD, Walsh KA, Haddad RJ. "Interface mechanism and bone ingrowth into porous Co-Cr-Mo alloy implants." Clin Orthop 193 (1985): 271-280.

73-Thomas KA, Cook SD. "An evaluation of variables influencing implant fixation by direct bone apposition." J Biomed Mater Res 19 (1985): 875-901.

74-Engh CA, Bobyn JD, Glassman AH. "Porous-coated hip replacement, the factors governing bone ingrowth, stress shielding and clinical results." J Bone Joint Surg 69B (1987): 45-55.

75-Havelin LI, Engesaeter LB, Espehaug B, Furnes O, Lie SA, Vollset SE. "The norvegian arthroplasty register: 11 years and 73000 arthroplasties." Acta Orthop Scand 71 (2000): 337-353.

76-Hildebrand HF, Hornez JC. "Biological response and biocompatibility ." Metals as biomaterials Ed. Helsen JA, Breme HJ Chichester, UK: John Wiley & Sons, 1998. 265-290.

77-Pan J. "Oxide film characterization by means of electrochemical impedance spectroscopy and surface analysis." PhD thesis, Royal institute of technology Stockholm, Sweden 1996.

78-Tengvall P, Lundstrom I. "Physico-chemical considerations of titanium as biomaterial." Clinical Materials 9 (1992): 115-134.

79-Serre CM, Boivin G, Obrant KJ, Linder L. "Osseointegration of titanium implants in the tibia. Electron microscopy of biopsies from 4 patients." Acta Orthop Scand 56 (1994): 323-327.

80-Carlsson L, Regner L, Johansson C, Gottlander M, Heberts P. "Bone response to hydroxyapatite-coated and commercially pure titanium implants in the human arthritric knee." J Orthop Res 12 (1994): 274-285.

81-McCutchen JW, Collier JP, Mayor MB. "Osseointegration of titanium implants in total hip arthroplastry." Clin Orthop 261 (1990): 114-125

82-Albrektsson T, Branemark PI, Hansson HA, Lindstrom J. "Osseointegrated titanium implants. Requirements for ensuring a long-lasting, direct bone-to-implant anchorage in man." Acta Orthop Scand 52 (1981): 155-170.

83-Barth E, Johansson C, Albrektsson T. "Histologic comparison of ceramic and titanium implants in cats." Int J Orla Maxillofac Implants 5 (1990): 227-231.

84-Chou L, Firth JD, Uitto VJ, Brunette DM. "Effects of titanium substratum and grooved surface topography on metalloproteinase-2 expression in human fibroblasts." J Biomed Mater Res 39 (1998): 437-445.

85-Eisenbarth E, Meyle J, Nactigall W, Breme J. "Influence of the surface structure of titanium materials on the adhesion of fibroblasts." Biomaterials 17 (1996): 1399-1403.

86-Deligianni DD, Katsala N, Ladas S, Sotiropoulou D, Amedee J, Missirlis YF. "Effect of surface roughness of the titanium alloy Ti6Al4V on human bone marrow cell response and on protein adsorption." Biomaterials 22 (2001): 1241-1251.

87-Boyan BD, Hummert TW, Dean DD, Schwartz Z. "Role of material surfaces in regulating bone and cartilage cell response." Biomaterials 17 (1996): 137-146.

88-Piattelli A, Scarano A, Piattelli M, Calabrese L. "Direct bone formation on sand-blasted titanium implants: an experimental study." Biomaterials 17 (1996): 1015-1018.

89-Rahal MD, Branemark PI, Osmond DG. "Response of bone marrow to titanium implants: osseointegration and the establishment of a bone marrow-titanium interface in mice. ." Int J Oral Maxillofac Implants 8 (1993): 573-579.

90-Buser D, Schenk RK, Steinemann S, Fiorellini JP, Fox CH, Stich H. "Influence of surface characteristics on bone integration of titanium implants. A histomorphometric study in miniature pigs." J Biomed Mater Res 25 (1991): 889-902.

91-Pilliar RM. "Porous-surfaced metallic implants for orthopedic applications." J Biomed Mater Res Appl Biomat 21.A1 (1987): 1-33.

92-Gotfredsen K, Berglundh T, Lindhe J. "Anchorage of titanium implants with different surface characteristics: an experiemental study in rabbits." Clin Implant Dent Relat Res 2 (2000): 120-128.

93-Gotfredsen K, Berglundh T, Lindhe J. "Bone reaction adjacent to titanium implants with different surface charactetristics subjected to static load. A study in the dog (II)." Clin Oral Implants Res 12 (2001): 196-201.

94-Chang YS, Oka M, Kobayashi M, Gu HO, Li ZL, Kitsugi T, NAkamura T. "Bone formation and remodelling around implanted materials under load-bearing conditions." Clin Mater 17 (1994): 181-187.

95-de Groot K, de Putter C, Sillevis Smit PAE, Driessens AA. "Mechanical failure of artificial teeth made of dense calcium-hydroxyl-apatite. Science of Ceramics 11 (1981): 433-437

96-de Groot K. Ceramics based on calcium phosphates, in: Ceramics in Surgery, Ed Vicenzini P Elsevier, Amsterdam, 1983

97-de Groot K, Geesink R, Klein CPAT, Serekian P. "Plasma sprayed coatings of hydroxylapatite." J Biomed Mater Res 21 (1987): 1375-1381.

98-Wolke JGC. "Sprayed and sputtered calcium phosphate coatings for medical implants." PhD thesis Catholic University of Nijmegen: 1997.

99-Geesink RGT. "Hydroxylapatite-coated total hip prostheses: Two years clinical and roentgenographic results of 100 cases." Clin Orthop Rel Res 261 (1990): 39-58.

100-Epinette JA. "Hydroxylapatite-coated implants for total hip replacement: clinical experience in France." Hydroxylapatite coatings in orthopaedic surgery Ed. Geesing RGT, Manley MT New-York, USA: Raven Press, Ltd, 1993. 227-248.

101-Bauer TW, Geesink RCT, Zimmerman R, McMahon JT. "Hydroxyapatite-coated femoral stems." J bone and joint surg 73-A (1991): 1439-1452.

102-Jansen JA, van der Waerden JPCM, Wolke JGC, de Groot K. "Histologic evaluation of the osseous adaptation to titanium and hydroxyapatite-coated titanium implants." J Biomed Mater Res 25 (1991): 973-989.

103-Tisdel CL, Goldberg VM, Parr JA, Bensusan JS, Staikoff LS, Stevenson S. "The influence of hydroxyapatite and tricalcium phosphate coating on bone growth into titanium fiber metal implants." Journal Bone Joint Surg 76 (1994): 159-171.

104-Dhert WJA, Klein CPAT, Wolke JGC, van der Velde EA, Vriesde RC, de Groot K, Rozing PM. "A mechanical investigation of fluoroapatite, magnesiumwhitlockite and hydroxylapatite plasma-sprayed coatings in goats." J Biomed Mater Res 25 (1991): 1183-1200.

105-Soballe K, Hansen ES, Brockstedt-Rasmussen, Bunger C. "Gap healing enhanced by hydroxyapatite coatings in dog." Clin Orthop 272 (1991): 300-307.

106-Clemens JAM, Klein CPAT, Vriesde RC, Rozing PM, de Groot K. "Healing of large (2mm) gaps around calcium phosphate-coated bone implants: a study in gaots with a follow-up of 6 months." J Biomed Mater Res 40 (1998): 341-349.

107-Sakkers RJB, Dalmeijer RAJ, Brand R, Rozing PM, van Blitterswijk CA. "Assesment of bioactivity for orthopedic coatings in a gap healing model." J Biomed Mater Res 36 (1997): 265-273.

108-McDonald DE, Betts F, Stranick M, Doty S, Boskey AL. "Physicochemical study of plasma-sprayed hydroxyapatite-coated implants in humans." J Biomed Mater Res 54 (2001): 480-490.

109-Ogiso M, Yamashita Y, Matsumoto T. "The process of physical weakening and dissolution of the HA-coated implant in bone and soft tissue." J Dent Res 77 (1998): 1426-1434.

110-Takeshita F, Matsushita Y, Ayukawa Y, Suetsugu T. "Fractures of hydroxyapatite-coated blade implants connected with natural teeth. A histological study using SEM, light microscopy, and an image processing system." J Periodontol 67 (1996): 86-92.

111-Bloembaum RD, Dupont JA. "Osteolysis from a press-fit hydroxyapatite-coated implant." J Arthropl 8 (1993): 195-202.

112-Bloembaum RD, Beeks D, Dorr LD, Savory CG, Dupont JA, Hofman AA. "Complication with hydroxylapatite particulate separation in total hip replacement." Clin Orthop 298 (1994): 19-26.

113-Hayashi K, Mashima T, Uenoyama K. "The effect of hydroxyapatite coating on bony ingrowth into grooved titanium implants." Biomaterials 20 (1999): 111-119.

114-Rivero DP, Fox J, Urban RM, Galante JO. "Calcium phosphate-coated porous titanium implants for enhanced skeletal fixation." J Biomed Mater Res 22 (1988): 191-201.

115-Wolke JGC, de BlieckHogevorst JMA, Dhert WJA, Klein CPAT,de Groot K. "Studies on the thermal spraying of apatite bioceramics." J Themal Spary Technology 1 (1992): 75-82.

116-de Groot K. "Calcium phosphate coatings: alternatives to plasma spray". Bioceramics 11 (1998): 41-43

117-Kokubo T, Kushitani H, Abe Y, Yamamuro T. "Apatite coating on various substrates in simulated body fluids." Bioceramics 2 (1989): 235-242.

118-Kokubo T, Kushitani H, Sakka S, Kitsugi T, Yamamuro T. "Solutions able to reproduce *in vivo* surface-structure changes in bioactive glass-cermics A-W3." J Biomed Mater Res 24 (1990): 721-734.

119-Mullin JW. "Crystallization" 3rd edition. Oxford, UK: Butterworth-Heinemann Ltd, 1993.

120-Heughebaert JC, Nancollas GH. "Mineralization kinetics: the role of octacalcium phosphate in the precipitation of calcium phosphates." Colloids and surfaces 9 (1984): 89-93.

121-Koutsoukos PG, Nancollas GH. "Crystal growth of calcium phosphates - Epitaxial considerations." J Crystal Growth 53 (1981): 10-19.

122-Royer P, Amrah-Bouali S, Freche M, Rey C, Rouquet N, Bonel G. "Nucleation of calcium phosphate salts onto biomaterial surfaces." Bioceramics 5 (1992): 95-102.

123-Moreno EC, Varughese K. "Crystal growth of calcium apatites from dilute solutions." J Crystal Growth 53 (1981): 20-30.

124-Boskey AL, Posner AS. "Formation of hydroxyapatite at low supersaturation." The Journal of Physical Chemistry 80 (1976): 40-45.

125-Nancollas GH, Tomazic B. "Growth of calcium phosphate on hydroxyapatite crystals. Effect of supersaturation and ionic medium." The Journal of Physical Chemistry 78 (1974): 2218-2225.

126-Cheng PT, Pritzker PH. "Solution Ca/P ratio affects calcium phosphate crystal phases." Calcif Tissue Int 35 (1983): 596-601.

127-Christoffersen MR, Dohrup J, Christoffersen J. "Kinetics of growth and dissolution of calcium hydroxyapatite in suspension with variable calcium to phosphorus ratio." J crystal growth 186 (1998): 283-290.

128-de Rooij JF, Heughebaert JC, Nancollas GH. "A pH study of calcium phosphate seeded precipitation." J of Colloids and Interface Science 100 (1984): 350-358.

129-Hohl H, Koutsoukos PG, Nancollas GH. "The crystallization of hydroxyapatite and dicalcium phosphate dihydrate; representation of growth curves." J Crystal Growth 57 (1982): 325-335.

130-McDowell H, Gregory TM, Brown WE. "Solubility of Ca5(PO4)3OH in the system Ca(OH)$_2$-HPO$_3$-H$_2$O at 5, 15, 25, and 37ºC." Journal of Research of the National Bureau of standards-A. Physics and Chemistry 81A (1977): 273-281.

131-Wu W, Nancollas GH. "Kinetics of nucleation and crystal growth of hydroxyapatite and fluoroapatite on titanium oxide surfaces." Colloids and Surfaces B: Biointeraces 10 (1997): 87-94.

132-Li P, Ohtsuki C, Kokubo T, Nakanish K, Soga N, de Groot K. "A role of hydrated silica, titania and alumina in forming biologically active bone-like apatite on implants." J Biomed Mater Res 28 (1994): 7-15.

133-Healy KE, Ducheyne P. "The mechanism of passive dissolution of titanium in a model physiological environment." J Biomed Mater Res 26 (1992): 319-338.

134-Combes C. "Croissance cristalline de phosphates de calcium sur des substrats d'interet biologique: le titane et le collagene." These d'Etat Toulouse, France: INP, 1996.

135-Abbona F, Franchini-Angela M. "Crystallization of calcium and magnesium phosphates from solutions of low concentrations." J Crystal Growth 104 (1990): 661-671.

136-Abbona F, Lundager HE, Madsen, Boistelle R. "The initial phases of calcium and magnesium phosphates precipitated from solutions of high to medium concentrations. 1986;74:581-590." J Cryst Growth 74 (1986): 581-590.

137-Kibalczyc W, Christoffersen J, Christoffersen MR, Zielenkiewicz A, Zielenkiewicz W. "The effect of magnesium ions on the precipitation of calcium phosphates." J Crystal Growth 106 (1990): 355-366.

138-Nancollas GH, Tomazic B, Tomson M. "The precipitation of calcium phosphates in the presence of magnesium." Croatia Chemica Acta 48 (1976): 431-438.

139-Salimi MH, Heughebaert JC, Nancollas GH. "Crystal growth of calcium phosphate in the presence of magnesium ions." Langmuir 1 (1985): 119-122.

140-Tomazic B, Tomson M, Nancollas GH. "Growth of calcium phosphates on Hydroxylapatite crystals: the effect of magnesium." Archs oral Biol 20 (1975): 803-808.

141-Eanes ED, Rattner SL. "The effect of magnesium on apatite formation in seeded supersaturated solutions at pH=7.4." J Dent Res 60 (1981): 1719-1723.

142-Termine JD, Peckauskas RA, Posner AS. "Calcium phosphate formation *in vitro* II. Effect of environment on amorphous-crystalline transformation." Archives of biochemistry and biophysics 140 (1970): 318-325.

143-Onuma K, Ito A. "Cluster growth model for hydroxyapatite." Chem Mater 10 (1998): 3346-3351.

144-Oyane A, Onuma K, Ito A, Kokubo T. "Clustering of calcium phosphate in SBF and in the system CaCl$_2$-H$_3$PO$_4$-KCl-H$_2$O." Bioceramics 12 (1999): 157-160.

145-Christoffersen J, Christoffersen MR, Kibalczyc W, Andersen FA. "A contribution to the understanding of the formation of calcium phosphates." J Crystal Growth 94 (1989): 767-777.

146-Christoffersen MR, Christoffersen J, Kibalczyc. "Apparent solubilities of two amorphous calcium phosphates and octacalcium phosphate in the temperature range 30-42ºC." J Crystal Growth 96 (1990): 349-354.

147-Abbona F, Baronnet A. "A XRD and TEM study on the transformation of amorphous calcium phosphate in the presence of magnesium." J Crystal Growth 165 (1996): 98-105

148-Harries JE, Hukins DWL, Holt C, Hasnain SS. "Conversion of amorphous phosphate into hydroxyapatite investigated by EXAFS spectroscopy." J Crystal Growth 84 (1987): 563-570.

149-van Blitterswijk CA, Bakker D, Leenders H, van der Brink J, Hesling SC, Bovell YP, Radder AM, Sakkers RJ, Gaillard ML, Heinze PH, Beumer GJ. "Interfacial reactions leading to bone-bonding with PEO/PBT copolymers (Polyactive®)." Bone-bonding biomaterials Ed. Ducheyne P, Kokubo T, van Blitterswijk CA Leiderdorp, The Netherlands: Reed Healthcare Communications, 1993. 13-30.

150-Miyazaki T, Kim HM, Miyaji F, Kokubo T, Nakamura T. "Apatite-forming ability of sodium tantalate gels." Bioceramics 11 (1998): 481-484.

151-Miyazaki T, Kim HM, Kokubo T, Kato H, Nakamura T, Ohtsuki C. "Bonelike apatite formation on niobium oxide gels in simulated body fluids." Bioceramics 13 (2000): 43-46.

152-Uchida M, Kim HM, Miyaji F, Kokubo T, Nakamura T. "Apatite forming ability of zirconia gel in modified SBF solutions." Bioceramics 11 (1998): 77-80.

153-Leitao E, Barbosa M, de Groot K. "Influence of substrate material and surface finishing on the morphology of the calcium phosphate coating." J Biomed Mater Res 36 (1997): 85-90.

154-Tengvall P, Elwing H, Sjoqvist L, Lundstrom I, Bjursten LM. "Interaction between hydrogen peroxide and titanium: a possible role in the biocompatibility of titanium." Biomaterials 10 (1989): 118-120

155-Combes C, Freche M, Rey C. "Nucleation and crystal growth of dicalcium phosphate dihydrate on titanuim powder." J Mat Sci Mat Med 6 (1995): 699-702.

156-Hanawa T. "Titanium and its oxide film: a substrate for formation of apatite." The Bone-Biomaterial interface Ed. Davies JE 1991. 49-61.

157-Healy KE, Ducheyne P. "Hydratation and preferential molecular adsorption on titanium in vitro." Biomaterials 13 (1992): 553-561.

158-Li P. "In vitro and in vivo calcium phosphate induction on gel oxides." PhD Thesis Leiden University, 1993.

159-Sutherland DS, Forshaw PD, Allen GC, Brown IT, Williams KR. "Surface analysis of titanium implants." Biomaterials 14 (1993): 893-899.

160-Li P, Ducheyne P. "Quasi-biological apatite film induced by titanium in a simulated body fluid." J Biomed Mater Res 41 (1998): 341-348.

161-Peltola T, Patsi M, Rahiala H, Kangesniemi I, Yli-Urpo. "Calcium phosphate induction by sol-gel-derived titania coatings on titanium substrates in vitro." J Biomed Mater Res 41 (1998): 504-510.

162-Kim HM, Miyaji F, Kokubo T, Nakamura T. "Preparation of bioactive Ti and its alloys via simple chemical surface treatment ." J Biomed Mater Res 32 (1996): 409-417.

163-Wen HB, Wolke JGC, de Wijn JR, Liu Q, Cui FZ, de Groot K. "Fast precipitation of calcium phosphate layers on titanium induced by simple chemical treatment." Biomaterials 18 (1997): 1471-1478.

164-Wen HB, de Wijn JR, Cui FZ, de Groot K. Preparation of bioactive Ti6Al4V surfaces by a simple method, Biomaterials 19 (1998) pp. 215-221

165-Combes C, Rey C, Freche M. "XPS and IR study of dicalcium dihydrate nucleation on titanium surfaces." Colloids and Surfaces B: Biointerfaces 11 (1998): 15-27.

166-Du C, Klasens P, Haan RE, Bezemer J, Cui FZ, de Groot K, Layrolle P. "Biomimetic calcium phosphate coatings on Polyactive 1000/70/30." J. Biomed. Mater. Res 59 (2002):535-546.

167-Wen HB, de Wijn JR, Li SH, Cui FZ, de Bruijn JD, van Blitterswijk CA, de Groot K. "Co-precipitation of bovine serum albumin in calcium phosphate coating on titanium: a model protein delivery system." J Biomed Mater Res 46 (1999): 245-252.

168-Liu Y, Layrolle P, de Bruijn J, van Blitterswijk C, de Groot K. "Biomimetic coprecipitation of calcium phopshate and bovine serum albumin on titanium alloy." J Biomed Mater Res 57 (2001): 327-335.

169-Stigter M, de Groot K, Layrolle P. "Incorporation of tobramycin into biomimetic hydroxyapatite coating on titanium." Biomaterials (submitted)

170-LeGeros RZ, Kijkowska R, LeGeros JP. Formation and transformation of octacalcium phosphate, OCP: a preliminary report. Scanning Electron Microscopy 1984; 1:1771-1777

171-Ban S, Matsuura M, Arimoto N, Hayashizaki J, Itoh Y, Hasegawa J. "Factors affecting the transformation of octacalcium phosphate to apatite in vitro." Dent Mater J 12 (1993): 106-117.

172-Sasano Y, Kamakura S, Homma H, Suzuki O, Mizoguchi I, Kagayama M. "Implanted octacalcium phosphate (OCP) stimulates osteogenesis by osteoblastic cells and/or committed osteoprogenitors in rat calvarial periosteum." Anat Rec 256 (1999): 1-6.

173-de Bruijn JD, Yuan HP, Dekker R, van Blitterswijk CA. "Osteoinduction by biomimetic calcium phosphate coatings and their potential use as tissue engineering scaffolds." Bone engineering Ed. Davies JE Toronto, Canada: : em squared incorporated, 2000.

174-Doi Y, Shibutani T, Moriwaki Y, Kajimoto T, Iwayama Y. "Sintered carbonate apatites as bioresorbable bone substitutes." J Biomed Mater Res 39 (1998): 603-610.

175-Barralet J, Akao M, Aoki H, Aoki H. "Dissolution of dense carbonate apatite subcutaneously implanted in Wistar rats." J Biomed Mater Res 49 (2000): 176-182.

176-Anderson RE, Jee WSS, Woodbury DM. "Stimulation of carbonic acid anhydrase in osteoclasts by parathyroid hormone." Calcif Tissue Int 37 (1985): 646-650.

CHAPTER 2

INFLUENCE OF IONIC STRENGTH AND CARBONATE ON THE CALCIUM PHOSPHATE COATING FORMATION FROM SBFx5 SOLUTION

F. Barrère, C.A van Blitterswijk, K. de Groot and P. Layrolle

ABSTRACT

Biomimetic calcium phosphate (Ca-P) coatings were applied on titanium alloy (Ti6Al4V) by using a Simulated Body Fluid concentrated by a factor 5 (SBFx5). The production of SBFx5 solution was possible by decreasing the pH of the solution to approximately 6 using carbon dioxide (CO_2) gas. The subsequent release of this mildly acidic gas led to a pH rise and thus, an increase of supersaturation. After immersion for 5h1/2, a Ca-P coating on the Ti6Al4V plates and a precipitate simultaneously formed at pH=6.8. Sodium chloride (NaCl) and carbonate (HCO_3^-) contents were studied in relation to CO_2 release and coating formation, by changing their individual concentration in SBFx5 solution. On one hand, NaCl-free or low NaCl content SBFx5 solution led to earlier precipitation in the solution than for SBFx5 solution. In contrast, Ca-P coating was formed later and was thinner than the coating obtained in regular SBFx5 solution. High ionic strength delayed precipitation and favored Ca-P heterogeneous nucleation on Ti6Al4V. On the other hand, HCO_3^- content increased the pH of the solution due to its buffering capacity, and influenced the release rate of dissolved CO_2. Thus, HCO_3^- content strongly affected the supersaturation and Ca-P structure. Furthermore, HCO_3^- favored the attachment of Ca-P mineral on Ti6Al4V by decreasing Ca-P crystal size resulting to a better physical attachment of Ca-P coating on Ti6Al4V substrate.

INTRODUCTION

Titanium (Ti) and its alloys are widely used in orthopedic surgery because of their excellent mechanical properties required for load bearing applications like hip prostheses or dental plugs. These Ti implants are often coated with calcium phosphate (Ca-P) coatings in order to enhance bone-bonding [1-8]. Furthermore, studies have shown that Ca-P crystals could nucleate easily on Ti and alloys *in vitro* [9-13] and *in vivo* [14-15], being thereby integrated into bone. In order to create Ca-P coatings onto Ti and alloys, different techniques have been developed [16-20]. Currently, Hydroxylapatite (HA) coatings are deposited by plasma-spraying technique onto Ti substrate. Despite excellent clinical results [1-8], plasma-sprayed HA coatings have specific drawbacks related to the extremely high processing temperatures and line of sight application.

The biomimetic route is nowadays very promising for coating implants with Ca-P, overcoming plasma-spraying drawbacks. The biomimetic process consists at soaking implants under mild conditions of pH and temperature into Simulated Body Fluid (SBF) solutions that have a similar inorganic content as human blood plasma [20]. Because of these physiological conditions, it is possible to coat heat-sensible materials such as polymers, and to cover complex shaped materials such as porous implants. Furthermore, this technique allows the covering of implants with new Ca-P phases [21-22] that could not be produced at high temperature. These new biomimetic coatings have different structures and dissolution behavior depending on their crystal size and phase composition [23]. These specific characteristics could be highly beneficial for bone formation as compared with HA-plasma sprayed coating.

However, the development of such biomimetic Ca-P coatings was limited by long immersion periods of about 7 to 14 days with daily refreshments for achieving uniform Ca-P layers on various substrates [20,24-26]. Several studies have shown that chemical treatment of Ti surface could enhance the deposition of apatite-like layers [27-29]. Another possibility for shortening the coating process is to concentrate SBF solution. However, SBF solutions are supersaturated at physiological pH and increasing the concentrations is limited by the low solubility of Ca-P.

The idea of our work was thereby to increase the solubility of Ca-P phases by the use of a mildly acidic gas like carbon dioxide (CO_2). Bubbling CO_2 allows the preparation of a stable five-times concentrated SBF (so-called SBFx5 solution). Once CO_2 supply is stopped, the gas is released out of the solution leading to an increase of pH and thus, to the formation of Ca-P salt in the solution and onto the Ti substrate [12]. In this work we investigated the release kinetics of CO_2 in relation to SBFx5 composition and Ca-P coating formation. Since ionic strength or amphoteric ions are thought to affect gas solubility, we studied the influence of sodium chloride (NaCl) and carbonate

(HCO_3^-) contents on CO_2 release. Thereafter, we changed individually the concentration of either NaCl or HCO_3^- in relation to Ca-P formation in the soaking solution and onto Ti alloy (Ti6Al4V) samples.

MATERIALS AND METHODS

Several simulated body fluids solutions were prepared by changing salt concentrations as summarized in table 1. All of these solutions were derived from the classical SBF solution [20], in which ionic concentrations were multiplied by five (SBFx5). Overall the experiments, the chemicals used for the study were reagents grade (Merck) precisely weighted. Each solution was prepared by dissolution of the salts into 1000 ml of demineralized water saturated with CO_2 gas at approximately 0.2 bar. The starting point of the experiments was set when CO_2 bubbling was stopped (t=0h). All of the experiments were performed in a 1.5l-reactor thermostated at 37±1°C with a soaking time of 24h. The solutions were stirred with a magnetic bar at a speed of 200 rounds per minutes (rpm). The head plate of the reactor had open ports for a natural exchange of CO_2 with air.

Reference solutions

Prior to investigating the Ca-P coating formation into highly concentrated SBF solutions, the CO_2 release mechanism was studied in simple media (REF1, REF2, REF3 and REF4, see table 1). The CO_2 release from a medium was expected to be influenced by HCO_3^- content and by ionic strength in the solution related to NaCl content. REF1 solution was simply composed of demineralized water. REF2 solution contained additionally $NaHCO_3$ salt in the same concentration than in SBFx5 solution. REF3 solution had a similar NaCl content than SBFx5. Finally, REF4 combines similar ionic strength and [HCO_3] than SBFx5. The pH of the REF solutions was recorded every 30 minutes for 24 hours with a combined electrode (pHmeter, Portamess). Prior to measurements, the pH electrode was calibrated at room temperature with two buffer solutions at pH=4.01 and pH=7.00 (IUPAC standards, Radiometer Copenhagen).

Influence of the ionic composition of SBF solution on the Ca-P coating formation

Various highly concentrated SBF solutions (SBFx5) were prepared with different NaCl and HCO_3^- contents. SBFx5(NaClx0) and SBFx5(NaClx3) were respectively a NaCl-free solution and a NaCl-concentrated by three solution. On the other hand, SBFx5 (HCO_3x0) was HCO_3-free solution and SBFx5 (HCO_3x3) was an SBFx5 solution where HCO_3^- content was reduced to three times. Besides HCO_3^- and NaCl contents, leftover salts, i.e. Mg^{2+}, Ca^{2+} and HPO_4^{2-} remained similar to SBFx5 (see table 1). Twenty Ti6Al4V plates were

soaked into each solution in order to investigate the coating formation mechanism.

Prior to the immersion, the Ti6Al4V plates were ultrasonically and successively cleaned into acetone, ethanol 70% and demineralized water for 15 minutes. These plates were then etched for 10 minutes by Kroll's reagent (a mixture of 2ml HF (40%) and 4ml HNO_3 (66%) in 1000ml of water) in order to create a fresh titanium oxide (TiO_2) layer. The average roughness (R_a) of the substrate was not affected by etching and remained around $R_a=0.80\mu m$. The plates were individually and vertically fixed to polyethylene sample holders. Finally, Ti6Al4V plates were soaked into each solution at 37ºC for 24h while pH was monitored.

	NaCl	$MgCl_2.6H_2O$	$CaCl_2.2H_2O$	$Na_2HPO_4.2H_2O$	$NaHCO_3$
HBP	146.7	1.5	2.5	1.0	27.0
SBF	146.7	1.5	2.5	1.0	4.2
SBFx5	733.5	7.5	12.5	5.0	21.0
REF1	0.0	0.0	0.0	0.0	0.0
REF2	0.0	0.0	0.0	0.0	21.0
REF3	733.5	0.0	0.0	0.0	0.0
REF4	733.5	0.0	0.0	0.0	21.0
SBFx5(HCO_3x0)	733.5	7.5	12.5	5.0	0.0
SBFx5(HCO_3x3)	733.5	7.5	12.5	5.0	12.6
SBFx5(NaClx0)	0.0	7.5	12.5	5.0	21.0
SBFx5(NaClx3)	440.1	7.5	12.5	5.0	21.0

Table 1: Inorganic composition (mM) of human blood plasma (HBP), regular Simulated Body Fluid (SBF), references (REF) solutions and experimental SBF solutions

A kinetic study was performed by measuring the pH of the solution, by taking out two Ti6Al4V plates every hour, and by determining visually when the precipitation occurred in the solution. The pH of the solutions was recorded in the same conditions as the reference solutions. The removed Ti6Al4V plates were ultrasonically cleaned for 10min into demineralized water in order to eliminate loose particles and to avoid late Ca-P formation. These samples were then dried overnight in air at 50°C. They were firstly observed macroscopically. Secondly, after carbon sputtering, these plates were then observed microscopically using Environmental Scanning Electronic Microscope equipped with a Field Emission Gun (ESEM, Philips, model XL-30, 15keV). Energy Dispersive for X-Ray analysis (EDX, Philips) were performed to check the presence of any Ca-P coating (data not shown). All of the precipitates formed during the experiments were filtrated through a Whatman paper n°5 and dried as previously described. Thereafter, precipitates were characterized by Fourier

Transform Infra-Red spectroscopy (FTIR, 8 scans, Perkin-Elmer, Spectrum 1000) and by X-ray Diffraction (XRD, Rigaku Miniflex goniometer). X-rays were produced by a monochromatic source (Cu Kα, λ=1.54Å, 30 KV, 15 mA). The entire XRD patterns were recorded in the same conditions (scan range: 2θ=3.00 to 60.00°, scan speed: 2.00°/min, scan step: 0.02°).

RESULTS

Reference solutions

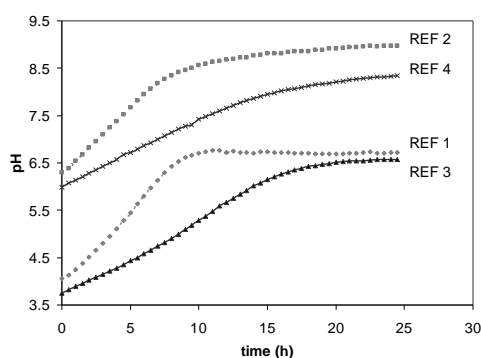Figure 1 exhibits the pH curves versus time for the various reference solutions.

Figure 1: pH profile versus time (h) for the various reference solutions: REF1 (a), REF2 (b), REF3 (c) and REF4 (d)

In the case of REF1 and REF3, the starting pH was rather similar, respectively pH=4.06 and pH=3.75, whereas in the case of REF2 and REF4, the starting pH was higher, respectively pH=6.29 and pH=5.99. This pH difference was due to the buffering capacity of HCO_3^-. Increasing HCO_3^- content resulted into higher initial and final pH values. Furthermore, the initial pH was slightly lower when the solution contained more NaCl. This indicated a slightly higher solubility of CO_2 gas for high ionic strength. For REF1 and REF2 solutions, the pH increased quickly with a rate of, respectively, 0.23 and 0.27 pH-units/hour during the first 6 or 7 hours. For REF3 and REF4 solutions, the pH increased slowly with an initial rate of respectively 0.15 and 0.145 pH-units/hour. NaCl considerably affected the pH rise. After 7h, the pH of REF1 solution reached a plateau at pH=6.7 indicating that this solution reached an equilibrium state. In the case of REF2 solution, this plateau was also observed at approximately pH=8.95 after 20h. The pH of REF3 evolved also less rapidly at the end than at the beginning of the experiments. After 23h, pH remained rather stable at pH=6.55. Similarly, in the case of REF4 solution, pH increased less rapidly at the end of the experiment but did not remain stable. Depending on the HCO_3^- and NaCl contents, the pH evolution was different. This evolution was totally

related to CO_2 gas release. Thereafter, it appeared that NaCl content, i.e ionic strength of the solution influenced the solubility of CO_2 gas while HCO_3^- content buffered the solutions.

Influence of the ionic composition of SBF solution on the Ca-P coating formation

All the results concerning the kinetic study and the Ca-P structures are summarized table 2.

Experiment	Precipitation		Coating		Precipitate	Slope
	pH	Time	pH	Time	structure	(/h)
SBFx5	6.7	4h1/2	6.8	5h1/2	AmCO₃-CaP	0.11
SBFx5(HCO₃x0)	6.2	18h	6.2	18h	DCPD	0.15
SBFx5(HCO₃x3)	6.8	6h1/2	6.8	6h1/2	AmCO₃-CaP	0.15
SBFx5(NaClx0)	6.0	0h	7.4	13h	CO₃-Ap	0.21
SBFx5(NaClx3)	6.8	4h1/2	6.8	4h1/2	AmCO₃-CaP	0.17

Table 2: Kinetics of precipitation and coating formations of the various experiments, and structure of the precipitate (AmCO₃-CaP: amorphous carbonated apatite, CO₃-Ap: carbonated apatite, DCPD: brushite)

SBFx5

As shown in figure 2a, the initial pH of SBFx5 solution was 6.2. During the overall experiment, the pH progressively raised to pH=8.0 after 24h. During the first 4h, the pH increased with a slope of 0.100 pH-unit/h. Later on, the pH curve increased more slowly than at the beginning. Finally, after 24h of soaking, the pH reached 8.0. At t=5h1/2, the solution became whitish: a precipitation occurred into the solution. The XRD pattern of the precipitate exhibited two wide bumps located at about $2\theta=30°$ and at $2\theta=45°$. These bumps are characteristic of the broadening of apatitic diffraction lines indicating a poorly crystallized structure (fig2b). The FTIR spectrum corroborates previous XRD observations. Intense and broad bands assigned to O-H stretching and bending of H_2O were observed at, respectively, 3435 and 1646cm^{-1}. Additionally, three bands were assigned to CO_3^{2-} groups (ν_3 mode at 1497 and 1428cm^{-1} and ν_2 mode at 868cm^{-1}). The broad and one-component bands at 1043 and 560cm^{-1} corresponded to the ν_3 and ν_4 P-O vibration modes of phosphate groups (PO_4^{3-}) while the band located at 868 cm^{-1} corresponded to P-(OH) stretching of HPO_4^{2-} groups. These featureless PO_4^{3-} bands were characteristic of a disordered environment. Therefore, the precipitate formed in SBFx5 is characteristic of a poorly crystallized or amorphous carbonated Ca-P phase. Simultaneous to the precipitation phenomenon, at t=5h1/2 and pH=6.8,

a colorful layer appeared on the Ti6Al4V plates corresponding to a Ca-P layer. ESEM observations of the final coating after 24h of immersion in SBFx5 indicated that the plate was covered by a uniform and dense Ca-P film composed of globules of 1 to 5μm in size (2d). At high magnification (x20000) the globules exhibited nanometric spherical particles indicating that the film was composed of an amorphous or nanocrystalline apatite.
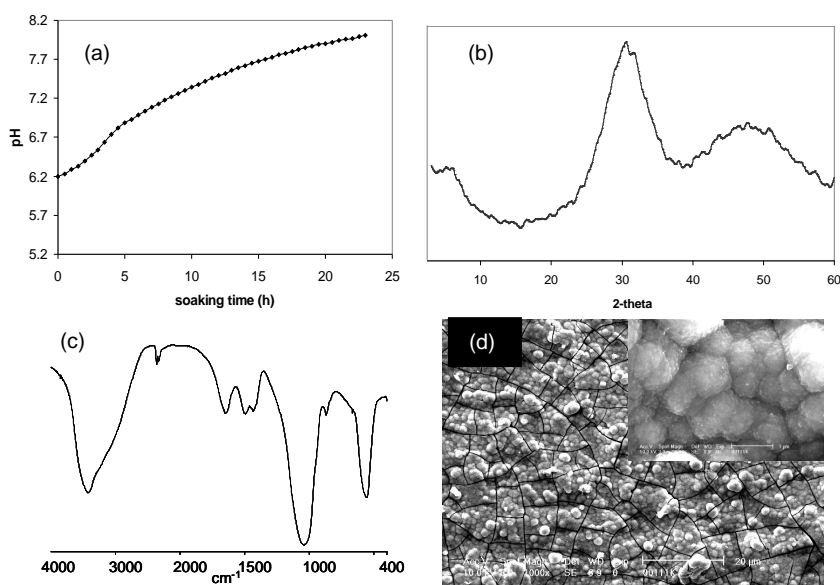
Figure 2: SBFx5 experiment: (a) pH versus soaking time, (b) XRD, (c) FTIR, (d) ESEM photos at magnification x1000 and x20000

Influence of Sodium Chloride

In the case of NaCl-free solution (SBFx5(NaClx0)), the starting pH value was 6.0. During approximately the 2 first hours, the pH increased rapidly with a slope of 0.21 pH-units/h. Subsequently, pH remained stable for 1h1/2 at pH=6.25 and started to rise again. At the end of the experiment, pH of SBFx5(NaClx0) solution reached 8.0 (fig 3a). A precipitation occurred immediately after adding the salts into SBFx5(NaClx0) solution, thus at pH=6.0. As shown in figure 3b, XRD pattern of this precipitate gathered at t=24h exhibits broad diffraction lines. The peak at $2\theta=32.06°$ corresponded to the overlapping of (211), (112), (300) and (202) diffraction plans of apatitic structure. The FTIR spectrum of SBFx5(NaClx0) precipitate (fig 3c) showed intense and broad bands assigned to O-H stretching and bending of H_2O (3435 and 1646cm^{-1}), three bands corresponding to CO_3^{2-} groups (v_3 mode at 1497 and 1428cm^{-1} and v_2 mode at 868cm^{-1}). PO_4^{3-} groups were located at 1028cm^{-1} (v_3 mode), at 960cm^{-1} (v_1 mode) and at 602 and 563cm^{-1} (v_4 mode).

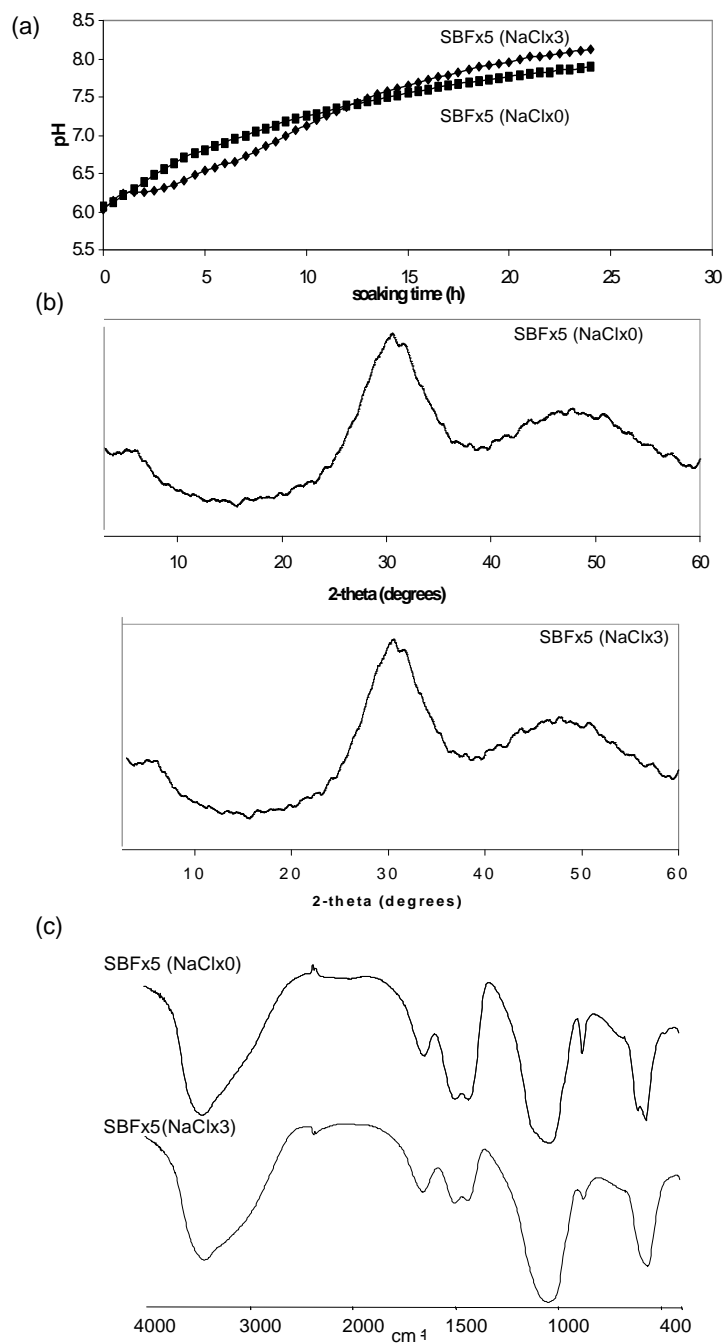Figure 3: SBFx5(NaClx0) and SBFx5(NaClx3) experiments: (a) pH versus soaking time, (b) XRD, (c)FTIR
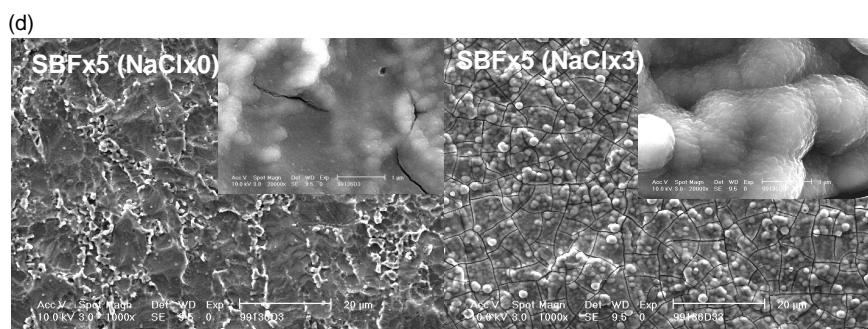
(d)

Figure 3 (*continued*): SBFx5(NaClx0) and SBFx5(NaClx3) experiments: (d) ESEM photos at magnification x1000 and x20000

Furthermore HPO_4^{2-} groups were detected at $1108cm^{-1}$ (ν_3 mode). This indicated a Ca-deficient carbonated apatitic structure. Thereby SBFx5(NaClx0) precipitate has a Ca-deficient carbonated apatitic structure. After 13h of soaking, at pH=7.4 a Ca-P film was detected by EDX on Ti6Al4V substrate. After 24h of soaking, ESEM photos of the final coating showed that this layer was uniform and contained few globules smaller than $1\mu m$ (fig 3d). Ti6Al4V texture was still visible beneath, indicating a very thin film. At high magnification (x20000), ESEM photos indicated that the substrate was uniformly coated with a Ca-P film. This film contained few cracks and it was composed of nano-sized Ca-P nuclei.

In the case of SBFx5(NaClx3) solution ([NaCl]=440mM), the starting pH was pH=6.1. During approximately the first 6 hours, the pH increased rapidly with a slope of 0.17 pH-units/h (fig 3a). Subsequently, pH rose slower. A precipitation in SBFx5(NaClx3) solution occurred at t=4h1/2 at pH=6.8. XRD and FTIR spectra (respectively fig 3b and fig 3c) of the final precipitate gathered at the end of the experiments indicated totally similar features than SBFx5 precipitate. In other words, the precipitate formed in SBFx5(NaClx3) has an amorphous or nano-crystalline carbonated Ca-P structure. At t=6h1/2 (pH=6.8), a colorful Ca-P layer appeared on Ti6Al4V substrate. By ESEM, the final Ca-P layer was dense, though showing cracks, and it covered homogeneously the Ti6Al4V plate (fig 3d). The Ca-P coating was composed of numerous Ca-P globules of 1 to $5\mu m$ in diameter. At high magnification (x20000), the dense layer was composed of expended globules containing nano-sized particles. No crystals could be detected. From these two experiments, we could see how NaCl content can affect the coating structure. Indeed, when ionic strength is high, it delays precipitation kinetics, allowing coating formation whereas for low ionic strength, precipitation occurs shortly leading to apatitic salts in the solution in detriment to the coating formation.

Influence of carbonate

In the case of HCO_3-free solution SBFx5(HCO_3x0), the starting pH was pH=5.3. During the first 10 hours, the pH increased with a slope of 0.15 pH-units/h. Subsequently, the pH reached a plateau at t=10h for pH=6.7. Suddenly at t=18h, the pH dropped until pH=6.2 at the end of the experiment (t=24h) (fig 4a). A precipitation into SBFx5(HCO_3x0) solution started to occur at t=18h. XRD pattern of the precipitate gathered at the end of the experiments exhibited sharp peaks indicating a highly crystallized structure.

The diffraction lines at 2θ=11.7° and at 2θ=29.3° are characteristic of a brushite structure (DCPD, $CaHPO_4,2H_2O$, fig 4b). FTIR spectrum confirmed previous XRD investigations, phosphate and hydrogenphosphate bands are characteristic of DCPD structure (1220, 1134 1074, 1059, 1000 and 986cm^{-1} for P-O ν_3 mode, 874cm^{-1} for P-O(H) ν_1 mode and 525cm^{-1} for P-O ν_4 mode) (fig 4c). Tiny Ca-P crystals appeared on the Ti6Al4V surface at t=18h, simultaneously with the precipitation. After 24h of soaking in SBFx5(HCO_3x0) solution, a whitish film covered approximately 50% of the Ti6Al4V surface. ESEM photos at magnification x1000 showed that the Ti6Al4V plate was partially covered with tiny Ca-P crystals of approximately 1 to 2μm in size (fig 4d). At high magnification (x20000), this layer seemed to be attached on some parts to the Ti6Al4V substrate. On other parts, the crystals seemed to lie on the surface without anchorage. This could suggest that the crystals were too large to remain attached on the Ti6Al4V substrate in the contrary of the small crystals that remained on to Ti6Al4V surface.

In the case of SBFx5(HCO_3x3) solution ($[HCO_3]$=12.6mM), the starting pH was pH=5.9. During approximately the first 6 hours, the pH increased rapidly with a slope of 0.15 pH-units/h. Subsequently, the pH increased more slowly than at the beginning. At t=24h, pH reached 7.6 (fig 4a). A precipitate formed into the solution at t=6h1/2 (pH=6.8). XRD and FTIR spectra (respectively fig 4b and fig 4c) of the final precipitate gathered at the end of the experiments indicated totally similar features than SBFx5 and SBFx5(NaClx3) precipitates. In other words, the precipitate formed in SBFx5(HCO_3x3) has an amorphous or nano-crystalline carbonated Ca-P structure. At t=6h1/2 (pH=6.8), a colorful layer appeared on the substrate corresponding to the Ca-P coating as indicated EDX. The ESEM observations of the final coating indicated that the coating was dense, though cracks, and uniformly composed of globules of 0.5 to 1μm in diameter (fig 4d). At high magnification (x20000), the dense layer was composed of dense globules connected together. These globules were composed of nano-sized particles. No crystals were visible. From these two experiments, it is suggested that the size of the crystals, which formed onto Ti6Al4V is critical for the homogeneity of the coating.
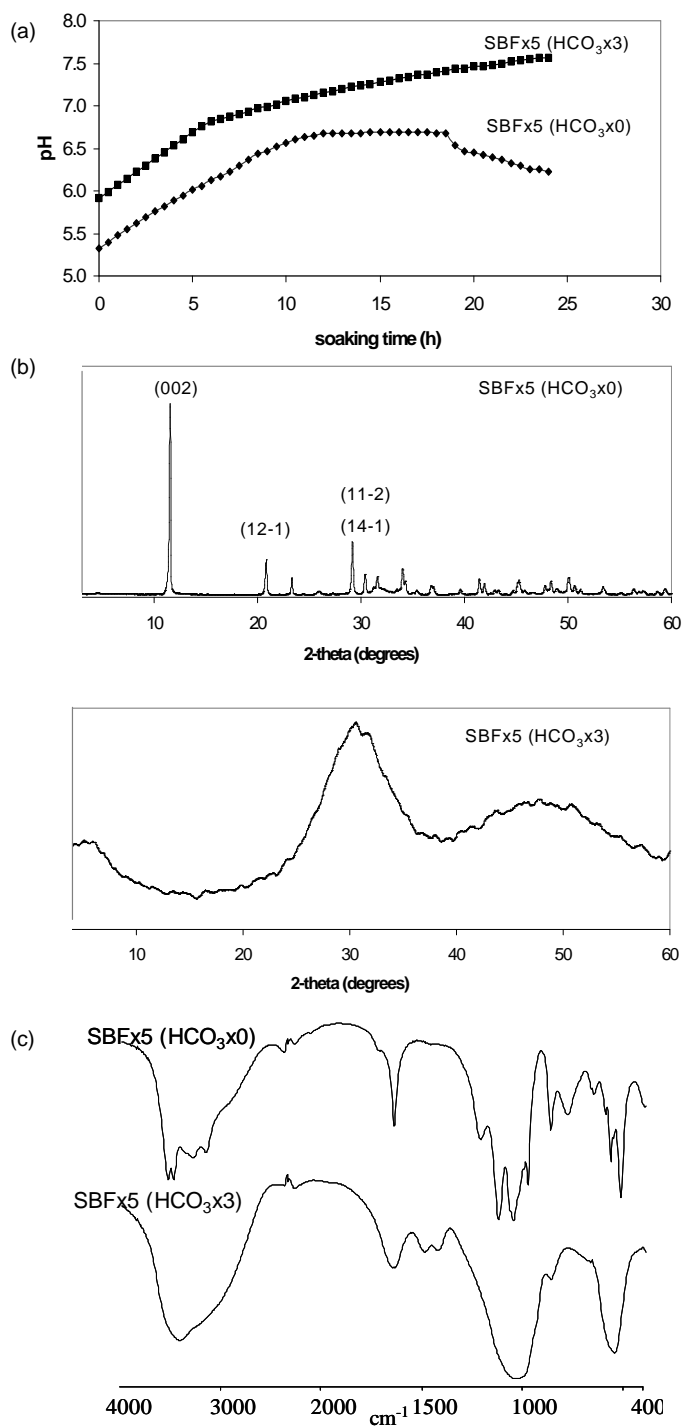
Figure 4: SBFx5(HCO$_3$x0) and SBFx5(HCO$_3$x3) experiments: (a) pH versus soaking time, (b) XRD, (c)FTIR

(d)
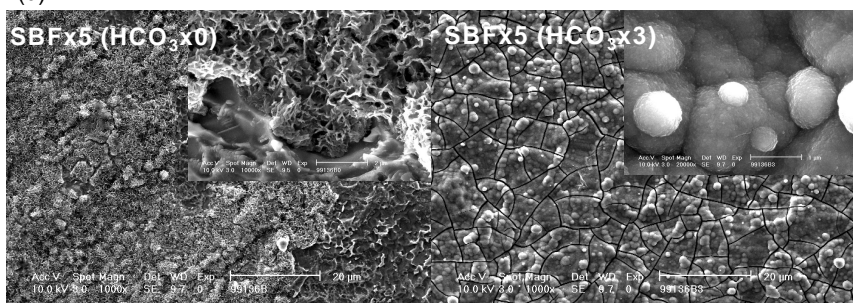
Figure 4 (*continued*): SBFx5(HCO$_3$x0) and SBFx5(HCO$_3$x3) experiments: (d) ESEM photos at magnification x1000 and x20000

DISCUSSION

The above experiments have demonstrated the possibility of producing Ca-P coatings on Ti6Al4V substrate within less than 24h from highly concentrated SBF solutions. Visual observations reveal that the initial Ca-P film is colorful. This phenomenon is due to visible light diffraction by the coating thickness. Indeed, the coating is less than 1µm thick, i.e. nearly equal to visible light wavelength.

Effect of carbon dioxide

The stability of this highly concentrated solution (SBFx5) is due to the introduction of an acidic gas. It is very well known that the solubility of Ca-P salts increases with a decrease of pH [30]. Dissolution of CO_2 gas (solubility of 33.6mmol/l at 25ºC) leads to the formation of carbonic acid H_2CO_3 (reaction (1)). Immediately, this acid can be considered totally dissociated into HCO_3^- and CO_3^{2-} species (reaction (2) and (3)).

$$CO_2 + H_2O \leftrightarrow H_2CO_3 \ (1)$$
$$H_2CO_3 + H_2O \leftrightarrow HCO_3^- + H_3O^+ \ (2), \quad pK_2 = 6.3$$
$$HCO_3^- + H_2O \leftrightarrow CO_3^{2-} + H_3O^+ (3), \quad pK_3 = 10.3$$
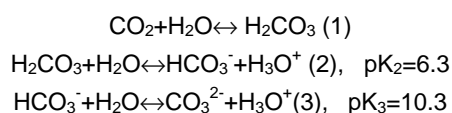
Under these acidic conditions, it is possible to obtain stable highly concentrated solution like the SBFx5 solution. Once the CO_2 supply is stopped, the system returns to equilibrium by releasing dissolved CO_2 gas to air. The system, being open, trends to lower the pressure by releasing into the atmosphere. Thus, the gas release out of the solution leads to a slow and homogeneous pH increase following the left trend of relations (1), (2) and (3) as experimentally observed in the reference solutions REF1 to REF4. In the case of HCO$_3$-free reference solutions (REF1 and REF3), the final pH in the solution remains constant at about 6.7, indicating that all the CO_2 gas has been released. This final pH of the solution approaches that of pure water. In the case of HCO$_3$-containing

reference solutions, the initial pH was higher than the HCO_3-free solutions due to the buffering effect of HCO_3^-/CO_3^{2-}. In the same way than for HCO_3-free reference solutions, the system returns to equilibrium by releasing CO_2 gas out of the solution. The equilibrium pH for this system is set according to the equation applicable for conjugated weak acido-basic couples (4):

$$pH=1/2(pK_2+pK_3) \quad (4)$$

In the case of H_2CO_3/HCO_3^- and HCO_3^-/CO_3^{2-} couples, the equilibrium pH is theoretically 8.3. The final pH values of the two carbonated reference solutions were slightly higher than this theoretical pH value. This might be due to an additional buffering effect of the amphoteric ion HPO_4^{2-}. In the case of the various SBFx5 solutions, the gas release induces a rise in pH. Progressively, the calcifying solutions reach their supersaturation point leading to Ca-P precipitation into the solution. Usually, Ca-P precipitation leads to a decrease of pH due to H_3O^+ release according to the general reaction (5):

$$(10\text{-}x)Ca^{2+}+6HPO_4^{2-}+3H_2O \leftrightarrow Ca_{10\text{-}x}(HPO_4)_x(PO_4)_{6\text{-}x}(OH)_{2\text{-}x}+(6\text{-}x)H_3O^+ \quad (5)$$
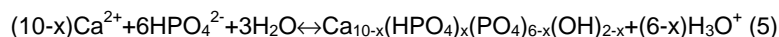
In our experiments, there is a combination of increase and decrease of pH due respectively to CO_2 release and Ca-P formation. The pH drop due to Ca-P precipitation was not always observed. This decrease in pH might be compensated by CO_2 release. However, a pH drop was observed for HCO_3-free SBF solution (SBFx5(HCO_3x0)). Two reasons can explain this phenomenon in this particular case. The absence of HCO_3^- reduces markedly buffering capacity of SBFx5 solution, thus enhancing pH variations especially during Ca-P precipitation. Furthermore, HCO_3^- is known to reduce apatitic growth rate [31-33]. So in a HCO_3-free SBFx5 solution, apatite can precipitate more suddenly leading to a sudden decrease in pH.

Study of Ca-P precipitation process
The precipitation indicates the stage when SBFx5 solutions reach saturation. From the visual observations of precipitation in the various SBFx5 solutions, we can define three different groups. Firstly, in the case of NaCl-free solution, precipitation occurs immediately at the end of CO_2 supply at pH=6.0. Secondly, precipitation occurs at pH=6.8 in the case of low NaCl and HCO_3^- content solutions (SBFx5(NaClx3) and SBFx5(HCO_3x3)) and in the case of the regular SBFx5 solution. Thirdly, in the case of HCO_3-free solution, precipitation occurs at pH=6.2. So, NaCl and HCO_3^- contents affect precipitation kinetics and precipitate structure. With regard to NaCl influence, i.e. ionic strength, the reference solutions showed that CO_2 content is quite similar for high or low ionic strength, but CO_2 is released at a faster rate at low ionic strength.

Thereby, at the starting point of the experiments, in SBFx5(NaClx0) solution fizzes in a larger extend than for all other calcifying solutions. In other words, the lower ionic strength is, the more nucleation sites are present in the solution. The increase in nucleation sites enhances obviously Ca-P precipitation in the solution. In addition, ionic diffusion is enhanced by low ionic strength favoring spontaneous precipitation even at low pH value of 6.0. Interestingly, by comparing SBFx5 and SBFx5(NaClx0), despite their similar Mg^{2+} and HCO_3^- contents (well known as crystal growth inhibitors [31-35]) the precipitate appears more crystalline than the precipitate formed with a lower ionic strength than SBFx5. Indeed as we saw above, the ionic diffusion is enhanced by low ionic strength, so crystal growth is accelerated. It overcomes for a certain extend the inhibitory effect of HCO_3^- and Mg^{2+}. Regarding HCO_3^- influence, a lack in HCO_3^- contents in the reference solutions leads to a lack of buffer capacity in the system. So the pH values in HCO_3-free solution are lower than the HCO_3-containing solutions. Under these mildly acidic conditions, this solution is supersaturated towards DCPD [36-37], wich precipitates following reaction (5).

$$Ca^{2+}+H_2PO_4^{2-}+3H_2O \rightarrow CaHPO_4.2H_2O+H_3O^+ \quad (5)$$
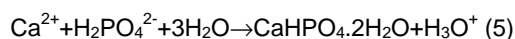
Additionally HCO_3^- species have also an inhibitory effect on Ca-P formation. It is difficult to compare the Ca-P precipitation kinetics versus $[HCO_3^-]$ because this concentration strongly affects the pH in the solution and thus the supersaturation. However, HCO_3^- inhibits apatite crystal growth in favor to poorly carbonated apatite. According to the position of CO_3^{2-} bands, CO_3^{2-} groups substitute PO_4^{3-} groups [38-39]. This carbonated apatite is so-called type B substitution. This substitution leads a distortion of the crystallographic lattice: a-axis contraction and c-axis extension. These distortions lead to a low crystallinity of apatite [31-33].

Study of Ca-P coating process
From the overall experiments, it can be conducted that Ca-P formed from SBFx5 solution on Ti6Al4V substrate. The various Ca-P films are formed between 4h30 and 18h00 of immersion time. Thereby, this process is significantly accelerated as compared to regular supersaturated SBF solution buffered at pH=7.4 [20,24-26]. This fast deposition indicates that highly supersaturated calcifying solutions accelerate significantly the Ca-P coating formation on Ti6Al4V substrate. Similarly to the precipitation, the coating deposition depends on the composition of the soaking solution. In the case of SBFx5, SBFx5(HCO_3x0), SBFx5(HCO_3x3) and SBFx5(NaClx3) Ca-P coating forms simultaneously with the precipitation. So, the coating forms when the supersaturation in the solution is reached. In the case of SBFx5(NaClx0) experiment, due to a low ionic strength, Ca-P coating forms on Ti6Al4V

substrate later than precipitation in the solution. This early and sudden precipitation lowers markedly the supersaturation of the solution. Thereby, less ionic species are available in the solution for the Ca-P nucleation on Ti6Al4V. Furthermore, there is a competition between early-formed Ca-P salt acting as seed and, heterogeneous nucleation on Ti6Al4V surface. When Ca-P forms too fast in the solution, the competition is detrimental to the coating formation. This explains the thin Ca-P coating obtained after 24h of soaking in NaCl-free solution. Therefore, Ca-P coating formation on Ti6Al4V depends on the precipitation kinetics throughout the soaking in SBFx5 solution. If the precipitate appears early in the solution, it delays the coating formation process due to a low remaining supersaturation. Additionally, the amount of HCO_3^- into SBFx5 solution influences Ca-P coating structure. The heterogeneity and the crystal size of the coating formed from SBFx5(HCO_3x0) suggest that Ca-P crystal size is also critical for coating stability. When Ca-P crystals are small, they remain well adhered onto the substrate whereas when the layer is composed of large crystals, the Ca-P layer detaches from the Ti6Al4V substrate. Indeed loading forces are greater for large and vertical crystals than for tiny Ca-P globules fixed into substrate cavities. It appears that HCO_3^- contributes efficiently to control the Ca-P crystal size due to apatite crystal distortion and, therefore physical attachment of Ca-P coating onto Ti6Al4V substrate.

CONCLUSION

The use of a mildly acidic gas CO_2 into a highly concentrated Simulated Body Fluid solution allowed the formation of a Ca-P coating on Ti6Al4V within less than 24h. This biomimetic method avoids particular surface treatment for Ti and refreshing of metastable SBF solutions. The coating deposition kinetics is influenced by the ionic strength of the solution and HCO_3^- content. NaCl controls the ionic strength of the solution and thereby, it controls CO_2 release, i.e. pH profile. Furthermore ionic strength delays Ca-P precipitation in SBFx5 solution allowing Ca-P to nucleate on Ti6Al4V. HCO_3^- acts as a buffer with the dissolved CO_2 gas. Furthermore HCO_3^- reduces apatite crystals size of the coating allowing a better physical attachment on Ti6Al4V substrate. From these experiments two important parameters can be highlighted on the biomimetic Ca-P formation process from SBFx5 solutions. Firstly, precipitation in the solution must be delayed in order to favor heterogeneous nucleation on Ti6Al4V. Secondly, Ca-P particles deposited on the substrate must be nano-sized to remain physically attached on Ti6Al4V.

References

1-T.W. Bauer, R.C.T. Geesink, R. Zimmerman and J.T. McMahon. Hydroxylapatite-coated femoral stems: Histological analysis of components retrieved at autopsy. J Bone and Joint Surgery 1991;73:1439-1452

2-R.G.T. Geesink. Hydroxyalapatite-coated hip implants: Five year clinical and radiological results. In: Hydroxylapatite coatings in orthopedic surgery. Ed: R.G.T. Geesink and M.T. Manley, Raven Press New York U.S., 1993

3-J.A.M. Clemens, C.P.A.T. Klein, R.C. Vriesde, P.M. Rozing and K. de Groot. Healing of large (2mm) gaps around calcium phosphate coated bone implants: A study in goats with a follow-up of 6 months. J Biomed Mater Res 1998; 40: 341-349

4- A. Moroni, P. Aspenberg, S. Toksvig-Larsen, G. Falzarano, S. Giannini. Enhanced fixation with hydroxyapatite coated pins. Clin Orthop 1998;346: 171-177

5- P.O. Kroon and M.A. Freeman. Hydroxyapatite coating of hip prostheses. Effect on migration into the femur. J Bone Joint Surg Br 1992;74: 518-522

6- P. Frayssinet, D. Hardy, N. Rouquet, B. Giammara, A. Guilhem and J. Hanker. New observations on middle term hydroxyapatite-coated titanium alloy hip prosthesis. Biomaterials 1992;13: 668-674

7- R.J. Furlong and J.F. Osborn. Fixation of hip prosthesis by hydroxyapatite ceramic coating. J Bone Joint Surg Br 1991;73: 741-745

8- K. Soballe, S. Toksvig-Larsen, J. Gelineck, S. Fruensgaard, E.S. Hansen, L. Ryd, U. Lucht and C. Bunger. Migration of hydroxyapatite coated femoral prostheses. A Roentgen Stereophotogrammetric study. J Bone Joint Surg Br 1993;75: 681-687

9- C. Combes, C. Rey and M. Freche XPS and IR study of dicalcium phosphate dihydrate nucleation on titanium surfaces. Colloids and surfaces B: Biointerfaces 1998;11: 15-27

10- P. Li. *In vitro* and *in vivo* calcium phosphate induction on gel oxide.1993. PhD thesis, Leiden University, The Netherlands

11- K.E. Healy and P. Ducheyne. Hydration and preferential molecular adsorption on titanium *in vitro*. Biomaterials 1992;13: 553-561 (1992)

12- F. Barrere, P. Layrolle, C.A. van Blitterswijk and K. de Groot. Fast formation of Ca-P coating on Ti6Al4V. Mat Res Soc Symp Proc 2000;599: 135-140

13- J.L. Ong and L.C. Lucas. Auger electron spectroscopy and its use for characterization of titanium and hydroxyapatite surface. Biomaterials 1998;19: 455-464

14- T. Hanawa. Titanium and its oxide film: a substrate for formation of apatite. In: The bone-biomaterial interface. 1990. Ed: J.E. Davies. University Toronto Press, Toronto Canada.Toronto, p49-61

15- W.Q. Yan, T. Nakamura, M. Kobayashi, H.M. Kim, F. Miyaji and T. Kokubo. Bonding of chemically treated titanium implants to bone. J Biomed Mater Res 1997;37: 267-275

16- K. de Groot, R.G.T. Geesink, C.P.A.T. Klein and P. Serekian. Plasma-sprayed coatings of hydroxylapatite. J. Biomed Mat Res 1987;21:1375-1381

17- J.A. Jansen, J.G.C. Wolke, S. Swann, J.V.P.M. van der Waerden and K. de Groot. Application of magnetron sputtering for the producing ceramic coating on implant materials. Clinical Oral Implant Research 1994;28: 1477-1484

18- P. Ducheyne, S. Radin, M. Heughebaert and J.C. Heughebaert. Calcium phosphate ceramic coating on porous titanium: effect: effect of structure and composition on electrophoretic deposition, vacuum sintering and *in vitro* dissolution. Biomaterials 1990;11: 244-254

19- G. Sardin, M. Varela and J.L. Morenza. Deposition of hydroxyapatite coatings laser ablation. In: Hydroxyapatite and related materials. Ed: Brown PW, Constanz B. London CRC press, London, UK. 1994:225-230

20- T. Kokubo, H. Kushitani, S. Sakka, T. Kitsugi and T. Yamamuro. Solutions able to reproduce *in vivo* surface-structure changes in bioactive glass-ceramics A-W[3]. J Biomed Mater Res 1990;24: 721-734

21- F. Barrere, P. Layrolle, C.A van Blitterswijk and K. de Groot. Biomimetic Coatings on Titanium: A crystal Growth Study of Octacalcium phosphate. J Mat Sci Mat Med 2001;12: 529-534

22- F. Barrere, P. Layrolle, C.A van Blitterswijk and K. de Groot. Biomimetic Ca-P coating on Ti6Al4V: Crystal growth study of Octacalcium phosphate and inhibition by Mg^{2+} and HCO_3^-. Bone 1999;25: 107S-111S

23- F. Barrere, M. Stigter, P. Layrolle, C.A. van Blitterswijk and K. de Groot. *In vitro* dissolution of various Calcium phosphate coatings on Ti6Al4V. Bioceramics 13 (2000): 67-70

24- P. Li, I. Kangasniemi, K. de Groot and T. Kokubo. Bonelike hydroxyapatite induction by a gel-derived titania on a titanium substrate. J Am Ceram Soc 1994;77: 1307-1312

25- T. Peltola, M. Patsi, H. Rahiala, I. Kangasniemi and A. Yli-Urpo. Calcium phosphate induction by sol-gel-derived titania coatings on titanium substrates *in vitro*. J Biomed Mater Res 1998;41: 504-510

26- P. Li and P. Ducheyne. Quasi-biological apatite film induced by titanium in a Simulated Body fluid, J Biomed Mater Res 1998;41: 341-348.

27- H.B. Wen, J.G.C. Wolke, J.R. de Wijn, F.Z. Cui and K. de Groot. Fast precipitation of calcium phosphate layers on titanium induced by simple chemical treatment. Biomaterials 1997;18: 1417-1478

28- C. Ohtsuki, H. Iida, S. Hayakawa and A. Osaka. Bioactivity of titanium treated with hydrogen peroxide solutions containing metal chloride. J Biomed Mater Res 1997;35: 39-47

29- H.M. Kim, F. Miyaji, T. Kokubo, T. Nakamura. Preparation of bioactive Ti and its alloys via simple chemical surface treatment. J Biomed Mater Res 1996;32: 409-417

30- J.C. Elliot, in Structure and chemistry of the apatites and other calcium orthophosphates. 1994. Edited by Elsevier, Amsterdam, The Netherlands

31- J. Barralet, S. Best and W. Bonfield. Carbonate substitution in precipitated hydroxyapatite: an investigation into the effects of reaction temperature and bicarbonate concentration. J Biomed Mater Res 1998;41: 79-86

32- N.S. Chikerur, M.S. Tung and W.E. Brown. A mechanism for incorporation of carbonate into apatite. Calcif Tissue Int 1980;32: 55-62

33- H. Newesely. Changes in crystal types of low solubility calcium phosphates in the presence of accompanying ions, Arch Oral Biol. Special supplement 1961;6: 174-180

34- B. Tomazic, M. Tomson and G.H. Nancollas. Growth of calcium phosphates on hydroxyapatite crystals: the effect of magnesium. Arch oral Biol 1975;20: 803-808

35- M.H.Salimi, J.C. Heughebaert and G.H. Nancollas. Crystal Growth of Calcium Phosphates in the presence of magnesium ions. Langmuir 1985;1: 119-122

36- C. Combes, M. Freche and C. Rey. Nucleation and crystal growth of dicalcium phosphate dihydrate on titanium powder. J. Mater Sci Mater Med 1995;6: 699-702

37- J.F. de Rooij, J.C. Heughebaert and G.H. Nancollas. A pH study of calcium phosphate seeded precipitation. J Colloid Interface Sci 1984;100: 350-358

38- J.C. Heughebaert, Contribution a l'etude de l'evolution des orthophosphates de calscium precipites amorphes en orthophosphates apatitiques. 1977. These d'Etat INP Toulouse, France

39- D.G.A. Nelson and J.D.B Featherstone, Preparation, analysis and characterization of carbonated apatites, Calcif Tissue Int 1982;34: S69-S81.

CHAPTER 3

INFLUENCE OF MAGNESIUM ON THE CALCIUM PHOSPHATE COATING NUCLEATION FROM SBFx5 SOLUTION

F. Barrère, C.A van Blitterswijk, K. de Groot and P. Layrolle

ABSTRACT

Biomimetic calcium phosphate (Ca-P) coatings were applied by using five times concentrated Simulated Body Fluid (SBFx5) using carbon dioxide gas. This process allows the deposition of a uniform Ca-P coating within 24h. A previous study of our process emphasized the importance of carbonate ions (HCO_3^-), a crystal growth inhibitor. The aim of the present study was to investigate the role of the other crystal growth inhibitor present in SBFx5, Magnesium (Mg^{2+}), on the Ca-P coating formation. Several SBFx5 solutions were prepared with various Mg^{2+} and HCO_3^- contents. No Ca-P deposits were detected on Ti6Al4V substrate soaked for 24h in a Mg-free SBFx5 solution, whereas by increasing HCO_3^- content in a Mg-free SBFx5 solution, a Ca-P coating developed on Ti6Al4V substrate. Therefore, it appeared that Mg^{2+} has a stronger inhibitory effect on apatite crystal growth than HCO_3^-. Nevertheless, Mg^{2+} plays also another important role as suggested by depth profile X-ray Photoelectron Spectroscopy (XPS) of the Ca-P coating obtained from SBFx5 solution. Ca^{2+} and Mg^{2+} contents increased significantly at the titanium/coating interface. Therefore, Ca^{2+} and Mg^{2+} initiated Ca-P coating from SBFx5 solution. The relatively high interfacial concentration in Mg^{2+} favors heterogeneous nucleation of tiny Ca-P globules onto the substrate. So physical adhesion is enhanced at the early stage of the coating formation.

INTRODUCTION

Biomimetic calcium phosphate (Ca-P) coatings have been obtained on titanium (Ti) substrates by the use of supersaturated solutions like Simulated Body Fluids (SBF) [1]. Such coatings are initiated by the heterogeneous nucleation of Ca-P globules. However, the formation of uniform Ca-P coating takes at least 7 days with regular refreshing of the solution [1-4]. The slowness of this process is due to the metastability of SBF at physiological conditions (37°C, pH=7.25). In this study, a biomimetic Ca-P coating was obtained by soaking Ti6Al4V plates in a 5 times more concentrated SBF (so-called SBFx5) with CO_2 gas [5-6]. This approach renders unnecessary the refreshing of the metastable solution, and it significantly accelerates the coating process. Our aim was to understand Ca-P nucleation mechanism on Ti6Al4V substrate.

Heterogeneous nucleation on a foreign substrate requires physical and chemical considerations. Several previous studies have shown that Ca-Ps have strong chemical and physical affinities for Ti substrate [5, 7-13]. On one hand, Ca-P nucleation on Ti substrates is promoted by chemical affinities, which are related to surface charge of the titanium oxide (TiO_2) layer that covers any Ti and alloys substrate [14-15]. On the other hand, the texture of the substrate can inhibit or promote, *in vitro* and *in vivo*, Ca-P nucleation depending on surface roughness [16-18]. Furthermore, we have shown in a previous study that Ca-P coating crystallinity influences coating attachment and homogeneity on Ti6Al4V substrate: the lower HCO_3^- content in SBFx5 was, the fewer the Ca-P developed on Ti6Al4V substrate [6]. The growing of small globules resulted in a more stable and homogeneous Ca-P coating.

In this study, our aim was to investigate chemical and physical affinities that lead to Ca-P coating formation from SBFx5 solution onto Ti6Al4V substrate. First, we analyzed the biomimetic Ca-P coating formed from SBFx5 solution by depth profile X-Ray Photoelectron (XPS) in order to enlighten favored Ca-P/Ti interactions. Second, since Magnesium (Mg^{2+}) is also known to inhibit apatite crystal growth [19-30], we studied its influence on Ca-P coating formation from SBFx5 solution. We compared also its role with HCO_3^- ions role, since HCO_3^- lowers Ca-P coating crystallinity [6]. Therefore, we prepared several SBFx5 solutions. On one hand, Mg^{2+} content was individually changed, whereas the other salts content remained similar to SBFx5 solution composition. On the other hand, we prepared two additional solutions, in which one of the crystal growth inhibitor (Mg^{2+} or HCO_3^-) content was discarded and the other crystal growth inhibitor content was increased eight times.

MATERIALS AND METHOD

Ti6Al4V plates were ultrasonically cleaned successively in acetone, ethanol (70%) and finally demineralized water. These plates were then etched for 10 minutes in a mixture of 2ml HF (40%) and 4ml HNO_3 (66%) in 1000ml of water.

The average roughness (R_a) of the substrate was not affected by etching and remained at $R_a=0.80\mu m$. Ti6Al4V plates were thereafter soaked into various SBF solutions (so-called SBFx5). The composition of these various solutions is summarized in table 1. Throughout the experiments, reagents grade chemicals were used (Merck). Each solution was prepared by dissolution of the salts into 1000ml of demineralized water in which CO_2 gas was bubbled. The starting point of the experiments was set when CO_2 bubbling was stopped (t=0h). All the experiments were performed in a 1.5l-reactor thermostated at $37\pm1°C$ for 24h of soaking. The solutions were stirred with a magnetic bar with a speed of 200 rounds per minutes (rpm). The pH of the calcifying solutions was recorded every 30 minutes with a combined electrode (pHmeter Portamess). Prior to experiments, the pH electrode was calibrated with two buffer solutions at pH=4.01 and pH=7.00 (IUPAC standards, Radiometer Copenhagen). After 24h of immersion Ti6Al4V plates were removed out of the SBF solution.

	NaCl	$MgCl_2.6H_2O$	$CaCl_2.2H_2O$	$Na_2HPO_4.2H_2O$	$NaHCO_3$
HBP	146.7	1.5	2.5	1.0	27.0
SBF	146.7	1.5	2.5	1.0	4.2
SBFx5	733.5	7.5	12.5	5.0	21.0
SBFx5(Mgx0)	733.5	0.0	12.5	5.0	21.0
SBFx5(Mgx3)	733.5	4.5	12.5	5.0	21.0
SBFx5(Mgx8, HCO$_3$x0)	733.5	12.0	12.5	5.0	0.0
SBFx5(Mgx0, HCO$_3$x8)	733.5	0.0	12.5	5.0	33.6

Table 1: Inorganic composition (mM) of human blood plasma (HBP), regular Simulated Body Fluid (SBF), experimental SBFx5 solutions

Qualitative and quantitative analysis of the biomimetic Ca-P by XPS depth profile.

After 24h of immersion into SBFx5 solution, Ti6Al4V plates were taken out of the solution, ultrasonically cleaned with demineralized water, and finally dried at room temperature overnight. At the end of the experiment (t=24h) the precipitate formed in SBFx5 solution was filtrated through a Whatman paper n°5, and dried overnight in air at 50°C. Analysis of this precipitate was performed by Fourier Transform Infra-Red (FTIR, 8 scans, Perkin-Elmer, Spectrum 1000) and X-ray Diffraction (XRD, Rigaku Miniflex goniometer). The X-rays were produced by a monochromatic source (Cu Kα, $\lambda=1.54$Å, 30 KV, 15 mA). The XRD patterns were recorded as follows: scan range: $2\theta=3.00$ to $60.00°$, scan speed: $2.00°$/min, scan step: $0.02°$. Plates were microscopically investigated using Environmental Scanning Electron Microscopy with a Field

Emission Gun (ESEM-FEG, Philips, model XL-30, 10keV). The Ca-P coated Ti6Al4V plates were analyzed by X-Ray Photoelectron Spectroscopy (XPS, Surface Science Instrument M-Probe, United Kingdom) using a monochromatised source using Al Kα. An XPS depth profile qualitative analysis was performed by gradually removing the coating with an Argon (Ar) Ion Etch Gun, calibrated at 3nm/min. The detection limit of XPS depth profile analysis for atomic percentage was about 1%.

Influence of magnesium on the Ca-P coating formation

In order to investigate the role of magnesium (Mg^{2+}) in SBFx5 various highly concentrated SBF solutions were prepared (see table 1). SBFx5(Mgx0) was a Mg-free SBFx5 solution. SBFx5(Mgx3) was a solution where Mg^{2+} was increased to three times as compared with a regular SBF solution. The leftover salts concentrations remained similar to SBFx5 solution. Furthermore, in order to differentiate the role of magnesium ions (Mg^{2+}) and carbonate ions (HCO_3^-), two additional solutions were prepared. SBFx5(Mgx8,HCO$_3$x0) solution is an HCO$_3$-free solution with [Mg^{2+}] raised to eight times as compared with regular SBF solution. Contrarily, SBFx5(Mgx0,HCO$_3$x8) solution is an Mg-free solution whereby [HCO_3^-] was raised to eight times. Twenty Ti6Al4V plates were soaked in each solution (SBFx5(Mgx0), SBFx5(Mgx3), SBFx5(Mgx8,HCO$_3$x0) and SBFx5(Mgx0,HCO$_3$x8)). A kinetic study was performed for each experiment by measuring the pH of the solution, by taking out two Ti6Al4V plates every hour and by determining visually when the precipitation occurred in the solution. The presence of any Ca-P coating on the plates was checked with Energy Dispersive for X-Ray analysis (EDX, Philips). Filtration and analysis of the Ca-P precipitates, gathered at the end of the experiments, were performed by FTIR and XRD as mentioned above. The removed Ti6Al4V plates were cleaned, dried and observed by ESEM as mentioned above.

RESULTS

Qualitative and quantitative characterization of the biomimetic Ca-P obtained from SBFx5 solution

As shown in figure 1, the pH of SBFx5 solution raised from 5.9 at t=0h to 8.1 at t=24h. The XRD pattern of the precipitate exhibited two wide bumps located at about $2\theta=30°$ and at $2\theta=45°$. These bumps were characteristic of the broadening of apatitic diffraction lines indicating a poorly crystallized structure (fig1b). The FTIR spectrum (fig1c) corroborated previous XRD observations. Intense and broad bands assigned to O-H stretching and bending of H_2O were observed at, respectively, 3435 and 1646cm^{-1}. Additionally, three bands at 1497 and 1428cm^{-1} at 868cm^{-1} were assigned to CO_3^{2-} groups. The broad and one-component bands at 1043 and 560cm^{-1} corresponded to phosphate

groups (PO_4^{3-}), while the band located at 868cm^{-1} corresponded to HPO_4^{2-} groups. These featureless PO_4^{3-} bands were characteristic of a disordered environment. Therefore, the precipitate formed in SBFx5 was a poorly crystallized or amorphous carbonated Ca-P phase. ESEM photos of the final coating after 24h of immersion in SBFx5 indicated that a uniform Ca-P layer covered the plate as a dense Ca-P film composed of globules of 1 to 5µm in size (fig. 1d). At high magnification (x20000), the globules exhibited nanometric nuclei indicating that the film was composed of an amorphous or nanocrystalline compound.
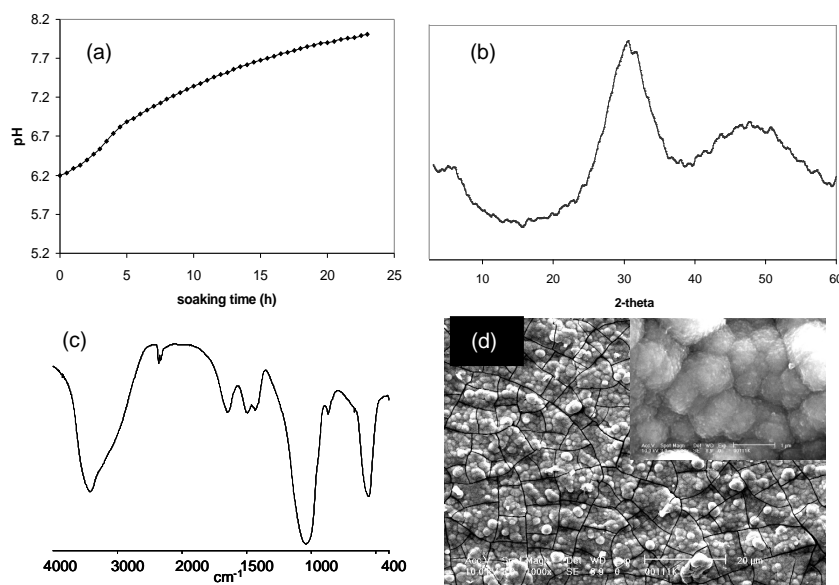
Figure 1: SBFx5 experiment: (a) pH versus soaking time, (b) XRD, (c) FTIR, (d) ESEM photos at magnification x1000 and x20000

Figure 2 shows the quantitative variation of the elements present in the Ca-P coated Ti6Al4V sample (Ca%, P%, Mg% and Ti%) versus cumulative Ar etching time, related to the depth analysis. Considering the depth profile, from 0s to 1383s of etching, Ca, P and Mg were the main elements detected by XPS. P%, Ca% and Mg% remained quite stable at respectively 15.0%, 22.0% and 3.0%. This first part corresponded uniquely to Ca-P coating. Beyond 1383s of etching, P%, Ca% and Mg% started to significantly evolve. For example, after 1623s of etching, %P decreased to 9.8%, while the %Ca raised to a maximum of 29.8%, and %Mg remained stable at 3.7%. At this etching time, 1623s, the calculated atomic ratios were Ca/P=3.0, Ca/Ti=12.9 and P/Ti=4.3. Deeper in the sample, at 1743s, %Ti started to increase rapidly at 7.2%, indicating the approach of Ti6Al4V substrate, and corresponding to the

coating/substrate interface. Considering the other elements after 1743s of etching, %P, %Ca and %Mg were respectively 4.8%, 28.1% and 4.6%. Ca and Mg were highly present in comparison to P at the interface as indicated by the atomic ratios Ca/P=5.9, Ca/Ti=3.9 and P/Ti=0.6. The high Ca/P ratio could not correspond uniquely to any Ca-P phase. For 1983s of etching, %P, %Ca and %Mg continued decreasing, whereas %Ti increased to 23.6%. However a similar tendency was observed. %Ca and %Mg were still relatively high as compared with %P. Beyond 1983s of etching, Ti was the main detectable element indicating the end of the interface, and herewith the unique Ti6Al4V substrate.
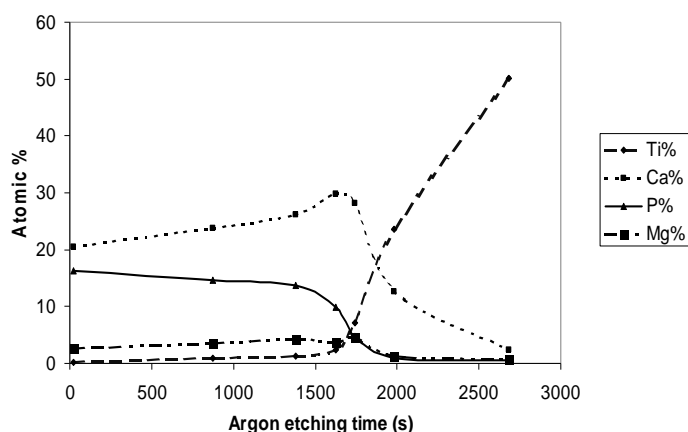
Figure 2: XPS depth profile of the biomimetic Ca-P coating obtained from SBFx5 solution. Atomic percentages of the elements (Calcium (Ca), Phosphorus (P), Magnesium (Mg), and Titanium (Ti) are plotted versus Argon etching time (s)

Influence of magnesium on the Ca-P coating formation

Experiment	Precipitation		Coating		Precipitate	Slope
	pH	Time	pH	Time	structure	(/h)
SBFx5	6.7	4h1/2	6.8	5h1/2	AmCO$_3$-CaP	0.11
SBFx5 (Mgx0)	6.7	6h	-	-	CO$_3$-Ap	0.14
SBFx5 (Mgx3)	6.7	4h	6.8	4h1/2	AmCO$_3$-CaP	0.15
SBFx5 (Mgx8, HCO$_3$x0)	6.6	15h1/2	6.6	15h1/2	DCPD	0.12
SBFx5 (Mgx0, HCO$_3$x8)	6.4	1h1/2	7.0	10h	CO$_3$-Ap/calcite	0.12

Table 2: Kinetics of precipitation and coating formations of the various experiments (AmCO$_3$-CaP: amorphous carbonated apatite, DCDP: brushite, CO$_3$-Ap: carbonated apatite)

All the results concerning the kinetic study and the Ca-P structures are summarized in table 2

Influence of magnesium content on Ca-P formation

Regarding the Mg-free solution SBFx5(Mgx0), the starting pH was pH=5.8 (fig 3a). During the first 6 hours, the pH increased with a slope of 0.14 pH-units/h. At t=6h, the pH suddenly dropped from 6.8 to 5.7 within 30min. Subsequently, pH increased again and reached pH=7.9 at t=24h. By t=6h during the pH drop, a precipitate appeared through the whole solution. XRD analysis of this precipitate gathered at t=24h exhibited quite broad diffraction lines (fig3b). The position of these diffraction lines indicated an apatitic structure. The peak at $2\theta=32.1°$ corresponded to the overlapping of (211), (112), (300) and (202) diffraction plans. In addition the peak at $2\theta=25.8°$ corresponding to diffraction plan (002) of apatitic structure indicated that SBFx5(Mgx0) precipitate was composed of tiny apatitic crystals. The FTIR characterization confirmed this observation (fig 3c). The spectrum showed intense and broad bands assigned to O-H stretching and bending of H_2O (3435 and $1646cm^{-1}$), three bands corresponding to CO_3^{2-} groups (ν_3 mode at 1497 and $1428cm^{-1}$ and ν_2 mode at $868cm^{-1}$). PO_4^{3-} groups were located at $1028cm^{-1}$ (ν_3 mode), at $960cm^{-1}$ (ν_1 mode), and at 602 and $563cm^{-1}$ (ν_4 mode). Furthermore HPO_4^{2-} groups were detected at 1108cm-1 (ν_3 mode). This indicated a Ca-deficient carbonated apatitic structure. In contrast to the Ca-P precipitation in SBFx5(Mgx0) solution, Ti6Al4V surface did not exhibit any changes for 24h of experiments. ESEM pictures of the removed Ti6Al4V plates did not show any Ca-P traces but only substrate texture (fig 3d). The EDX analysis of this sample only indicated Ti and Al peaks. Thereby, the immersion of the Ti6Al4V samples into SBFx5 (Mgx0) did not lead to the formation of any Ca-P trace on the substrate.

Regarding the SBFx5(Mgx3) ([Mg]=4.5mM), the starting pH is pH=6.0. Within approximately the 5 first hours, the pH increased rapidly with a slope of 0.15 pH-units/h. Subsequently, the pH slope was quite reduced. At the end of the experiments, pH reached 7.8 (fig 3a). A precipitate formed in the solution at t=4h (pH=6.7). XRD and FTIR spectra (respectively fig 3b and fig 3c) of the final precipitate gathered at the end of the experiments indicated a one-component and broad PO_4 FTIR band and wide XRD bumps. In other words, the precipitate formed in SBFx5(Mgx3) was a poorly crystallized carbonated Ca-P structure. Simultaneously to precipitation (t=4h1/2, pH=6.8), a colorful layer appeared on the Ti6Al4V plates corresponding to a Ca-P layer as indicated EDX analysis. By ESEM, at magnification x1000, the final coating appeared dense and presented some cracks. This Ca-P coating covered uniformly the Ti6Al4V surface and it was composed of numerous Ca-P globules of approximately 1 to 5µm in diameter (fig 3d). At high magnification

(x20000), these globules were dense and they were composed of nanometric globules. No crystals could be observed on Ti6Al4V substrate following its immersion in SBFx5(Mgx3).
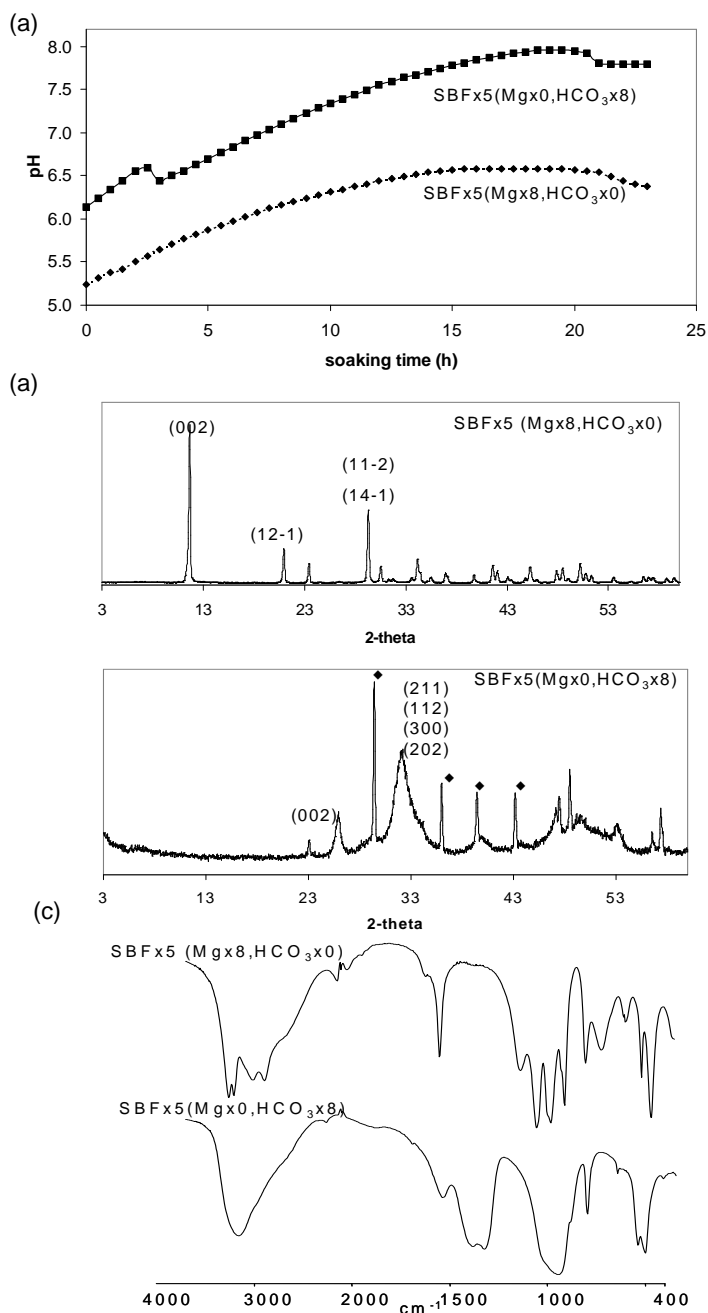
(a)

(a)

(c)

Figure 3: SBFx5 (Mgx0) and SBFx5 (Mgx3) experiments: (a) pH versus soaking time, (b) XRD, (c) FTIR
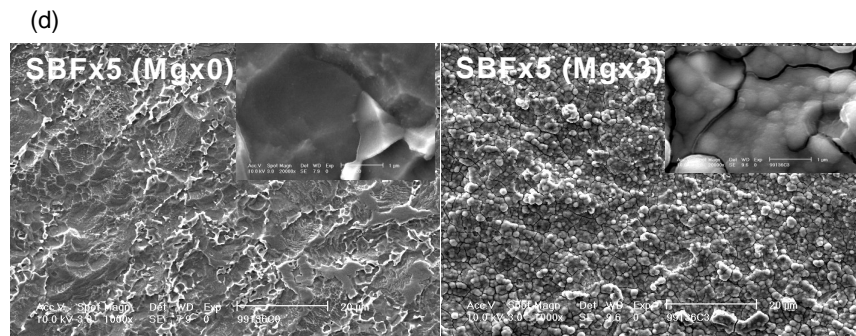
(d)

Figure 3 (*continued*): SBFx5 (Mgx0) and SBFx5 (Mgx3) experiments: (d) ESEM photos at magnification x1000 and 20000.

Distinction between carbonate and magnesium role

In the case of SBFx5(Mgx8,HCO$_3$x0) ([Mg]=12mM, [HCO$_3$]=0mM), the starting pH was 5.3. During the 3 first hours, the pH increased with a slope of 0.13 pH units/hour. At t=16h, pH reached a plateau at 6.6 (fig 4a). Meanwhile, a precipitation occurred into SBFx5 (Mgx8, HCO$_3$x0) solution. The XRD spectrum of this precipitate gathered at the end of the experiments exhibited sharp peaks indicating a highly crystallized structure (fig 4b). The diffraction lines at 2θ=11.7° and at 2θ=29.3° are characteristic of a DCPD. FTIR spectrum (fig 4c) was in compliance with the previous XRD investigations, the phosphate and hydrogenophosphate bands are characteristic of DCPD structure (1220, 1134 1074, 1059, 1000 and 986cm^{-1} for P-O ν$_3$ mode, 874cm^{-1} for P-O(H) ν$_1$ mode and 525cm^{-1} for P-O ν$_4$ mode). Simultaneously to the precipitation into SBFx5(Mgx8,HCO$_3$x0) solution, a colorful Ca-P film was formed. At t=24h, ESEM photos of the final coating exhibited a dense and smooth morphology with some Ca-P globules of approximately 2μm in diameter (fig 4d). At high magnification (x20000), this smooth layer was composed of expanded globules containing nano-sized globules.

In the case of SBFx5(Mgx0,HCO$_3$x8) solution ([Mg]=0mM, [HCO$_3$]=33.6mM), the starting pH was 6.1 (fig 4a). During the first 3 hours, the pH increased with a slope of 0.12 pH-units/h. Subsequently, pH dropped from 6.6 (t=2h1/2) to 6.4 (t=3h). Further, pH stared to rise and reached pH=7.9. This pH remained stable until t=18h1/2. Subsequently, pH decreased again to pH=7.8 at the end of the experiments (t=24h). At t=1h1/2 (pH=6.4), a precipitation occurred in SBFx5(Mgx0,HCO$_3$x8). The XRD pattern of the precipitate gathered at t=24h exhibited both sharp and broad diffraction lines (fig 4b). The sharp diffraction lines could be assigned to calcite structure, whereas the broad diffraction lines could be assigned to apatitic structure where the peak at 2θ=32.06° corresponded to the overlapping of (211), (112), (300) and (202) diffraction plans. Besides PO$_4$$^{3-}$ groups located at 1028cm^{-1} (ν$_3$

mode), at 960cm^{-1} (ν_1 mode), at 602 and 563cm^{-1} (ν_4 mode) and HPO_4^{2-} groups at 1108cm^{-1} (ν_3 mode), FTIR spectrum of the precipitate (fig 4c) exhibited strong and large CO_3^{2-} bands at 1480 and 1416cm^{-1} (ν_3 mode) and at 868cm^{-1} (ν_2 mode) corresponding to carbonated Ca-P structure. Additionally two sharp and fine bands located at 1793 and 713cm^{-1} were assigned to calcite structure ($CaCO_3$). At t=10h (pH=7.0), a whitish layer covered uniformly the Ti6Al4V substrate. EDX of this layer indicated the formation of a Ca-P film. At the end of the experiments, the ESEM photos of the final sample revealed an heterogeneous coating morphology (fig 4d). The coating seemed to be first covered with tiny crystals. These crystals were partially covered by nano-sized globules. Though calcite was detected in the precipitate, the microstructure of this coating suggested the formation of Ca-P compounds on the Ti6Al4V substrate rather than $CaCO_3$.
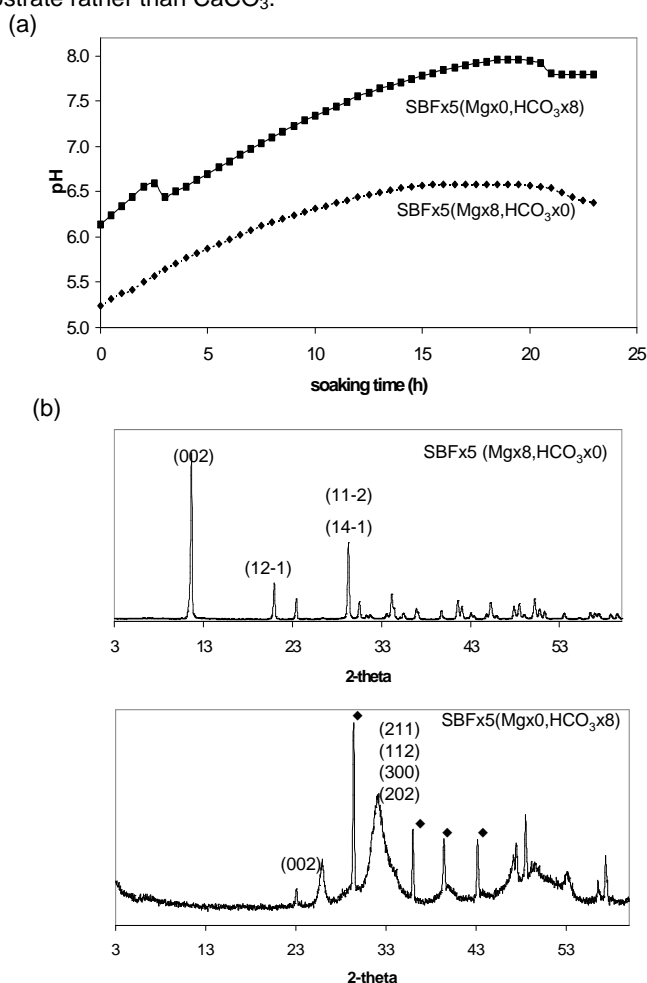
Figure 4: SBFx5 (Mgx8,HCO$_3$x0) and SBFx5 (Mgx0,HCO$_3$x8) experiments: (a) pH versus soaking time, (b) XRD (♦ correspond to calcite).

(c) SBFx5 (Mgx8,HCO₃x0)

SBFx5(Mgx0,HCO₃x8)

(d)
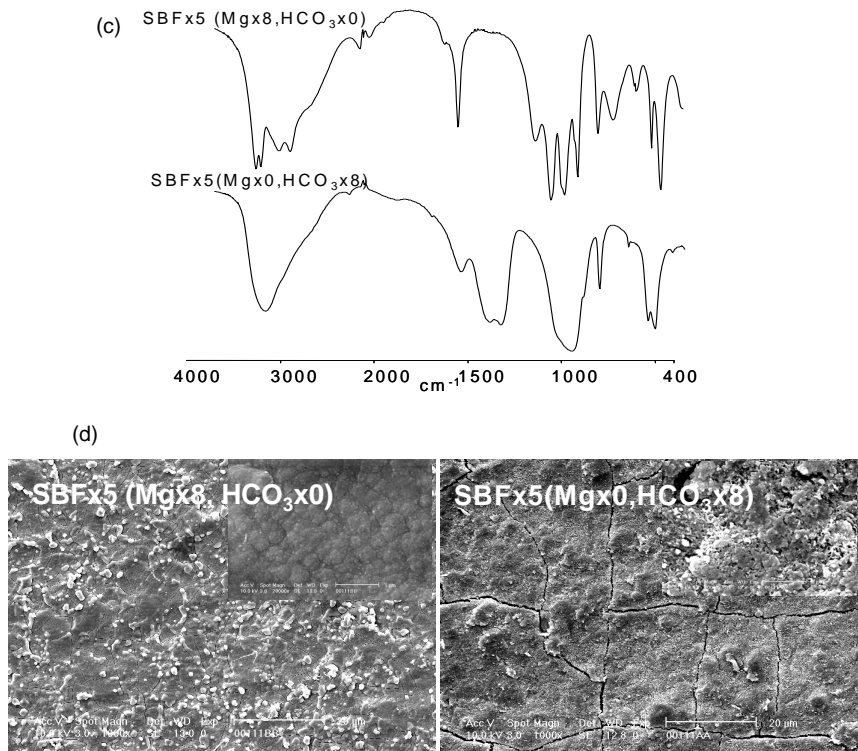
Figure 4 (*continued*): SBFx5 (Mgx8,HCO$_3$x0) and SBFx5 (Mgx0,HCO$_3$x8) experiments (c) FTIR, (d) ESEM photos at magnification x1000 and x20000

DISCUSSION

Role of magnesium in SBFx5 solution

From the overall experiments, Mg^{2+} strongly affects the Ca-P coating formation and structure. This important effect is emphasized by XPS depth profile of the final Ca-P coating obtained from SBFx5 solution. As previously shown [6], immersion of Ti6Al4V plates into SBFx5 led to the deposition of a uniform and thin amorphous carbonated Ca-P layer within 5h1/2. This coating, together with a precipitate, formed while CO_2 gas is released out of the solution. This CO_2 release induces a pH raise leading to an increasing supersaturation of SBFx5 solution, and to Ca-P nucleation in the solution and onto the Ti substrate. Mg^{2+} affects Ca-P coating process at different stages, related to its Ca-P crystal growth inhibitory effect [19-21, 27]. When Mg^{2+} is lowered, pH curve is affected. As discussed elsewhere, CO_2 release prevented the drop in pH that is usually observed during Ca-P formation [6]. In the particular case of Mg-free SBFx5 solutions (SBFx5(Mgx0) and SBFx5(Mgx0,HCO₃x8)), pH suddenly decreases simultaneously to precipitation in the solution. When Mg^{2+} is absent of SBFx5

solution, Ca-P precipitation occurs suddenly, leading to a drop in pH. Kibalczyc et al. have already reported dependence of pH drop versus the amount of Mg^{2+} contents: higher Mg^{2+} content is, smaller is the pH drop [24]. The pH decreases slower in the case of Mg-containing SBF solutions as compared to Mg-free SBF solutions. Additionally, Ca-P precipitation is delayed and the precipitate structure is changed into amorphous or poorly crystallized apatite when Mg^{2+} content increased in SBFx5 solution. Indeed Mg^{2+} is known to poison Ca-P surfaces by disturbing the crystal growth process and by stabilizing ACP phases in detriment to apatitic phases [24-30]. In the particular case of SBFx5(Mgx8,HCO$_3$x0), the precipitate has a highly crystallized DCPD structure. It appears that Mg^{2+} does not affect DCPD formation as it was already shown by previous studies [20-21, 30].

As Mg^{2+} affects the precipitation, it strongly affects coating formation as well. When comparing coatings obtained from SBFx5(Mgx3) and from SBFx5, Ca-P globules were larger with low Mg^{2+} content. When Mg^{2+} content is increased in SBFx5(Mgx8,HCO$_3$x0) solution, though without HCO$_3^-$, the coating is evenly composed of smaller globules. This difference in size is obviously due to the inhibitory effect of Mg^{2+} as mentioned above. On the other hand, when Mg^{2+} content is removed from SBFx5 solution, no Ca-P trace was detected on Ti6Al4V substrate. This experiment suggests that Mg^{2+} is essential for the Ca-P coating formation.

At this stage three hypotheses can be considered. First, Ca-P crystals might have been too large to remain on Ti6Al4V substrate. Due to a lack of Mg^{2+}, Ca-P crystals could have grown as it partially happened in the case of HCO$_3$-free SBFx5 solution [6]. Secondly, due to the absence of Mg^{2+}, precipitation occurs suddenly in the solution. Consequently, the energy required to grow Ca-P homogeneously in the solution is lower than energy required for heterogeneous nucleation on the substrate. These two last hypotheses implicate that a critical amount of Mg^{2+} is required related to its "inhibitory strength". This can be supported by experiment SBFx5(Mgx0,HCO$_3$x8), whereby a Ca-P coating grew on Ti6Al4V substrate despite the absence of Mg^{2+} in this solution. So, it suggests that Mg^{2+} is not essential for the coating formation. However, our first hypothesis seems rather improbable since Ti6Al4V plates were analyzed every hour and any Ca-P trace had never been detected by ESEM/EDX.

In a third hypothesis, additionally to a comparable tailoring effect of both crystal growth inhibitors, Mg^{2+} seems to have an important role at the Ca-P coating/substrate interface. Indeed, XPS depth profile of this thin Ca-P coating formed from SBFx5 solution indicated that, like Ca%, Mg% reaches its maximum at the interface. This suggests that the coating formation was initiated by positive ions certainly due to a negatively charged oxide passive surface. Because the isoelectric point of this TiO$_2$ layer is approximately

pH=6.0-6.2 [14-15], in the case of SBFx5 solution the Ti6Al4V substrate is slightly negatively charged. Via the passive TiO_2 layer therefore, cationic species like Ca^{2+} and Mg^{2+} are preferably attracted. The high Mg^{2+} content at the vicinity of Ti6Al4V substrate inhibits Ca-P growth favoring tiny Ca-P globules on Ti6Al4V substrate. So the Ca-P coating, being composed of tiny globules, is stabilized on evenly smooth Ti6Al4V substrate.

General scheme of Ca-P coating formation from SBFx5 solution

This study of Mg^{2+} role on Ca-P coating deposition on Ti6Al4V from SBFx5 solution clarifies the Ca-P coating formation process. From a previous publication we established that Ca-P formation, in the solution and on the substrate, must be simultaneous in order to balance both phenomena [6]. Precipitation must not occur too fast in order to allow nucleation on heterogeneous substrate.

Additionally HCO_3^-, like Mg^{2+}, reduces apatitic crystal growth. Consequently, both these ions reduce Ca-P crystal size and thereby, Ca-P entities remain more stabilized on a relatively flat Ti6Al4V substrate. Theoretically, heterogeneous nucleation on a substrate requires chemical and physical affinities and Mg^{2+} in SBFx5 solution seems to influence on both chemical and physical affinities. Indeed, in our study, cationic species, i.e. Ca^{2+} and Mg^{2+} are favorably attracted onto the TiO_2 passive layer covering Ti6Al4V plates. Both affinities towards Ca-P nucleation onto Ti and alloys have been already widely studied [5-11]. It is not clear yet to which extend each parameter, physical or chemical affinity is important. For example, chemical treatments have been performed on Ti substrates in order to accelerate the Ca-P nucleation process [31-33]. These drastic treatments affect both surface composition as well as surface roughness. So it is ambiguous to investigate at which extend, each parameter influences Ca-P nucleation. In our experiments, surface texture is kept similar throughout all the experiments. We only change ionic composition of SBFx5.

However, we hypothesize that initial Ca-P nucleation step is primarily favored by chemical affinity. Indeed, Li compared the ability of various substrates on Ca-P formation. The author has shown that alumina substrates, positively charged at pH=7.4 do not initiate any Ca-P nuclei whereas silica and titania substrate lead to Ca-P nucleation due to their negatively charged surface at pH=7.4 [8]. Concerning the nature of chemical bonding between Ca-P and Titanium remains quite ambiguous. Some authors claim chemical bonding occurring between Ti and Ca^{2+} [8,10,34] whereas others claim a chemical bonding between Ti and HPO_4^{2-} [4,6-8]. We think that these two kinds of binding actually are possible and occur during Ca-P coating formation on Ti6Al4V [5]. All these studies have been performed under different conditions

of soaking solutions and analysis. This enables a definitive conclusion concerning a general scheme of chemical bonding.

Concerning the physical affinity, it appears that the stability of this Ca-P coating is related to Ca-P globule development kinetics on the Ti6Al4V substrate. The uniform Ca-P coatings obtained in our experiments exhibit globules being amorphous or nano-crystalline as suggested FTIR and XRD analyses of the precipitates. These globules seem to have expanded during the formation process all over the surface to finally link with surrounding Ca-P globules growing as well. When Ca-P crystals were detected by ESEM, the Ca-P coating was heterogeneous due to the detachment of the largest Ca-P crystals. Thereby, in order to create a stable biomimetic Ca-P coating, this coating must first be composed of tiny Ca-P globules. The presence of Mg^{2+} present at the vicinity of the negatively charged surface inhibits apatite crystal growth in favor to poorly crystallized Ca-P globules. This leads to a strong attachment of the Ca-P coating on Ti6Al4V substrate.

CONCLUSION

The use of a five times more concentrated SBF solution allows the deposition of an homogeneous Ca-P coating within 24h. The formation and attachment of this coating is strongly related to Mg^{2+} content. Indeed, Mg^{2+} is a key-factor for Ca-P coating formation from SBFx5 solution. It inhibits precipitation in the solution and it favors the formation of an amorphous Ca-P coating on the Ti6Al4V surface because of its relatively high concentration at the substrate vicinity. Magnesium stabilizes small amorphous Ca-P globules that can physically attach more easily on the relatively flat Ti6Al4V.

References

1. Kokubo T, Kushitani H, Sakka S, Kitsugi T, Yamamuro T. Solutions able to reproduce *in vivo* surface-structure changes in bioactive glass-ceramics A-W[3]. J Biomed Mater Res 1990; 24: 721-734.

2. Li P, Kangasniemi I, de Groot K, Kokubo T. Bonelike hydroxyapatite induction by a gel-derived titania on a titanium substrate. J Am Ceram Soc 1994; 77:1307-1312.

3. Peltola T, Patsi M, Rahiala H, Kangasniemi I, Yli-Urpo A. Calcium phosphate induction by sol-gel-derived titania coatings on titanium substrates *in vitro*. J Biomed Mater Res 1998; 41: 504-510.

4. Li P, Ducheyne P. Quasi-biological apatite film induced by titanium in a Simulated Body fluid. J Biomed Mater Res 1998; 41: 341-348.

5. Barrere F, Layrolle P, van Blitterswijk CA, de Groot K. Fast formation of biomimetic Ca-P coatings on Ti6Al4V. Mat Res Soc Symp Proc 2000; 599: 135-140.

6. Barrere F, van Blitterswijk, de Groot K, Layrolle P. Nucleation of a biomimetic Ca-P coating on Ti6Al4V from a highly SBF solution: influence of magnesium. Submitted in Biomaterials (2001).

7. Combes C, Freche M, Rey C. Nucleation and crystal growth of dicalcium phosphate dihydrate nucleation on titanium powder. J Mater Sci: Mater Med 1995; 6: 699-702.

8. Li P. In: *In vitro* and *in vivo* calcium phosphate induction on gel oxide, PhD thesis 1993, Leiden University.

9. Healy KE, Ducheyne P. Hydration and preferential molecular adsorption on titanium *in vitro*, Biomaterials 1992; 13: 553-561.

10. Ong JL, Lucas LC. Auger electron spectroscopy and its use for characterization of titanium and hydroxyapatite surface. Biomaterials 1998; 19: 455-464.

11. Hanawa T. Titanium and its oxide film: a substrate for formation of apatite. In: Davies JE, editor. The bone-biomaterial interface. University Toronto Press, 1990. p. 49-61.

12. Yan WQ, Nakamura T, Kobayashi M, Kim HM, Miyaji F, Kokubo T. Bonding of chemically treated titanium implants to bone. J Biomed Mater Res 1997; 37: 267-275.

13. Combes C, Rey C, Freche M. XPS and IR study of dicalcium phosphate dihydrate nucleation on titanium surface. J Colloids and Surfaces B: Biointerfaces 1998; 11: 15-27.

14. Thull R. In: Helsen JA, Breme HJ, editors. Wiley, England, 1998. Metals as biomaterials. p291-315.

15. Tengvall P, Lundström I. Physico-chemical considerations of titanium as a biomaterial. Clin Mater 1992; 9: 115-134.

16. Leitao E, Barbosa MA, de Groot K. Influence of substrate material and finishing on the morphology of the calcium phosphate coating. J Biomed Mater Res 1997; 36: 85-90.

17. Buser D, Schenk RK, Steinemann S, Fiorellini JP, Fox CH, Stich H. Influence of surface characteristics on bone integration of titanium implants. A histomorphometric study in miniature pigs. J Biomed Mater Res 1991;25: 889-902.

18. Thomas KA, Cook SD. An evaluation of variables influencing implant fixation by direct bone apposition. J Biomed Mater Res 1985; 19: 875-901.

19. Tomazic B, Tomson M, Nancollas GH. Growth of calcium phosphates on hydroxyapatite crystals: the effect of magnesium. Archs oral Biol 1975; 20: 803-808.

20. Salimi MH, Heughebaert JC, Nancollas GH. Crystal Growth of Calcium Phosphates in the presence of magnesium ions. Langmuir 1985; 1: 119-122.

21. Eanes ED, Rattner SL. The effect of magnesium on apatite formation in seeded supersaturated solutions at pH=7.4. J Dent Res 1980; 60: 1719-1723.

22. Termine JD, R.A. Peckauskas RA, Posner AS. Calcium phosphate formation *in vitro*. II Effect of environment on amorphous-crystalline transformation. Arch Biochem Biophys 1970; 140: 318-325.

23. Martens CS, Harriss RC. Inhibition in the marine environment by magnesium ions. Geochim Cosmochim Acta 1970; 34: 621-625.

24. Kibalczyc W, Christoffersen J, Christoffersen MR, Zielenkiewicz A , Zielenkiewicz W. The effect of Magnesium ions on the precipitation of calcium phosphates. J Cryst Growth 1990; 106: 355-366.

25. Newesely H. Changes in crystal types of low solubility calcium phosphates in the presence of accompanying ions. Arch Oral Biol 1961; 6: SS174-SS180.

26. Boskey AL, Posner AS. Magnesium stabilization of amorphous calcium phosphate: a kinetic study. Mat Res Bull 1974; 9: 907-916.

27. Nancollas GH, Tomazic B, Tomson M. The precipitation of calcium phosphate in the presence of magnesium, Croat Chem Acta 1976; 48: 431-438.

28. Bachara BN, Fisher HRA. The effect of some inhibitors on the nucleation and crystal growth of apatite. Calc Tiss Res 1969; 3: 348-357.

29. Blumenthal NC. Mechanism of inhibition in calcification, Clin Orth Rel Res 1989; 247: 279-289.

30. Abbona F, Lundager Madsen HE, Boistelle R. The initial phases of calcium and magnesium phophates precipitated from solutions of high to medium concentrations. J Cryst Growth 1986; 74: 581-590.

31. Wen HB, Wolke JGC, de Wijn JR, Cui FZ, de Goot K. Fast precipitation of calcium phosphate layers on titanium induced by simple chemical treatment. Biomaterials 1997; 18: 1471-1478.

32. Kim HM, Miyaji F, Kokubo T, Nakamura T. Preparation of bioactive Ti and its alloys via simple chemical surface treatment. J Biomed Mater Res 1996; 32: 409-417.

33. Ohtsuki C, Iida H, Hayakawa S, Osaka A. Bioactivity of titanium treated with hydrogen peroxide solutions containing metal chloride. J Biomed Mater Res 1997; 35: 39-47.

CHAPTER 4

CALCIUM PHOSPHATE INTERACTIONS WITH TITANIUM OXIDE AND ALUMINUM OXIDE: AN XPS STUDY

F. Barrère, C. A. van Blitterswijk, K. de Groot, C. Rey and P. Layrolle

ABSTRACT

Besides the excellent mechanical properties of titanium and alumina (Al_2O_3) in the case of load bearing applications, their osseointegration properties are very different. So far, this calcification dissimilarity between the natural passive titanium oxide layer (TiO_2) and Al_2O_3 was attributed to respectively their negative and positive surface charge under physiological conditions. The present study aims at studying the chemical interactions between TiO_2 and Al_2O_3 with calcium (Ca)-solutions, phosphate (HPO_4)-solutions and Simulated Body Fluids (SBF), buffered with trishydroxymethyl aminomethane (TRIS) at pH=6.0 and pH=7.4. After 1h of immersion, TiO_2 and α-Al_2O_3 powders were analyzed by X-ray Photoelectron Spectroscopy (XPS). The results indicated that when Ca and/or HPO_4 groups were present in the studied solutions, Ca and orthophosphate groups were detected on TiO_2 surface. In addition, orthophosphate groups were found to be in a higher amount than Ca on TiO_2, which does not comply with the surface charge theory. With regard to Al_2O_3 surface, little orthophosphate was detected after immersion in HPO_4-solutions compared to TiO_2 substrate, and no Ca was detected after immersion in Ca-solutions. Regarding SBF experiments, Al_2O_3 did not show any affinity towards Ca and HPO_4 ions. In addition, TRIS bound to Al_2O_3 substrate in all of the immersion experiments. The fact that both Ca and HPO_4 interacted with TiO_2 might be at the origin of its calcification ability. On the other hand, the poor affinities between Ca and HPO_4 with Al_2O_3 substrate might explain why this substrate is a poor Ca-P nucleator.

INTRODUCTION

In hip and joint surgery, titanium (Ti) and alloys, and alumina ceramics (Al_2O_3) are widely used because of their excellent mechanical properties, which are required for load bearing applications. Both biomaterials have a successful clinical history in load-bearing applications, they are biocompatible, but they react differently in the body. In a bony environment, a rather thick fibrous tissue envelope usually covers Al_2O_3 implants. The presence of fibrous tissue layer affects bone fixation on the implants, leading at long term to decalcification [1,2], and to the loosening of the implant [3,4]. With regard to Ti implants, direct bone contact is often observed without intervention of fibrous tissues [5-8]. The superior osseointegration of titanium is attributed to the passive oxide (TiO_2) layer forming immediately on the surface in air or aqueous solutions, which could calcify.

It is clear that the physico-chemical properties of these two sorts of biomaterials affect their calcification ability. *In vitro* studies have shown that Al_2O_3 is not an efficient calcium phosphate (Ca-P) nucleator when soaked in calcifying solutions, whereas titanium with its passive oxide layer (TiO_2) is [9,10]. Li attributed this phenomenon to the difference of surface charge of these substrates immersed in simulated body fluids (SBFs) [10]. At physiological pH, Al_2O_3 is positively charged, whereas TiO_2 is slightly negatively charged [10,11]. Additionally, TiO_2 surface has a gel-like structure in the presence of aqueous fluids [11-14]. With regard to TiO_2 surface charge, one should expect a higher amount of cationic species such as Ca^{2+} than anionic species such as HPO_4^{2-} on TiO_2 substrate. Experimentally, the initiation of Ca-P formation on Ti substrates from supersaturated calcifying solutions remains under discussion. Depth profile analyses of Ca-P coatings formed in SBF indicate that calcium and magnesium are detected deeper at the coating/substrate interface than HPO_4 groups [15,16]. On the other hand, analyses performed on Ti materials soaked for various times in calcifying solutions indicate usually first the presence of HPO_4^{2-} on the substrate, and second a lower amount of Ca^{2+} compared with HPO_4^{2-} [13,17]. With regard to Al_2O_3 surface charge, one should expect interaction with HPO_4^{2-} due to its positively charged surface at physiological pH=6-7. If it is the case, why Ca-P does not form on Al_2O_3 substrate?

The goal of this study was to analyze the surface of TiO_2 and Al_2O_3 powder soaked in SBF solution at pH=6.0 and pH=7.4. Both substrates were analyzed by X-ray Photoelectron Spectroscopy (XPS) in order to quantify which elements are bound to the substrate, and to evaluate which chemical interactions favor the formation of Ca-P on inorganic substrates, and thus their calcification ability.

MATERIALS AND METHODS

Materials
Titanium oxide powder (TiO_2, pure anatase, Prolabo) had an average particle size of 40nm. Aluminum oxide (Al_2O_3, pure α-phase) had an average particle size of 100nm, and was a gift from Dr. A.J.A. Winnubst (Twente University, The Netherlands).

Method
Firstly, two SBF solutions were prepared by dissolving $CaCl_2.2H_2O$, $MgCl_2.6H_2O$, $Na_2HPO_4.2H_2O$, $NaHCO_3$ and $NaCl$. These solutions were buffered with trishydroxymethyl aminomethane (TRIS, $(CH_2OH)_3CNH_2$) and HCl (1M). SBF-7.4 was buffered at pH=7.4 whereas SBF-6 was buffered at pH=6.0. Secondly, Ca- and HPO_4-solutions were prepared by dissolving on one hand NaCl and $CaCl_2.2H_2O$, and on the other hand NaCl and $Na_2HPO_4.2H_2O$ in similar concentrations as SBF solution. These so-called Ca- and HPO_4-solutions were buffered respectively at pH=6.0 and pH=7.4. They were named Ca-6, Ca-7.4 for Ca-containing solution respectively buffered at pH=6.0 and pH=7.4, and HPO_4-6, HPO_4-7.4 for HPO_4-containing solutions respectively buffered at pH=6.0 and pH=7.4. Ca-6, Ca-7.4, HPO_4-6 and HPO_4-7.4 had a similar ionic strength as SBF solution. All of the chemicals were reagent grade (Prolabo) and they were precisely weighted. Table 1 summarizes the composition of the various solutions.

	pH	NaCl	$MgCl_2.6H_2O$	$CaCl_2.2H_2O$	Na_2HPO_4	$NaHCO_3$	TRIS
SBF-6	6.0	140.0	1.5	2.5	1.0	4.2	50.0
SBF-7.4	7.4						
Ca-6	6.0	140.0	0.0	2.5	0.0	0.0	50.0
Ca-7.4	7.4						
HPO_4-7.4	6.0	140.0	0.0	0.0	1.0	0.0	50.0
HPO_4-6	7.4						

Table 1: Composition of the various solutions in mM

XPS analyses
TiO_2 and Al_2O_3 powder were individually soaked into Ca-6, Ca-7.4, HPO_4-6, HPO_4-7.4, SBF-6 and SBF-7.4 at ambient temperature (250mg/500ml). After 1h of soaking, the powder was filtrated through Millipore filter (0.2μm). Thereafter, the particles were gently washed with demineralized water and dried in a dessicator overnight. XPS analyses allowed the determination of the elemental composition of the first surface atomic layers up to a depth of 30-40 Å and the identification of surface species. The analyses were performed using

a spectrometer ESCALAB MK II (VG Scientific, France). X-Ray source was generated by the Al Kα: 1486.6eV, with a power of 250W. The resolution of the spectrometer was 1eV. The aliphatic C 1s peak (284.6eV) was used as an internal standard to correct the peak shifts due to the accumulation of surface charge on insulating samples. The relative atomic concentrations were determined on C1s, O1s, Ti2p, Ca2p, P2p, Mg1p and Al2p bands using the Scofield sensitivity coefficients. The peaks were fitted using the VGS 5000 ESCA software. The atomic ratios calculated with the semi-quantitative analyses were given with an uncertainty of about 5%. Three determinations have been performed for each sample.

RESULTS

TiO$_2$

The general spectrum of TiO$_2$ powder prior to immersion exhibited the Ti2p, O1s and C1s bands (figure 1a). The Ti2p band was composed of Ti2p$_{3/2}$ at 458.3 eV and Ti2p$_{1/2}$ at 464.1 eV (fig 1b). The O1s bands were asymmetrical, with shoulders tending to higher binding energies (fig 1c). After deconvolution, raw TiO$_2$ exhibited a three-component O1s band that can be attributed to a combination of the oxygen from the titanium dioxide, titanium hydroxide and associated water molecules onto the substrate [12].
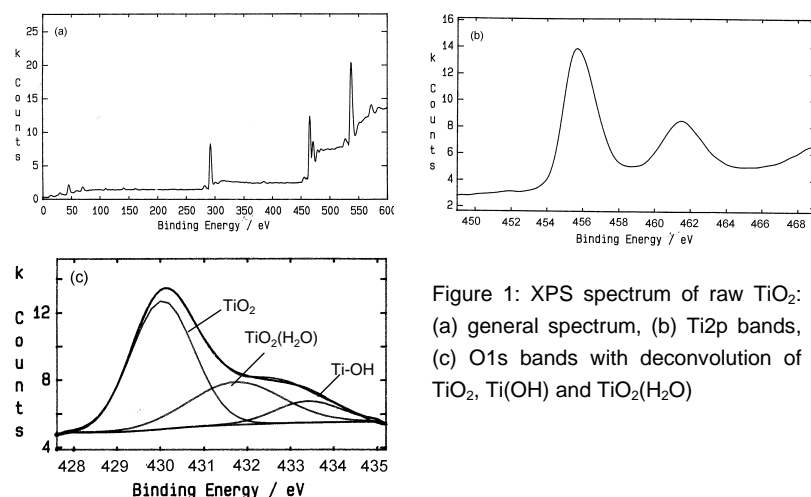
Figure 1: XPS spectrum of raw TiO$_2$: (a) general spectrum, (b) Ti2p bands, (c) O1s bands with deconvolution of TiO$_2$, Ti(OH) and TiO$_2$(H$_2$O)

Table 2 summarizes the band positions of the various elements detected for all the studied samples. The position and symmetry of the O1s and Ti2p$_{3/2}$ peaks did not change with the diverse immersions. When Ca^{2+} ions were present in the solution, the Ca2p$_{3/2}$ peak was detected between 436.3 and 436.7 eV. When HPO$_4^{2-}$ ions were present in the solution, the P2p peak

was detected between 132.5 and 133 eV. The values were in the range of binding energies determined for orthophosphate groups [13]. Magnesium was never detected.

TiO$_2$	Raw	Ca-6	Ca-7.4	HPO$_4$-6	HPO$_4$-7.4	SBF-6	SBF-7.4
Ti2p$_{3/2}$	458.3	458.4	458.3	458.5	458.5	458.3	458.3
O1s	529.7 (60%)	529.7 (70%)	529.6 (70%)	529.9 (73%)	529.7 (71%)	529.6 (64%)	529.9 (74%)
	531.3 (29%)	531.4 (19%)	531.2 (22%)	531.3 (19%)	531.1 (23%)	531.2 (32%)	531.5 (19%)
	533.0 (11%)	532.9 (11%)	532.8 (8%)	532.9 (8%)	532.8 (6%)	533.0 (5%)	533.0 (6%)
Ca2p$_{3/2}$	nd	346.7	346.7	nd	nd	346.7	346.3
P2p	nd	nd	nd	132.6	133	132.8	132.5
C1s	284.6	284.6	284.6	284.6	284.6	284.6	284.6

Table 2: XPS binding energies (eV) and the corresponding elements detected on TiO$_2$ powder in the diverse studied conditions. In the case of O1s, the position and the relative contribution (%) of three O1s bands are indicated after deconvolution. nd: not detected

As an example, figure 2 displays the XPS spectrum of TiO$_2$ powder immersed into SBF-7.4 solution. In addition to the initial Ti2p, O1s and C1s bands, Ca2p$_{3/2}$ and Ca2p$_{1/2}$ bands at 346.3eV and 349.7 eV respectively (figure 2b), and P2p band at 132.5eV (figure 2c) were detected.
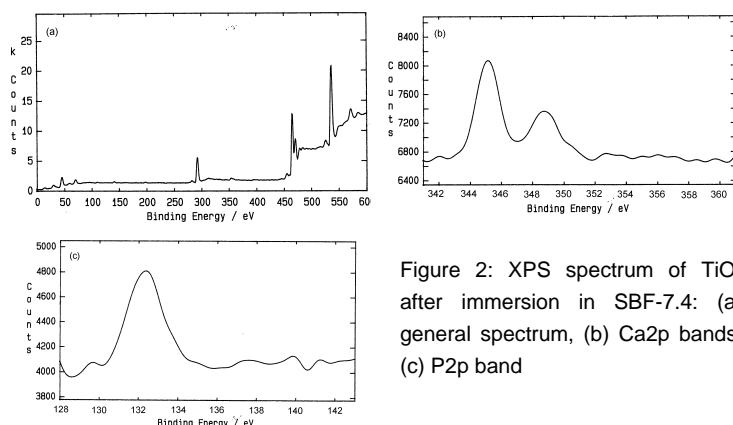
Figure 2: XPS spectrum of TiO$_2$ after immersion in SBF-7.4: (a) general spectrum, (b) Ca2p bands, (c) P2p band

Table 3 summarizes the quantification of various elements detected on TiO$_2$ samples. The raw TiO$_2$ powder was P- and Ca-free, its O/Ti ratio appeared much higher than that of the theoretical ratio at 2. This excess of oxygen decreased significantly for all samples treated in aqueous media but the O/Ti ratio still remained well above 2. With regard to HPO$_4$-6 and HPO$_4$-7.4

solutions the Ti/P ratio was quite similar for both pH. When TiO_2 was soaked into Ca-containing solutions at pH=6.0 and pH=7.4, the Ti/Ca ratio depended on the pH. In these solutions, the Ca-amount was two times higher at pH=7.4 than at pH=6.0. In SBF-6 and SBF-7.4 experiments the Ca- and HPO_4-amount were relatively independent of pH. Ca-amount was comparable to Ca-7.4 experiment, and HPO_4-amount was comparable to HPO_4-6.0 and HPO_4-7.4 experiments. The quantity of orthophosphate groups was two times higher than the quantity of Ca^{2+} ions.

	Ti	P	Ca	O	Ti/Ca	Ti/P	O/Ti
TiO_2	1	0	0	3.225	-	-	3.225
HPO_4-7.4	1	0.077	0	2.571	-	13.0	2.571
HPO_4-6	1	0.088	0	2.73	-	11.4	2.73
Ca-7.4	1	0	0.049	2.897	20.4	-	2.897
Ca-6	1	0	0.023	2.842	43.5	-	2.842
SBF-7.4	1	0.084	0.057	2.909	17.5	11.9	2.909
SBF-6	1	0.093	0.046	2.977	21.7	10.8	2.977

Table 3: Relative quantification of the elements detected by XPS on TiO_2 powder in the diverse studied conditions.
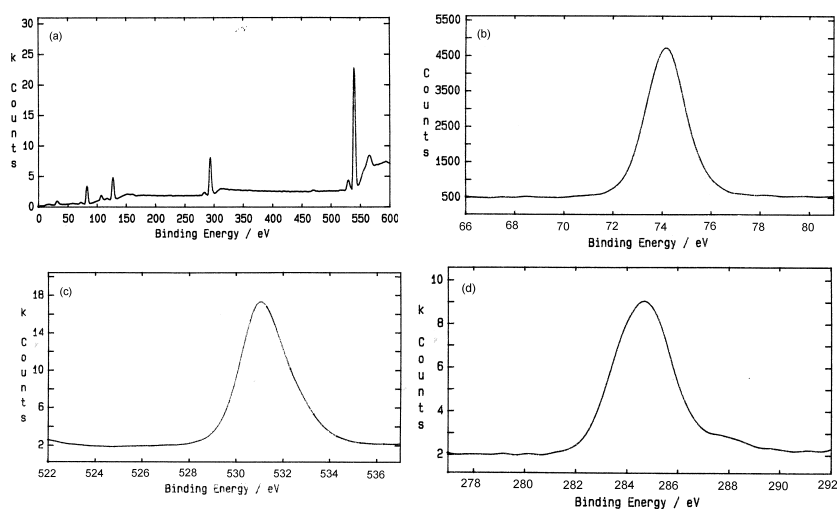
α-Al_2O_3

Figure 3:XPS spectrum of raw α-Al_2O_3: (a) general spectrum, (b) Al2p band, (c) O1s band, (d) C1s band.

Figure 3a exhibits the general XPS spectrum of α-Al_2O_3 powder prior to immersion. The Al2p band at 74.1 eV, the O1s bands at 531.0 eV, and the C1s band at 284.6 eV were detected respectively in figures 3b, 3c and 3d. All of the bands were symmetrical, and the O1s band corresponded to aluminum oxides and hydroxides compounds [18,19].

Table 4 summarizes the peak positions for the α-Al_2O_3 samples. The peak position of Al2p was found between 73.9 and 74.1 eV, in agreement with α-Al_2O_3 materials [20,21]. Hereby, the surface chemistry of Al_2O_3 was not affected by immersion in the various solutions. Despite the presence of Ca^{2+} ions in the working solutions, Ca2p peak was never detected onto the surface of α-Al_2O_3 powder. When α-Al_2O_3 powder was immersed in HPO_4-containing solutions, P2p transition band was detected (figure 4b). The P2p peak position could be attributed to orthophosphate group [13]. Despite the presence of HPO_4^{2-} in SBF6 and SBF7.4 solution, P2p peak could not be detected on α-Al_2O_3 surface.

α-Al_2O_3	Raw	Ca-6	Ca-7.4	HPO_4-6	HPO_4-7.4	SBF-6	SBF-7.4
Al2p	74.1	73.9	73.9	74	73.9	74.2	73.9
O1s	531.0	530.7	530.8	530.9	530.8	531.1	530.7
Ca2p$_{3/2}$	nd	nd	nd	nd	nd	nd	nd
P2p	nd	nd	nd	133.9	133.6	nd	nd
C1s	284.6 (100%)	284.6 (49%)	284.6 (64%)	284.6 (40%)	284.6 (45%)	284.6 (50%)	284.6 (52%)
	nd	282.5 (51%)	283.3 (36%)	281.9 (60%)	281.7 (55%)	282.0 (50%)	282.2 (48%)

Table 4: XPS binding energies (eV) and the corresponding elements detected on α - Al_2O_3 powder in the diverse conditions. In the case of C1s, the position and the relative contribution (%) of the two C1s bands are indicated after deconvolution. nd: not detected.

Additionally to the C1s peak attributed to aliphatic C-H at 284.6eV, a second C1s band was detected between 281.7eV and 283.3eV, and contributed for approximately 50 % of the total C band (figure 4c). This band was detected for all of the samples, except for raw α-Al_2O_3, indicating that solely the immersion of α-Al_2O_3 in the various solutions affected the C1s band. According to literature, this binding energy could correspond to C1s transition for carbures (Al-C) or Al-O-C. In the later case though, this C1s value was found for polyethylene containing Al [20].
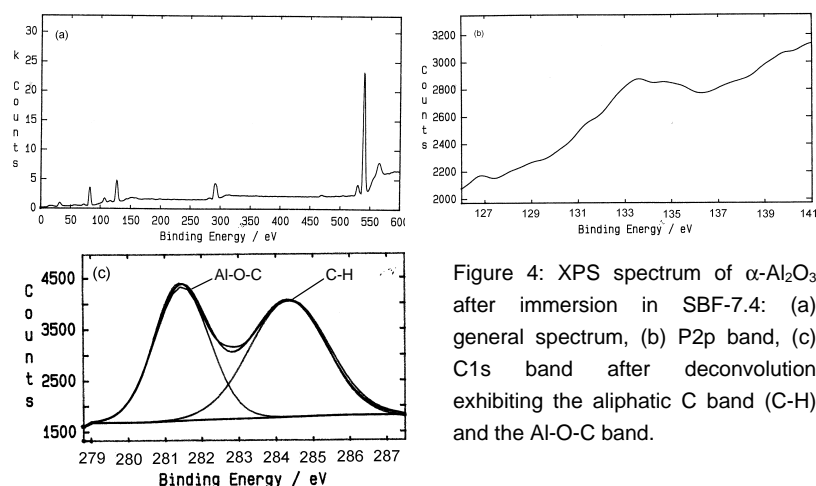
Figure 4: XPS spectrum of α-Al_2O_3 after immersion in SBF-7.4: (a) general spectrum, (b) P2p band, (c) C1s band after deconvolution exhibiting the aliphatic C band (C-H) and the Al-O-C band.

Table 5 summarizes the quantification of various elements detected on α-Al_2O_3 samples. The O/Al ratio of the raw α-Al_2O_3 substrate appeared close to that expected for the theoretical O/Al ratio at 1.5. This ratio remained similar for the immersion performed at pH=6.0 whereas the amount of oxygen slightly increased for the immersions in solutions at pH=7.4. The sole Al/P ratios that could be calculated were for HPO_4-6 and HPO_4-7.4 experiments; they were respectively 47.6 and 37.0.

|	Al	P	Ca	O	Al/Ca	Al/P	O/Al
α-Al_2O_3	1	0	0	1.511	-	-	1.511
HPO_4-7.4	1	0.027	0	1.59	0	37.0	1.59
HPO_4-6	1	0.021	0	1.525	0	47.6	1.525
Ca-7.4	1	0	0	1.44	-	-	1.44
Ca-6	1	0	0	1.525	-	-	1.525
SBF-7.4	1	0	0	1.565	-	-	1.565
SBF-6	1	0	0	1.52	-	-	1.52

Table 5: Relative quantification of the elements detected by XPS on α-Al_2O_3 powder in the diverse studied conditions.

DISCUSSION

TiO_2 and α-Al_2O_3 are oxides, for which the isoelectric point (iep) is respectively 6.2 and 8.5 [11]. Below iep, their surfaces are positively charged, having more positively charged sites than negative ones. Vice versa, above the iep, their surfaces are negatively charged, exhibiting more negatively charged sites than positive ones. In water, their surface can hydrolyze according to the equilibrium (1):

$$Me\text{-}O + H_2O \leftrightarrow Me\text{-}(OH)_2 \quad (1)$$
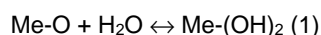
Depending on the iep, and on the nature of the Me-OH bonds, these hydroxylated surfaces can then show acidic or alkaline properties, according to the equilibria (2) and (3):

$$Me\text{-}OH + H_2O \leftrightarrow Me\text{-}O^- + H_3O^+ \quad (2)$$
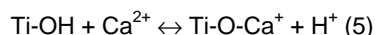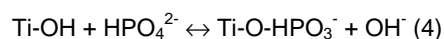$$Me\text{-}OH \leftrightarrow Me^+ + OH^- \quad (3)$$
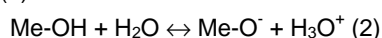
In both cases, an increase of the pH shall lead to a more negative surface either due to a decrease of the positive charges and/or to an increase of the negative charges.

With regard to TiO_2, the XPS analysis of the raw TiO_2 substrate exhibits solely oxygen element (O) and, respectively, titanium (Ti), with an O/Ti ratio greater than the theoretical ratio of 2, indicating the presence of hydroxyl groups as exposed in equilibrium (1). The position of the 3-components O1s band is in agreement with the titanium dioxide hydrolysis [12,13]. The TiO_2 surface may be therefore represented as $TiO_{2-x}(OH)_{2x}.nH_2O$. In aqueous solutions, the O/Ti ratio partially decreases. The water content of the surface layer seems to depend on the solution composition, related probably to faint surface alteration due to the fixation of mineral ions.

With regard to $\alpha\text{-}Al_2O_3$ the O/Al ratio remains close to the theoretical ratio of 1.50. After immersion at pH=6.0, the O/Al ratio remains similar to the raw powder, whereas the amount of oxygen slightly increases for $\alpha\text{-}Al_2O_3$ powder immersed in all of the solutions at pH=7.4. This systematic increase for higher pH may be consistent with the partial hydrolysis of $\alpha\text{-}Al_2O_3$ surface according to equilibrium (1).

The various atomic ratios calculated for TiO_2 and $\alpha\text{-}Al_2O_3$ reveal significant differences. With regard to TiO_2, Ca and P, under orthophosphate form, are detected on the surface, whereas Mg is never detected. The Ca- and P-amounts are identical for the overall immersion experiments, except for Ca-6 solution. This indicates that the TiO_2 surface has a double affinity for HPO_4^{2-} and Ca^{2+} according to the reactions (4) and (5):

$$Ti\text{-}OH + HPO_4^{2-} \leftrightarrow Ti\text{-}O\text{-}HPO_3^- + OH^- \quad (4)$$
$$Ti\text{-}OH + Ca^{2+} \leftrightarrow Ti\text{-}O\text{-}Ca^+ + H^+ \quad (5)$$

The HPO_4-amount is higher than Ca-amount, as already observed by similar analysis technique [12,13,17]. However, this is in disagreement with surface charge considerations and previous depth profile analyses, whereby Ca was present in a higher amount than HPO_4 at the Ca-P/Ti or TiO_2 interface [15,16]. Anatase shall be slightly negatively charged under our experimental

condition since its isoelectric point (iep) has been determined at iep=6.2 [11]. Above this value, the surface exhibits a higher density of negative charges compared to positive charges. Electrostatically, TiO_2 substrate should therefore attract more cations than anions, which is in disagreement with the present results. The bonding of HPO_4^{2-} might be kinetically and chemically favored with the positive, i.e. acidic, sites despite the negative surface charge of the TiO_2 substrate. The bonding between TiO_2 substrate and the solvated Ca^{2+} might be less favored, but might occur in a later stage of the Ca-P formation on the substrate. In the later stage, at the vicinity of TiO_2 substrate, the supersaturation in Ca^{2+} and HPO_4^{2-} may be reached, leading the heterogeneous nucleation of Ca-P.
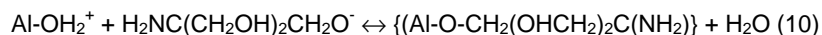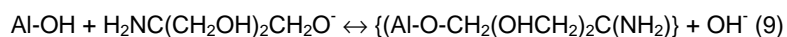
With regard to α-Al_2O_3 substrate, HPO_4 groups are detected on the surface after immersion in HPO_4-6 and HPO_4-7.4 solutions. The Al/P ratio depends on pH, suggesting that HPO_4^{2-} interacted with the hydrolyzed sites of α-Al_2O_3 substrate according to the reaction (6):

$$Al\text{-}OH + HPO_4^{2-} \leftrightarrow Al\text{-}O\text{-}HPO_3^- + OH^- \quad (6)$$
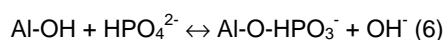
In the case of the SBF-6 and SBF-7.4 immersion experiments, HPO_4 groups were not detected on the α-Al_2O_3 substrate. On the other hand, the marked presence of non-aliphatic C1s suggested a Al-O-C binding [20], as a probable result of the grafting of TRIS on Al_2O_3 substrate. TRIS is a weak monoacidic base, which follows equilibrium (8) in water (pKa=7.82 at 37°C) [21]:

$$H_2NC(CH_2OH)_3 + H_2O \leftrightarrow H_2NC(CH_2OH)_2CH_2O^- + H_3O^+ \quad (8)$$

TRIS anions may interact with Al_2O_3 substrate according to equilibrium (9) or (10):

$$Al\text{-}OH + H_2NC(CH_2OH)_2CH_2O^- \leftrightarrow \{(Al\text{-}O\text{-}CH_2(OHCH_2)_2C(NH_2)\} + OH^- \quad (9)$$
$$Al\text{-}OH_2^+ + H_2NC(CH_2OH)_2CH_2O^- \leftrightarrow \{(Al\text{-}O\text{-}CH_2(OHCH_2)_2C(NH_2)\} + H_2O \quad (10)$$

The interaction with anionic species complies with the positively charged surface of α-Al_2O_3 (iep~9 [11]). However, despite the positive surface charge of α-Al_2O_3, the HPO_4-amount is significantly lower on α-Al_2O_3 than on the slightly negatively charged TiO_2 surface. This lower HPO_4-amount might result from a competition in favor to the bonding with TRIS. In addition, α-Al_2O_3 does not display any affinity for Ca^{2+} ions from Ca- and SBF solutions since Ca is never detected on its surface. With regard to SBF, a competition might take place between the solvated Ca^{2+}, HPO_4^{2-} and the acidic α-Al_2O_3 substrate, resulting in a stronger affinity in the solution between Ca^{2+} and HPO_4^{2-} rather than

HPO_4^{2-} with α-Al_2O_3 substrate. Therefore the supersaturation at the vicinity of the substrate cannot be reached enabling the further formation of Ca-P.

This inability of α-Al_2O_3 to calcify seems to be inherent to the material. Besides the surface charge characteristics, the dielectric constant values (ε) of the studied materials are markedly different: Al_2O_3 ε=5 to 10, TiO_2 (anatase) ε=48 [11]. TiO_2 has a rather equal value with dielectric constant of water (ε=78), whereas Al_2O_3 has a dielectric constant significantly lower than water and TiO_2. The close dielectric constant values between water and TiO_2 suggests a water-like behavior of the surface, whereas the difference in dielectric constant values between α-Al_2O_3 substrate and water leads to the polarization of the surface, which is beneficial for interaction with hydrated macromolecules [11]. This may be consistent with the strong affinity between TRIS and Al_2O_3. In relation with this low dielectric constant, Al_2O_3 ceramics are relatively less hydrophilic than other bioceramics [22], exhibiting a lower wettability angle than TiO_2 and Ti substrates [23]. Besides the surface charge considerations, the approach of solvated cations might be therefore inhibited, enabling the further Ca-P nucleation on Al_2O_3 substrates.

CONCLUSION

The overview of the present study enlightens that TiO_2 and Al_2O_3 have a marked diverse reactivity towards SBF solution at pH=6.0 and pH=7.4. TiO_2 has a double affinity towards cations and anions. Ca and in a greater amount HPO_4 bound to TiO_2 substrate, resulting locally in a relatively high supersaturation. On the other hand, Al_2O_3 exhibits a low density of OH groups precluding interactions with the mineral ions present in SBF solutions. The local supersaturation is therefore to low at the vicinity of Al_2O_3 substrate to stimulate the Ca-P formation.

References

1-Talwar HS, Reddi AH, Menczel J, Thomas Jr WC, Meyer JL. "Influence of aluminium on mineralization during matrix-induced bone development." Kidney International 29 (1986): 1038-1042.

2-Stea S, Savarino L, Toni A, Sudanese A, Giunti A, Pizzoferrato A. "Microradiographic and histochemical evaluation of mineralization inhibition at the bone-alumina interface." Biomaterials 13 (1992): 664-667.

3-Boehler M, Knahr K, Plenk H, Walter A, Salzer M, Schreiber V. "Long-term results of uncemented alumina acetabular implants." J Bone Joint Surg Br 76 (1994): 53-59.

4-Darvell BW, Samman N, Luk WK, Clark RKF, Tideman H. "Contamination of titanium casting by aluminium oxide blasting." J Dentistry 23 (1995): 319-322.

5- McCutchen JW, Collier JP, Mayor MB. "Osseointegration of titanium implants in total hip arthroplastry." Clin Orthop 261 (1990): 114-125

6-Serre CM, Boivin G, Obrant KJ, Linder L. "Osseointegration of titanium implants in the tibia. Electron microscopy of biopsies from 4 patients." Acta Orthop Scand 56 (1994): 323-327.

7-Carlsson L, Regner L, Johansson C, Gottlander M, Heberts P. "Bone response to hydroxyapatite-coated and commercially pure titanium implants in the human arthritric knee." J Orthop Res 12 (1994): 274-285.

8-Albrektsson T, Branemark PI, Hansson HA, Lindstrom J. "Osseointegrated titanium implants. Requirements for ensuring a long-lasting, direct bone-to-implant anchorage in man." Acta Orthop Scand 52 (1981): 155-170.

9-Royer P, Amrah-Bouali S, Freche M, Rey C, Rouquet N, Bonel G. "Nucleation of calcium phosphate salts onto biomaterial surfaces." Bioceramics 5 (1992): 95-102.

10-Li P, Ohtsuki C, Kokubo T, Nakanish K, Soga N, de Groot K. "A role of hydrated silica, titania and alumina in forming biologically active bone-like apatite on implants." J Biomed Mater Res 28 (1994): 7-15.

11-Tengvall P, Lundstrom I. "Physico-chemical considerations of titanium as biomaterial." Clinical Materials 9 (1992): 115-134

12-Healy KE, Ducheyne P. "The mechanism of passive dissolution of titanium in a model physiological environment." J Biomed Mater Res 26 (1992): 319-338.

13-Combes C, Rey C, Freche M. "XPS and IR study of dicalcium dihydrate nucleation on titanium surfaces." Colloids and Surfaces B: Biointerfaces 11 (1998): 15-27.

14-Sutherland DS, Forshaw PD, Allen GC, Brown IT, Williams KR. "Surface analysis of titanium implants." Biomaterials 14 (1993): 893-899.

15- Barrère F, van Blitterswijk CA, de Groot K, Layrolle P. "Nucleation mechanism of Ca-P coating formed from SBFx5 solution: influence of magnesium." Biomaterials, in press.

16-Li P. In: *In vitro* and *in vivo* calcium phosphate induction on gel oxides. PhD thesis, Leiden University, The Netherlands (1993).

17-Healy KE, Ducheyne P. "Hydratation and preferential molecular adsorption on titanium *in vitro*." Biomaterials 13 (1992): 553-561.

18-Sherwood PMA. "Introduction to Studies of Aluminum and its Compounds by XPS ." Surface Science Spectra 5 (1998): 1-13.

19-Thomas S, Sherwood P. M. A. "Valence Band Spectra of Aluminum Oxides, Hydroxides, and Oxyhydroxides Interpreted by Xalpha Calculations ." Anal. Chem 64.2488 (1992): 2495

20-Droulas JL, Jugnet Y, Duc TM. Etudes des proprietes interfactiales des depots par evaporation et pulverization d'aluminum sur polyethylene terephtalate. Le vide, les couches minces. 1991; suppl 258:39-41

21-In:The Merck Index, Budavari S Ed., 12th edition, Merck & co Inc, Whitehouse station, USA, 1996 p9899.

22-Milleding P, Gerdes S, Holmberg K, Karlsson S. "Surface energy of non-corroded and corroded dental ceramic materials before and after contact with salivary proteins." Eur J Oral Sci 107 (1999): 384-392.

23- Smith DC, Pilliar RM, Chernecky R. Dental implants. I. Some effects of preparative procedures on surface topography. J Biomed Mater Res 25, 1045-1068 (1991).

CHAPTER 5

NUCLEATION AND GROWTH OF CALCIUM PHOSPHATE ON TITANIUM: A NANO-SCALE STUDY

F. Barrère, M. M. E. Snel, C. A. van Blitterswijk, K. de Groot, P. Layrolle

ABSTRACT

The nucleation and growth of a calcium phosphate (Ca-P) coating from a simulated body fluid solution concentrated by five (SBFx5) was investigated. A group composed of smooth titanium alloy (s-Ti6Al4V) with a maximum roughness R_{max}<0.10µm, and a group of rough Ti6Al4V (r-Ti6Al4V) with a R_{max}<0.25 µm were used in the present study. They were examined by Environmental Scanning Electronic Microscopy (ESEM) and Atomic Force Microscopy (AFM) after immersion in SBFx5 solution during 10min to 4h. Scattered Ca-P nuclei of 15nm in diameter appeared after 10min of immersion in SBFx5, they grew up to 60 to 100nm after 4h for both s- and r-Ti6Al4V substrates. The Ca-P coating developed by the packing of Ca-P nuclei of tens of nm in diameter, forming bigger globules. A direct contact between the Ca-P coating and the Ti6Al4V surface was found, composed partially of nuclei and partially of an amorphous matrix. This interfacial matrix might ensure the adhesion between the Ca-P coating and the Ti6Al4V substrate. However, failures appeared within this matrix in the case of s-Ti6Al4V substrate, whereas the Ca-P film did not detach from r-Ti6Al4V, and extended on the whole surface. The present study suggested that the primary heterogeneous nucleation of Ca-P was immediate and did not depend on the Ti6Al4V surface topography or on the increasing supersaturation of SBFx5. Whereas, the further stability and mechanical attachment of the final Ca-P coating strongly depended on the surface, for which a rough topography was beneficial.

INTRODUCTION

The nucleation and growth of calcium phosphates (Ca-P) on titanium and certain of its alloys have been extensively investigated because of their relevance in orthopedic applications. *In vivo*, a direct bone contact has been often observed between the hosting bone and titanium implants. This calcification is attributed to 1) the supersaturation in calcium and phosphate of the body fluids, and 2) the surface properties of titanium (Ti) [1-8]. Regarding the surface chemistry, Ti is naturally covered by an oxide layer, which is hydrated in aqueous media. The presence of hydroxyl groups favors chemical bonding with calcium and phosphate ions from supersaturated solutions [1,2,4,5,8]. The degree of supersaturation in the solution influences also the calcification ability of titanium and titanium oxides [3,7]. Regarding the Ti surface morphology, Ca-P nucleation and growth can be also affected by the substrate roughness, when immersed in Hank's Balanced Salt Solution, i.e. a simulated physiological solution [6].

Resulting from these physico-chemical properties, the idea to create a Ca-P coating under simulated physiological conditions has risen. A so-called biomimetic coating process has been developed. It is based on heterogeneous nucleation of Ca-P from simulated body fluids (SBFs), which are supersaturated towards hydroxyapatite at pH=7.25 and at 37ºC [9]. By this technique, bone-like apatite coatings could be deposited within 7 days [10]. Knowing that Ca-P nucleation and growth is enhanced when the supersaturation of the solution increases [3,7], and that the solubility of Ca-P increases when pH decreases [11], a SBF solution concentrated by five (SBFx5) could be produced at pH=6.0 by bubbling a weak gaseous acid carbon dioxide (CO_2). A previous study has shown that a homogeneous Ca-P coating could be deposited on a titanium alloy (Ti6Al4V) when the limit of metastability state of SBFx5 was attained, passing to the labile state [12]. In addition, the magnesium content in the solution was found to be critical for the formation of a Ca-P coating on Ti6Al4V substrate [8]. The goal of the present study was to investigate the early events in the nucleation and growth of Ca-P occurring on the Ti6Al4Vsurface. For this purpose, Atomic Force Microscopy (AFM) and Environmental Scanning Electronic Microscopy (ESEM) have been utilized in order to detect at the nanometer scale the primary Ca-P nucleated on the substrate, to evaluate in which way the Ca-P coating attaches to the Ti6Al4V substrate, and to investigate how the Ca-P coating develops on Ti6Al4V.

MATERIALS AND METHODS

Materials

Forty Ti6Al4V plates, of 1cm^2 in surface area, were used for these experiments. Twenty Ti6Al4V plates were polished mechanically until a maximum roughness peak-to-valley R_{max}<0.25μm. The leftover twenty Ti6Al4V plates were polished mechanically until a maximum roughness peak-to-valley R_{max}<0.1μm. Because of these different surface finishing, the batch polished up to R_{max}<0.25μm was called rough Ti6Al4V (r-Ti6Al4V), and the batch polished up to R_{max}<0.1μm was called smooth Ti6Al4V (s-Ti6Al4V). Thereafter, the Ti6Al4V plates were ultrasonically cleaned in acetone, ethanol 70% and demineralized water, 15 minutes for each step. The plates were finally dried at 50ºC.

Biomimetic coating

A highly concentrated simulated body fluid solution was prepared by dissolving carbon dioxide gas (CO_2), into a solution made of reagent grade NaCl (40g), $CaCl_2.2H_2O$ (1.84g), $MgCl_2.6H_2O$ (1.52g), $NaHCO_3$ (1.76g) and $Na_2HPO_4.2H_2O$ (0.89g) salts in 1l of demineralized water at 37ºC. The starting point of the experiments (t=0min) was set when the supply of CO_2 was stopped [12].

The Ti6Al4V plates were fixed vertically in sample holders, and they were immersed into SBFx5 for various immersion times. When the samples were taken out, they were thoroughly rinsed with demineralized water, and they were dried overnight at 50ºC in air. Subsequently, the samples were observed by Field Emission Gun Environmental Scanning Electron Microscopy (FEG-ESEM, XL-30 Philips, Eindhoven, The Netherlands) after gold sputtering. Energy Dispersive X-rays analysis (EDX) was performed to control the nature of the substrate over time. In addition, the samples were studied by Atomic Force Microscopy (AFM, Nanoscope III Multimode, Digital Instruments, Santa Barbara, CA, USA). The measurements were performed in constant force mode with oxide-sharpened tips with a spring constant of 0.12N/m as specified by the manufacturer (Digital Instruments, Santa Barbara, CA, USA). All images shown are flattened raw data. The cross-sections were used to determine the diameter of the observed Ca-P globules.

RESULTS

Prior to the immersion study, the surface of the r-Ti6Al4V and the s-Ti6Al4V substrates was examined by AFM (figure 1). Scratches due to the mechanical polishing were visible in both cases. The r-Ti6Al4V substrate appeared less flat

than s-Ti6Al4V, suggesting that r-Ti6Al4V and s-Ti6Al4V had distinct surface topographies
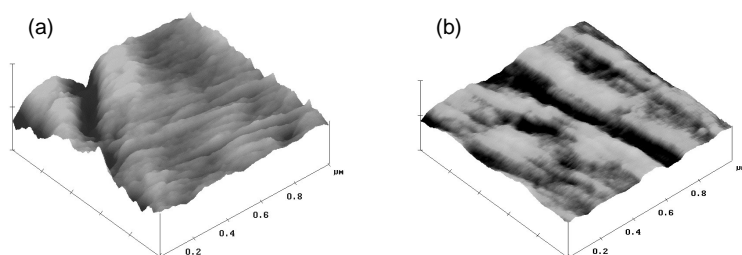

Figure 1: AFM images of (a) r-Ti6Al4V, and (b) s-Ti6Al4V; window 1µm

After 30min of immersion in SBFx5, scattered Ca-P nuclei appeared on r-Ti6Al4V substrate even if no precipitation was visible in the solution. Their diameter varied from 50 up to 100nm (fig 2a). The 100nm-globules seemed to be composed of smaller nuclei. After 2h of immersion, part of r-Ti6Al4V substrate was covered with a Ca-P film (fig2b). This film was composed of linked globules of an approximate diameter of 100 to 500nm, which were composed of nuclei of an approximate diameter of tens of nm.
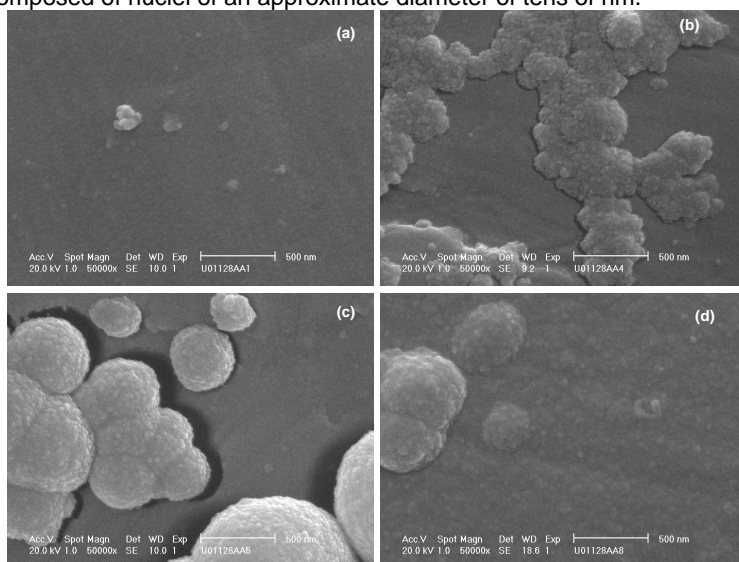

Figure 2: ESEM photos of r-Ti6Al4V versus soaking time in SBFx5 (magnification x50000): (a) 30 minutes, (b) 2hours, (c) 3hours, (d) 4hours.

With increasing immersion time, the film covered a larger part of r-Ti6Al4V substrate (fig 2c). After 3h of immersion in SBFx5, figure 2c indicated that the film was composed of Ca-P globules linked to each other. In other areas,

individual globules were still lying on the Ti6Al4V substrate. Nuclei of tens of nm in diameter were clustered into large globules. The diameter of these globules varied approximately from 500nm to 1µm. These Ca-P globules were larger than for the previous immersion time. After 4h of immersion in SBFx5, Ca-P nuclei of tens of nm in diameter covered the whole r-Ti6Al4V substrate (fig 2d). On the top of this Ca-P film, bigger globules were detected, composed of similar nuclei of tens of nm in diameter, as previously observed. In all cases, the Ca-P deposited on r-Ti6Al4V were composed of two entities: 1) more or less large globules depending on the immersion time in SBFx5, 2) these globules were formed by the clustering of smaller Ca-P nuclei of approximately tens of nm.
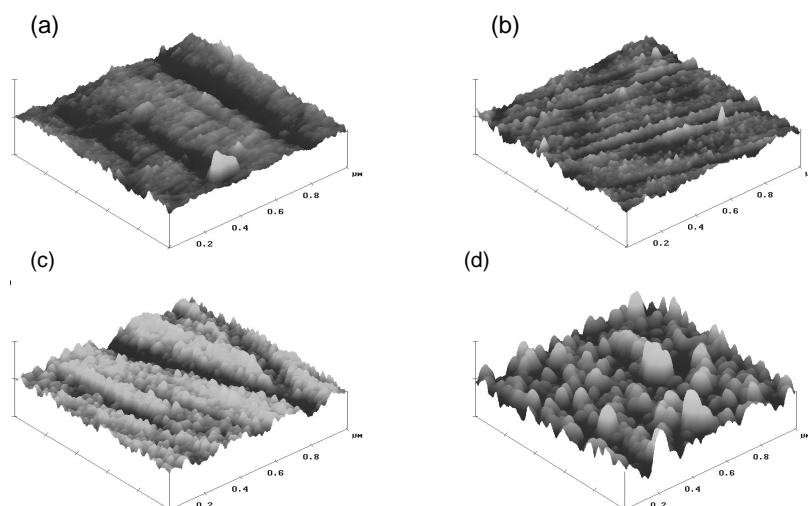

Figure 3: AFM images r-Ti6Al4V substrate immersed for (a) 30min, (b) 1h, (c) 2hours, (d) 4hours.

Figure 3 shows that the r-Ti6Al4V surface topography evolved versus immersion time in SBFx5. At the first measured point (30min), the r-Ti6Al4V sample exhibited already scattered nuclei on its surface suggesting the heterogeneous nucleation of Ca-P (fig 3a). The size of these nuclei was a few nm in diameter. For immersion times of 1h and longer, nuclei became bigger, and they covered homogeneously the whole observed area (fig 3), and their diameter reached approximately 50 to 100nm.

Figure 4 shows that the s-Ti6Al4V surface topography evolved versus immersion time in SBFx5. Already at the first measured point at 10min, s-Ti6Al4V sample exhibited scattered globules on its surface suggesting the heterogeneous nucleation of Ca-P (fig 4a). These nuclei were a few nm in

diameters. Up to 1h, nuclei grew in diameter and covered more and more the s-Ti6Al4V substrate (fig 4b, c). For longer immersion time, nuclei were not homogeneously present on the surface (fig 4d), and their size was approximately 50nm in diameter.
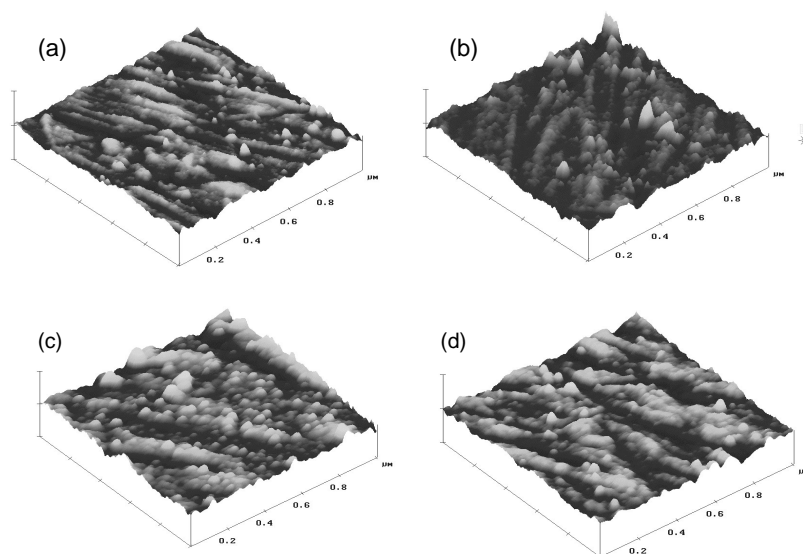

Figure 4: AFM images r-Ti6Al4V substrate immersed for (a) 30min, (b) 1h, (c) 2hours, (d) 4hours.

After 20min, some Ca-P nuclei were scattered on the s-Ti6Al4V substrate (fig5a). Their diameter varied from tens of nm to 300nm and they were in direct contact with the surface of s-Ti6Al4V. In few zones of about $5\mu m^2$, a continuous Ca-P film covered the s-Ti6Al4V substrate. This film was composed of spherical globules of $0.2\mu m$ to $1\mu m$, for which no direct contact with the substrate could be observed (fig 5b). At higher magnification, when the film was composed of smaller and flatter globules a direct contact could be detected in some sites (fig 5c). There, Ca-P nuclei of tens of nm in diameter were lying between s-Ti6Al4V and the Ca-P film. After 40min and 1h of immersion in SBFx5, Ca-P film had developed on s-Ti6Al4V surface. In figure 5d, the Ca-P film was composed of relatively big globules, which were composed of relatively tiny nuclei of tens of nm, as previously observed. In addition, beneath the Ca-P film, a glassy halo surrounded the whole film. At higher magnification (fig 5e,f), this glassy interface was partially composed of nuclei apparently in direct contact with s-Ti6Al4V.
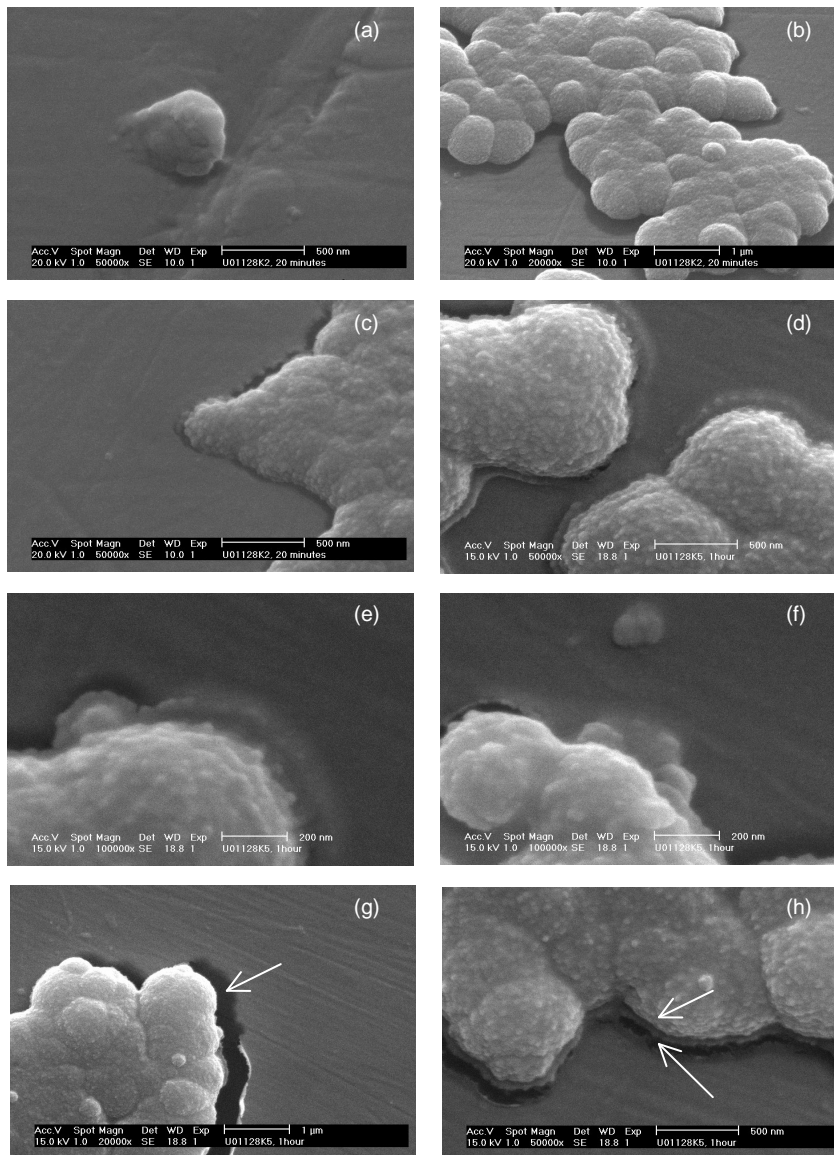
Figure 5: ESEM photos of s-Ti6Al4V versus soaking time in SBFx5 at various magnifications. After 20min: (a) Ca-P globule growing on r-Ti6Al4V (x50000), (b) Ca-P film (x20000), (c) bonding of Ca-P film on r-Ti6Al4V (x50000). After 1h (d) Ca-P film and its glassy halo on r-Ti6Al4V substrate (x50000), (e) and (f) details of the glassy interface between Ca-P globules and r-Ti6Al4V (x100000). The photos (g) and (h) display the detachment of the Ca-P film from r-Ti6Al4V substrate within the glassy interface indicated by white arrows at magnification (g) x20000, (h) x50000, at t=1h.

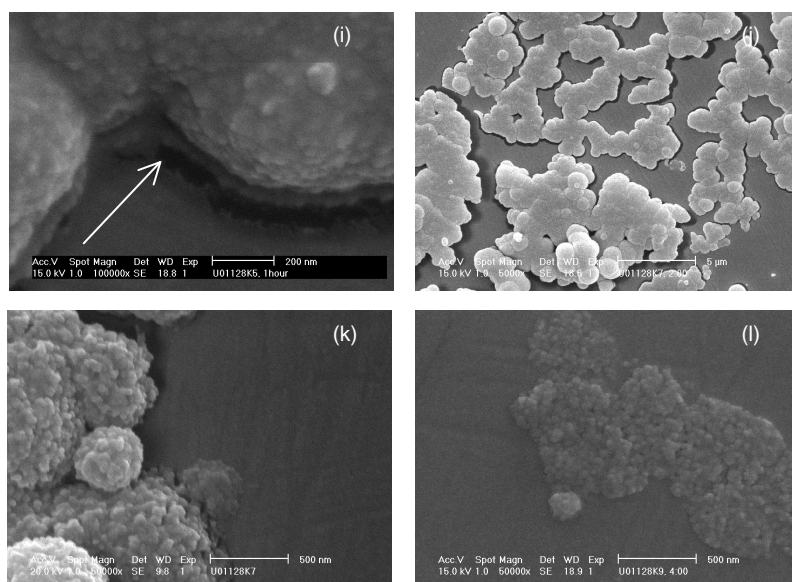Figure 5 (*continued*): ESEM photos of s-Ti6Al4V versus soaking time in SBFx5 at various magnifications: The photo (i) displays the detachment of the Ca-P film from r-Ti6Al4V substrate within the glassy interface indicated by white arrows at magnification x100000. After 2h, (j) development of the Ca-P film (x5000), (k) morphology of the Ca-P film (x50000). After 4h, (l) morphology of the Ca-P.

The diameter of these nuclei varied between tens of nm to 100nm. In other areas, the Ca-P film started to detach from the s-Ti6Al4V substrate. A failure was observed at the glassy interface: part of the glassy interface remained on Ti6Al4V, and the other part remained attached to the Ca-P film (fig 5g,h,i). For longer immersion times up to 2h, the Ca-P film developed and covered larger areas of the s-Ti6Al4V substrate (fig 5j). In other areas, the globules appeared however rougher than previously, and less bonded to each other's (fig 5k). After 4h of immersion in SBFx5, figure 5l exhibited a Ca-P film, which was present solely in scattered areas of s-Ti6Al4V. Contrarily to the earlier immersion periods, the Ca-P coating appeared flat, but always composed of nuclei of tens of nm in diameter.

DISCUSSION

In a previous study, we have shown that after stopping the CO_2 supply, the gas released out of the SBFx5 solution. Consequently, the pH of SBFx5 solution increased from pH of 6.0 to pH of 8.0 within 24h. Above pH=6.8, i.e. after approximately 5h, SBFx5 reached the labile state materialized by the precipitation of Ca-P in the solution, and to the homogeneous deposition of an amorphous Ca-P coating on the whole Ti6Al4V substrate [12]. In the present

study, the formation of Ca-P on Ti6Al4V occurs already after 10 min of immersion in SBFx5 solution, i.e. at the starting pH of 6.0. The heterogeneous nucleation on Ti6Al4V substrate occurs therefore before SBFx5 reaches the labile state illustrated by the formation of a Ca-P precipitate in the solution. The chemical affinity between Ti6Al4V and Ca-P solutions [1,2,4] might stimulate the heterogeneous nucleation prior to the attainment of the labile state. This early heterogeneous nucleation would be also stimulated by the high concentrations in SBFx5 solution.

Therefore, the initialization of the Ca-P coating starts at early immersion times, by the heterogeneous nucleation of Ca-P nuclei scattered on Ti6Al4V substrate. The average diameter of these primary globules is a few nm in diameter. With an increasing immersion time, these globules expand on Ti6Al4V up to approximately 50-100nm after 4h of immersion for r-Ti6Al4V and s-Ti6Al4V (fig 3,4). These nm-scale globules are hardly detected as sole entities by ESEM, but as building entities at the surface of bigger globules, suggesting that the bigger globules are formed by a secondary nucleation mechanism of Ca-P entities. After Ca-P nuclei have directly formed on Ti6Al4V substrate, other Ca-P nuclei have developed on the surface of the primary Ca-P nuclei. The extension of these secondary globules seems to be limited to a diameter of approximately 1μm. These secondary globules can be found individually or bond to others, creating a film that extends on the Ti6Al4V substrate. The globular shape and the nm-diameter of the Ca-P entities indicate an amorphous state [12-14].

A glassy matrix was observed at the interface between Ti6Al4V substrate and the globular Ca-P film (fig 5d,e,f). This interfacial unstructured matrix partially contains nuclei of tens of nm in diameter. The chemical composition of this matrix cannot be clearly established, however this matrix could be composed of smaller Ca-P entities derived from Posner's clusters [15]. According to Posner, the formation of amorphous Ca-P starts with the packing of spherical clusters $Ca_9(PO_4)_6$ packed by water. Recently, the existence and the stability of these clusters have been demonstrated in a magnesium-free and carbonate-free SBF solution. From pH=5.28 to pH=7.40, their diameter was constant between 0.7 and 1.0nm [16]. In a regular SBF solution, containing magnesium and carbonate, the diameter of the clusters was not significantly affected by these two apatite crystal growth inhibitors, but their diameter was slightly higher in a 1.5 more concentrated SBF solution (SBFx1.5) [17]. In the present study, one can expect that the unstructured matrix might be composed of relatively similarly packed clusters, although certainly larger in diameter due to the higher supersaturation of SBFx5. The presence of magnesium ions at the Ca-P coating/Ti6Al4V substrate interface detected in a previous study [8] may stabilize these tiny amorphous Ca-P entities [13,19].

This glassy matrix remarkably illustrates the way in which the Ca-P film forms on Ti6Al4V and binds to the surface. In some parts, this unstructured matrix insures a direct contact between the Ca-P globules and the Ti6Al4V substrate (fig5d). The presence of an interface composed of very small entities may create an efficient adhesion of the final Ca-P coating [18,8]. The small dimensions and the granular shape of these nuclei may be beneficial for the adhesion of Ca-P coatings on the substrate because of a relative insensibility of mechanical stresses compared to more geometrical Ca-P shapes [20]. The importance of the tiny size of the interfacial nuclei accentuates the fact that magnesium is a critical element in the deposition of the Ca-P coating. In decreasing the Ca-P nuclei size, magnesium acts as a gluing agent between the Ca-P film and Ti6Al4V substrate. In some other zones, Ca-P detaches from the substrate and the failure appears to be within this matrix (fig 5g,h,I). Part of the matrix remains attached to Ti6Al4V, and the other part remains with the bigger Ca-P globules. This failure in the middle of this interface indicates that the bonding between the matrix and the Ti6Al4V substrate is as strong as the matrix and the Ca-P globules, suggesting a chemical bonding between Ca-P and Ti6Al4V.

Besides a comparable Ca-P growth observed for s-Ti6Al4V and r-Ti6Al4V substrates, the final surface state differs for the two substrates. With regard to r-Ti6Al4V, Ca-P nuclei grow with time, and they significantly spread all over the substrate between 2h1/2 and 3h. On the contrary, Ca-P film significantly disappears from s-Ti6Al4V substrate after 2h of immersion in SBFx5 solution. Solely few parts remain covered for longer immersion time, and the morphology of the Ca-P film changes. The behavior of r-Ti6Al4V plates is in accordance with the usual Ca-P coating process mentioned previously [12]. The Ca-P coating grew over time on Ti6Al4V of an average roughness of 0.8μm, i.e rougher than r-Ti6Al4V and s-Ti6Al4V of the present study. The behavior of s-Ti6Al4V towards Ca-P has a behavior proper to its surface characteristics. Nevertheless, the initial heterogeneous nucleation of Ca-P is not affected by the substrate topography. As illustrated in fig 5a, the Ca-P globule does not grow specifically in a scratch but on an apparently flat zone. However, surface topography might affect the reactivity of the substrate, exhibiting more active sites towards SBFx5 solution. In addition, surface topography affects the stability of the Ca-P coating; the very smooth s-Ti6Al4V might not be able to anchor sufficiently the growing Ca-P globules. Over immersion time, the thickness of the Ca-P film increases, as well as the load in the coating [21], which induces the failure in the interfacial matrix. As the result of low roughness and liquid flow, the Ca-P coating detaches from s-Ti6Al4V substrate (fig 5g, h, i). The relative irregular topography of r-Ti6Al4V might stabilize the deposited Ca-P film, and its continuous growth over time. With regard to s-Ti6Al4V, the detachment of the Ca-P film leads to the release of

Ca-P flakes in SBFx5 solution, and the further growth of Ca-P might occur in the solution nucleating onto the detached Ca-P flakes rather than onto Ti6Al4V substrate.

As the supersaturation of SBFx5 solution continuously increases with time, the formation of new Ca-P globules took place on s-Ti6Al4V, but not sufficiently to cover the whole substrate. On the other hand, the r-Ti6Al4V is suddenly and completely covered by a layer of small Ca-P globules, indicating that SBFx5 attained labile state. Therefore, two distinct events occurrs on the Ti6Al4V substrate. Firstly, a heterogeneous nucleation of Ca-P on Ti6Al4V is initiated spontaneously on Ti6Al4V certainly because of chemical affinities between the Ca-P nuclei and the titanium substrate [1,2,4] followed by a secondary nucleation from the initial Ca-P globules already deposited on the substrate. This event appears to be independent of the topography of the substrate. Secondly, the labile state of SBFx5 solution is attained, and a marked Ca-P nucleation and growth takes place. The initial Ca-P film already developed on r-Ti6Al4V substrate acts as a stable basis for the development of the final spreading and the complete covering of r-Ti6Al4V. Thereby, the surface roughness of the substrate has a secondary effect on the Ca-P coating formation: a smooth surface does not preclude the initial Ca-P nucleation but the further stability of the Ca-P coating.

CONCLUSION

The formation mechanism of the Ca-P coating from SBFx5 solution can be divided in two subsequent steps. Firstly, the heterogeneous nucleation of Ca-P is initiated at the earliest point of the immersion in SBFx5. Secondly, the coating develops all over the substrate when the labile state of SBFx5 solution is attained. The heterogeneous nucleation and growth of Ca-P on Ti surface is initiated by chemical bonding of nanosized clusters forming an interfacial unstructured matrix, which is certainly stabilized by the presence of magnesium ions. The surface roughness did not affect the development of the Ca-P globules. However, a rougher substrate allows the final Ca-P coating to remain on the surface, whereas a smoother substrate is not efficient for the anchorage of the final Ca-P coating. In summary, the heterogeneous nucleation of Ca-P did not depend on the surface morphology, whereas the stability of the Ca-P coating requires a Ti6Al4V substrate of a roughness higher than 0.10μm.

References

1-Tengvall P, Lundstrom I. Physico-chemical considerations of titanium as biomaterial. Clinical Materials 1992;9: 115-134.

2-Healy KE, Ducheyne P. Hydratation and preferential molecular adsorption on titanium *in vitro*." Biomaterials 1992;13: 553-561.

3-Combes C, Freche M, Rey C. Nucleation and crystal growth of dicalcium phosphate dihydrate on titanuim powder. J Mat Sci Mat Med 1995;6: 699-702

4-Combes C, Rey C, Freche M. XPS and IR study of dicalcium dihydrate nucleation on titanium surfaces. Colloids and Surfaces B: Biointerfaces 1998;11: 15-27.

5-Li P, Ohtsuki C, Kokubo T, Nakanish K, Soga N, de Groot K. A role of hydrated silica, titania and alumina in forming biologically active bone-like apatite on implants. J Biomed Mater Res 1994; 28: 7-15.

6-Leitao E, Barbosa M, de Groot K. Influence of substrate material and surface finishing on the morphology of the calcium phosphate coating. J Biomed Mater Res 1997;36: 85-90

7-Wu W, Nancollas GH. Kinetics of nucleation and crystal growth of hydroxyapatite and fluoroapatite on titanium oxide surfaces. Colloids and Surfaces B: Biointeraces 1997; 10: 87-94

8-Barrere F, van Blitterswijk CA, de Groot K, Layrolle P. Nucleation mechanism of Ca-P coating formed from SBFx5 solution: influence of magnesium. Biomaterials, under press

9-Kokubo T, Kushitani H, Abe Y, Yamamuro T. Apatite coating on various substrates in simulated body fluids. Bioceramics 1989;2: 235-242.

10-Li P, Ohtsuki C, Kokubo T, Nakanishi K, Soga N, Nakamura T, Yamamuro T. Effects of ions in aqueous media on hydroxyapatite induction by silica gel and its relevance to bioactivity of bioactive glasses and glass-ceramics. J Appl Biomater 1993;4: 221-229.

11-Mc Dowell H, Gregory TM, Brown WE. Solubility of $Ca_5(PO_4)_3OH$ in the system $Ca(OH)_2$-HPO_3-H_2O at 5, 15, 25, and 37ºC. Journal of Research of the National Bureau of standards-A. Physics and Chemistry 1977;81A: 273-281.

12-Barrere F, van Blitterswijk CA, de Groot K, Layrolle P. Influence of ionic strength and carbonate on the Ca-P coating formation from SBFx5 solution. Biomaterials, under press

13-Abbona F, Baronnet A. A XRD and TEM study on the transformation of amorphous calcium phosphate in the presence of magnesium. J Crystal Growth 1996; 165: 98-105.

14-Christoffersen J, Christoffersen MR, Kibalczyc W, Andersen FA. A contribution to the understanding of the formation of calcium phosphates. J Crystal Growth 1989; 94: 767-777.

15-Posner AS, Betts F. Synthetic amorphous calcium phosphate and its relation to bone mineral structure. Acc Chem Res 1975;8: 273-281.

16-Onuma K, Ito A. Cluster growth model for hydroxyapatite. Chem Mater 1998;10: 3346-3351

17-Oyane A, Onuma K, Ito A, Kokubo T. Clustering of calcium phosphate in SBF and in the system $CaCl_2$-H_3PO_4-KCl-H_2O. Bioceramics 1999; 12: 157-160

18-Wolke JGC, van Dijk K, Schaeken HG, de Groot K, Jansen JA. Study of the surface characteristics of magnetron-sputter calcium phosphate coatings. J Biomed Mater Res 1994;28: 1477-1484.

19-Boskey AL, Posner AS. Magnesium stabilization of amorphous calcium phosphate: a kinetic study. Mat Res Bull 1974;9: 907-916.

20-Cleries L, Martinez E, Fernandez-Pradas JM, Sardin G, Esteve J, Morenza JL. Mechanical properties of calcium phosphate coatings deposited by laser ablation. Biomaterials 2000; 21: 967-971.

21-Fernandez-Pradas JM, Cleries L, Martinez E, Sardin G, Esteve J, Morenza JL. Influence of thickness on the properties of hydroxyapatite coatings deposited by KrF laser ablation. Biomaterials 2001;22: 2171-2175.

A CRYSTAL GROWTH STUDY OF
OCTACALCIUM PHOSPHATE COATING

F. Barrère, P. Layrolle, C.A. van Blitterswijk and K. de Groot

ABSTRACT

The biomimetic approach allows the coating of metal implants with different calcium phosphate (Ca-P) phases. Films elaborated at physiological conditions exhibited structures closely resembling those of bone mineral. For instance, octacalcium phosphate (OCP, $Ca_8(HPO_4)_2(PO_4)_4,5H_2O$) crystals have been deposited on titanium through a two-step procedure. After cleaning and etching, Ti6Al4V plates were immersed for 24 hours into a Simulated Body Fluid (SBFx5). A thin amorphous carbonated Ca-P layer precipitated on the metal substrate. Secondly, these thinly Ca-P coated titanium substrates were immersed for 48 hours into a Supersaturated Calcifying Solution (SCS1). The thin amorphous carbonated Ca-P layer induced the fast precipitation of a second Ca-P layer of 55µm in thickness composed of OCP crystals. The measurements of Ca and P concentrations *versus* soaking time in SCS1 showed that the carbonated Ca-P layer partially dissolved before the deposition of the OCP coating. X-Ray Diffraction (XRD) revealed that OCP crystals grew epitaxially on the substrate. The biomimetic route allows therefore the formation of novel Ca-P coatings that may be promising for orthopaedic applications.

INTRODUCTION

Hydroxylapatite (HA) and related calcium phosphate (Ca-P) ceramics have been widely used in orthopedic surgery because of their favorable biocompatibility and osteoconductive properties. However, these bioceramics have disadvantages such as difficulty in shaping and low mechanical properties. Many studies have been conducted using Ca-P coatings on metal implants to combine the biocompability of ceramics with the excellent strength of metals. HA plasma-sprayed coating on titanium prostheses is successfully used for joint reconstruction [1]. However, the plasma-spraying technique presents several drawbacks. For instance, 1) it is not possible to evenly deposit HA coating on porous implants and 2) it is not possible to process many Ca-P phases, like octacalcium phosphate (OCP, $Ca_8(HPO_4)_2(PO_4)_4,5H_2O$), because they decompose at high temperature. Recently, a biomimetic approach for coating metal implants with Ca-P has been developed [2-4]. This method consists of soaking metal implants into supersaturated Ca-P solutions at physiological pH and temperature. Bone-like apatite films have been deposited on chemically treated titanium surfaces [5-7], by soaking into Simulated Body Fluids (SBFs) over a long soaking time. These thin films were less than 4μm in thickness.

Although HA coatings have been widely applied to titanium, OCP might be also considered for coating metal implants by a biomimetic approach. Indeed, OCP has been proposed as one of the Ca-P that participates in the early stage of biomineralization of calcified tissues [8,9]. The biodegradability and osteoconductivity of OCP have been demonstrated *in vivo* [10,11]. The aim of this work was firstly to deposit a biomimetic OCP coating within a two-step procedure by immersing into two different supersaturated Ca-P solutions under physiological conditions; secondly to study the nucleation and growth of the OCP coating on the Ti6Al4V substrate.

MATERIALS AND METHODS

Materials

Plates (10 x 10 x 1 mm^3) were cut from a Ti6Al4V sheet (Smitford Staal BV, The Netherlands). The plates were ultrasonically cleaned for 15 min in acetone, then ethanol (70 %) and finally demineralized water, respectively. The samples were subsequently etched for 10 minutes in Kroll's reagent: a mixture of 2 ml hydrofluoric acid (40%), 4 ml nitric acid (66%) and 994ml of demineralized water. After etching, the Ti6Al4V plates were thoroughly washed with demineralized water.

Preparation of the biomimetic Ca-P coating

The biomimetic calcium phosphate coatings were produced in two steps as previously mentioned [12]. The Ti6Al4V plates were first soaked into a SBFx5 solution in order to pretreat the Ti6Al4V substrate with Ca-P nuclei. Later, the samples were immersed into a second solution (SCS1) in order to grow the biomimetic coating.

Soaking of Ti6Al4V plates into SBFx5

SBFx5 was prepared by dissolving NaCl, $CaCl_2.2H_2O$, $MgCl_2.6H_2O$, $NaHCO_3$ and $Na_2HPO_4.2H_2O$ salts into demineralized water under mildly acidic conditions. All of the chemicals were weighted with a confidential interval of 10 mg. This solution was prepared with reagent pure chemicals (Merck). The plates were soaked into the first solution SBFx5 for 24 hours at 37°C. The preparation of SBFx5 is mentioned elsewhere [4].

Soaking of seeded Ti6Al4V plates into SCS1

SCS1 was prepared by dissolving NaCl, $CaCl_2.2H_2O$ and $Na_2HPO_4.2H_2O$ salts into demineralized water. Crystal growth inhibitors, such as Mg^{2+} and HCO_3^{2-}, were excluded from SCS1 solution, while the ionic strength was kept constant by adding NaCl. This solution was prepared with reagent pure chemicals (Merck). SCS1 solution was buffered at pH=7.05 at 37°C by adding a mixture of tris-hydroxymethylaminomethane (TRIS, 50 mM) and 1M HCl. All the chemicals have been weighted with a confidential interval of 10mg. Finally the solution was filtrated trough a 0.22μm Millipore membrane. Subsequently to pretreatment in SBFx5, the plates were immersed into the SCS1 for 48h at 37°C. As control, 2 etched Ti6Al4V plates were immersed into SCS1 solution without previous pretreatment into SBFx5 solution.

	Na^+	Mg^{2+}	Ca^{2+}	Cl^-	HPO_4^{2-}	HCO_3^{2-}
HBP	142.0	1.5	2.5	103.0	1.0	27.0
SBFx5	733.5	7.5	12.5	740.0	5.0	21.0
SCS1	140.4	0.0	4.0	142.9	2.0	0.0

Table 1: Inorganic composition in (mM) of the various minerals contained in Human Blood Plasma (HBP), SBFx5 and SCS1

Kinetic study

The kinetic study is based on the characterization of the coating as well as the composition of SCS1 versus soaking time. The experiments have been repeated 5 times.

Analyses of the coating versus soaking time

Twenty seeded Ti6Al4V samples were individually and vertically placed in polystyrene vials containing 60 ml of SCS1 solution. The vials were sealed and incubated in a calibrated shaking water-bath at 37°C. For each sampling time (1, 2, 3, 4, 5, 6, 7, 8, 12, 24 and 48 hours of soaking), two soaked plates were taken out from SCS1. The samples were subsequently cleaned with demineralized water and dried overnight in air. The coating morphology was observed by Environnemental Scanning Electronic Microscopy with Field Emission Gun (ESEM, Philips, model XL-30 ESEM-FEG) coupled with Energy Dispersive for X-Ray analysis (EDX, Philips). The coating thickness has been determined by using a magnetic induction probe (Electrophysik, Minitest 2100, Germany). The measuring range of this apparatus is between 0 and 100μm. The probe was calibrated with standard polymer films 10μm thick on a Ti6Al4V plate etched and cleaned in the same conditions as the other samples. The measurements were repeated 10 times on each sample. For every Ca-P coated plates, the thickness value was determined by averaging the data. The structure was determined by Fourier Transform Infrared spectrometry (FT-IR, Perkin-Elmer, Spectrum 1000) using transparent KBr pellets of 250 mg and containing 1mg of Ca-P coating. An X-Ray diffractometer (XRD, Philips, model APDW40C) rebuilt for thin-film (TF) applications was used to determine the crystal phase of Ca-P deposited on Ti6Al4V. The monochromatic source was a Cu generator (40kV, 50mA) and TF-XRD were patterned for raising angles $3^\circ < 2\theta < 60^\circ$ with a step-size of 0.5°.

Analyses of SCS1 versus soaking time

Two treated Ti6Al4V samples were individually and vertically placed in polystyrene vials containing 60 ml of SCS1 solution. The vials were sealed and incubated in a calibrated shaking water-bath at 37°C for 48h. For comparison, a SCS1 control vial without a Ti6Al4V plate was placed in the mean time under similar conditions. A sampling from each vials of 1ml of SCS1 solution was performed after 1, 2, 3, 4, 5, 6, 7, 8, 12, 24 and 48 hours of soaking. The pH of SCS1 solution was measured in the same conditions after calibration with 2 buffer solutions pH=4.01 and pH=7.00 (IUPAC standards, Radiometer Copenhagen). A combined pH electrode (Portamess 913, Knick Eletctronische Messgerate, Holland) was used. The calcium concentrations [Ca] in SCS1 solutions were measured by Atomic Absorption Spectroscopy (AAS, Varian SpectrAA-300, Australia). Standard solutions were made by diluting 1000ppm Ca stock solution with demineralized water to a level of 20, 40, 60, 80 and 100ppm. A $LaCl_3$ solution (about 0.6 vol%) was used as a releasing agent to eliminate the depression of Ca absorption by the acetylene flame. Both the standard and sample solution (0.1 ml of each) were diluted with 3.0 ml of the lanthanum solution and then analyzed. The measurements were done in

triplicate for each standard and sample solutions. The phosphorus concentrations [P] were determined by spectrophotometry of a phospho-molybdate complex at 820nm (Vitalab 21, Vital scientific, Holland). Standard solutions were made by diluting 1000ppm P-stock solution with demineralized water to a level of 50 and 100ppm. Measurement involved 0.1ml of each solution, including the P standards, with 7ml of ammonium molybdate acidified with condensed sulfuric acid in the presence of ascorbic acid. After the mixed solutions have been kept at 37°C for 90 minutes, a blue color (molybdene blue) developed. The blue solutions were vortexed and the phosphate concentration [P] was determined after calibration with the standard solutions. The optical density of the complex was measured 3 times.

RESULTS
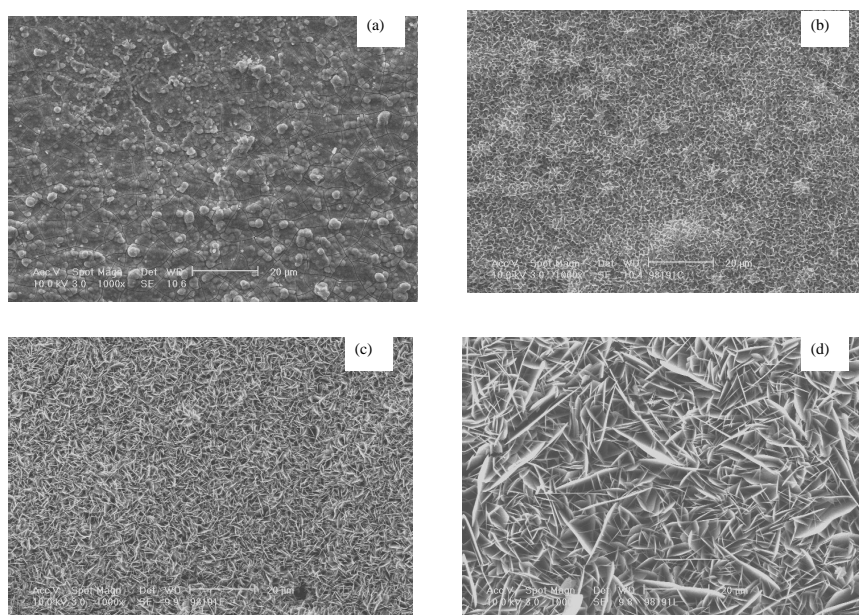
Analyses of the coating versus soaking time

Figure 1: Morphology evolution of the Ca-P coating versus soaking time:(a) pretreated surface; (b) after 2 hours of soaking;(c) after 5 hours of soaking;(d) after 48 hours of soaking into SCS1 solution.

After 24h of pretreatment into SBFx5, ESEM and EDX observations indicated that a dense and uniform Ca-P film was deposited on the Ti6Al4V plates (figure 1a). This layer was composed of spherical Ca-P globules of about 0.1μm in diameter. After soaking into SCS1 solution, no coating was deposited on the non-pretreated Ti6Al4V plates whereas Ca-P coatings were

detected on the pretreated plates in SBFx5 solution. After soaking for 2 hours in SCS1 solution, the initial Ca-P film already changed in morphology. Ca-P globules increased in size and are covered by small crystals of less than 5μm in length (figure 1b). As soaking time increased, these crystals appeared larger and the globules were no more visible. After 48 hours of soaking, these sharp crystal plates were approximately 30μm in length and 0.1μm in thickness. The crystalline coating covered uniformly the surface of Ti6Al4V plates. During the whole experiments, any homogeneous precipitation did not occurred in SCS1 solution. As shown in figure 2, the Ca-P layer became thicker as the soaking time increased. The thickness curve plotted versus the logarithm of soaking time exhibits indicated a hyperbolic shape. After 48h of soaking into SCS1 solution the coating had a thickness of 55μm.
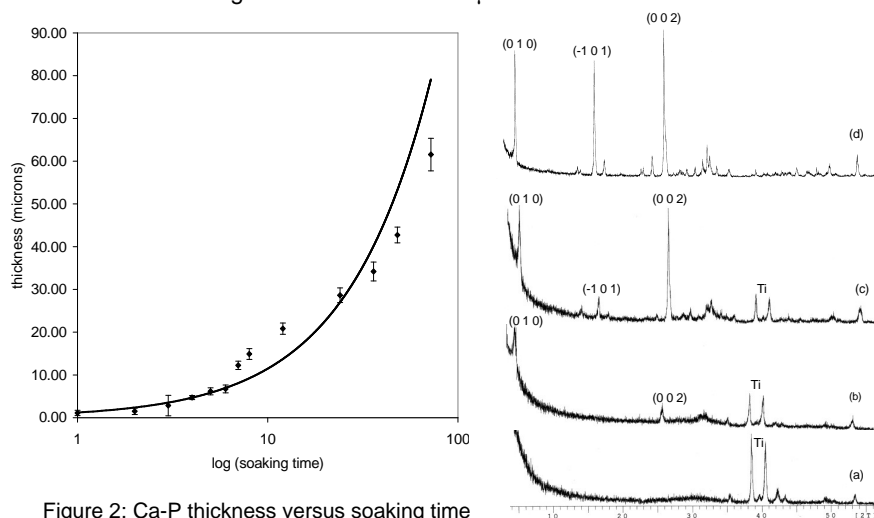
Figure 2: Ca-P thickness versus soaking time

Figure 4: XRD characterization: Crystal features of the coating versus soaking time: (a) pretreated surface; (b) after 2 hours; (c) after 5 hours; (d) after 48 hours.
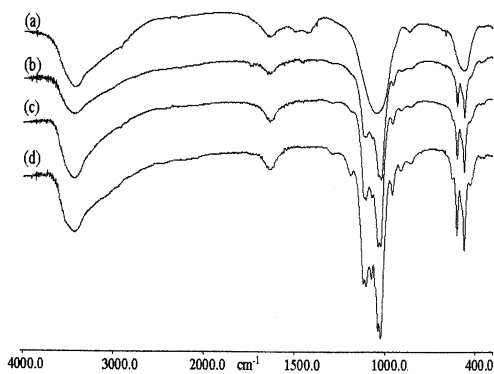
Figure 3: FTIR spectra of the coating, structure evolution versus soaking time. (a) pretreated surface; (b) after 2 hours; (c) after 5 hours; (d) after 48 hours

102

FTIR spectra of the coating are gathered in figure 3. As the soaking time evolved, the structure of coating changed. Initially, the FTIR spectrum of the seeded Ti6Al4V substrate after soaking into SBFx5 (fig 3a) showed featureless phosphate and carbonate bands. Phosphate groups exhibited broad and single bands at 560 cm^{-1} (P-O deformation in PO$_4$ (ν_4)) and 1041 cm^{-1} (P-O stretching in PO$_4$ (ν_3)). The carbonate bands were also observed at 1410 cm^{-1} and 1450 cm^{-1}. The spectrum of the Ca-P film is typical of an amorphous carbonated calcium phosphate. For 2 hours soaking, FTIR spectrum (fig 3b) exhibited a mixture of 2 phases. The single large P-O band at 560 cm^{-1} evolved to sharp bands at 560 cm^{-1} and 600 cm^{-1}, respectively. The broad and single P-O band at 1041 cm^{-1} exhibited a fine structure with vibrations and shoulders at 1025 cm^{-1} and 1011 cm^{-1}. The coating appeared more crystalline. Moreover new bands appeared at 906 cm^{-1} and 852 cm^{-1}, which are typical of HPO$_4^{2-}$ bands in OCP structure [13]. The OCP phase appeared predominant and unique after 48h of soaking into SCS1 (fig 3c-d).
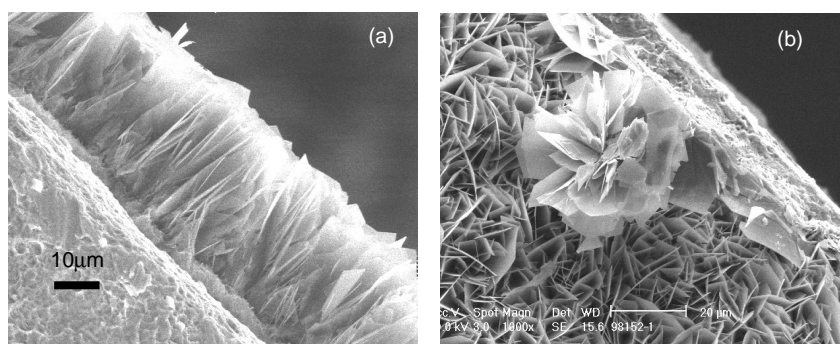

Figure 5: OCP specific crystal growth. (a) OCP crystals growing vertically on the top of the Ca-P seeded Ti6Al4V, (b) secondary OCP growth with a rose-like shape.

The XRD patterns (figure 4) corroborated the previous results obtained by FTIR spectroscopy. The pretreated Ti6Al4V surface pattern (fig 4a) showed a halo or bump located at approximately 30° typical of a Ca-P amorphous state. The other sharp peaks at 2θ=35.5°, 38.6°, 39.6°, 40.5° and 42.2° were assigned to the Ti6Al4V substrate. After 2hours of soaking into SCS1 (fig 4b), additional sharp diffraction lines appeared at 2θ=4.7° corresponding to (010) diffraction line and at 2θ=25.5° corresponding to the (002) plan, both typical of triclinic OCP crystals [14]. After 5hours of soaking, the diffraction lines of the titanium substrate were less intense as compared to earlier immersion time (fig 4c). Furthermore a new line appeared at 2θ=16.8° corresponding to the plan (-101) in the OCP structure. This indicated that the highly crystalline coating had grown on Ti6Al4V plates. However, the relative intensities of the OCP diffraction peaks present mismatches with the typical

OCP pattern. Indeed, the diffraction line (002) had the highest in intensity of the XRD-pattern whereas the diffraction line (010) is the most intense peak for the pattern of typical triclinic OCP crystals. Moreover the diffraction line (-101) at $2\theta=16.8°$ is much more intense in our OCP coating than the typical triclinic OCP crystals [14]. This suggested that the OCP crystals have grown on the substrate after the favorite directions (-101) and (002).

This specific growth is well shown in figure 5, the OCP crystals are all perpendicularly oriented to the substrate. Figure 5b exhibited also the vertical crystals growing from the substrate whereas the rose-like OCP crystal on the top of coating spread over x, y and z-axis. This indicated that the substrate influences the OCP crystal growth.

Characterization of SCS1 versus soaking time

Figure 6 shows the concentrations of Calcium [Ca] and Phosphorus [P] in SCS1 solution (control and samples) as a function of soaking time.
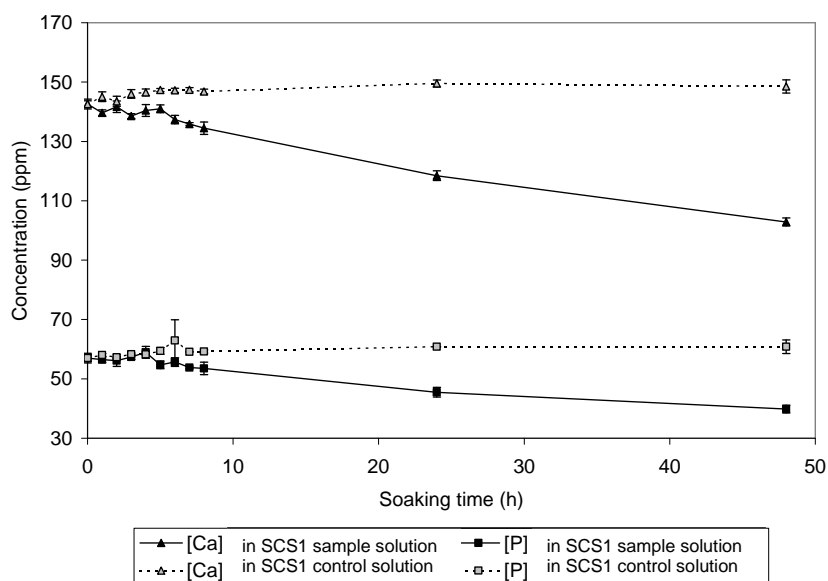
Figure 6: Ca and P concentration in SCS1 solution (sample and control) versus soaking time.

The composition of the control SCS1 solution remains constant whereas the concentrations in the sample SCS1 solution decreased with soaking time. Calcium and phosphorus concentrations (respectively [Ca] and [P]) graphs versus soaking time showed similar behaviors. [Ca] and [P] in SCS1 solution mainly decreased with the soaking time indicating the deposition of a Ca-P coating. During the 10 first hours, an oscillating tendency between uptake and

release of Ca and P was observed. Both ions were partially released from the seeded Ti6Al4V surface and Ca-P reprecipitated from the solution. The OCP crystals grew on the top of this Ca-P layer. After soaking for 48 hours, [Ca] and [P] concentrations are approximately 100 ppm and 40 ppm, respectively. The initial pH of the buffered control SCS1 solution remained at pH=7.05 during the 48h of soaking at 37°C. Whereas the pH in the soaking SCS1 solution slightly decreased to pH=6.95 which is characteristic of Ca-P formation.

DISCUSSION

The results show that a calcium phosphate coating of 55µm in thickness deposited on Ti6Al4V after 48hours of soaking. This layer is composed of pure OCP crystal plates that grow vertically on top of a thin amorphous carbonated Ca-P layer at physiological conditions (fig 5a). The absence of any Ca-P coating on the 2 control Ti6Al4V plates indicates that this layer was essential to induce precipitation of the Ca-P coating. This first Ca-P film deposited on the Ti6Al4V substrate acts as a seeding surface, on which OCP crystals grow. This formation is a dynamic process involving the partial dissolution of the primary Ca-P film and the reprecipitation of the crystalline phase from SCS1 solution. The supersaturation of SCS1 solution increases at the vicinity of the substrate and thereby leads to the heterogeneous nucleation of Ca-P crystals. The continuous oscillating phenomenon can be due to an Ostwald ripening process of Ca-P nuclei: the smallest seeds dissolve in favor to the biggest seeds. Works on the soaking of Ca-P seeds into supersaturated calcifying solutions have shown that fast changes of the precipitates' phases occurred when the soaking time increase [15,16]. This suggests that these metastable phases might dissolve before the precipitation of another subsequent Ca-P phase. However, in our experimental conditions, no intermediates were observed. Furthermore, this oscillating process occurs for about 10h, while the XRD pattern of the coating obtained after 2 hours (figure 4) of soaking in SCS1 solution shows already diffraction line (010) of triclinic OCP crystals. This could indicate a unique deposited phase. It seems that OCP crystals grow directly on the top of the first Ca-P film that dissolves partially in SCS1 solution. When the first Ca-P layer dissolves, it can initiate the deposition of OCP ($Ca_8H_2(PO_4)_6,5H_2O$). Its precipitation resulted in a slight decrease of pH in SCS1. This mechanism can be illustrated by the following the reaction (1):

$$8Ca^{2+} + 6HPO_4^{2-} + 5H_2O \rightarrow Ca_8H_2(PO_4)_6,5H_2O + 4H^+ \ (1)$$
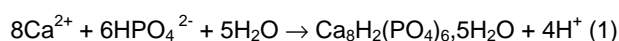
Besides the influence of the seeding role of the Ca-P film on the nature of the subsequent Ca-P coating, authors have shown that the formed phase depends on the characteristics of the soaking supersaturated solution [17-20]. Furthermore several phases can precipitate at the same conditions. It has been

quite well established that the precipitation of Ca-P obeyed to solubility and kinetics of the different possible phases in the supersaturated solution [20]. Indeed the most soluble product is kinetically favored. In our experiments, SCS1 solution is supersaturated in respect to both HA and OCP phases. HA is the most thermodynamically stable Ca-P phase at physiological conditions but OCP, more soluble than HA, is thus kinetically favored compared to HA [21]. Subsequently OCP, being a metastable phase, can transform into more thermodynamically stable Ca-P phases [15,20,22]. For instance, OCP has been detected *in vitro* as an intermediate before the formation of HA [15,20]. However, other studies [12,19,21] have isolated stable OCP crystals at physiological conditions. In our study, the thick OCP layer is stable while the soaking time is increasing. The OCP coating continuously grows while the supersaturation in SCS1 solution decreases.

The crystals appear perpendicularly oriented to the substrate. However the crystal growth evolves during the coating formation. Firstly, the crystals start to nucleate allover the sample surface at the vicinity of each other, growing mainly along the (010) direction (fig. 4b), and they spread allover the substrate following the 3 dimensions in the space as shown in fig 1b. Subsequently, OCP crystals grow following (-101) and (002) plans to the detriment to (010) plan (fig 4c-d), indicating a specific oriented growth along the z-axis. This specific orientation is mainly due to the relative substrate flatness. The crystals cannot extend anymore freely on the Ti6Al4V surface along the x and y-axis due to a steric effect. This hindrance is well illustrated in figure 5, whereby the primary OCP crystals rose perpendicularly to the substrate (fig 5a), the rose-like OCP crystal nucleated on the top of the primary crystals, could grow freely along x, y and z-axis.

CONCLUSION

A two-step biomimetic procedure allowed the formation of an OCP coating of 55 μm in thickness. First a thin and amorphous carbonated Ca-P film was uniformly deposited on Ti6Al4V substrate. Subsequently, this film induced the nucleation and growth of OCP crystals with a specific orientation, by soaking into a second solution. The biomimetic approach allows thereby the formation of new Ca-P phases as coatings on Ti6Al4V substrate that need to be tested *in vitro* and *in vivo*

References

1- R.G.T. Geesink and N.H.M. Hoefnagels, *J. Bone and Joint Surg.*, **77B** (1995) p534.

2- T. Kokubo, H. Kushitani, Y. Abe and T. Yamamuro, *Bioceramics* **2** (1990) p235.

3- P. Layrolle, C.A. van Blitterswijk and K. de Groot, *Bioceramics* **11** (1998) p465.

4- F. Barrere, P. Layrolle, C.A. van Blitterswijk, K. de Groot, in Proceedings of the Material Research Society on Mineralization in natural and synthetic biomaterials, 2000, under press

5- P. Li, I. Kanganesniemi, K. de Groot and T. Kokubo, *J. Am. Ceram. Soc.* **77** (1994) p1307.

6- T. Peltola, M. Patsi, H. Rahiala, I. Kangasniemi and A. Yli-Urpo, *J. Biomed. Mater. Res.* **41** (1998) p504.

7- P. Li and P. Ducheyne, *J. Biomed. Mater. Res.* **41** (1998) p341.

8- Legeros, R.Z, in "Biological and synthetic apatites. In Hydroxyapatite and Related Materials" edited by P.W. Brown and B. Constanz (CRC Press, Roca-Batton, 1994) p3.

9- Brown W.E., *Nature* **196** (1962) p1048

10- F. Sugihara, H. Oonishi, S. Kushitani, N. Iwaki, Y. Mandai, K. Minamigawa, E. Tshuji, M. Yoshikawa and T. Toda, *Bioceramics* **8** (1995) p89.

11- O. Suzuki, M. Nakamura, Y. Miyasaka, M. Kagayama and M. Sakurai, "Bone formation on synthetic precursors of hydroxyapatite", *Tohoku J. Exp. Med.* **164**, 37-50 (1991)

12- F. Barrere, P. Layrolle, C.A. van Blitterswijk and K. de Groot, *Bone* **25** (1999) p107S.

13- B.O.Fowler, M. Markovic and W.E. Brown, *Chem. Mater* **15** (1993) p1417.

14- Joint Comity for Powder Diffraction Standards, OCP 26-1056 (1992)

15- E.D. Eanes and J.L. Meyer, *Calcif. Tiss. Res.* **23** (1977) p259.

16- E.C. Moreno and K. Varughese, *J. Crystal Growth* **53** (1981) p20.

17- R.Z. LeGeros, R. Kijkowska and J.P. LeGeros, *Scanning Electron Microscopy* **IV** (1984) p1771.

18- P.T.Cheng and K.P.H. Pritzker, *Calcif. Tissues Int.* **35** (1983) p596.

19- M. Iijima, H. Kamemizu, N. Wakamatsu, T. Goto, Y. Doi and Y. Moriwaki, *J. Crystal Growth* **112** (1991) p467.

20- M.J.J.M. van Kemenade and P.L. de Bruijn, *J. Colloid and Interface Science* **118** (1987) p564

21- J.C. Heughebaert and G.H. Nancollas, *J. Phys. Chem.* **88** (1984) p 2478.

22- R.Z. Le Geros, G. Daculsi, I. Orly, T. Abergas and W. Torres, *Scanning Microscopy* **1** (1989), p129.

A CRYSTAL GROWTH STUDY OF OCTACALCIUM PHOSPHATE COATING AND INHIBITION BY MAGNESIUM AND CARBONATE

F. Barrère, P. Layrolle, C.A. van Blitterswijk and K. de Groot

ABSTRACT

The biomimetic approach for coating metal implants allows the deposition of new calcium phosphate (Ca-P) phases. Films elaborated at physiological conditions might have structures closer to bone mineral than Hydroxylapatite (HA) plasma-sprayed coatings. In this study, different Ca-P coatings have been deposited through a two-step procedure. After cleaning and etching, Ti6Al4V plates were pre-treated by soaking into a Simulated Body Fluid concentrated by five (SBFx5): a thin amorphous carbonated Ca-P layer precipitated on the metal substrate. Secondly, by soaking these thinly coated metal substrates into another Supersaturated Calcifying Solution (SCS), with different concentrations, the thin amorphous carbonated Ca-P layer led to the fast precipitation of a second and thick Ca-P layer. From the SCS containing only Ca^{2+} and HPO_4^{2-} ions, an OCP layer grew epitaxially on the substrate. When Mg^{2+} was added into this SCS, the coating was composed of Ca-deficient apatite crystals. While the addition of HCO_3^- in SCS led to the formation of a B-carbonated apatite layer. Magnesium and carbonate acted as inhibitors of OCP growth. The 3 phases obtained by our biomimetic process are significantly different in structure composition in comparison with plasma-sprayed HA coatings. Thereby, the obtained results may be particularly relevant for further *in vivo* investigations to evaluate the bioactivity of these novel biomimetic Ca-P coatings.

INTRODUCTION

Titanium alloys (Ti6Al4V) coated with plasma sprayed hydroxylapatite (HA) are currently used as orthopedic hip prostheses. Despite excellent clinical results [1], plasma-sprayed HA coatings have specific drawbacks related to the extremely high processing temperatures and lines of sight application. For instance, one can only plasma-spray a limited number of calcium phosphate (Ca-P) phases. Octacalcium phosphate $Ca_8H_2(PO_4)_6,5H_2O$ (OCP) which has been proposed as bone mineral precursor [2,3], or carbonated apatites closer to bone mineral structure [4] cannot be obtained by plasma-spraying. However these Ca-P phases may demonstrate, *in vivo*, bioactive specificities beneficial for the osseointegration of implants.

Recently, several groups have focused their attention to a biomimetic approach for coating implants [5,6]. This technique consists at soaking metals into Simulated Body Fluids (SBF) that mimic the inorganic composition of human blood plasma. As a result, bone-like apatite coatings have been deposited on their surface under modulated nucleation and crystal growth conditions. In contrast to plasma-spraying technique, the biomimetic method offers the possibility to cover complex shaped implants. In addition, different Ca-P phases can be elaborated as coatings, knowing that the nucleation and growth of Ca-P crystals can be controlled by the composition and concentrations of the salts in the soaking solutions [7,8].

In this study, the various Ca-P coatings were prepared from calcifying solutions by changing their composition. In particular, the addition of magnesium and carbonate has been studied. Indeed both ions are known to play a role of inhibition of crystal growth in bone biomineralization process [9].

MATERIALS AND METHODS

The principle of our biomimetic process is a two-step procedure. Firstly the samples were pretreated by soaking into SBFx5 solution for 24 hours. Secondly, pretreated samples were soaked into SCS1 containing only Ca^{2+} and HPO_4^{2-}, SCS2 containing Mg^{2+} or SCS3 containing HCO_3^- (table 1).

Pretreatment of the Ti6Al4V substrate

Ti6Al4V ($10x10x1mm^3$) plates were ultrasonically cleaned successively in acetone, ethanol (70%) and finally demineralized water. These plates were then etched for 10 minutes in a mixture of 2ml HF (40%) and 4ml HNO_3 (66%) in 1000ml of water. Subsequently, these Ti6Al4V plates were firstly soaked in SBFx5 solution (table 1), under high heterogeneous nucleation conditions for 24 hours at 37°C.

Calcifying treatments

The concentrations of the various calcifying solutions (SBFx5, SCS1, SCS2 and SCS3) are given table 1. The salts (Reagent grade, Merck) were precisely weighted (±0.01g) and dissolved into demineralized water. These calcifying solutions were buffered at physiological pH=7.40 at room temperature with TRIS-HCl 50mM, and they were filtrated trough a 0.22μm Millipore membrane.

	Na^+	K^+	Mg^{2+}	Ca^{2+}	Cl^-	HPO_4^{2-}	SO_4^{2-}	HCO_3^-
HBP	142.0	5.0	1.5	2.5	103.8	1.0	0.5	27.0
SBFx5	733.5	0.0	7.5	12.5	740.0	5.0	0.0	21.0
SCS1	140.4	0.0	0.0	3.1	142.9	1.86	0.0	0.0
SCS2	140.4	0.0	1	3.1	142.9	1.86	0.0	0.0
SCS3	140.4	0.0	0.0	3.1	142.9	1.86	0.0	5

Table 1: Inorganic composition (mM) of Human Blood Plasma (HBP), SBFx5 and the supersaturated calcifying solutions (SCS1, SCS2 and SCS3).

Calcification by SCS1: structure and kinetic study

Two non-pretreated samples as control and six pretreated samples were soaked individually and were placed vertically in a polystyrene vial containing 50ml of SCS1. The vials were sealed and incubated in a calibrated shaking water-bath at 37°C. After 2, 5 and 48 hours of immersion two samples were then taken out, rinsed with demineralized water and dried in air. The structure of the deposited Ca-P layer has been investigated by FTIR (Perkin-Elmer, Spectrum 1000), SEM/EDX (Philips, Model 525, 15 kV). Its evolution was studied by TF-XRD (Philips, model APDW40C).

Calcification by SCS2 and SCS3: influence of Mg^{2+} and HCO_3^- on coating structure

The soaking procedure was similar to the above procedure. For each solution, the 2 non-pretreated samples and 2 pretreated samples were soaked individually. After 48h of immersion, the samples were taken out, rinsed and dried in similar conditions than above. The structure and morphology of coatings were investigated as above by FTIR and SEM/EDX.

RESULTS

Pretreatment leading to Ca-P seeding on Ti6Al4V

After the first soaking step into SBFx5, SEM photo (fig 1a) showed a thin Ca-P layer uniformly deposited on the Ti6Al4V surface. By EDX (fig 2a), Mg, Na, Ca, P (from the coating) and Ti (from the substrate) were detected. Ti peaks as high as Ca peak indicated that the Ca-P film was very thin. The FTIR spectrum

(fig 3a) of this first layer showed featureless phosphate and carbonate bands. Phosphate groups exhibited broad and single bands at 560cm^{-1} (P-O deformation in PO$_4$ (ν_4)) and 1041cm^{-1} (P-O stretching in PO$_4$ (ν_3)). The carbonate bands were also observed at 1410cm^{-1} and 1450cm^{-1}. The FTIR spectrum was characteristic of a carbonated amorphous Ca-P. The TF-XRD pattern, displayed between 5° and 60°, of this Ca-P layer (fig 4a) corroborates with the FTIR observations. The halo or bump located at approximately 30° is typical of an amorphous phase, the other sharp peaks at 35.5°, 35.6°, 39.6° and 40.5° present were assigned to the Ti6Al4V substrate.

Calcifying treatments

Calcification by SCS1: structure and kinetic study

By soaking into SCS1, no precipitation occurred on the control sample. Whereas a macroscopically visible coating was deposited on the pretreated plates. Flake-like crystals of 35μm in length were seen (fig 1b) on the Ti6Al4V plates. All the crystal plates were oriented more or less perpendicularly to the surface of the plates. EDX (fig 2b) indicated that only Ca, P and O were present in the coating. The absence of Ti peak showed that the coating is thicker than the Ca-P seeded surface. The FTIR spectrum of the coating after 48hours of immersion is typical of OCP (fig 3b) [10]. The single large P-O band of the Ca-P seeded surface at 560cm^{-1} evolved to 2 fine bands at 560cm^{-1} and 600cm^{-1}, with two thin shoulders at 628cm^{-1} (H$_2$O libation) and 527cm^{-1} (ν_4 HPO$_4^{2-}$ bend). The broad and single P-O band at 1041cm^{-1} exhibited a fine structure with vibrations and shoulders at 1025cm^{-1} and 1011cm^{-1}. Characteristic HPO$_4^{2-}$ bands of OCP were also noticed at 906cm^{-1} and 852cm^{-1}. The OCP phase appeared predominant and its proportion increased with the soaking time as we can see on the TF-XRD patterns (fig 4b, c, d). The diffraction lines of the Ti6Al4V substrate and the Ca-P seeded surface disappeared while sharp diffraction lines of OCP were appearing. This indicates that the coating has grown and presents a high crystallinity. The diffraction lines (-101) at 16.09° and (002) at 26.10° had the highest relative intensity (fig 4d).

Calcification by SCS2 and SCS3: influence of Mg^{2+} and HCO$_3^-$ on coating structure

By soaking into SCS2, no precipitation occurred on the control sample. Whereas a macroscopically visible coating was deposited on the pretreated plates. As compared to the original OCP coating, SEM photo of the coating (fig 1c) showed that the layer was denser and exhibited smaller crystals (approximately 1μm). On the EDX spectrum (fig 2c), one can see that a minor

Ti peak remains present while it was absent for the original OCP coating (fig 2b). Soaking into SCS2 led to a thinner layer than soaking into SCS1. EDX measurements indicated also that Mg and Na were incorporated in the Ca-P layer. The incorporation of magnesium ions was estimated by measuring the peaks counts. It resulted that 1 Mg^{2+} was present in the coating for 27 Ca^{2+} (Mg/Ca=0.037), i.e. approximately 11.5% of Mg^{2+} from the solution precipitated in the coating in that time period. Furthermore, the structure of the coating was different from OCP, as shown by the FTIR spectrum (fig 3d). The phosphate bands were broad and characteristic of less crystallized structures. The thin shoulders at 630cm^{-1} (H_2O libation) and 527cm^{-1} (v_4 HPO_4 bend) and the OCP band at 906cm^{-1}, as originally seen in fig 3b, were not detected. One single HPO_4 stretching (P-(OH)) remained at 870cm^{-1} and one single v_1 PO_4 stretching remains at 960cm^{-1}. Thereby, the structure of this layer was typical of a Ca-deficient apatite.

By soaking into SCS3, no precipitation occurred on the control sample. Whereas a macroscopically visible coating was deposited on the pretreated plates. SEM photo of the coating showed a denser coating with smaller crystals (fig 1d) than the Ca-deficient layer (fig 1c). EDX spectrum (fig 2d) showed only Ca, P and O elements in contrast to the Ca-deficient coating where Ti peak was present. Soaking into SCS3 led to a denser and thicker layer than by soaking into SBF2. The FTIR spectrum of this coating (fig 3c) exhibited carbonate bands at 1460cm^{-1} and at 1416cm^{-1}. Similar phosphate bands than the previous structure were observed (fig 3d): HPO_4 stretching (P-(OH)) at 870cm^{-1} and one single v_1 PO_4 stretching at 960cm^{-1}. Therefore, the deposited coating was composed of a B-carbonated apatite [12].
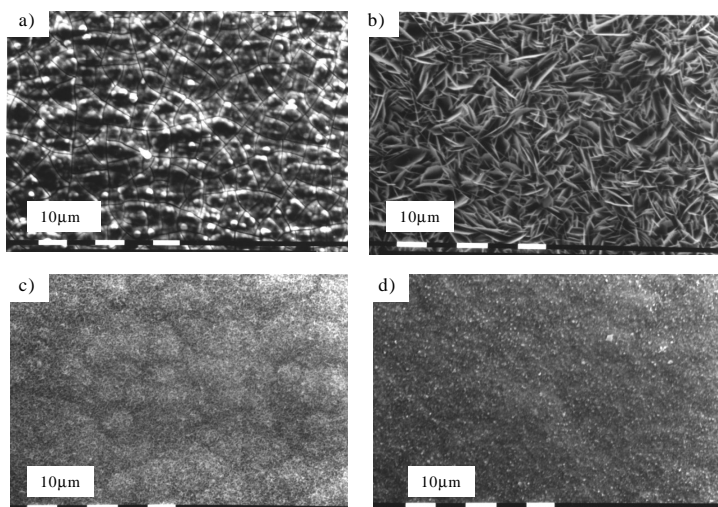

Figure 1: SEM photos of a) Ca-P seeded substrate obtained after immersion in SBFx5, b) coating obtained after 48hours immersion in SCS1, b) coating obtained after 48hours soaking in SCS2, d) coating obtained after 48 hours soaking in
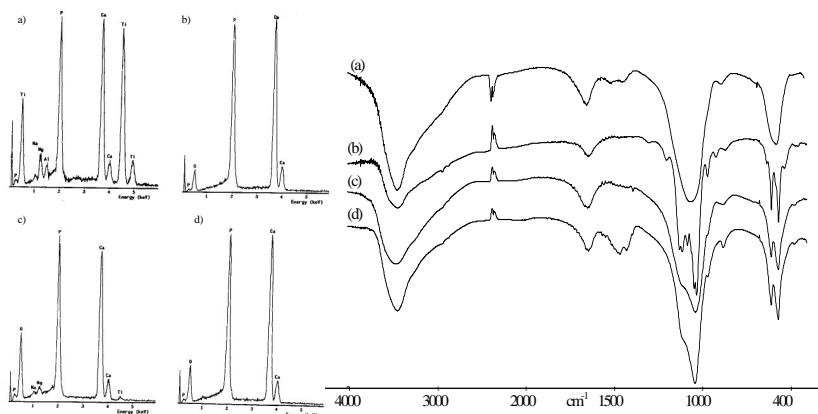
Figure 2: EDX spectra after immersion in a) SBFx5, b) SCS1, c) SCS2, d) SCS3

Figure 3: FTIR spectra of the various coatings after immersion in a) SBFx5 b) SCS1, c) SCS2, d) SCS3
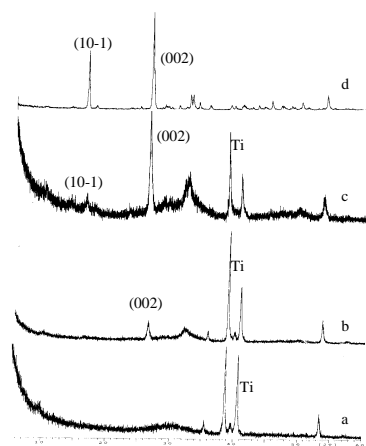

Figure 4: Evolution of the Ca-P coating obtained by immersion in SCS1 at a) t=0h, b) t=2h, c) t=5h, d) t=48h.

DISCUSSION

Pretreatment leading to Ca-P seeding on Ti6Al4V

As no precipitation occurred on any control samples, the Ca-P seeded surface was mandatory to induce the deposition of different Ca-P phases. The amorphous particles of this thin layer obviously act as nucleation sites for growth of additional Ca-P crystals; we could suggest that a partial dissolution process of the Ca-P nuclei might initiate the deposition of the second layer. At

the interface between the substrate and the solution, the supersaturation would increase and subsequently would initiate the precipitation of the Ca-P coating.

Calcifying treatments

Calcification by SCS1: structure and kinetic study

By immersing into SCS1, a unique phase composed of OCP crystals grew epitaxially on the substrate. The formation can be illustrated by the reaction (1):

$$8Ca^{2+} + 6HPO_4^{2-} + 5H_2O \rightarrow Ca_8H_2(PO_4)_6,5H_2O + 4H^+ \quad (1)$$
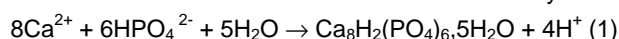
Unlike previous results [13,14], the thick OCP layer is stable during the entire experiment and the coating continuously grows while the supersaturation of SCS1 decreases as the soaking time increases. As, in our experiments, a unique phase grew epitaxially on the substrate OCP crystals may contain very few defaults through its lattice. Thus, the absence of failures in the crystal improves its stability and avoids its hydrolysis into other Ca-P phases.

Calcification by SCS2 and SCS3: influence of Mg^{2+} and HCO_3^- on coating structure

The addition of magnesium led to the deposition of a poorly crystallized Ca-deficient apatite coating containing Mg^{2+}. As previously reported, depending on Ca/Mg ratio and pH, magnesium is known to retard or inhibit the crystallization of several Ca-P phases [15-19]. Our results are comparable to those reported by Eanes et al [17]: few Mg^{2+} from the solution were incorporated into the precipitate. He concluded that Mg^{2+} markedly influence Ca-P crystallization without being significantly incorporated in the precipitate. The magnesium ions hardly enter the lattice but interfere with the formation OCP by favoring Mg-P complexes rather than Ca-P complexes [15]. If we maintain the hypothesis that the Ca-P seeded surface partially dissolves in the calcifying solution, the phosphate ions released in SCS2 might complex more easily with Mg^{2+} than with Ca^{2+}. Thereby, the Ca-P deposition should be affected leading to a precipitation of a less crystalline layer i.e. Ca-deficient apatite instead of OCP.

The presence of carbonate ions in SCS3 affects also OCP precipitation. In spite of a similar inhibitory effect, the mechanism of inhibition by HCO_3^- is different than the one with Mg^{2+}. Indeed, the incorporation of carbonate ions in the crystal lattice is obviously shown on FTIR spectrum (fig 3c), indicating a substitution of phosphate by carbonate in the lattice. Iijima et al. [18] showed that OCP growth was favored even in presence of carbonate, at physiological conditions. In our experiments, for similar carbonate concentration, but for higher Ca/P ratios, the structure of the coating is a B-carbonated apatite. If we consider as supposed above that the seeded Ca-P layer partially dissolves in SCS3, Ca^{2+}, Mg^{2+} and HPO_4^{2-}, HCO_3^- ions are released at the vicinity of the substrate. The supersaturation is raised at the

interface solid-solution and, thereby leading to the precipitation of B-carbonated apatite instead of OCP. In the mean time, Mg^{2+} released from the Ca-P seeded surface can also enhance the inhibitory effect of carbonate ions, as discussed by Iijima et al. [20]. Indeed, Mg^{2+} might complex with phosphate ions present in SCS3 and thereby, favor the substitution by carbonate ions.

CONCLUSION

After seeding Ti6Al4V plates with an amorphous carbonated Ca-P layer, the immersion in various SCS solutions led to the deposition of different Ca-P phases, depending on the composition of the calcifying solution. OCP crystals grew epitaxially on this Ca-P seeded surface when immersed in SCS1. Magnesium and carbonate ions markedly affected the structure of the Ca-P coating by different mechanisms. At pH=7.4 and at 37°C, by soaking into SCS2, a Ca-deficient apatite coating was obtained, and by soaking into SCS3, a B-carbonated apatite was deposited. These three Ca-P phases are unable to be elaborated by high temperature processes such as plasma-spraying. Further *in vitro* and *in vivo* investigations shall be conducted in order to evaluate their osteogenic potential.

References

1-Havelin LI, Engesaeter LB, Espehaug B, Furnes O, Lie SA, Vollset SE. "The norvegian arthroplasty register: 11 years and 73000 arthroplasties." Acta Orthop Scand 71: 337-353; 2000

2-LeGeros, R.Z. Biological and synthetic apatites. In Hydroxyapatite and Related Materials. Ed P.W. Brown and B. Constanz, CRC Press; 1994.

3-Brown W.E., Octacalcium phosphate and hydroxyapatite. Nature 196:1048-55; 1962.

4-Rey, C. Calcium phsphate biomaterials and bone mineral. Differences in composition, structures and properties. Biomaterials 11:13-15; 1990.

5-Kokubo, T., Kushitani, H., Abe, Y., Yamamuro, T. Apatite coating on various substrates in Simulated Body Fluid. Bioceramics 2:235-242, 1989.

6-Wen, H.B. Calcium Phosphate Coatings Based on Mineralization in Natural Hard Tissues. PhD; 1998.

7-Cheng, P.T. and Pritzker, K.P.H. Solution Ca/P ratio affects calcium phosphate crystal phases. Calcif. Tissues Int 35:596-601; 1983.

8-de Rooij, J.F., Heughebaert, J.C. and Nancollas, G.H. A pH study of calcium phosphate seeded precipitation. J. Colloid Interface Sci. 100.2:350-358; 1984.

9-Fleisch, H. Inhibitors of calcium phosphate precipitation and their role in biological mineralization. J. Crystal Growth 53:120-134; 1981

10-Fowler, B.O., Markovic, M. and Brown, W.E. Octacalcium Phosphate. 3. Infrared and Raman Vibrational Spectra. Chem. Mater l5:1417-1423; 1993.

11-JCPDS. OCP 26-1056; 1992.

12-Heughebaert, J.C. Contribution a l'etude de l'evolution des orthophosphates de calcium precipites amorphes en orthophosphates apatitiques. These d'Etat INP Toulouse; 1977.

13-Eanes, E.D. and Meyer, J.L., The maturation of crystalline calcium phosphates in aqueous suspensions at physiological pH. Calcif. Tiss. Res. 23:259-269; 1977.

14-Moreno, E.C. and Varughese, K. Crystal growth of calcium apatite from dilute solutions. J. Crystal Growth 53:20-30; 1981.

15-Bachara, B.N. and Fisher, H.R.A. The effect of some inhibitors on the nucleation and crystal growth of apatite. Calc. Tiss. Res 3:348-357; 1969.

16-Nancollas, G.H., Tomazic, B. and Tomson, M. The precipitation of calcium phosphates in the presence of Magnesium. Croatia Chem. Acta 48:431-438; 1976.

17-Eanes, E.D. and Rattner, S.L. The effect of magnesium on apatite formation in seede supersaturated solutions at pH=7.4. J. Dent. Res 60:1719-1723; 1981.

18-Iijima, M., Kamemizu, H., Wakamatsu, N., Goto, T., Doi, Y. and Moriwaki, Y. Effects of CO_3^{2-} ion on the formation of octacalcium phosphate at pH=7.4 and 37°C. J.Crystal Growth 135:229-234 ;1994.

19-Kibalczyc, W., Christoffersen, J., Christoffersen, M.R., Zielenkiewicz, A. and Zielenkiewicz, W. The effect of magnesium ions on the precipitation of calcium phosphates. J. Crystal Growth 106:355-366; 1990.

20-Iijima, M. and Moriwaki, Y. Effect of inorganic on morphology of octacalcium phosphate grown on cation selective membrane at physiological temperature and pH in relation to enamel formation. J. Crystal Growth 96:59-64; 1989.

CHAPTER 7
Section 1

PHYSICAL AND CHEMICAL CHARACTERISTICS
OF PLASMA-SPRAYED AND BIOMIMETIC APATITE COATING

F. Barrère, P. Layrolle, C.A. van Blitterswijk and K. de Groot

ABSTRACT

Hydroxylapatite (HA) coatings on titanium alloy (Ti6Al4V) implants are widely used in orthopaedics because of the strong mechanical properties of this metal combined with the osteoconductive properties of calcium phosphate (Ca-P). HA coatings are commonly applied on metal prostheses by plasma spraying. However, this technique presents important drawbacks: inability to cover porous implants and to incorporate biologically active agents, delamination and particles release. Recently, a biomimetic approach has been developed for coating metal implants. This method, which mimics biomineralization allows the deposition of a bone-like apatite layer on metal prosthesis. In this study, cleaned and etched Ti6Al4V samples were firstly immersed into a Simulated Body Fluid concentrated by 5 (SBFx5) solution at 37ºC and secondly into a modified simulated body fluid solution containing less inhibitors of crystal growth (e.g. Mg^{2+}, HCO_3^-). A bone-like apatite layer of about 15µm precipitated on the titanium alloy surface. Scratch testing showed that biomimetic carbonate apatite coating (BCA) is more elastic than the brittle HA-PSC. Both coatings present similarities and dissimilarities, which are mainly due to their microstructure specific to the processing.

INTRODUCTION

Hydroxylapatite (HA) coatings on metal prostheses enhance bone growth because of their osteoconductive property. Several techniques, such as plasma-spraying, have been developed for coating HA on metals. Despite the excellent clinical results up to 10 years with HA plasma-sprayed coatings (HA-PSC), there are specific drawbacks such as the inability to cover porous shapes and to incorporate biologic agents, delamination and particle release of insoluble HA particles. In view of such disadvantages, there is an increasing interest to develop a biomimetic strategy for the preparation of apatite coatings on metal implants [1-3], which might possess many favourable characteristics. This method, that resembles the biomineralization process of calcified tissues, involves the nucleation and growth of bone-like apatite crystals on metal surfaces from supersaturated solutions at ambient temperatures. The advantages of the biomimetic technique are that porous shapes can be covered; biologically active agents can possibly be incorporated into the biomimetic coating, and the deposition of new Ca-P phases as coatings. In this study, the chemical and physical properties of both biomimetic carbonate apatite coating (BCA) and HA-plasma sprayed coating (HA-PSC) are compared.

MATERIALS AND METHODS

Preparation of the samples
Commercially available plasma-sprayed HA coated titanium alloy (Ti6Al4V) plates of 20x20x1 mm^3 were used as reference.
Prior to applying the biomimetic coating, the Ti6Al4V plates were sand-blasted. The samples were then cleaned successively by acetone, ethanol (70%) and finally demineralized water. The plates were firstly soaked into a Simulated Body Fluid concentrated by 5 (SBFx5) [3] under high heterogeneous nucleation conditions for 24 hours at 37°C. Secondly the plates were immersed into a modified SBF solution containing less inhibitors of crystal growth (i.e. Mg^{2+} and HCO_3^-) at 50°C. Finally, the coated plates were cleaned with demineralized water and dried in air over night.

Chemical and structural characterisation of HA-PSC and BCA
Both calcium phosphate (Ca-P) coatings were studied in the same experimental conditions. Ca/P ratio of both coatings was determined by Atomic Absorption Spectrometry (AAS) for [Ca] and by spectrophotometry for [P]. The structure of the coating was investigated by Infra-Red spectroscopy (FTIR, Perkin Elmer 1000), Scanning Electronic Microscopy (SEM, Philips 525) and Thin Film-X-Rays Diffraction (TF-XRD, Philips APDW40C). The crystallinity was calculated according to ASTM standards [4]. The thickness of the coating was determined by magnetic induction (Electrophysik Minitest 2100).

Scratch testing of HA-PSC and BCA

Scratch tests were performed by applying a progressive load (0-30N) with a spherical diamond stylus of 100 μm (MST-CSEMEX®). Critical load (L_c) has been defined at a constant acoustic emission sensitivity.

Dissolution study of HA-PSC and BCA

The dissolution of the coating has been performed by soaking into Simulated Physiological Solutions [5] (SPS) and buffered at pH=3 with a mixture of Khphtalate and HCl 1M, and at pH=7.3 with a mixture of TRIS and HCl 1M. Each coated plate was individually soaked into 10ml of SPS at 37°C. 100μl of SPS pH=3 or pH=7.3 was performed after 10, 30, 60, 120, 180, 300 and 540min. [Ca] released in SPS was measured in triplo by AAS.

RESULTS

Chemical and structural characterisation of HA-PSC and BCA

The atomic ratio Ca/P of HA-PSC was 1.67 that corresponds to stoichiometric HA, $Ca_{10}(PO_4)_6(OH)_2$ and the FTIR spectrum (fig1a) was typical of HA. TF-XRD (fig1b) of HA-PSC showed thin diffraction lines characteristic of HA above a bump corresponding to an amorphous phase. The crystallinity of HA-PSC was 67%, and the thickness was about 50μm.

The atomic ratio Ca/P of BCA was 1.55 typical of a Ca-deficient apatite. The FTIR spectrum shows bands assigned to AB-carbonated apatite (fig1a). TF-XRD pattern of BCA (fig1b) exhibited broad diffraction lines characteristic of tiny apatite crystals, indicating that BCA was 55% crystalline and the thickness was about 15μm.
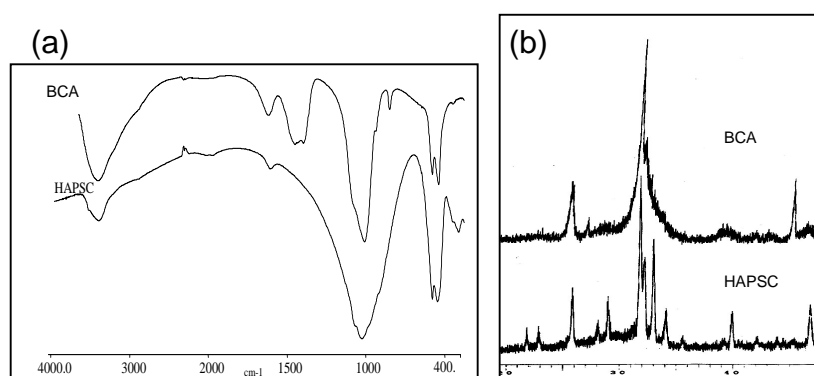

Figure 1 (a):FTIR spectra of BCA and HA-PSC, (b):XRD patterns of BCA and HA-PSC

Scratch testing of HA-PSC and BCA

HA-PSC failed at a critical load L_c=22N. A partial delamination of the coating around the track was observed (fig 2a). For BCA, the critical load occurred for a value L_c=7.5N. However, no coating delamination or spall off was observed in this case (fig 2b). BCA is more elastic than the brittle HA-PSC.
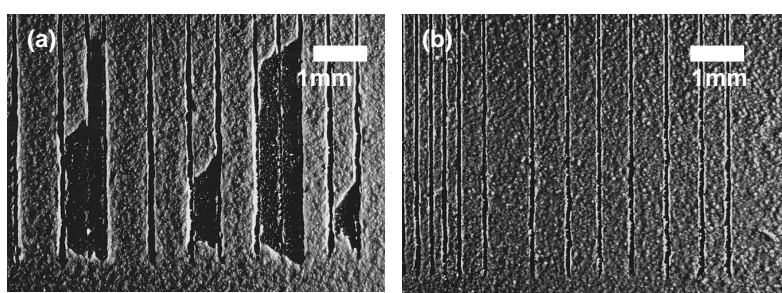

Figure 2: Micrographs of (a) HA-PSC and (b) BCA after scratch testing

Dissolution study

In acidic medium (pH=3), a fast dissolution was observed for both coatings (fig 3a). In the case of HA-PSC, the initial dissolution rate was about 1.8 ppm/min. Later, [Ca] was released slower and reached 373ppm after 540min of immersion into SPS. In the case of BCA, [Ca] increased rapidly in SPS solution with an initial rate of 2.65 ppm/min. Subsequently, the curve reached a plateau at 95ppm. The coating was completely dissolved after 60min of immersion in SPS pH=3. BCA dissolved faster than HA-PSC. However, both coatings were totally dissolved at the end of the experiments.

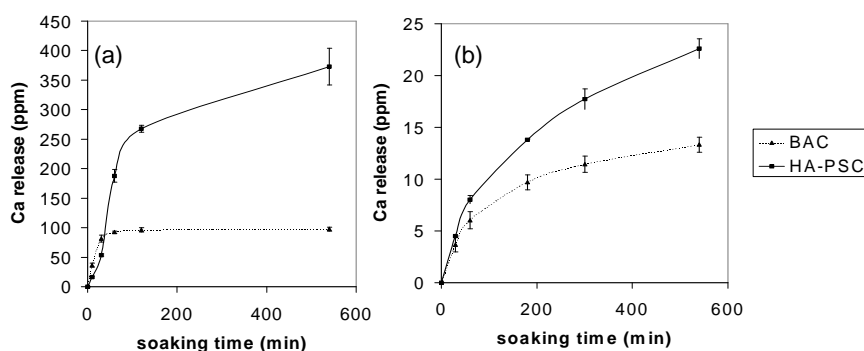Figure 3: Cumulative Calcium release from SPS at pH=3 (a) and from SPS at pH=7.3 (b)

At neutral pH, Ca^{2+} release curves of BCA and HA-PSC increased with the soaking time (fig 3b). The dissolution profile was similar for BCA and HA-PSC. Both coatings dissolved relatively rapidly during the first soaking hour with initial rates of 0.130 and 0.100 ppm/min for HA-PSC and BCA, respectively. At

the end of the experiments (540min) both coatings were partially dissolved: 22.6 ppm of Ca^{2+} is released from HA-PSC whereas 13.3 ppm of Ca^{2+} was released from BCA.

DISCUSSION

HA-PSC and BCA are structurally different. HA-PSC is composed of HA, whereas BCA is composed of AB-carbonated apatite. In composition, BCA contains CO_3 substituted groups as bone like mineral. In addition, the XRD pattern of both coatings showed that the HA-PSC is composed of two distinct phases: a purely amorphous and a purely crystalline phase. Their relative contribution in HA-PSC was respectively 33% and 67%. On the contrary, the XRD pattern of BCA indicated broader diffraction lines, signifying that the crystals composing this coating are relatively small compared to the crystalline HA phase. These XRD patterns emphasized marked microstructural differences: on one hand, HA-PSC is composed of two distinct phases, and on the other hand BCA is uniformly composed of small apatitic crystals. These differences in microstructure and composition were emphasized in the mechanical tests and in the *in vitro* dissolution test.

On one hand, scratch tests indicated that HA-PSC has better adhesion properties than BCA. However, BCA is more elastic than the brittle HA-PSC. The observed delamination is due to the propagation of micro-cracks and failures through HA-PSC. These micro-cracks can possibly to initiate particles release and delamination of plasma-sprayed coatings *in vivo.*

On the other hand, the dissolution rate was different for BCA and for HA-PSC. This difference is most likely due to the coating composition. Indeed, previous studies showed that the dissolution rate for HA is slower than for synthetic carbonated apatite [6]. In addition, the dissolution of the two coating is also certainly based upon the coatings microstructure. The amorphous phase composing the HA-PSC shall dissolve much faster than the crystalline HA, whereas BCA shall dissolve in a more gradual manner due to the uniformity of its microstructure.

Finally, BCA is closer in structure to bone mineral than HA-PSC. Similar layer forms *in vivo* at the interface between the Ca-P implant and the hosting bone [7,8]. The implantation of a synthetic bone-like apatite should be investigated in order to evaluate whether mimicking bone mineral would be beneficial towards bone response.

CONCLUSION

The biomimetic method on Ti6Al4V implants led to the deposition of a bone-like apatite layer of 15μm in thickness. This film is less brittle than HA-plasma-sprayed coating, and it is more uniform in structure. These specific features

intrinsic to the biomimetic process might be beneficial to prevent delamination, and release of insoluble coating's particles *in vivo*.

References

1-T. Kokubo, H. Kushitani, Y. Abe and T. Yamamuro, *Bioceramics*, 2, 235-242, 1990.

2-P. Li, I. Kanganesniemi, K. de Groot and T. Kokubo, *J. Am. Ceram. Soc.*, 77, 1307-1312, 1994.

3-F. Barrere, C.A. van Blitterswijk, K. de Groot and P. Layrolle. *Biometarials* (in press).

4-J.S. Flach, L.A. Shimp, C.A. van Blitterswijk and K. de Groot, *ASTM STP 1196*, 1993.

5-P. Ducheyne, S. Radin, M. Heughebaert and J.C. Heughebaert, *Biomaterials*, 11, 1990.

8-D.G.A. Nelson, J.D.A. Featherstone, J.F. Duncan and T.W. Cutress, *Caries. Res*, 17, 200-211, 1983

6-R.Z. LeGeros, G. Daculsi, I. Orly, M. Gregoire, M. Heughebaert, M. Gineste and R. Kijkowska. In: *Bone-bonding biomaterials*, 201-212, 1993.

7-J. Wolke, K. de Groot and J.A. Jansen. *J. Biomed Mater. Res.*, 39, 524-530, 1998.

IN VITRO DISSOLUTION OF VARIOUS CALCIUM PHOSPHATE COATINGS ON TITANIUM

F. Barrère, M. Stigter, P. Layrolle, C.A. van Blitterswijk and K. de Groot

ABSTRACT

The biomimetic route allows the formation of various calcium phosphate (Ca-P) coatings that cannot be produced by the most usual technique: plasma-spraying. Amorphous carbonated Ca-P (ACCP), octacalcium phosphate (OCP) and carbonated apatite (BCA) coatings could be prepared by the biomimetic route on titanium alloy (Ti6Al4V) plates. The *in vitro* dissolution of these biomimetic Ca-P coatings were compared with a commercially available Hydroxyapatite (HA) plasma-sprayed coating. The overall coatings of similar thickness (~30μm) were soaked into various media: simulated physiological solution at pH=7.3 (physiological conditions), pH=5.0 (inflammatory conditions) and pH=3.0 (total dissolution), and in a cell-culture medium (α-MEM). The dissolution rate of these various Ca-P coatings was determined by measuring the calcium release by Atomic Absorption Spectroscopy. Our results showed that the more acidic the medium was, the faster the coating dissolved. Furthermore, depending on the pH, the dissolution sequence of decreasing dissolution rate differs: at pH=7.3, ACCP>HA>BCA>OCP; at pH=5.0 ACCP<OCP<HA<BCA and at pH=3.0 ACCP<OCP<BCA<HA. These different dissolution rates can be explained by specific solubilities, crystal size and microstructure of the coatings. On the other hand, all the Ca-P coatings soaked into α-MEM evolved to a carbonated apatite structure resulting from ionic exchanges between the coating and the surrounding medium.

INTRODUCTION

Calcium phosphate (Ca-P) coatings on titanium (Ti) and alloys (Ti6Al4V) are widely used in orthopedic surgery because of the excellent mechanical properties of metals combined with osteoconductivity of bioceramics. The bioactivity of Ca-P is due to a controlled dissolution of this coating in bony environment. The Ca^{2+} release activates osteoblasts, enhancing bone formation onto the implant. Plasma-spraying technique has been successfully used for hydroxylapatite (HA) coating on metallic implants. However, plasma-spraying can only deposit thermally stable phases like HA on flat implants. The biomimetic route, which occurs in aqueous media and at low temperature [1-3], allows the even deposition of various Ca-P coating structures on porous implants. The aim of this work was to study the *in vitro* dissolution rates of various biomimetic Ca-P coatings and to compare their dissolution behavior with a commercially available HA-plasma sprayed coating.

MATERIALS AND METHODS

Biomimetic Ca-P coating preparation

First, 20 grit-blasted Titanium alloy plates (Ti6Al4V, 20x20x1 mm^3) were cleaned in acetone, ethanol (70%) and demineralized water under sonification. Secondly, these plates were soaked into a highly supersaturated calcifying solution (SBFx5) in order to seed Ti6Al4V plates with Ca-P nuclei. Thirdly, these plates were soaked into another calcifying solution: 6 plates were soaked several times into SBFx5 solution, 6 plates were immersed into a supersaturated calcifying solution (SCS1), and 6 into a modified SBFx5 solution (mSBFx5) containing less Mg^{2+} and HCO_3^- than in SBFx5 solution (table 1).

	Na^+	Mg^{2+}	Ca^{2+}	Cl^-	HPO_4^{2-}	HCO_3^-
HBP	142.0	1.5	2.5	103.0	1.0	27.0
SBF	142.0	1.5	2.5	147.8	1.0	4.2
SBFx5	733.5	7.5	12.5	740.0	5.0	20.0
SCS1	140.4	0.0	3.1	142.9	1.86	0.0
mSBFx5	702.0	2.5	12.5	714.5	5.0	10.0

Table 1: Composition in mM of Human Blood Plasma (HBP), regular SBF solution and the various Supersaturated Calcifying Solutions (SBFx5, SCS1, mSBFx5)

The preparation of SBFx5 and mSBFx5 solutions was possible by the supply of carbon dioxide (CO_2) gas [4], whereas SCS1 was buffered at pH=7.4 by addition of TRIS and HCl. The plates were soaked as long as the final thickness for all the Ca-P coatings was approximately 30µm. The final Ca-P

coatings were characterized by Fourier Transform Infra-Red (FTIR) and Environmental Scanning Electronic Microscopy (ESEM).

Initial dissolution rate determination

Dissolution tests were repeated three times for a Ca-P coating at one pH value. The test consisted at soaking Ca-P coated plates into simulated physiological solutions (SPS) buffered at pH=3.0, 5.0 and 7.3 at 37°C. Calcium ions (Ca^{2+}) release was measured by Atomic Absorption Spectroscopy (AAS) versus soaking time. The dissolution rate was determined at the early stage of the experiments.

Structure evolution of the coating in α-MEM

The various Ca-P coated Ti6Al4V plates were soaked into a cell culture medium, α-MEM (Gibco) for 1 week at 37°C in an incubator. The atmosphere of the incubator was maintained at 5% of CO_2 so that α-MEM was naturally buffered at pH=7.3. The structure of the coating was analyzed by FTIR spectroscopy and the coating morphology was observed by ESEM.
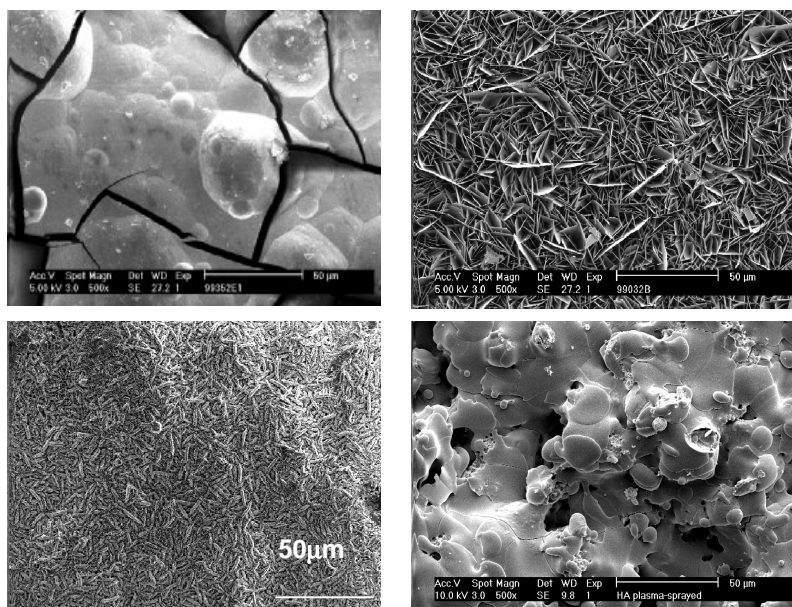
RESULTS

Figure 1: ESEM pictures of the various Ca-P coatings (bar 10μm): a) ACCP, b) OCP, c) BCA, d) HA plasma-sprayed coatings

Soaking into SBFx5 led to an amorphous carbonated Ca-P (ACCP) coating. The coating was smooth and dense (fig1a). In the case of soaking into SCS1,

ESEM photos showed that the coating was composed of sharp octacalcium phosphate (OCP) crystals vertically oriented of 30µm in length and 0.2µm in width (fig1b). Finally, soaking into mSBFx5 led to a carbonated apatitic (BCA). By FTIR, the position of the carbonate (CO_3) groups indicated that the BCA coating had type AB carbonated apatite. This coating is composed of tiny crystals of approximately 2µm in size (fig1c). Finally the HA plasma-sprayed coating exhibited a smooth morphology that was composed of globules corresponding to the solidified HA droplets (fig1d).

Initial dissolution rate determination
For all the Ca-P coatings, the dissolution rates were pH-dependent. At low pH, the dissolution rates were higher than at neutral pH. Furthermore, the dissolution rate varied with the composition and structure of each coating. At pH=7.3, ACCP coating dissolved faster than the others as shown by the sequence ACCP>HA>BCA>OCP. At pH=5.0, ACCP exhibited also the fastest dissolution rate and the dissolution sequence was ACCP<OCP<HA<BCA. Finally, at pH=3, all the coatings were totally dissolved in 2-3 hours while ACCP was again more soluble than others as indicated by the dissolution sequence ACCP>OCP>BCA>HA (table 2).

pH	ACCP	OCP	BCA	HA
7.3	23.0	4.73	12.5	13.5
5.0	170.2	98.1	60.0	80.0
3.0	250.0	180.0	160.0	123.0

Table 2: Dissolution rate (in ppm/h) of the various Ca/P coatings

Structure evolution of the coating in α-MEM
Independently to their initial composition, all of the Ca-P coatings evolved into a carbonated apatitic structure already after 1 week of immersion into α-MEM. Figure 3 displays the initial FTIR structures of the various studied coatings, and figure 4 displays the FTIR structures of the coatings after 2 weeks of immersion in α-MEM. After immersion in α-MEM, the carbonate band appeared for OCP and HA coatings, and this band became more intense for ACCP and BCA coatings. In addition, ACCP coating became more crystalline as indicated by the splitting of the HPO_4^{2-} bands at approximately 560cm^{-1}.

DISCUSSION
Depending on the composition of SCS solutions, it is possible to change the structure and crystallinity of biomimetic Ca-P coatings. Previous studies *in vitro* [5,6] and *in vivo* [7] showed that the crystallinity, structure and morphology

were markedly influencing bone formation onto the Ca-P coated implants. Our biomimetic coatings might have different bioactivity upon implantation.
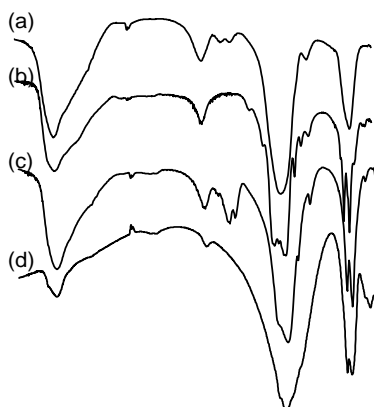

Figure 3: FTIR spectra of the various coatings prior to immersion of (a) ACCP, (b) OCP, (c) BCA, (d) HA coatings
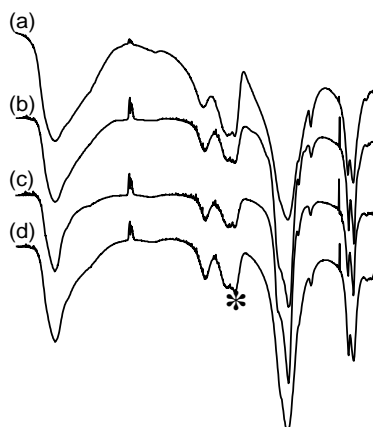
Figure 4: FTIR spectra of the various coatings after 2 weeks of immersion in α-MEM of (a) ACCP, (b) OCP, (c) BCA, (d) HA coatings. Note the presence of the CO_3 band (*).

For this reason, we studied their *in vitro* dissolution by soaking into various media. It was possible to compare the dissolution rates of various coatings in salt and buffered solutions, like SPS. The dissolution rates depend on pH since Ca-Ps are more soluble in acidic than neutral media. Several parameters can play a role in dissolution of Ca-Ps: specific solubility of each Ca-P phase, crystal size and morphology of each coating.

ACCP coating dissolves at the fastest rate whatever the pH value of SPS. At physiological pH of 7.3, OCP coating dissolves markedly slower than apatitic coatings BCA and HA. Indeed at this pH and temperature conditions, solubility isotherm of OCP is higher than HA [8]. This indicates that the dissolution behavior does not depend only on thermodynamics and kinetics but also on the crystallinity and morphology of the coating. Indeed, the OCP coating is highly crystallized with a crystallinity index close to 100% [8]. This structure is thereby more stable at neutral pH due to long-range order as compared to the 55% crystalline BCA coating and the 67% crystalline HA coatings. However, this OCP coating dissolves faster than BCA and HA at pH=5.0 and 3.0. In acidic conditions, the dissolution behavior follows the solubility isotherms. Furthermore, OCP coating is composed of vertical crystals leading to a large open structure where media can go through. In the case of BCA coating, the presence of HCO_3^- and Mg^{2+} inhibits crystal growth resulting in small and distorted crystals. Whereas HA plasma-sprayed coating is composed of solidified HA droplets. The core of these droplets is composed of

sintered HA crystals and the outer surface of these droplets is composed of amorphous Ca-P due to a sudden cooling down. Thereby, at pH=7.3 and pH=5.0, the initial dissolution rate of HA plasma-sprayed coating corresponds mainly to the dissolution of the amorphous outer layer. Whereas at highly acidic pH there is a competition between sintered HA crystals versus tiny BCA crystals. From these experiments, we can see that all the coating's morphology, composition and structure are important parameters that affect their initial dissolution rate.

Interestingly, the various Ca-P coatings evolved all into carbonated apatitic structure by soaking into α-MEM at neutral pH. The α-MEM medium is a more complete medium containing amino-acids, calcium, phosphate, magnesium and carbonate ions and thereby resembling body fluids. The presence of Ca^{2+} and HPO_4^{2-} maintains the medium supersaturated and thus reduces the dissolution rate of the coating. Mg^{2+}, HCO_3^- and amino-acids present in α-MEM might inhibit the crystal growth during dissolution-reprecipitation. The conversion of various coatings into carbonated apatite might result from ionic exchanges between the coating and the surrounding medium. These ionic exchanges might be enhanced by crystal size and coating morphology and modulated by crystal growth inhibitors.

CONCLUSION

This *in vitro* study showed that dissolution behavior of various Ca-P coating does not only depend on acidity but it also relates to microscopic parameters such as crystal size, coating composition and microstructure. Furthermore, the immersion into α-MEM, which is "more physiologic" than SPS, leads to a conversion of all the Ca-P coating into a carbonated apatitic structure. These first dissolution investigations emphasized different and specific reactivates, thus this study should be completed with bone marrow cell culture in order to evaluate cell-material interactions. Finally, *in vivo* implantation should be preformed to compare the different dissolution rates of coatings.

References

1-T. Kokubo, H. Kushitani, S. Sakka, T. Kitsugi and T. Yamamuro, J. Biomed. Mater. Res. **24**, 1990, pp721-734

2-P. Li, I. Kangasniemi, K. de Groot and T. Kokubo, J. Am. Ceram. *Soc.* **77**, 1994, pp1307-1312

3-F. Barrere, P. Layrolle, C.A. van Blitterswijk and K. de Groot, Bone **25**, 1998, pp107S-111S

4-F. Barrere, P. Layrolle, C.A. van Blitterswijk and K. de Groot, Mineralization in natural and synthetic biomaterials in MRS Fall Meeting 1999, to be published

5-J.D. de Bruijn, J.E. Davies, J.S. Flach, C.P.A.T Klein, K. de Groot and C.A. van Blitterswijk, Cells and Materials 3, pp115-127 (1993)

6-J.D. de Bruijn, C.P.A.T Klein, K. de Groot and C.A. van Blitterswijk, Cells and Materials 3, pp407-417 (1994)

7-J.G.C. Wolke, K. de Groot and J.A. Jansen, J. Biomed. Mat. Res. 39, pp524-530 (1998)

8-R. LeGeros, in Calcium phosphate in oral biology and medicine, vol 15, p27 (1991)

CHAPTER 8

IN VITRO AND *IN VIVO* DEGRADATION OF OCTACALCIUM PHOSPHATE AND CARBONATE APATITE COATINGS ON TITANIUM IMPLANTS

F. Barrère, C.M. van der Valk, R.A.J. Dalmeijer, C.A. van Blitterswijk, K. de Groot and P. Layrolle

ABSTRACT

In load-bearing applications for bone repair, calcium phosphate (Ca-P) coatings have been applied onto titanium alloys prostheses in order to combine the strength of metals with the bioactivity of Ca-P. It has been clearly shown in many publications that Ca-P coating accelerates bone formation around the implant. However, longevity of the Ca-P coating for an optimal bone apposition onto the prosthesis remains controversial. Biomimetic bone-like carbonate apatite (BCA) and octacalcium phosphate (OCP) coatings were deposited on Ti6Al4V samples in order to evaluate their *in vitro* and *in vivo* dissolution properties. The coated plates were soaked in α-MEM for 1, 2 and 4 weeks, and they were analyzed by Back Scattering Electron Microscopy (BSEM) and by Fourier Transform Infra Red spectroscopy (FTIR). Identical coated plates were implanted subcutaneously in Wistar rats for similar periods. BSEM, FTIR and histomorphometry were performed on the explants. *In vitro* and *in vivo*, a carbonate apatite (CA) formed onto OCP and BCA coatings via a dissolution-precipitation process. *In vitro*, both coatings dissolved overtime, whereas *in vivo* BCA calcified, and OCP partially dissolved after one week. Thereafter, OCP remained stable. This different *in vivo* behavior can be attributed to 1) different organic compounds that might prevent or enhance Ca-P dissolution, 2) a greater reactivity of OCP due to its large open structure, or 3) different thermodynamic stability between OCP and BCA phases. These structural and compositional differences promote either the progressive loss or calcification of the Ca-P coating and might lead to different osseointegration of coated implants.

INTRODUCTION

In the case of load-bearing applications, hydroxyapatite (HA) coatings are applied onto a metal substrate in order to combine the strength of metal with the bioactivity of calcium phosphates (Ca-P). Recent clinical results in total hip arthroplasty showed the significant improvement in bone fixation by using plasma sprayed HA-coated metallic prosthesis as compared to non-coated implants [1]. Extensive studies have shown that Ca-P materials have a highly attractive biologic profile because of their ability to bind directly with bone. Such materials are called bioactive; i.e. they interact dynamically with the local environment in order to favor and to enhance bone formation. When a bioactive material is implanted, one of the first events is an ionic exchange between the Ca-P in contact with body fluids [2,3]. This dissolution leads to an increase of supersaturation at the vicinity of the implant, and thereafter to a precipitation onto the substrate of a bone-like carbonate apatitic structure [3-6].

At the first stage of implantation, Ca-P dissolution ability appears to be essential for an optimal bone formation and fixation onto the implants. The optimization of the Ca-P dissolution ability can be achieved by varying the crystallinity [7-10] or the composition [11-14], the microstructure [11,13,15,16], or a combination of the aforementioned parameters. With regard to HA plasma-sprayed coating, longevity is subject to discussion. A fast Ca-P dissolution enhances a fast bone remodeling activity and high interfacial bonding strength at early implantation time [8,17]. At late implantation time, non-soluble and stable Ca-P coating lead to a better interfacial stability of bone-bonding according to some studies [12,17], whereas clinical failure reports of such coatings are due to the coating delamination that induces unstable coating-implant interface [18-20]. Up to now, these studies have exclusively concerned HA plasma-sprayed coatings with various crystallinities.

Besides the well-known plasma-spraying technique, other coating routes have been developed, among which the biomimetic approach. The principle of the biomimetic route is to immerse a substrate into simulated body fluids, favoring the nucleation and growth of bone-like apatite under physiological conditions of temperature and pH [21]. In addition, this physiological method enlarges the variety of Ca-P phases that can be deposited, such as Octacalcium phosphate (OCP) or bone-like carbonate apatite (BCA) [22]. The biomimetic process is even, nowadays, shortened up to 24h [23]. So far, a limited amount of studies have been conducted to evaluate the bioactivity of these novel coatings. *In vitro*, dissolution rates in a saline solution indicated that OCP dissolved slower than BCA at pH=7.3, whereas OCP dissolved faster than BCA at pH=5.0 [24]. OCP and BCA coatings reacted differently towards osteoclastic resorption assays *in vitro* [25]. *In vivo*, OCP coating applied onto porous metal implants could induce bone in muscles of dog, and OCP and BCA coatings combined with cultured bone marrow cells

induced bone, when subcutaneously implanted [26]. The reasons explaining these interesting results are not yet fully established. In view of this open question, the present work aims at focusing on the physicochemistry of OCP and BCA coatings dissolution. This dissolution behavior will be tested both *in vitro* under simulated physiological conditions, and *in vivo* by subcutaneous implantation in rats.

MATERIALS AND METHODS

Materials

Medical grade sandblasted titanium alloy (Ti6Al4V) were used as substrate ($R_a \sim 2.8 \mu m$). The size of the plates were square-like ($10 \times 10 \times 1 mm^3$), the four corners were smoothened in order to avoid any subcutaneous injury. Prior to the coating procedure, the plates were ultrasonically cleaned by subsequent immersion into acetone, ethanol 70% and demineralized water. These plates were then etched for 10 minutes with Kroll reagent, a mixture of 2ml of fluorohydric acid (40%), 4ml nitric acid and 994ml demineralized water. Ti6Al4V samples were then dried overnight at 50°C. In the experiments, the chemicals used for the study were reagents grade (Merck), and they were precisely weighted with a confidential interval of 10%.

Biomimetic coatings preparation

Ca-P coatings were produced within a two-steps biomimetic process. First, the plates were pre-treated by soaking at 37±1°C for 24h into a Simulated Body Fluid solution concentrated by a factor five (SBFx5, table 1).

	Na^+	Mg^{2+}	Ca^{2+}	Cl^-	HPO_4^{2-}	HCO_3^-
HBP	142.0	1.5	2.5	103.0	1.0	27.0
SBF	142.0	1.5	2.5	147.8	1.0	4.2
SBFx5	733.0	7.5	12.5	720.0	5.0	21.0
SCS1	140.4	0.0	3.1	142.9	1.86	0.0
mSBFx5	702.0	2.5	12.5	714.5	5.0	10.0

Table 1: Composition in mM of Human Blood Plasma (HBP), regular SBF solution and the various soaking solutions (SBFx5, SCS1 and mSBFx5)

The solubility of SBFx5 was controlled by supplying carbon dioxide gas at 0.2 bars prior to immersion of the plates. After coating, the plates were ultrasonically cleaned into demineralized water for 10 minutes. Secondly, these pre-treated plates were divided into two groups. Each group was soaked into a second calcifying supersaturated solution in order to grow a Ca-P coating. One Ti6Al4V group was soaked into the supersaturated calcifying solution SCS1 for

48h at 37ºC. The other Ti6Al4V group was soaked into the modified SBFx5 solution (SBFx5), for 24h at 50ºC. The composition of all these solutions is summarized table 1. After immersion, the coated Ti6Al4V plates were thoroughly cleaned with demineralized water. These samples were then dried overnight in air at 50°C.

Characterization of the biomimetic Ca-P coatings

Morphology of the coatings was checked by Environmental Scanning Electron Microscopy (ESEM, XL-30 Philips, Eindhoven, The Netherlands), and their crystallinity was determined according to ASTM STP 1196 [27]. Prior to dissolution studies, for each group, coated Ti6Al4V plates were embedded in polymethylmetacrylate (PMMA). Cross-section of the embedded plates was performed using a diamond saw (Microtome Saw SP 1600, Leica Instruments GmbH, Nussloch, Germany), as described figure 1.
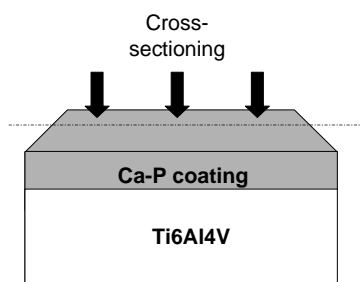

Figure 1: Three-dimensional scheme of cross sectioning. After embedding in PMMA, the diamond the Ca-P coated plate was sawed perpendicularly to the plate (10x10mm^2), approximately in its middle. The sectioning was in parallel with two sides of the Ti6Al4V square. After sawing, a two dimensional observation of the Ca-P coating on Ti6Al4V was performed by BSEM

The cross-sectioned sample was polished (1200 and 2400 grid), and was observed by Back Scattering Electron Microscopy (BSEM, XL-30, Philips, Eindhoven, The Netherlands). The 2d picture of the Ca-P coating on Ti6Al4V plate obtained by BSEM was used to determine the Ca-P coating surface area using an image analysis software (VIDAS). Finally, Ca-P coating structures were characterized by Fourier Transform Infra-Red spectroscopy (FTIR, 8 scans, Spectrum 1000 FT-IR, Perkin-Elmer, Oosterhout, The Netherlands).

***In vitro* study of the biomimetic Ca-P coatings**

The OCP and BCA coated Ti6Al4V plates, and bare Ti6Al4V plates were individually soaked into sterile polystyrene vials containing 50ml of simulated physiological medium (α-MEM, Gibco, Life Technology). The vials were placed into an incubator at 37°C in humid atmosphere containing 5% CO_2, in order to

buffer naturally the α-MEM solution at pH=7.3. After each incubation time (1, 2 and 4 weeks), 2 plates were removed, and cleaned with demineralized water. After immersion, the evolution of coatings' structure and morphology was investigated in a similar manner as the initial coatings by ESEM, BSEM and FTIR.

In vivo study of the biomimetic Ca-P coatings

The Dutch comity for animal experimentation (DEC) has approved this study, and the implantations were performed according to Good Laboratory Practice (GLP) in the University Hospital of Utrecht (AZU, The Netherlands). Gamma sterilized Ti6Al4V plates were subcutaneously implanted in male Wistar rats. A total of 12 Male Wistar rats (approx. 200-300 g, age) were anaesthetized using a combination of 100 µg/ml Ketamine, 50 mg/ml Xyalizine and 0.5 mg/ml atropine (1.75:1.5:0.5 ml). Four plates (10x10x1 mm^3) were implanted under the skin of each animal following a latin square implantation scheme. Bare Ti6Al4V plates were also implanted as negative control. The incisions were closed using 5.0 polyglycolic acid suture. After 1, 2 and 4 weeks of survival period, the rats were killed with CO_2-gas. Implants were removed with surrounding tissue.

Three out of four retrieved coated implants were soaked into Karnovsky's fixative for several days, the samples were immersed in phosphate buffer saline for at least one day. The plates with surrounding tissue were dehydrated through a grade series of alcohol and individually embedded into PMMA solution. The embedded implants were partially sectioned at a thickness of approximately 10 µm with a diamond saw (Microtome Saw SP 1600, Leica Instrument GmbH, Nussloch, Germany) and stained with methylene blue and basic fuchsine. The sections were examined by light microscopy. The second part of cross-sectioned samples was observed by BSEM as mentioned above in order to quantify the two-dimensional (2d) surface area of the coating.

The fourth retrieved coated implant was soaked into Karnovsky's fixative, dehydrated through a graded series of alcohol and the surrounding tissue was removed. Finally these latter implants were dried with CO_2 critical point drying. The coating was scraped off, and analyzed by FTIR.

RESULTS

Characterization of the biomimetic coatings

OCP coating

The initial coating morphology exhibited sharp crystals that grew perpendicularly to the Ti6Al4V substrate (figure 2a,b). In figure 3a, FTIR spectrum of the initial OCP coating displayed sharp P-O bands at 1100, 1070 and 1023 cm^{-1} (P-O stretching in phosphate (PO_4^{3-}) and hydrogenophosphate

(HPO_4^{2-})), and a HPO_4^{2-} band at 906 cm^{-1} (P-O stretching in HPO_4^{2-}), typical of an OCP structure. The two sharp P-O bands at 560 cm^{-1} and 600 cm^{-1} (P-O deformation in PO_4^{3-}) exhibited shoulders at 624 cm^{-1} (H_2O libation) and 526cm^{-1} (P-O twisting in HPO_4^{2-}) [28]. This OCP coating was 100% crystalline.

BCA coating

The BCA coating was initially composed of a thick dense layer, on the top of which crystals grew perpendicularly (figure 4a). In figure 5a, the FTIR spectrum of the initial BCA coating exhibited a broad 1041 cm^{-1} band with 2 shoulders at 1104 and 960cm^{-1} (P-O stretching in PO_4^{3-} and HPO_4^{2-}) and two relatively sharp bands at 603 and 562cm^{-1}. Additionally, the FTIR spectrum displayed carbonate bands at 1494, 1476 and 1417cm^{-1}. The position of these CO_3^{2-} bands indicated that carbonate groups replace phosphate and hydroxyl group in the crystals, i.e. typical of AB carbonated apatitic structure [29]. The crystallinity of BCA coating was 60%.

In vitro study

After immersion in α-MEM, the bare Ti6Al4V plates did not show any surface modification.

After 2 weeks of immersion in α-MEM, the biomimetic OCP coating was covered by a dense thin layer (figure 2c). After 4 weeks, the OCP coating appeared denser, due to a thickening of each initial crystal that suggests a horizontal binding between the OCP crystals through the whole thickness of the coating (fig2d). Additionally, the OCP coating became thinner when immersion time was longer. The FTIR spectra of the OCP coating versus immersion in α-MEM time showed changes in the coating structure (figure 3). After 2 weeks of immersion in α-MEM, the phosphate vibration bands located at of the initial OCP coating became less sharp and less numerous as shown on the PO_4^{3-} and HPO_4^{-} bands at 1110, 1070 and 1023cm^{-1} (figure 3b), indicating a decrease in crystallinity. Furthermore the HPO_4^{2-} band at 906cm^{-1} became less distinct. In addition, carbonate bands (C-O of CO_3^{2-}) appeared at 1472, 1447 and 1417 cm^{-1} indicating the formation of a carbonated apatitic phase among the OCP phase. The position of CO_3^{2-} bands indicated that CO_3^{2-} groups replaced PO_4^{3-} and OH^{-} groups, suggesting an AB-carbonated apatitic phase. After 4 weeks of immersion in the medium, the HPO_4^{2-} band at 906cm^{-1} disappeared completely, and only two large PO_4^{3-} bands remained at 1104 and 1029cm^{-1} (figure 3c). CO_3^{2-} bands remained similar to the FTIR spectrum at 2 weeks. Thereby, after 4 weeks of immersion into α-MEM, the OCP coating was totally converted into an AB-carbonated apatite coating. From the initial typical sharp OCP crystals (fig 2b) tiny crystals that we attributed to carbonated apatite (CA) had grown sideward and on the detriment to OCP phase (fig2e).
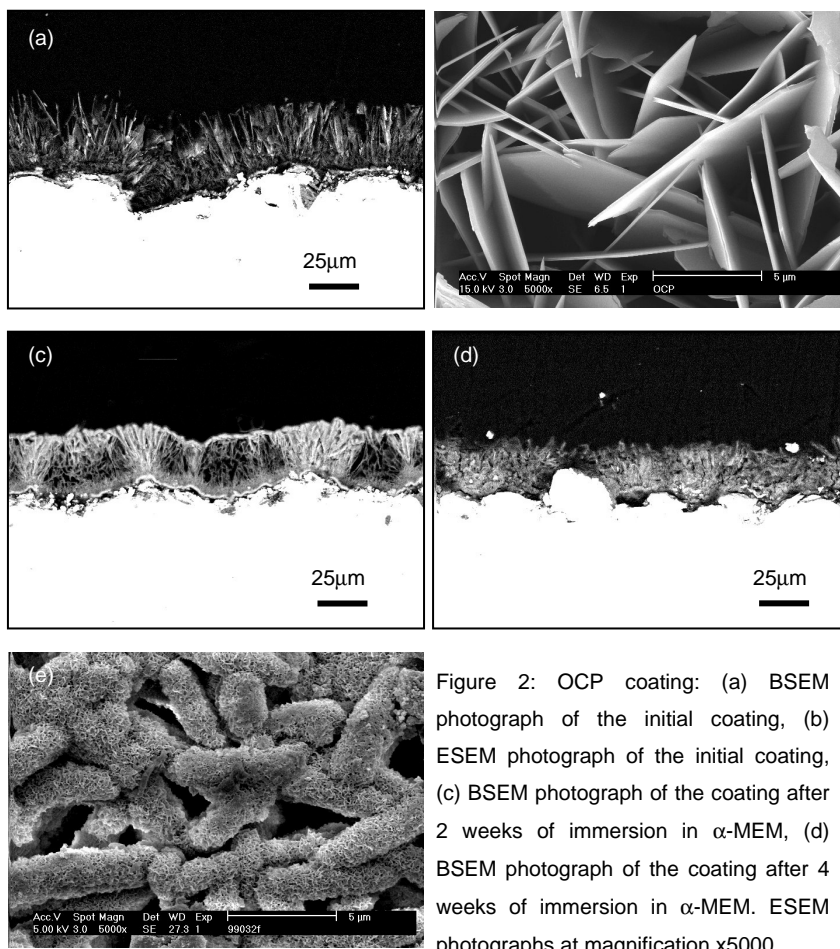
Figure 2: OCP coating: (a) BSEM photograph of the initial coating, (b) ESEM photograph of the initial coating, (c) BSEM photograph of the coating after 2 weeks of immersion in α-MEM, (d) BSEM photograph of the coating after 4 weeks of immersion in α-MEM. ESEM photographs at magnification x5000
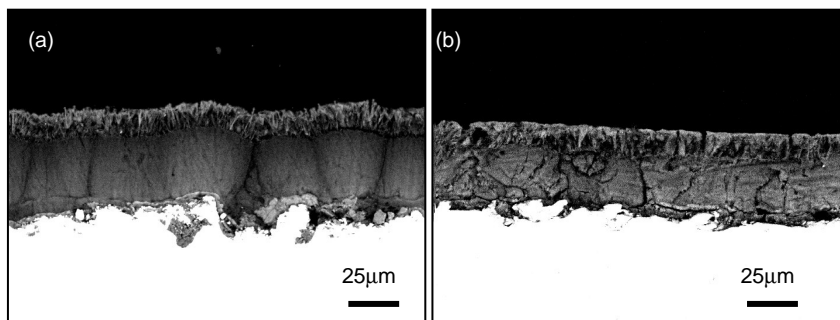

Figure 4: BSEM photos of BCA coating: (a) initial coating, (b) after 4 weeks of immersion
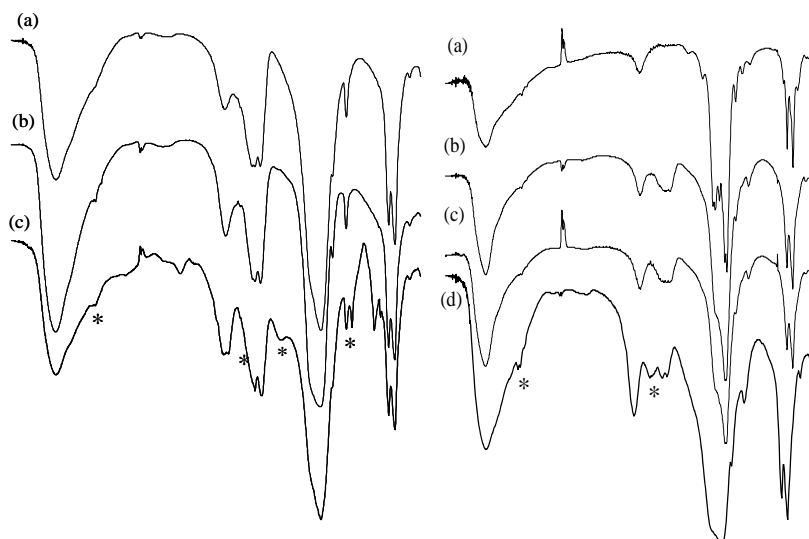
Figure 3: FTIR spectra of OCP coating: (a) initial coating, (b) in vitro after 2 weeks of immersion, (c) in vitro after 4 weeks of immersion, and (d) *in vivo* after 4 weeks of implantation. (∗) Bands attributed to organic compounds.

Figure 5: FTIR spectra of BA coating: (a) initial coating, (b) *in vitro* after 4 week of immersion, and (c) *in vivo* after 4 weeks of implantation. (∗) Bands attributed to organic compounds.

In the case of BCA coating, after 4 weeks of immersion in α-MEM, the dense layer exhibited cracks that might be due to a long hydration time followed by drying. On the top of this dense layer the crystals appeared slightly denser than the initial top crystal layer (figure 4b). In addition, the coating became thinner overtime. The FTIR spectrum recorded after 4 weeks into α-MEM was accurately similar to the initial BCA coating (fig 5b). Therefore the soaking of BCA coated Ti6Al4V plates into α-MEM affected the coating morphology, but not its structure, which remained composed of CA crystals.

***In vivo* study**

Figure 6 shows the histological slides of the three sorts of explants after 4 weeks. No systemic toxic effects or inflammatory reaction could be observed following 1, 2 and 4 week of *in vivo* exposure. No significant foreign body giant cell reaction was noted in any of the evaluated sections. Light microscopy showed no signs of debris or coating delamination. In addition, the coating did not disappear *in vivo*. The entire titanium alloy surface was still covered with a uniform coating after 1, 2 and 4 weeks implantation under the skin.
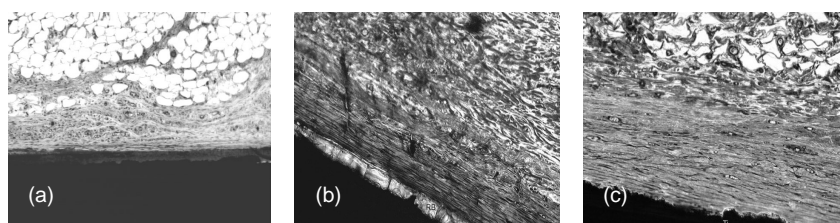
Figure 6: Light microscopy for the three groups of implants after 4 weeks of implantation (magnification x100): (a) OCP coating, (b) BCA coating, (c) bare Ti6Al4V. The black part represents Ti6Al4V substrate. Above, in the case of fig 6a and 6b, the bright purple layer represents the Ca-P phase. The dark purple mixed with dark blue represents fibrous tissues surrounding the implants.

The FTIR spectra of the OCP coating after 4 weeks of implantation time exhibit changes in structure (figure 3d). Similarly to the *in vitro* study, OCP evolved into a CA. Additionally, other bands appeared at 2959 and 2871 cm^{-1} corresponding to C-H aliphatic vibrations and a band at 1546 cm^{-1} that could correspond to amine N-H vibrations. This suggested the incorporation of proteins or amino-acids while the initial OCP coating was converted into a carbonated apatitic coating. In the case of the BCA coating, the mineral structure remained the same (fig 5c). However, like previously observed for OCP coating, after 4 weeks of implantation, additional bands were detected at 2929 cm^{-1} corresponding to aliphatic C-H. The other bands at 1697, 1292 and 836 cm^{-1} were not detected in the case of the implanted OCP coating. Since these bands do not correspond to any phosphate or hydrogenophosphate bands, they should be assigned to organic compounds. For both coatings, organic compounds from the surrounding body fluids were incorporated into the coating during the subcutaneous implantation.

Table 2 represents the evolution of the measured surface area of both coating versus implantation time.

	OCP Coating area (μm^2)	BCA coating area (μm^2)
Week 0	884±54	501±28
Week 1	773±43	545±51
Week 2	777±317	579±36
Week 4	776±42	602±235

Table 2: Coating surface area in μm^2 before (week 0) and after one, two and four weeks of subcutaneous implantation for OCP and BCA. The measurements have been performed on BSEM pictures (magnification x40) of cross-sections. The given values are absolute.

The measurement of the cross-sectioned surface area of the coating indicated a decrease of $100\mu m^2$ after 1 week of subcutaneous implantation. Thereafter, for 2 and 4 weeks, the 2d-surface area did not evolve, remaining at approximately $775\mu m^2$. On the other hand, the morphology of OCP coating did not evolve after 1, 2 and 4 weeks of implantation. In contrast to the *in vitro* study, the coating kept its sharp crystals *in vivo*. In the case of BCA coating, the morphology of the cross-sectioned samples after 1, 2 and 4 weeks did not change overtime. However, the 2d-surface area of the coating slightly increased with time. This suggested a calcification of the coating by mineral ions contained in the surrounding body fluids.

DISCUSSION

Physicochemistry of the Ca-P coating evolution *in vitro* and *in vivo*
It is clear that the OCP coating transforms overtime into a CA. This OCP-to-CA structural evolution has been already described *in vitro* [30,31], and *in vivo* [5]. Under physiological conditions, Mg^{2+} inhibits the OCP-to-CA transformation, whereas Ca^{2+}, HPO_4^{2-}, HCO_3^- favors the OCP-to-CA transformation [30,31]. In the present study, α-MEM contains all of the aforementioned ions. In our case Mg^{2+} did not prevent the OCP-to-CA transformation, certainly due to the compensation of promoting ions like HCO_3^-. This *in vitro* OCP-to-CA transformation results from an interfacial dissolution-reprecipitation mechanism. Once immersed into α-MEM, Ca^{2+} and HPO_4^{2-} ions must be liberated from the surface to the medium. At the vicinity of the OCP coating, supersaturation in α-MEM is reached, resulting to Ca-P nucleation and growth. The presence of Mg^{2+} and HCO_3^- in the medium inhibits the growth of the OCP phase and favors the formation of poorly crystallized CA [22].

Irrespective to the continuous dissolution *in vitro*, OCP coating partially dissolved after 1 week of implantation, and thereafter remained stable for 2 and 4 weeks of implantation while being converted into CA from the first week on. This initial dissolution of OCP can be due to an environmental decrease in pH consequently to the inflammatory response after implantation. Subsequently, in the surrounding body fluids, pH trends to increase up to a neutral pH, ending the dissolution process. On the other hand this initial dissolution of OCP could result from a higher thermodynamic instability in body fluids CA, due to an initial lack of carbonate in OCP coating. Further, the incorporation of organic compounds can reduce the dissolution rate, as it has been shown for bovine serum albumin co-precipitated into a similar biomimetic OCP coating [32].

With regard to BCA coating, the analyses indicated that the mineral structure did not change. However, we hypothesize that a dissolution-precipitation mechanism could have taken place as crystal morphology has

changed with immersion time in α-MEM. After implantation, BCA coating contained organic compounds, which were either incorporated or adsorbed. *In vivo*, the BCA coating grew continuously over implantation period. Since histology did not reveal any bone formation, this growth can be interpreted as a surface calcification of the BCA coating from the body fluids. Our *in vivo* data are in accordance with Heughebaert et al. who quantified a similar calcification with sintered HA ceramics [4], whereas a weight loss occurred for sintered CA [33]. This suggests that the processing of the material, and therefore the microstructure and composition have a great influence on its stability *in vivo*.

Similarities and differences between OCP and BCA coatings
The biomimetic OCP and BCA coatings have a relatively comparable behavior both *in vitro* and *in vivo*. Initially, a partial dissolution takes place followed by the reprecipitation of a CA layer. In our study, the CA layer is detected in bone cell-free environment, and the CA formation results from a purely physicochemical process. However, *in vivo*, OCP partially dissolves, whereas BCA calcifies. Several parameters can explain this *in vivo* dissimilarity.

Influence of proteins
FTIR spectra of both coating displayed the presence of organic compounds. These compounds were incorporated or adsorbed in both implanted coatings. Even if we could not identify namely the interacting organic compounds, it is clear that they were not identical for the two coatings. FTIR spectra of implanted OCP exhibited an amino group band that can be reasonably attributed to proteins, whereas FTIR spectra of implanted BCA did not exhibit this band, suggesting that BCA did not incorporate proteins. This observation is in accordance with Johnsson et al. [34] who have shown that OCP and BCA have specific and distinct affinities for other compounds present in body fluids. These various compounds might promote or prevent dissolution. Besides direct interactions (adsorption or incorporation) between organic compounds and Ca-P, the sole presence of organics in the medium can influence the Ca-P stability. For example, serum albumin present in the medium interacts with free Ca^{2+}, enhancing HA dissolution [35,36]. Thus, the cocktail of numerous organic and inorganic compounds present in the body fluids can drastically influence the dissolution behavior of the implanted Ca-P phase.

Influence of microstructure
It is microscopically clear that OCP and BCA coating have different microstructures. The OCP coating is composed of large vertical crystals exhibiting a great open structure to the surrounding body fluids, whereas the BCA exhibits smaller and denser crystals. Since a greater surface is exposed to the body fluid, one might expect a higher reactivity between OCP coating

and its environment, than for BCA coating. Specific surface area measurements were not performed in this study because such analysis requires the scrapping off the coating, and thereby the exposed surface morphology would have been markedly modified, misleading the interpretation of the data. On the other hand, BCA crystallinity is significantly lower than OCP, due to the distortions and deficiencies created by the incorporation of carbonate in the apatitic lattice [29]. This lower crystallinity would suggest a faster dissolution of BCA compared to OCP.

Physicochemical aspect
In addition to the comparison of crystallinity, we have to compare two different crystal lattices. Under physiological conditions apatite is thermodynamically more stable than OCP, suggesting in theory a higher dissolution rate for OCP than for apatite. In summary, this dissolution study has shown a competition between two different Ca-P phases OCP and BCA, exhibiting a great *versus* small microstructure, a crystalline *versus* less-crystalline structure, and a more thermodynamically stable *versus* less thermodynamically stable structure. All of these features markedly influence the dissolution behavior, as already mentioned previously for dissolution rate determination in saline solutions [24]. Although α-MEM and body fluids are more complex than saline solution in term of composition, microstructure, crystallinity and thermodynamics, the dissolution behavior of OCP and BCA coatings seems to be also the result of a combination of those parameters.

Effect of dissolution on the bioactivity of OCP and BCA
The present results, and previous evaluations of BCA and OCP [24-26] suggest that these coatings might have a different bioactivity. At which extend these differences would be beneficial for clinical applications remains discussed. Relatively fast degradation of Ca-P coating favors early bone formation [7,18], whereas the *in vivo* longevity of the coating on implants is subjected to discussion. Dhert and Klein have shown under their experimental conditions that long lasting Ca-P coating were more beneficial for bone fixation [12,17], although the reported failure cases are due to a weakening between the implant and the hosting bone with the partially remaining Ca-P coating [18-20]. However, these *in vivo* studies were limited to plasma-sprayed Ca-P coatings, which are heterogeneous in morphology. The amorphous phase participates to the early dissolution, and the remaining crystalline HA participates to the interfacial stability. On the other hand, a long term bone reaction appeared similar for Ti or HA coated Ti implants [37-41]. In our view, an optimal Ca-P coating should dissolve in a rate similar to bone formation and should completely disappear after completion of the bone healing process. Further, the total resorption of the Ca-P coating would avoid possible

weakening that occur at the interfacial remaining Ca-P coating. OCP and BCA coatings are homogeneous throughout their whole thickness; therefore these biomimetic coatings should dissolve gradually and completely over implantation time. Recently, OCP was shown to be more resorbable than HA or β-TCP in rat cranial defects of rats, and OCP enhanced bone formation more than the two other Ca-P ceramics [42]. Therefore, because of a more open and more thermodynamically reactive structure, OCP may interact more dynamically than BCA in a bony environment, stimulating bone formation. On the other hand, since different organic compounds interact with OCP and BCA subcutaneously, the adsorption of diverse proteins may differ in bony environment as well. A different interaction may happen for OCP and BCA coatings towards bone morphogenetic proteins (BMP), leading to a distinct bioactive performance of the two coatings.

CONCLUSION

The biomimetic OCP and BCA coatings show similarities and dissimilarities in their *in vitro* and *in vivo* behavior. Whatever their environment, simulated physiological fluids or natural body fluids, the surface of these material interacts dynamically. Firstly, Ca-P partially dissolves and secondly, a carbonate apatitic phase grows onto the Ca-P substrate. Depending on the microstructure of their surface, and on the involved organic compounds, Ca-P dissolves in a more or less large extend, leading to the progressive loss or calcification of the coating. OCP and BCA coatings have specific *in vivo* properties that might be emphasized in osseous environment.

References

1-Havelin LI, Engesaeter LB, Espehaug B, Furnes O, Lie SA, Vollset SE. The norvegian arthroplasty register: 11 years and 73000 arthroplasties. Acta Orthop Scand 2000;71: 337-353.

2-Ducheyne P, Bianco P, Radin S, Schepers E. Bioactive materials: mechanism and bioengineering considerations. In: Bone-bonding biomatrials. Ducheyne P, Kokubo T, van Blitterswijk CA, editors. Leiderdorp, The Netherlands: Reed healthcare communications; 1992. p 1-12

3-LeGeros RZ, Orly I, Gregoire M, Daculsi G. Substrate surface dissolution and interfacial biological mineralization. In: Davies JE, editor. The Bone-Biomaterial Interface. Toronto, Canada: University of Toronto Press; 1991. p76-88.

4-Heughebaert M, LeGeros RZ, Gineste M, Guihlem A, Bonel G. Physicochemical characterization of deposits associated with HA ceramics implanted in nonosseous sites. J Biomed Mater Res Appl Biomat 1988; A3:257-268

5-Suzuki O, Nakamura M, Miyasaka Y, Kagayama M, Sakurai M. Maclura pomifera agglutin-binding glycoconjugates on converted apatite from synthetic Octacalcium phosphate implanted subperiosteal region of mouse calvaria. Bone and Mineral 1993; 20:151-166

6-Radin S, Ducheyne P. The effect of calcium phosphate ceramic composition and structure on *in vitro* behavior. II Precipitation. J Biomed Mater Res 1993; 27:35-46

7-Wolke JGC, de Groot K, Jansen JA. *In vivo* dissolution behaviour of various RF magnetron sputtered Ca-P coatings. J Biomed Mater Res 1998; 39:524-530

8-de Bruijn JD, Structural arrangements at the interface between plasma-sprayed calcium phosphate and bone tissue *in vivo*. Biomaterials 1994; 15:543-550.

9-Klein CPAT, Wolke JGC, de Blieck-Hogervorst JMA, de Groot K. Features of calcium phosphate plasma-sprayed coatings: an *in vitro* study. J Biomed Mater Res 1994; 28:961-967

10-Nagano M, Nakamura T, Kokubo T, Tanahashi M, Ogawa M. Diffrences of bone bonding ability and degradation behaviour *in vivo* between amorphous calcium phosphate and highly crystalline hydroxyapatite coating. Biomaterials 1996; 17:1771-1777.

11-Frayssinet P, Mathon D, Lerch A, Autefage A, Collard P, Rouquet N. Osseointegration of composite calcium phosphate bioceramics J Biomed Mater Res 2000; 50:125-130

12-Dhert WJA, Klein CPAT, Jansen JA, van der Velde EA, Vriesde RC, Rozing PM, de Groot K. A histological and histomorphometrical investigation of fluoroapatite, magnesiumwhitlockite, and Hydroxylapatite plasma-sprayed coatings in goats. J Biomed Mater Res 1993; 27:127-138

13-Hyakuna K, Yamamuro T, Kotoura Y, Oka M, Nakamura T, Kitsugi T, Kokubo T, Kushitani H. Surface reaction of calcium phosphate ceramics to various solutions. J Biomed Mater Res 1994; 24:961-967

14-Radin S, Ducheyne P. The effect of calcium phosphate ceramic composition and structure on *in vitro* behavior. I Dissolution. J Biomed Mater Res 1993; 27:25-34

15-Radin S, Ducheyne P. The effect of calcium phosphate ceramic composition and structure on *in vitro* behavior. III Porous versus dense ceramics. J Biomed Mater Res 1994; 28:471-488

16-Yuan H, de Bruijn JD, Yang Z, Li Y, de Groot K, Zhang X. Osteoinduction by calcium phosphates. J Mat Sci: Mat Med 1998;9: 723-726

17-Klein CPAT, Wolke JGC, de Blieck-Hogervorts JMA, de Groot K. Calcium Phosphate plasma-sprayed coatings and their stability: an *in vivo* study. J Biomed Mater Res 1994; 28:909-917.

18-Ogiso M, Yamashita Y, Matsumoto T. The process of physical weakening and dissolution of the HA-caoted implant in bone and soft tissue. J Dent Res 1998; 77:1426-1434.

19-McDonald DE, Betts F, Stranick M, Doty S, Boskey AL. Physicochemical study of plasma-sprayed hydroxyapatite-coated implants in humans. J Biomed Mater Res 2001; 54:480-490.

20-Takeshita F, Matsushita Y, Ayukawa Y, Suetsugu T. Fractures of hydroxyapatite-coated blade implants connected with natural teeth. A histological study using SEM, light microscopy, and an image processing system. J Periodontol 1996; 67: 86-92.

21-Kokubo T, Kushitani H, Abe Y, Yamamuro T. Apatite coating on various substrates in simulated body fluids. Bioceramics 1989; 2:235-242

22-Barrere F, Layrolle P, van Blitterswijk CA, de Groot K. Biomimetic Calcium phosphate Coatings on Ti6Al4V: a Crystal Growth Study of OctaCalcium Phosphate and Inhibition by Mg^{2+} and HCO_3^-. Bone 1998; 25:107S-111S

23-Barrere F, van Blitterswijk CA, de Groot K, Layrolle P. Influence of ionic strength and carbonate on the Ca-P coating formation form SBFx5 solution, Biomaterials (under press).

24-Barrere F, Stigter M, Layrolle P, van BlitterswijkCA, de Groot K. *In vitro* dissolution of various Calcium phosphate coatings on Ti6Al4V. Bioceramics 2000;13: 67-70

25-Leeuwenburgh S, Layrolle P, Barrere F, de Bruijn J, Schoonman J, van Blitterswijk CA, de Groot K. Osteoclastic resorption of biomimetic calcium phosphate coatings *in vitro*. J Biomed Mater Res 2001;56:208-215.

26-de Bruijn JD, Yuan HP, Dekker R, van Blitterswijk CA. Osteoinduction by biomimetic calcium phosphate coatings and their potential use as tissue engineering scaffolds. In: Davies JE, editor. Bone engineering. Toronto, Canada: em squared incorporated;2000.

27-Flach JS, Shimp LA, van Blitterswijk CA, de Groot K. A calibrated method for crystallinity determination of hydroxyl apatite coatings ASTM STP 1196, 1993

28-Fowler BO, Markovic M, Brown WE. Octacalcium Phosphate. 3. Infrared and Raman Vibrational Spectra. Chem. Mater 1993;15: 1417-1423

29-Rey C, Collins B, Goehl T, Dickson IR, Glimcher MJ. "The carbonate environement in bone mineral: a resolution-enhanced fourier transform infrared spectroscopy study." Calcif Tissue Int 1989;45:157-164.

30-Ban S, Matsuura M, Arimoto N, Hayashizaki J, Itoh Y, Hasegawa J. Factors affecting the transformation of octacalcium phosphate to apatite *in vitro*. Dent Mater J 1993;12:106-117

31-LeGeros RZ, Kijkowska R, LeGeros JP. Formation and transformation of octacalcium phosphate, OCP: a preliminary report. Scanning Electron Microscopy 1984; 1:1771-1777

32-Liu Y, Layrolle P, van Blitterswijk CA, de Groot K. Incorporation of proteins into biomimetic hydroxyapatite coatings. Bioceramics 2000; 13:71-74.

33-Barralet J, Akao M, Aoki H, Aoki H. Dissolution of dense carbonate apatite subcutaneously implanted in Wistar rats. J Biomed Mater Res 2000; 49:176-182

34-Johnsson MSA, Paschalis E, Nancollas GH. Kinetics of mineralization, demineralization, transformation of calcium phosphates at mineral and protein surface. In: Davies JE, editor. The Bone-Biomaterial interface Toronto, Canada: University of Toronto Press; 1991. p68-75.

35-Radin S, Ducheyne P, Bethold P, Decker S. Effect of serum proteins and osteoblasts on the surface transformation of a calcium phosphate coating: a physicochemical and ultrastructural study. J Biomed Mater Res 1998; 39:234-243.

36-Bender SA, Bumgardner JD, Roach MD, Bessho K, Ong JL. Effect of protein on the dissolution of HA coatings. Biomaterials 2000; 21:299-305

37-Rivero DP, Fox J, Urban RM, Galante JO. "Calcium phosphate-coated porous titanium implants for enhanced skeletal fixation." J Biomed Mater Res 22 (1988): 191-201.

38-Jansen JA, van der Waerden JPCM, Wolke JGC, de Groot K. Histologic evaluation of the osseous adaptation to titanium and hydroxyapatite-coated titanium implants. J Biomed Mater Res 1991; 25: 973-989

39-Hayashi K, Mashima T, Uenoyama K. The effect of hydroxyapatite coating on bony ingrowth into grooved titanium implants. Biomaterials 1999; 20: 111-119.

40-Carlsson L, Regner L, Johansson C, Gottlander M, Heberts P. Bone response to hydroxyapatite-coated and commercially pure titanium implants in the human arthritic knee. J Orthop Res 1994; 12: 274-285.

41- Wolke JGC, de BlieckHogevorst JMA, Dhert WJA, Klein CPAT,de Groot K. Studies on the tehrmal spraying of apatite bioceramics. J Themal Spary Technology 1992; 1: 75-82.
42-Kamakura S, Sasano Y, Shimizu T, Hatori K, Suzuki O, Kagayama, Motegi K. Implanted octacalcium phosphate is more resorbable than beta-tricalcium phosphate and hydroxyapatite. J Biomed Mater Res 2002; 59: 29-34.

CHAPTER 9

OSTEOGENICITY OF OCTACALCIUM PHOSPHATE COATINGS APPLIED ON POROUS METALLIC IMPLANTS

F. Barrère, C.M. van der Valk, R.A.J. Dalmeijer, G. Meijer,
C.A. van Blitterswijk, K. de Groot and P. Layrolle

ABSTRACT

Nowadays, the biomimetic route allows the homogeneous deposition of calcium phosphate (Ca-P) coatings on porous implants. These porous implants ensure a better fixation of prosthesis to bone. In addition, various Ca-P phases, which are solely stable at low temperature, can be deposited by using the biomimetic technique. Firstly, octacalcium phosphate (OCP) was applied on porous and dense cylinders by immersion in supersaturated Ca-P solutions. OCP coated and non-coated devices were thereafter implanted in the muscle of goats for 12 and 24 weeks. Secondly, OCP and bone-like carbonated apatite (BCA) coatings were respectively applied on porous cylinders. The implants were inserted in the femoral condyle with a gap of 1mm between the hosting bone and the implant. OCP coated porous cylinders induced ectopic bone after 12 weeks of implantation in goat muscles, as well as in the cavity of the coated dense cylinder. It appears that the confinement is an important factor for osteoinduction. A critical free calcium level might be maintained in the confined sites, triggering cell differentiation in bone cells. In the condyle, the gap was not healed in any of the cases. In contrast with BCA and bare porous cylinders, OCP coated cylinders exhibited bone formation in the centre of the implant. This suggests a higher osteogenic potential of OCP coating than BCA. The nature of the Ca-P coating, via its microstructure, its dissolution rate and its specific interactions with body fluids may influence osteogenicity of the Ca-P biomaterial.

INTRODUCTION

Calcium phosphate (Ca-P) coated metallic prostheses have been highly successful in orthopedic surgery due to their osteoconductive properties. The osseointegration of orthopedic implants is related to both their surface morphology and the nature of Ca-P coating. On one hand, porous surfaced-implants can enhance bone ingrowth as compared to dense implants *in vivo* [1-3]. On the other hand, Ca-P coated implants stimulate the early bone formation onto the implants as compared to non-coated implants *in vivo* [4-6], and Ca-P coated porous implants enhance bone ingrowth as compared to porous implants [7-9]. This bone stimulation is due to the dissolution of the Ca-P coating in the surrounding body fluids and the release of free Ca^{2+} [10, 11]. The osteogenic potential of Ca-P coating is still active in gaps up to 2mm created between the host bone and the Ca-P coated implant [12-14]. Ca-P ceramics have also shown osteoinductive properties. For example, some specific Ca-P porous materials induced bone in nonosseous environments [15-19]. Although the reasons behind osteoinduction by Ca-P remain unclear, osteoinduction strongly depends on the geometry of the material [20], the nature of the implanted Ca-P ceramics [21], and on the microporosity of the implant [22]. Such osteoinductive Ca-P biomaterials could be attractive for bone repair in clinics because they may facilitate bone formation by osteogenic cells, especially in revision of hip arthroplasty where press-fit of the implant cannot be always achieved.

So far, the deposition of Ca-P coatings on and in porous material has been incomplete because of the line of sight application of the current plasma-spraying coating technique. However, it is nowadays possible to coat evenly porous implants with Ca-P by using the biomimetic route. This biomimetic route is based on the nucleation and growth of Ca-P from supersaturated calcifying solutions called Simulated Body Fluids (SBF) [23]. Since the process occurs in aqueous media, it is now possible to coat complex shaped materials. Resulting from the physiological conditions of this technique, diverse Ca-P phases such as octacalcium phosphate (OCP) or bone mineral-like carbonated apatite (BCA) that are solely stable at low temperature, can be deposited [24-26]. So far, the biological evaluation of these two sorts of coatings has been conducted *in vitro* [27-30], subcutaneously in rats [30], and in muscles of dogs [32]. It has been shown that OCP and BCA coatings have a different *in vitro* and *in vivo* degradation behavior related to their different nature and microstructure [30].

The aim of this study was to evaluate the osteogenic potential of OCP and BCA biomimetic coatings in goats. First, OCP coating was applied on two sorts of implants: dense titanium alloy (Ti6Al4V) and porous (Hedrocel™) cylinders. Thereafter, they were implanted in muscle in order to validate the osteoinduction observed earlier in dogs [31], and in order to estimate the importance of the macrostructure, the microstructure, and the physicochemistry

of the implant. Second, OCP and BCA coatings were evaluated in a gap-healing model. Coated and bare porous cylinders were inserted in femoral condyle, where a gap of 1mm was created in between the implant and the host tissue. Because these coatings are applied on a similar porous scaffold, the importance of the structure and the physicochemistry of OCP and BCA coatings were evaluated.

MATERIALS AND METHODS

Materials

Metal implants

Dense titanium alloy (Ti6Al4V surgical grade, Smitford Staal BV, The Netherlands) and porous tantalum cylinders (Hedrocel^{TM}, Implex Corporation, USA) were used as implants. They had similar dimensions (5mm in diameter and 10mm in length). The Ti6Al4V cylinders had a dense surface. Inside, they were hollow with a diameter of 2.5mm, one side being open and the other side closed (see figures in Results). Hedrocel is a porous material fabricated by chemical vapor infiltration of pure tantalum onto a highly porous vitreous carbon skeleton. The porous structure possessed 70 to 75% porosity and a regular array of interconnecting pores averaging 400 to 500 µm.

The metal implants (Ti6Al4V and Hedrocel) were ultrasonically cleaned for 15 minutes in respectively acetone, ethanol 70% and demineralized water. The Ti6Al4V implants were etched with Kroll's reagent a mixture of 996ml of demineralized water, 2ml of fluorhydric acid (40 %) and 4ml of nitric acid (66 %), in an ultrasonic bath for 30 minutes. After etching, the samples were thoroughly rinsed with demineralized water for 10 minutes. Etching was only performed on Ti6Al4V in order to obtain a fresh oxide layer on the substrate.

Preparation of the Biomimetic Ca-P coatings

The procedure to produce the two biomimetic coatings has been mentioned elsewhere [24,26,28,30]. OCP coating is 100% crystalline, and it is composed octacalcium phosphate crystals (OCP, $Ca_8(HPO_4)_2(PO_4)_4.5H_2O$) that grew perpendicularly to the substrate. BCA coating is 65% crystalline, and it is composed of a carbonate apatite closely similar to bone mineral [26, 28]. The implants gamma-sterilized at 25 kGy.min (Gammaster, The Netherlands). Prior to implantation, uniformity, thickness and structure of the coatings were controlled by Environmental Scanning Electronic Microscopy (ESEM), Backscattering Scanning Electronic Microscopy (BSEM) and Infrared spectroscopy (IR). The coating thickness was approximately of 20-30 µm, for both the OCP and BCA coatings.

Animal Experiments

After approval by the Dutch Animal Care and Use Committee, a large animal study was performed on 14 Dutch milk goats of 60-70kg, housed by the Central Laboratory Animal Institute (GDL), Utrecht University. Prior surgery, all the animals were quarantined for at least four weeks. The general condition of the goats was checked daily. Prior to surgery, the goats were weighed and they were anaesthetized. A dose of Domosedan (Pfizer Animal Health BV, Capelle aan de Ijssel, The Netherlands) of 0.1 ml in 5 ml physiological salt solution (approx. 1 ml / 25 kg body weight) was administered by intravenous injection. The surgical procedure was performed under general inhalation anaesthesia. Thiopental (Nesdonal, about 400 mg / 70 kg body weight on indication, Rhone Merieux, Amstelveen, The Netherlands) was injected intravenously and anaesthesia was maintained by inhaling a gas mixture of nitrous oxide, oxygen and Halothane (ICI-Farma, Rotterdam, The Netherlands) through an endotracheal tube.

Intra-muscular implantation

Sixteen samples were implanted in total (4 OCP coated Hedrocel, 4 bare Hedrocel, 4 OCP coated Ti6Al4V, and 4 bare Ti6Al4V) for each survival period (12 and 24 weeks). Both lateral back muscles (left and right) of each goat were used. The skin was shaved and disinfected with Iodine (1 % in 70 % ethanol). Two skin incisions, on each side of the spine, of approximately 2 cm in length were made. An intra-muscular pocket was prepared by blunt dissection in which one implant was placed by using tweezers. In each side, two bare and two coated metal implants were inserted according to a defined implantation scheme. After insertion of all four implants, the muscle and skin was sutured with Vicryl 4-0 and 3-0 respectively.

Implantation in the femoral condyle

Under general anesthesia, a size defect of 7 mm in diameter was created in the lateral and medial condyle of both femurs (left and right) of goats by using a saline-cooled dental drill. For each goat, four implantation sites were used in total. Two bare and four coated (two OCP and two BCA) Hedrocel implants were inserted. The cylinders were held centered by placing o-ring Teflon spacers of 1 mm in thickness on each end of the plug. The Teflon washers created a 1 mm gap surrounding the implant. The coated or bare cylindrical implants were inserted in the 7 mm defect by using a special designed instrument. The incision was routinely closed with sutures.

Retrieval of the implants

The goats were sacrificed after 12 and 24 weeks by an intravenous overdose of Euthesaat (about 20 ml of 400 mg pentobarbital sodium/ml). The implants

with surrounding tissues were explanted by sharp dissection and immediately put into cold Karnovsky fixative (4 % Paraformaldehyde, 5 % Glutaraldehyde) and stored for at least one week at 4 ºC.

Histological analyses

After 1 week of storage in Karnovsky fixative at 4 °C. the implants were washed in phosphate buffered solution, dehydrated in graded series of alcohol 70% up to 100%. The implants were transferred to methylmethacrylate solution (MMA), which polymerized into polymethylmethacrylate (PMMA) at 37°C in one week. Longitudinal implants histology with a thickness of 10-15 μm was made on a modified interlocked diamond saw (Leica microtome, Rijswijk, The Netherlands). Sections were stained with 1% methylenblue and 0.3% basic fuchsin. The sections were examined by light microscopy. Half of the implant was polished, carbon sputtered and analyzed by Back Scatter Electron Microscopy (BSEM, Philips XL 30 ESEM/FEG).

RESULTS

ESEM photos of the cross-sectioned Hedrocel showed that both OCP and BCA coating were homogeneous (fig 1).
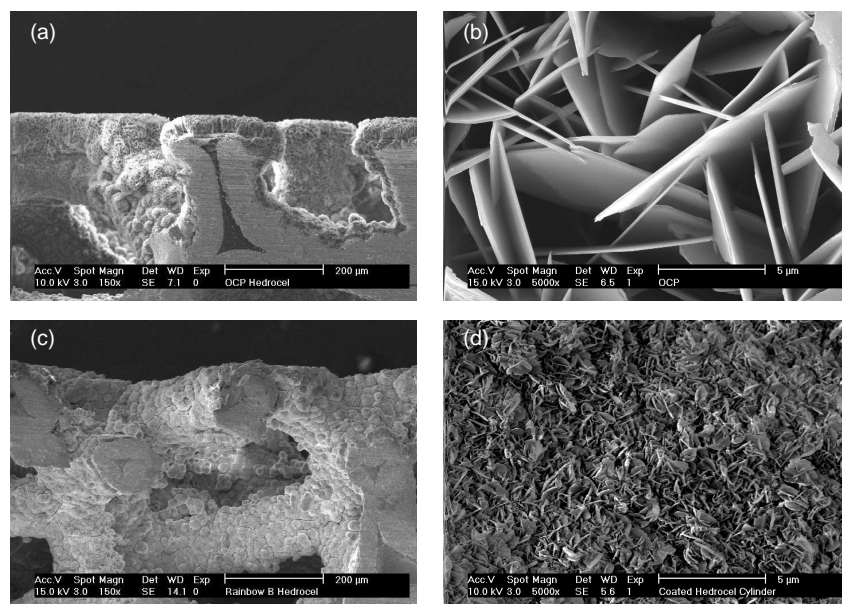

Figure 1: ESEM photos of Hedrocel implant coated with OCP at a) magnification x150, b) at magnification x5000), and with BCA c) at magnification x150, d) at magnification x5000.

OCP coating was somehow thicker at the exterior of the porous implant as compared to the interior. However, both coatings had a similar thickness of approximately 20-30μm. After implantation, the animals recovered quickly and there were no surgical complications. Within two hours post-operatively the animals were standing and walked without a limb. During the post-operative period, none of the animals has lost significant weight. After sacrifice, no gross abnormalities or no sign of infection were noticed around the implants.

Intramuscular implantation
Table 1 summarizes the bone incidence of the intramuscular implantations.

	12 weeks	24 weeks
Bare Ti6Al4V	0/4	0/4
OCP Ti6Al4V	1/4[*]	1/4[*]
Bare Hedrocel	0/4	0/4
OCP Hedrocel	3/4	0/4

Table 1: Bone incidence after intramuscular implantation in goats. (*) bone was detected in the cavity of the Ti6Al4V cylinder, and not on the outer surface

OCP coated and bare Ti6Al4V cylinders
After 12 and 24 weeks, OCP coating dissolved extensively, and remained in few random areas after 12 weeks of implantation. Fibrous tissue covered the Ti6Al4V implants. In two cases, one at 12 weeks and on at 24 weeks, histology showed ectopic bone formed in the inner cavity of the Ti6Al4V cylinders (figure 2).
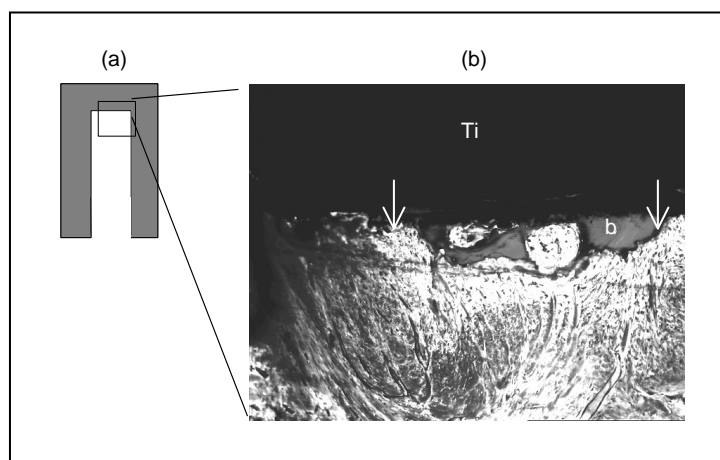

Figure 2: (a) Design of the Ti6Al4V cylinder implants. (b) ectopic bone (b) formed in the cavity of the Ti6Al4V cylinder, as shown by light microscopy (x200). The yellow arrows point out the remaining OCP coating.

OCP coated and bare Hedrocel cylinders

After 12 and 24 weeks of implantation, the OCP coating had completely disappeared. Three out of four OCP-coated Hedrocel implants exhibited bone in the pores after 12 weeks implantation (figure 3a,b). BSEM images indicated that bone was in direct contact with Hedrocel substrate without the intervention of fibrous tissue. However, in some places the OCP coating could be visible as an integrated layer in *de novo* bone (fig 3c). Bone was formed in the interior of the implants, and in several parts of the porous implants. After 24 weeks of implantation, two coated Hedrocel implants exhibited a random purple filling in the pores similar to bone stained in similar conditions. However, no bone cells-like could be detected, suggesting the presence of a calcified matrix.

Gap healing implantation in the femoral condyle

Table 2 summarizes the bone incidence of the gap-healing implantation in the femoral condyle.

	Gap healed	Direct bone contact	Bone in the centre
Bare Hedrocel	0/2	0/2	0/2
OCP Hedrocel	0/2	2/2	2/2
BCA Hedrocel	0/2	2/2	0/2

Table 2: Bone incidence in the porous implants in the gap (1mm) created in the femoral condyle of goats.

Bare Hedrocel cylinders

After 12 weeks of implantation, the original margins of the drill hole were still visible. At the drill margins of the trabeculae, newly formed bone could be seen. Bare Hedrocel implants showed columns of bone growth towards the implant, but bone was confined along the Teflon spacers and the outer perimeter of the implant. A fibrous tissue was observed between the newly formed bone and the Teflon spacer, as well as between the newly formed bone and the walls of the pores. The rest of the implant was mainly filled by fat cells and by fibrous tissues (fig 4a).

BCA coated Hedrocel cylinders

After 12 weeks of implantation, light microscopy of the two BCA coated implants showed similar features compared to bare Hedrocel cylinders: new bone formed in the gap between the cortical bone and the implants, and bone reached the implants only along the Teflon spacers (figure 4b). Additionally, BCA coating had almost completely disappeared. The coating could be rarely detected in the pores of the implant, and in some parts, it was integrated with *de novo* bone. Bone was in direct contact with Hedrocel cylinders. No evidence

of bone in the center of the implant could be detected. The rest of the implant was filled mainly by fat cells and fibrous tissue.

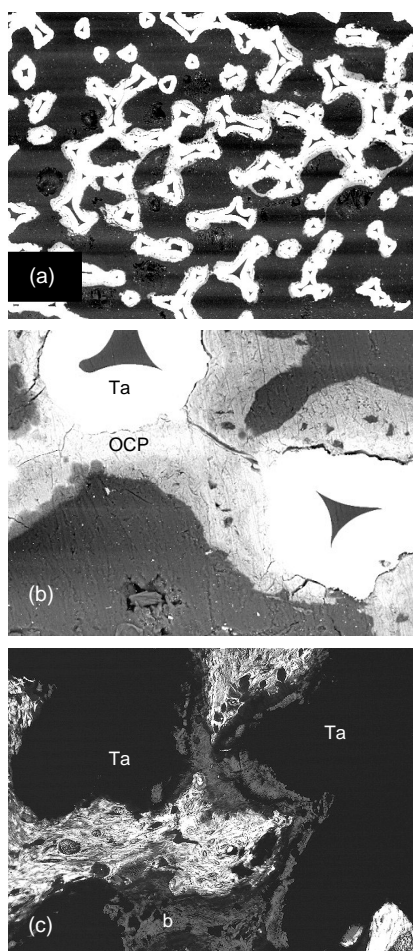### *OCP coated Hedrocel cylinders*

Figure 3: OCP coated Hedrocel explanted after 12 weeks from muscle of goats: a) BSEM (x25), b) BSEM (x250). White areas correspond to the tantalum pore walls (Ta), the dark grayish areas correspond to ectopic bone (b), and the light gray layer represents OCP coating (black arrow), c) light microscopy (x100). The arrows indicate the remaining OCP coating.
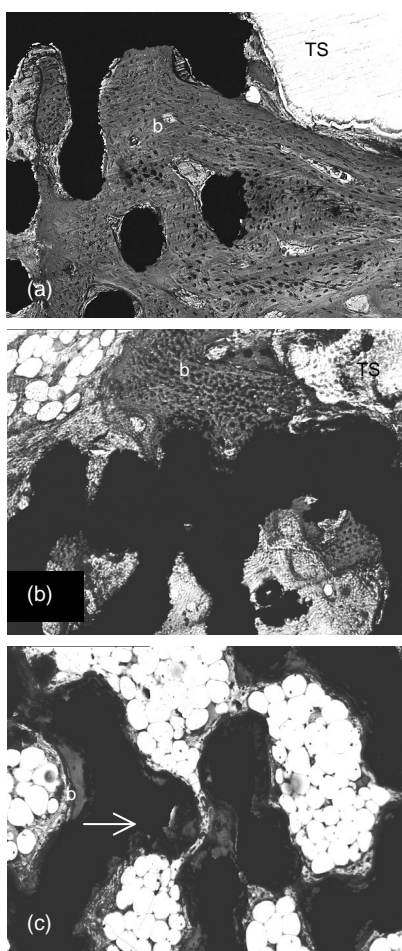
Figure 4: Bone formed on the three sorts of Hedrocel cylinders after 12 weeks of implantation in femoral condyle (gap-healing model). Magnification x100. Arrows indicate the remaining coating. (a) Bare Hedrocel: *de novo* bone (b) was only observed at the vicinity of the Teflon spacer (TS); (b) BCA coated Hedrocel; (c) OCP coated Hedrocel on partially remaining OCP coating.

After 12 weeks of implantation, light microscopy of the 2 OCP coated implants showed bone growth along the Teflon spacers towards the implant. The original margins of the drill hole were still visible. In contrast with BCA coating, OCP coating could still be detected after 12 weeks of implantation, and newly formed bone was also present in the center of the Hedrocel implants (fig 4c). BSEM revealed that OCP coating was integrated in the newly formed bone (fig 5a, 5b). In figure 5b, OCP crystals were visible and they were completely interlocked in *de novo* bone. The rest of the porous implant was filled mainly with fat cells and fibrous tissues.
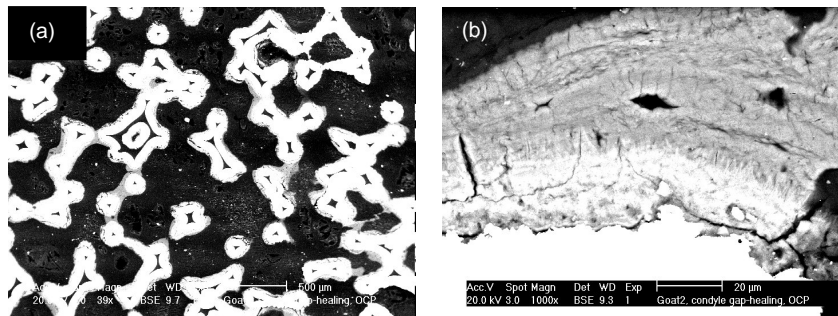

Figure 5: BSEM photo of bone in the center of OCP coated Hedrocel implanted in the femoral condyle (gap-healing model). a) at magnification x40, b) at magnification x1000: note the bonding between OCP and bone, the OCP crystals are interlocked with ectopic bone. White areas correspond to the tantalum pore walls (Ta), The dark grayish areas correspond to ectopic bone (b), and the light gray layer represents OCP coating (black arrow).

DISCUSSION

With regard to the intramuscular implantation in goats, it appears that OCP coating can induce bone formation in a nonosseous site. Firstly, bare materials -Ti6Al4V and Hedrocel cylinders– did not lead to intramuscular bone formation. Secondly, OCP coated porous structure induced bone formation, either in the Hedrocel pores, or in the inner cavity of the Ti6Al4V cylinder, but not on flat substrates such as Ti6Al4V cylinders. From these observations, two conditions seem to be required to induce ectopic bone formation: 1) the presence of a Ca-P coating, and 2) the architecture of the implant. These two conditions are simultaneously mandatory. Within porous implants, the sole surface composition of the pore walls rule the formation or not of bone. Vice versa, dense flat OCP coated implants did not lead to any bone formation, whereas in the cavity of the Ti6Al4V cylinder, bone could be found apparently formed following the intramembranous ossification route [32]. According to the BSEM imaging, OCP alone was not detected on the surface of the pores, indicating that the coating dissolves in contact with body fluids. On the other hand, OCP was fully integrated in the newly formed bone, without intervention of fibrous

tissues. In other areas where bone is present, no OCP coating could be detected, suggesting that OCP coating was completely resorbed. Bone was in direct contact with Hedrocel material.

Osteoinduction by porous Ca-P ceramics can be attributed to 1) the incorporation and concentration of Bone Morphogenetic Proteins (BMPs) by Ca-P crystals [32-34], 2) a low oxygen tension in the central region of the implant triggering the pericytes of microvessels to differentiate into osteoblasts, 3) a rough surface produced by the 3D microstructure causing the asymmetrical division of mesenchymal cells that would produce osteoblasts, 4) the surface charge of the substrate triggering cell differentiation, 5) the bone-like apatite layer formed *in vivo* that recognize mesenchymal cells, or 6) the local high level of free Ca^{2+} provided by the Ca-P material that triggers cell differentiation and bone formation [32]. In our experiments, as the presence of Ca-P and of a porous structure are two simultaneously required conditions for bone induction, the proposals 3), 4) and 5) concerning the rough 3D-microstructure, the surface charge and the bone-like apatite recognition cannot be the sole parameters. Otherwise, bone could have been induced on the OCP coated dense Ti6Al4V cylinders, and not only in the cavity of the Ti6Al4V implants. Incorporation of BMPs (proposal 1), and the presence of Ca^{2+} (proposal 6) are also expected from a flat and smooth substrate such as OCP coated Ti6Al4V, as observed under the skin of rats for OCP coated Ti6Al4V plates. OCP reacts dynamically towards the surrounding body fluids, and transforms into a bone-like apatite with the incorporation of organic compounds [30].

We hypothesize that a similar behavior occurs in the present study, in the case of intramuscular implantation in goats. OCP might therefore incorporate Bone Morphogenetic Proteins (BMPs). During the phase transformation, a probable release of Ca^{2+} and HPO_4^{2-} from the coating is expected. Hedrocel has a much greater specific surface area than dense Ti6Al4V cylinder. Therefore, the quantity of free Ca^{2+} is much higher for a porous substrate than for a dense one. In relation to the specific surface area of the implant, the possible incorporation of BMPs must be also in a greater extend in the case of a porous cylinder than in the case of a dense one. The amount of BMPs and free Ca^{2+} must to be highly critical in the osteoinduction phenomenon. On the other hand, bone also formed in the cavity of the Ti6Al4V cylinder, which suggest that the confinement is also a critical factor. In a confined site, the amount free Ca^{2+} released from OCP coating may remain quite stable, and high enough to trigger cell differentiation and bone formation (proposal 6). Therefore, it appears in the present study that the primary condition for inducing ectopic bone could be a quite stable critical level of free Ca^{2+}, which can be achieved in the pores of Hedrocel.

Bone formation is however limited in time. After 24 weeks of implantation no bone was observed in the four explanted Hedrocel. Ectopic bone could be detected solely in the cavity of one Ti6Al4V cylinder. However, in two out of four cases, a calcified matrix was detected in the pores. It is clear that bone does not continuously grow as function of time. As no more bone is detected on the 24-weeks implants, we can suggest that bone induced by OCP coating degraded with time. This resorption could be related to an interruption of Ca^{2+} supply from OCP coating, because of its complete dissolution. The implant being in a nonosseous site cannot benefit of a continuous differentiation into bone cell to pursue bone formation. On the other hand, the encapsulation of the implant by fibrous tissue could limit the flow of surrounding body fluids into the porous implant. This could lead to the degradation of the newly formed bone, which could be attributed to the calcified matrix observed in two porous implants after 24 weeks.

When OCP-coated, BCA-coated, and bare Hedrocel were implanted in a gap of 1mm in the condyle, marked distinctions could be noted between the three sorts of implant. Firstly, contact could be established between newly formed bone and Hedrocel along the Teflon spacer. Direct bone contact could be noted for BCA and OCP coated Hedrocel, whereas a fibrous tissue layer was often detected between the bare implant and the newly formed bone. Therefore, Ca-P coating allowed a direct bonding between the implant and the hosting bone. In all the cases OCP-coated, BCA-coated and bare Hedrocel, the gap of 1 mm was not healed, whereas bone was detected in the center of the OCP coated porous implant. Due to the high interconnectivity of Hedrocel, one cannot confirm that bone present in the center of the implant does not have a direct contact with host bone. Further, OCP coated Hedrocel could induce bone in nonosseous sites. Therefore, one can think that bone formed in the center of the implant is not necessarily connected with the host bone.

Nevertheless, this observation suggests that OCP coating has a markedly higher osteogenic potential than BCA coating. In relation to this osteogenicity difference, one could note that BCA coating had completely disappeared, whereas OCP coating remained partially after 12 weeks of implantation in trabeculae. When Hedrocel implants were inserted in femoral condyle, one must consider the strong influence of bone marrow cells. In a bony environment, the resorption of the coating depends strongly on the osteoclastic activity, ruled by the physicochemistry of the Ca-P coating [27,35,36]. The more soluble Ca-P is, the less osteoclastic activity is. [35,36]. In the case of OCP and BCA coatings, Leeuwenburgh et al. have shown that resorption pits had extended more on BCA coating *in vitro* [27]. Therefore, osteoclastic activity may be higher *in vivo* in the case of BCA than for OCP coating. A too fast osteoclastic resorption of BCA could therefore affect bone formation onto BCA coated Hedrocel.

On the other hand, the initial microstructure of the two coatings is markedly different: OCP exhibits a rough surface due to the sharp vertical crystals of approximately 20 to 30μm in length, whereas BCA exhibit a relatively smooth surface composed of globules containing tiny crystals of 1 to 3 μm in length. The initial microstructure can affect considerably osteogenic properties of Ca-P ceramics [22]: a rougher microstructure was beneficial for bone induction as compared to a smoother one. The relatively rough microstructure of OCP coating might influence positively bone formation, whereas the relatively smooth BCA might influence negatively bone formation. Independently of the material, cell adhesion, morphology and orientation are strongly affected by the implant roughness and surface physics and chemistry [37-45]. Redey et al. have shown that a difference in surface energy between a HA substrate and a type A carbonated apatite could influence significantly the early osteoblastic adhesion *in vitro*, although surface roughness of both material was similar [38]. Although the two substrates evolved into a type AB carbonated apatite with culturing time, and despite a similar final cell growth on the two materials, the authors observed differences in the kinetics of cell attachment. The relatively high-energy HA substrate accelerated cell attachment and spreading as compared to the low-energy type A carbonated apatite. In addition for a similar surface chemistry and roughness, the bigger the HA crystallite were, the higher the osteoblasts response was [43].

These two aforementioned studies are quite in accordance with our results: the large OCP crystals may favor osteoblastic activity, and the presence of carbonate in BCA may decrease its surface energy, inhibiting the early osteoblasts response towards BCA. Besides surface energy considerations, Knabe et al related a relative inhibition of osteoblasts growth *in vitro* with a relatively high phosphate-ion release [44, 45]. This observation is quite in accordance with the present study: OCP has an atomic calcium to phosphorus ratio (Ca/P) of 1.33, whereas BCA has a Ca/P=1.60 [29]. In addition BCA dissolves faster than OCP in the condyle, therefore a higher phosphate-ion release with BCA coating than with OCP coating.

CONCLUSION

The present study has shown that OCP coating has a stronger osteogenic potential as compared to BCA coating. In the muscle, the presence of OCP coating in a macroporous structure induced ectopic bone formation. In the condyle, although the 1mm-gap was not healed by bone in any of the cases, bone was detected in the center of OCP coated porous implants, whereas bone formed solely at the vicinity of the BCA coated porous implants. The nature of the Ca-P coating for a similar porous scaffold influences markedly the osteogenic potential of Ca-P biomaterials via the microstructure, the dissolution rate, the chemistry and the physics of their surface, and the specific

interactions with body fluids markedly influences osteogenicity of the Ca-P biomaterial.

References:

1-Overgaard S, Lind M, Glerup H, Bünger C, Søballe K. Porous-coated versus grit-blasted surface texture of hydroxyapatite-coated implants during controlled micromotion: mechanical and histomorphometric results. J Arthroplasty 1998;13: 449-458

2-Simmons CA, Valiquette N, Pilliar RM. Osseointegration of sintered porous-surfaced and plasma spray-coated implants: An animal model study of early postimplantation healing response and mechanical stability. J Biomed Mater Res 1999; 47:127-38

3-Deporter DA, Watson PA, Pilliar RM, Chipman ML, Valiquette N. A histological comparison in the dog of porous-coated vs. threaded dental implants. J Dent Res 1990; 69: 1138-1145.

4-Jansen JA, van der Waerden JPCM, Wolke JGC, de Groot K. Histologic evaluation of the osseous adaptation to titanium and hydroxyapatite-coated titanium implants. J Biomed Mater Res 1991; 25: 973-989.

5-Dhert WJA, Klein CPAT, Jansen JA, van der Velde EA, Vriesde RC, Rozing PM, de Groot K. A histological and histomorphometrical investigation of fluoroapatite, magnesiumwhitlockite, and Hydroxylapatite plasma-sprayed coatings in goats. J Biomed Mater Res.1993; 27: 127-138.

6-Klein CPAT, Wolke JGC, de Blieck-Hogervorts JMA, de Groot K. Calcium Phosphate plasma-sprayed coatings and their stability: an *in vivo* study. J Biomed Mater Res 1994; 28: 909-917

7-Cook SD, Thomas KA, Dalton JE, Kay JF. Enhanced bone ingrowth and fixation strength with hydroxyapatite-coated porous implants. Semin Arthroplasty 1991; 2: 268-279.

8-Pilliar RM, Deporter DA, Watson PA, Pharoah M, Chipman M, Valiquette N, Carter S, De Groot K. The effect of partial coating with hydroxyapatite on bone remodeling in relation to porous-coated titanium-alloy dental implants in the dog. J Dent Res 1991; 70: 1338-1345.

9-Cook SD, Enis J, Armstrong D, Lisecki E. Early clinical results with the hydroxyapatite-coated porous LSF Total Hip System. Dent Clin North Am 1992;36: 247-255.

10-Geesink RG, de Groot K, Klein CP. "Bonding of bone to apatite-coated implants. J Bone Joint Surg Br. 1988; 70B: 17-22.

11-Hanawa T, Kamira Y, Yamamoto S, Kohgo T, Amemyia A, Ukai H, Murakami K, Asaoka K. Early bone formation around calcium-ion-implanted titanium inserted into rat tibia. J Biomed Mater Res 1997; 36:131-136

12-Sakkers RJB, Dalmeijer RAJ, Brand R, Rozing PM, van Blitterswijk CA. Assessment of bioactivity for orthopedic coatings in a gap healing model. J Biomed Mater Res 1997; 36: 265-273.

13-Søballe K, Hansen ES, Brockstedt-Rasmussen, Bunger C. Gap healing enhanced by hydroxyapatite coatings in dog. Clin Orthop 1991; 272 : 300-307

14-Clemens JAM, Klein CPAT, Vriesde RC, Rozing PM, de Groot K. Healing of large (2mm) gaps around calcium phosphate-coated bone implant: a study in goats with a follow up of 6 months. J Biomed Mater Res 1998;40): 341-349

15-Yamasaki H. Ectopic bone formation around porous hydroxyapatite ceramics in the subcutis of dogs. Japan J Oral Biol 1990;32: 190-192.

16-Yuan H, de Bruijn JD, Yang Z, de Groot K, Zhang X. Osteoinduction by calcium phosphates. J Mat Sci Mat Med 1998; 9: 717-721.

17-Vargervik K. Critical sites for new bone formation. Bone grafts & bone substitute 1992: 112-120.

18-Ripamonti U. The morphogenesis of bone in replicas of porous hydroxyapatite obtained from conversion of calcium carbonate exoskeletons of coral. J Bone&Joint Surg 1991; 73A: 692-703.

19-Zhang X. A study of porous blocks HA ceramics and its osteogenesis." Bioceramics and the Human Body 1991: 408-415.

20-Magan A, Ripamonti U. Geometry of porous hydroxyapatite implants influences osteogenesis in baboons (Papio ursinus). J Craniofac Surg 1996;7: 71-78.

21-Yuan H, de Bruijn JD, Li Y, Feng Z, Yang K, de Groot K, Zhang X. Bone formation induced by Calcium phosphate ceramics in soft tissue of dogs: a comparative study between α-TCP and β-TCP. J Mat Sci Mat Med 2001;12:7-13

22-Yuan H, Kurashina K, de Bruijn JD, Li Y, de Groot K, Zhang X. A preliminary study on osteoinduction of two kind of calcium phosphate ceramics. Biomaterials 2000; 20: 1283-1290

23-Kokubo T, Kushitani H, Sakka S, Kitsugi T, Yamamuro T. Solutions able to reproduce *in vivo* surface-structure changes in bioactive glass-ceramics A-W3. J Biomed Mater Res 1990; 24: 721-734.

24-Barrère F, Layrolle P, van Blitterswijk CA, de Groot K. Biomimetic Calcium Phosphate coatings on Ti6Al4V: Growth study of OCP. J Mat Sci Mat Med 2001; 12: 529-534.

25-Barrère F, Layrolle P, van Blitterswijk CA, de Groot K. Biomimetic Calcium phosphate Coatings on Ti6Al4V: a Crystal Growth Study of Octacalcium Phosphate and Inhibition by Mg^{2+} and HCO3$^-$. Bone 1998; 25: 107S-111S.

26-Habibovic P, Barrère F, van Blitterswijk CA, de Groot K and Layrolle P. Biomimetic Hydroxyapatite coating on metal implants. J. Am. Ceram. Soc. accepted, in press.

27-Leeuwenburgh S, Layrolle P, Barrère F, de Bruijn J, Schoonman J, van Blitterswijk CA, de Groot K. Osteoclastic resorption of biomimetic calcium phosphate coatings *in vitro*. J Biomed Mater Res 2001; 56: 208-215

28-Barrère F, Layrolle P, van Blitterswijk CA, de Groot K. Physical and chemical characteristics of Plasma-sprayed and Biomimetic Apatite coating. Bioceramics 1999; 12: 125-128

29-Barrère F, Stigter M, Layrolle P, van Blitterswijk CA, de Groot K. *In vitro* dissolution of various Calcium phosphate coatings on Ti6Al4V." Bioceramics 2000; 13: 67-70.

30-Barrère F, van der Valk CM, Dalmeijer RAJ, van Blitterswijk CA, de Groot K, Layrolle P. *In vitro* and *in vivo* studies of biomimetic octacalcium phosphate and carbonate apatite coatings on titanium implants, J Biomed Mater Res, submitted 2001.

31-De Bruijn JD, Yuan HP, Dekker R, Layrolle P, van Blitterswijk CA. Osteoinduction by biomimetic calcium phosphate coatings and their potential use as tissue engineering scaffolds. In: Davies JE, editor. Bone engineering Toronto, Canada: em squared incorporated, 2000, p 421-434.

32-Yuan H, Osteoinduction by Calcium Phosphates, PhD thesis, Leiden University,The Netherlands 2001

33-Ripamonti U, Osteoinduction in porous hydroxyapatite implanted in ectopic sites of different animal models Biomaterials 1996; 17:31-35

34-Yuan H, Zou P, Yang Z, Zhang X, de Bruijn JD, de Groot K. Bone morphogenetic protein and ceramic-induced osteogenesis. J Mat Sci Mat Med 1998; 9: 717-721.

35-Doi Y, Iwanaga H, Shibutani T, Moriwaki Y, Iwayama Y. Osteocalstic responses to various calcium phosphates in cell cultures. J Biomed Mater Res 1999; 47: 424-433.

36-Yamada S, Heymann D, Bouler JM, Daculsi G. Osteoclastic resorption of calcium phosphate ceramics with different hydroxyapatite/β-tricalcium phosphate ratios. Biomaterials 1997; 18: 1037-1041.

37-Boyan BD, Hummert TW, Dean DD, Schwartz Z. Role of material surfaces in regulating bone and cartilage cell response. Biomaterials 1996; 17: 137-146.

38-Redey SA, Nardin M, Bernache-Assolant D, Rey C, Delannoy P, Sedel L, Marie PJ. Behavior of human osteoblastic cells on stoichiometric hydroxyapatite and type A carbonate apatite: role of surface energy. J Biomed Mater Res 2000; 50: 353-364.

39-Chou L, Firth JD, Uitto VJ, Brunette DM. Effects of titanium substratum and grooved surface topography on metalloproteinase-2 expression in human fibroblasts. J Biomed Mater Res 1998; 39: 437-445.

40-Lampin M, Warocquier-Clerout, Legris C, Degrange M, Sigot-Luizart MF. Correlation between substratum roughness and wettability, cell adhesion and cell migration. J Biomed Mater Res 1997; 36: 99-108.

41-Anselme K. Osteoblast adhesion on biomaterials. Biomaterials 2000; 21: 667-681.

42-Eisenbarth E, Meyle J, Nachtigall W, Breme J. Influence of the surface structure of titanium materials on the adhesion of fibroblasts. Biomaterials 1996; 17: 1399-1403.

43- Ong JL, Hoppe CA, Cardenas HL, Cavin R, Carnes DL, Sogal A, Raikar GN. Osteoblast precursor cell activity on HA surfaces of different treatments. J Biomed Mater Res 1998; 39: 176-183.

44-Knabe C, Gildenhaar R, Berger G, Ostapowicz W, Fitzner R, Radlanski RJ, Gross U. Morphological evaluation of osteoblasts cultured on different calcium phosphate ceramics. Biomaterials 1887; 18: 1339-1347.

45- Knabe C, Driessens FCM, Planell JA, Gildenhaar R, Berger G, Reif D, Fritzner R, Radlanski RJ, Gross U. Evaluation of calcium phosphates and experimental calcium phosphate bone cements using osteogenic cultures. J Biomed Mater Res 2000; 52: 498-508.

CHAPTER 10

GENERAL DISCUSSION
AND CONCLUSIONS

I-Physicochemistry of biomimetic calcium phosphate coating formation on titanium substrate (chapters 2 to 5)

The formation of biomimetic calcium phosphate coatings can be accelerated by using a SBF solution concentrated by a factor 5, saturated with carbon dioxide gas (CO_2).
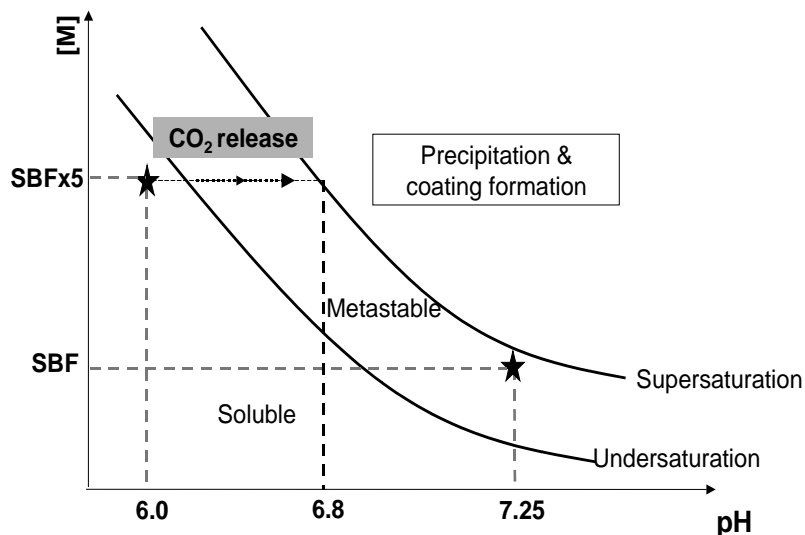

Figure 1: solubility isotherms of SBF solutions versus pH

Figure 1 illustrates the principle of the developed biomimetic process. SBF is a metastable solution at pH=7.25 and 37°C. The bubbling of CO_2 can maintain the solubility of SBFx5 at pH=6.0. When the gas supply is stopped, the CO_2 gas is liberated out of the solution, leading to a pH increase. The heterogeneous nucleation of calcium phosphate starts already after 10 minutes of immersion [1]. The full coverage is achieved at pH=6.8, when the limit of

supersaturation is passed. Meanwhile, calcium phosphate also precipitates in the solution. The formation of a uniform film depends upon the competition between the precipitation in the solution and onto the substrate. At high ionic strength, the coating formation is favored, while at low ionic strength, the precipitation in the solution is favored in detriment to the coating deposition. In addition, the buffering effect of carbonate ions, and the crystal growth inhibition by carbonate and magnesium ions contributed to the formation kinetics a homogeneous calcium phosphate film [2,3].
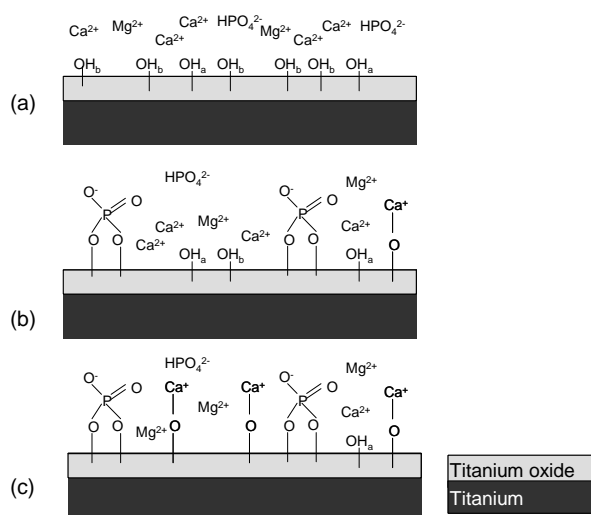

Figure 2

Chemically, the passive oxide layer covering naturally titanium substrates interacts with calcium and phosphate ions from SBF solutions as illustrated in figure 2. Under physiological conditions of pH=6-7.4, the titanium dioxide layer exhibits a slightly negative charge [4], i.e. a larger density of basic hydroxyl groups (OH_b) than acidic hydroxyl groups (OH_a). (figure 2a). Kinetically, and irrespective to the surface charge, the phosphate groups start to bind with the acidic hydroxyl groups (figure 2b) [5]. Thereafter, the calcium ions present at the vicinity of the substrate bind in a larger quantity than phosphate on the oxide layer due to its slightly negative surface charge (figure 2c). Although magnesium does not bind directly to the substrate, this crystal growth inhibitor was present at the calcium phosphate coating/ titanium interface, certainly incorporated in the calcium phosphate structure [3].

The primary calcium phosphate nuclei observed on the titanium substrate are of an approximate size of 15nm [1]. These nuclei grow over immersion time up to approximately 50 to 100nm. The coating is formed by the aggregation of these calcium phosphate nuclei to from bigger globules. The

interfacial cohesion between the substrate and the calcium phosphate film is achieved by a glassy matrix composed of tiny calcium phosphate nuclei [1]. These nanometer-scale nuclei are stabilized on the substrate due to a relatively high concentration in magnesium as previously mentioned [3,6]. This interfacial calcium phosphate layer acts as "glue" for the coating. Although carbonate was not specifically observed at the coating/substrate interface, like magnesium, this crystal growth inhibitor contributes to the formation of small and poorly crystallized calcium phosphate entities, and therefore contributes to a more efficient coating attachment [2,3]. Therefore crystal growth inhibitors chemically favor the attachment of the biomimetic calcium phosphate film.

With regard to the titanium texture, the initial heterogeneous nucleation process is not affected by different roughness. However, the density of calcium phosphate nuclei is higher for a rougher substrate [1], consistent with an increase of the surface reactivity by exposing more numerous active sites towards the solution, and probably to a greater wettability [7]. In addition, when the substrate is too smooth, the detachment of the calcium phosphate film occurs indicating that the adhesion of the calcium phosphate film requires a sufficient roughness [1]. Table 1 summarizes the different substrate parameters that can act on the formation of calcium phosphate from SBFs on a substrate. In summary, the uniformity and attachment of the biomimetic calcium phosphate film are a combination of salt composition in SBFs and properties of titanium substrate.

Titanium substrate	Surface Roughness	Surface Charge	Presence of hydroxyl groups
Calcium phosphate coating formation in vitro	♦ Tailoring Ca-P film morphology [8] ♦ Mechanical attachment ♦ Reactivity ♦ Hydrophobicity, wettability [7]	♦ Primary electrostatic interactions	♦ Basic and acidic character ♦ Density ♦ Bonding with HPO_4^{2-} and/or Ca^{2+} ♦ Hydrophobicity, wettability

Table 1

II-Flexibility of the biomimetic method (chapter 6)

Various novel calcium phosphate coatings can be produced by a two-step procedure. The amorphous calcium phosphate created by SBFx5 solution film acts as a seeding substrate, via a dissolution/reprecipitation process, to produce thick crystalline calcium phosphate coating by immersion in a subsequent supersaturated calcifying solution, containing less or no crystal

growth inhibitors [9,10]. The presence of the first film is mandatory, emphasizing the critical role and the critical amount of crystal growth inhibitors during the heterogeneous nucleation of calcium phosphate onto titanium substrate.

Depending on the pH and the composition of the supersaturated calcifying solution, different biomimetic calcium phosphate coatings can be deposited. For example, an octacalcium phosphate (OCP) coating can grow perpendicularly onto the titanium substrate [10]. The addition of magnesium or carbonate in the supersaturated calcifying solution induces the formation of carbonated apatitic phases or calcium-deficient apatitic phases [9]. By slight composition changes, the structure and microstructure of the biomimetic calcium phosphate coatings can be tailored.

III-Biological activity of biomimetic calcium phosphate coatings (chapters 7 to 9)

Bone formation on biomimetic calcium phosphate coatings results from the dynamic interactions between several physicochemical parameters and the body fluids. The initial structure, the microstructure, the crystallinity, and the surface morphology of calcium phosphate influence the dissolution rate [11-14], and the interaction with organic compounds and cells [15-21]. Vice versa, the organic compounds and cells present in the body fluids influence the degradation and dissolution rate, the surface morphology and the structure of the calcium phosphate [22-25].

In agreement with the above, the biological response towards the biomimetic carbonated apatite and octacalcium phosphate coatings differ. On one hand, carbonated apatite (BCA) coated porous metallic implants were found to be osteoconductive. On the other hand, octacalcium phosphate (OCP) coated porous metallic implants revealed osteoinductive properties [26]. This demonstrates that the osteogenic potential of calcium phosphate substrates depends strongly on the primary physicochemical features of the calcium phosphate coatings. Although all of the studied coatings evolve into a carbonated apatitic structure *in vitro* and *in vivo*, they incorporate selectively organic compounds certainly depending on their initial structure, composition and microstructure.

Yuan proposed several factors that could explain the osteoinduction by porous calcium phosphate ceramics, which are: 1) the incorporation and concentration of Bone Morphogenetic Proteins (BMPs) by calcium phosphate crystals, 2) a low oxygen tension in the central region of the implant triggering the pericytes of microvessels to differentiate into osteoblasts, 3) a particular microstructure causing the asymmetrical division of mesenchymal cells that

would produce osteoblasts, 4) the surface charge of the substrate triggering cell differentiation, 5) the bone-like apatite layer formed in vivo that recognize mesenchymal cells, or 6) the local high level of free Ca^{2+} provided by the calcium phosphate material that triggers cell differentiation and bone formation [27]

The recognition by mesenchymal cells of a bone-like apatite layer (proposal 5) does not comply with the present thesis since the biomimetic carbonated apatite, resembling to bone-mineral structure is not osteoinductive, whereas OCP is.
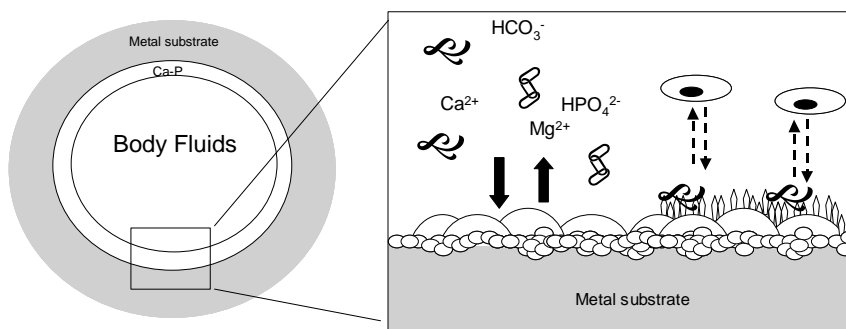

Figure 3: Schematic view of a coated porous implant *in vivo*. The biomimetic calcium phosphate coating (Ca-P) is "glued" on the pore walls with tiny calcium phosphate nuclei [this thesis]. The calcium phosphate coating surface is exposed to body fluids. With inorganic compounds the coating evolves into a carbonated apatitic structure, incorporating also organic compounds (⬡ and §). Depending on the structure and microstructure of the calcium phosphate coating, distinct organic compounds and distinct cells will interact in favor or not to bone formation.

As illustrated in figure 3, the factors affecting the osteoinductive properties of the calcium phosphate coatings on a porous implant can be related to:

> (i) The resorption rate of the calcium phosphate related to either the release of free calcium and free phosphate in the pores, or the osteoclastic activity in the case of the gap-healing model in the condyle,
>
> (ii) The interaction with specific organic compounds that can stimulate bone cells activity,
>
> (iii) A rough microstructure, rendering the calcium phosphate surface more reactive than smooth ones. The reactivity of the surface can influence the free-calcium level in the pore, or the amount of adsorbed BMPs,
>
> (iv) In addition, during the dissolution of the carbonated apatitic coating, a critical level of phosphate [18,19] and/or carbonate [28] may also affect bone cells response.

IV-Perspectives and conclusions

The acceleration of the biomimetic process by increasing the supersaturation of SBF solutions broadens the possibilities of applications. Firstly, this acceleration avoids the alkaline or precalcification treatments that weaken the substrate. Secondly, the biomimetic calcium phosphate coatings can be deposited on diverse substrates, such as heat sensitive materials, porous materials, or poor calcium phosphate nucleator. Therefore, one can imagine the broadening of engineered materials that can be coated, and that could enhance the osseointegration, the fixation and the longevity of the implant.

With regard to the biological activity, via a simple, low-temperature and aqueous process, it was possible to create an osteoinductive porous implants without the use of osteoinductive proteins. The intrinsic osteoinduction of such coatings could be applied in order to enhance osseointegration of the implant. However, to date the comparison between classical osteoconductive and osteoinductive calcium phosphate coatings on dense implants has not been investigated. Depending on the clinical application, the osteoinductive octacalcium phosphate (OCP) may or may not be beneficial for bone repair.

Because the structure and microstructure of the calcium phosphate coatings can be tailored by simple and slight changes in the supersaturated calcifying solutions, more fundamental studies could be performed to determine and evaluate at which extend the parameters evoked in this thesis influence the osteoinduction of a calcium phosphate substrate.

The plasma spraying of hydroxylapatite onto metallic implants has greatly improved the osseointegration and the longevity of hip prostheses. Nowadays, the biomimetic approach to coat prostheses broadens the possibilities to create novel calcium phosphate coatings with tailored structure, microstructure that influence considerably the biological response. As the composition and microstructure of the biomimetic calcium phosphate coatings are homogeneous in thickness, a more predictable resorption and thus bioactivity are expected in bony sites. The benefits of a tailored and a full resorption of the biomimetic coatings on bone bonding, bone fixation *in vivo* remains to be investigated.

References

1-Barrère F, Snel M, van Blitterswijk CA, de Groot K, Layrolle P. Nanoscale study of the nucleation and growth of a biomimetic Ca-P coating. Chem Mater (submitted).

2-Barrère F, van Blitterswijk CA, de Groot K, Layrolle P. Influence of ionic strength and carbonate on the Ca-P coating formation from SBFx5 solution. Biomaterials (in press).

3-Barrère F, van Blitterswijk CA, de Groot K, Layrolle P. Nucleation mechanism of Ca-P coating formed from SBFx5 solution: influence of magnesium. Biomaterials (in press).

4-Tengvall P, Lundstrom I. Physico-chemical considerations of titanium as biomaterial. Clinical Materials 9 (1992): 115-134.

5-Barrère F, van Blitterswijk CA, de Groot K, Rey C, Layrolle P. Calcium phosphate interactions with titanium oxide and aluminum oxide substrates: an XPS study. J Mat Sci Mat Med (submitted).

6-Boskey AL, Posner AS. Magnesium stabilization of amorphous calcium phosphate: a kinetic study. Mat Res Bull 9 (1974): 907-916.

7-Hazlett RD. On surface roughness effects in wetting phenomena. Contact angle, wettability and adhesion Ed. Mittal KL Utrecht, The Netherlands: VSP BV (1993): 173-181.

8-Leitao E, Barbosa M, de Groot K. Influence of substrate material and surface finishing on the morphology of the calcium-phosphate coating. J Biomed Mat Res 36 (1997): 85-90.

9-Barrère F, Layrolle P, van Blitterswijk CA, de Groot K. Biomimetic Calcium-Phosphate Coatings on Ti6Al4V: a Crystal Growth Study of OctaCalcium Phosphate and Inhibition by Mg^{2+} and HCO_3^-. Bone 25 (1999): 107S-111S.

10-Barrère F, Layrolle P, van Blitterswijk CA, de Groot K. Biomimetic Calcium Phosphate coatings on Ti6Al4V: Growth study of OCP. J Mater Sci Mater Med 12 (2001): 529-534.

11-Radin S, Ducheyne P. The effect of calcium phosphate ceramic composition and structure on in vitro behavior. I Dissolution. J Biomed Mater Res 27 (1993): 25-34.

12-Radin S, Ducheyne P. The effect of calcium phosphate ceramic composition and structure on in vitro behavior. II Precipitation. J Biomed Mater Res 27 (1993): 35-46.

13-Radin S, Ducheyne P. The effect of calcium phosphate ceramic composition and structure on in vitro behavior. III Porous versus dense ceramics. J Biomed Mater Res 28 (1994): 471-488.

14-Barrère F, Stigter M, Layrolle P, van Blitterswijk CA, de Groot K. In vitro dissolution of various Calcium-Phosphate coatings on Ti6Al4V. Bioceramics 13 (2000): 67-70.

15-Barrère F, van der Valk CM, Dalmeijer RAJ, van Blitterswijk CA, de Groot K, Layrolle P. In vitro and in vivo dissolution study of biomimetic calcium phosphate coatings on Ti6Al4V. J Biomed Mat Res (in press).

16-Redey SA, Nardin M, Bernache-Assolant D, Rey C, Delannoy P, Sedel L, Marie PJ. Behavior of human osteoblastic cells on stoichiometric hydroxyapatite and type A carbonate apatite: role of surface energy. J Biomed Mat Res 50 (2000): 353-364.

17-de Bruijn JD, Flach JS, Leenders H, van den Brink J, van Blitterswijk CA. Degradation and interface characteristics of plasma sprayed hydorxyapatite coatings with different crystallinities. Bioceramics 5 (1992): 291-298.

18-Knabe C, Gildenhaar R, Berger G, Ostapowicz W, Fitzner R, Radlanski RJ, Gross U. Morphological evaluation of osteoblasts cultured on different calcium phosphate ceramics. Biomaterials 18 (1997): 1339-1347.

19-Knabe C, Driessens FCM, Planell JA, Gildenhaar R, Berger G, Reif D, Fritzner R, Radlanski RJ, Gross U. Evaluation of calcium phosphates and experimental calcium phosphate bone cements using osteogenic cultures. J Biomed Mat Res 52 (2000): 498-508.

20-Leeuwenburgh S, Layrolle P, Barrère F, de Bruijn J, Schoonman J, van Blitterswijk CA, de Groot K. Osteoclastic resorption of biomimetic calcium phosphate coatings in vitro. J Biomed Mat Res 56 (2001): 208-215.

21-Johnsson MSA, Paschalis E, Nancollas GH. Kinetics of mineralization, demineralization, transformation of calcium phosphates at mineral and protein surface.

In: Davies JE, editor. The Bone-Biomaterial interface Toronto, Canada: University of Toronto Press (1991): 68-75.

22-Liu Y, Layrolle P, van Blitterswijk CA, de Groot K. Incorporation of proteins into biomimetic hydroxyapatite coatings. Bioceramics (2000): 71-74.

23-Liu Y, Layrolle P, de Bruijn JD, van Blitterswijk CA, de Groot K. Biomimetic coprecipitation of calcium phosphate and bovine serum albumin on titanium alloy. J Biomed Mater Res 57 (2001): 327-335.

24-Bender SA, Bumgardner JD, Roach MD, Bessho K, Ong JL. Effect of protein on the dissolution of HA coatings. Biomaterials 21 (2000): 299-305.

25-Radin S, Ducheyne P, Bethold P, Decker S. Effect of serum proteins and osteoblasts on the surface transformation of a calcium phosphate coating: a physicochemical and ultrastructural study. J Biomed Mater Res 39 (1998): 234-243.

26-Barrère F, van der Valk CM, Dalmeijer RAJ, Meijer G, van Blitterswijk CA, de Groot K, Layrolle P. Osteogenicity of octacalcium phosphate coatings applied on porous metallic implants. J Biomed Mat Res (submitted).

27-Yuan H, de Bruijn JD, Li Y, Feng Z, Yang K, de Groot K, Zhang X. Bone formation induced by Calcium phosphate ceramics in soft tissue of dogs: a comparative study between α-TCP and β-TCP. J Mater Sci Mater Med 12 (2001): 7-13.

28-Anderson RE, Jee WSS, Woodbury DM. Stimulation of carbonic acid anhydrase in osteoclasts by parathyroid hormone. Calcif Tissue Int 37 (1985): 646-650.

SUMMARY

Plasma-sprayed hydroxylapatite coatings on metallic prosthesis significantly increased the success rate of hip arthroplasty, namely from about 90% after 10 years for cemented hip stems to 98% for HA coated ones. Nowadays, the biomimetic approach has received increased interest because of the possible advantages of this route. The physiological conditions of the biomimetic process can broaden the variety of materials to be coated such as heat-sensitive or porous implants, and the variety of calcium phosphate phases, including those that are solely stable under mild temperature conditions. In addition, drugs and growth factors can be easily included into such coatings. The aim of this thesis was to accelerate and to optimize the biomimetic process, to study the physicochemistry involved in the formation of calcium phosphate on a heterogeneous substrate, to evaluate the flexibility of the biomimetic route, and finally to investigate the in vitro and in vivo behavior of these novel coatings.

Thick biomimetic calcium phosphate coatings (30 to 55 μm) on titanium substrates could be produced within less than 72h by a two-step procedure. First titanium plates were immersed in a simulated body fluid solution concentrated by 5 (SBFx5), supersaturated in carbon dioxide gas. After 24h, a homogeneous amorphous calcium phosphate film of 1 to 5 μm in thickness formed onto the titanium substrate via a chemical bonding (chapter 2-5). The subsequent immersion of these coated plates in a second supersaturated calcifying solution led to the growth of the final biomimetic calcium phosphate coating. Depending on the composition of the supersaturated calcifying solution, various calcium phosphate phases could be produced such as carbonated apatite or octacalcium phosphate coatings (chapter 6).

The developed biomimetic calcium phosphate coatings showed significant physicochemical differences compared to each other and to hydroxylapatite plasma sprayed coatings, due to different structure and microstructure. However, all of these coatings evolved into a carbonated apatitic structure when they were immersed in the simulated physiological fluid α-MEM, at pH=7.3 (chapter 7-8).

In vivo, the biomimetic carbonated apatite and octacalcium phosphate coatings showed significant differences. The two coatings incorporated different organic compounds when subcutaneously implanted in rats (chapter 8). These differences were emphasized in a goat study (chapter 9). Octacalcium phosphate coating on porous metallic implants was found to be osteoinductive, whereas carbonated apatite coating on similar porous implants was found to be solely osteoconductive. These different biological activities were correlated to the different physicochemical characteristics of the two studied biomimetic calcium phosphate coatings.

Summary

In addition to the variety of biomaterials that can be nowadays coated via the biomimetic method, this approach broadens the possibilities of biological activity of calcium phosphate coatings. This indicates that the biological activity of calcium phosphate coating can be improved.

SAMENVATTING

Hydroxyapatiet (HA) coatings op metalen protheses, aangebracht met behulp van de plasma spray techniek, hebben het slagingspercentage van heup revisies aanzienlijk verhoogd. Het percentage is 90% na 10 jaar voor gecementeerde heup implantaten en 98% voor hydroxyapatiet gecoate implantaten. Tegenwoordig is de biomimetische benadering voor het coaten van implantaten meer in de belangstelling gekomen, vanwege mogelijke voordelen van deze techniek. De fysische omstandigheden van het biomimetische proces vergroten de diversiteit van de te coaten materialen, zoals hitte-gevoelige en poreuze implantaten, en de diversiteit van coatings zelf omdat ook fasen die alleen stabiel zijn bij lagere temperaturen die behulp van deze techniek op implantaten aangebracht kunnen worden. Daarnaast kunnen geneesmiddelen en groeifactoren gemakkelijk ingesloten worden in biomimetische coatings. Het doel van dit onderzoek was (1) het versnellen en het optimaliseren van het biomimetische coating proces, (2) het bestuderen van fysico-chemische wetten die betrokken zijn bij de vorming van calciumfosfaat op een heterogene onderlaag, (3) het evalueren van de flexibiliteit van de biomimetische coating techniek, en afsluitend het onderzoeken van het *in vitro* en het *in vivo* gedrag van deze coatings.

Biomimeticshe calciumfosfaat coatings van 30 tot 55 μm kunnen op een titanium substraat verkregen worden in minder dan 72 uur door middel van een tweestaps procedure. Eerst wordt het titanium substraat ondergedompeld in een 5 maal geconcentreerde gesimuleerd lichaamsvloeistof (SBFx5), die oververzadigd is met koolstofdioxide gas. Na 24 uur heeft zich een homogene amorfe calciumfosfaat film met een dikte van 1 tot 5 μm gevormd op het titanium substraat via een chemische binding (hoofdstuk 2-5). In een volgende stap worden deze gecoate plaatjes ondergedompeld in een tweede oververzadigde calciumhoudende oplossing, resulterend in de groei van de uiteindelijke biomimetische calciumfosfaat coating. Afhankelijk van de samenstelling van de oververzadigde calcium oplossing, kunnen verscheidene calciumfosfaat fasen worden verkregen zoals carbonaat-apatiet of octacalciumfosfaat (hoofdstuk 6).

De beschreven biomimetische calciumfosfaat coatings laten aanzienlijke verschillen zien in fysico-chemische eigenschappen: niet alleen in vergelijking met elkaar, maar ook met coatings die zijn aangebracht door middel van de plasma spray techniek. Deze verschillen kunnen voornamelijk verklaard worden door de verschillen in (macro)structuur en microstructuur. Echter, al deze coatings transformeren in een carbonaat-apatiet structuur na onderdompeling in gesimuleerd fysiologisch vloeistof α-MEM bij pH=7.3

(hoofdstuk 7-8), zodat na implantatie uiteindelijk de oppervlakte structuur voor al deze coatings op elkaar zouda kunnen gaan gelijken.

Biomimetisch carbonaat-apatiet en octacalciumfosfaat coatings vertonen belangrijke verschillen *in vivo*. Een verschil is dat ze verschillende organische componenten opnemen na subcutane implantatie studie in ratten (hoofdstuk 8). Deze verschillen worden bevestigd in een studie na subcutane implantatie in de geit (hoofdstuk 9). Een belangrijke verschil is dat octacalcium-fosfaat (OCP) coatings op poreuze metalen implantaten osteninductief werken, terwijl carbonaat-apatiet op vergelijkbare implantaten osteoconductief werken. Dit verschil in biologische activiteiten zijn gerelateerd aan verschillen in de fysio-chemische eigenschappen van de twee biomimetische calciumfosfaat coatings.

Naast de diversiteit aan biomaterialen die met de biomimetische coating techniek gecoat kunnen worden, vergroot deze techniek de mogelijkheden van sturing van biologische activiteit van calciumfosfaat coatings. Dit geeft aan dat de potentiële biologische activiteit van gecoate protheses als gecoate poreuze blokken kunnen worden gestuurd. In dit opzicht moet men bijvoorbeeld denken aan octacalciumfosfaat, één van de meestbelovende nieuwe biomimetische coatings: poreuze blokken met een OCP coating zijn sterk botinductief, en zodoende niet alleen wellicht de eerste keuze voor tissue engineering van bot, maar ook voor een verbeterde generatie botvullers als zodanig.

AKNOWLEDGEMENTS

I would like to thank Pierre Layrolle, Clemens van Blitterswijk and Klaas de Groot to accept me as PhD student at IsoTis despite my so poor English when I came for my interview. Thank you, Pierre, for your daily and enthusiastic help. You were always available and open for discussion at any time. Thank you Clemens and Klaas for your fruitful and critical insight throughout my research.

Thanks also to Christian Rey who informed me on my voice mail about the PhD position in the *so far* and *so cold* Netherlands! Thank you also for your input during my thesis: it has been always fruitful. I wish to thank you and the all "36-Ponts" team for the "bonne ambiance" and "bonne humeur" in your lab. *Merci* Albert, Angélique, Annabelle, Christelle, Christian, Diane, Dominique, Gaby, Gerard, Jean-Louis, Lilian, Maite, Michelle, Sophie, Stephane, Stephanie et Stephanie.

I would like to thank Sandra Mendes, my Portuguese and dear colleague but above all dear friend. You made me feel comfortable as soon as I arrived in the "Berg en Bosch" villa. With Manuela, you brought me a lot of sun in Bilthoven, in the middle of the forest, in the middle of the winter. I will always remember these four years that we have spent together indoors and outdoors. *Obrigada* for your generous hart and understanding.

Thank you again for all my IsoTis colleagues. It has always been nice to spend time with you in both working and social way! *Bedankt* to the "rainbow team" and your kindness and your grateful help. Thanks to Remco for teaching me the informal english and dutch words! Thanks also to Martin for his fruitful analytical-chemistry-expertise! Thank you also for De Zaak, Tivoli, even for De Griek! You facilitated my integration into the Dutch culture! I would like to thank also (yes again) the other "rainbowers" who arrived later in the team: "do you want a cup of tea" Inge, "put my name on your acknowledgments, if you want a cup of tea" Pamela, "geweldig" Jeroen. I have spent excellent moments with you. You kept me informed with the most trendy news, Dutch slang and gossips! Because you served me very often tea, thank you, Pamela, for your friendliness and the moments we have spent outside IsoTis (e.g. Jesi). Thank you also, Chantal, for your great help with the animal studies. You have been always keen to share your expertise. Many thanks go to the entire team for your sympathy: ShiHong Li, Frederic, Maria, Ferry, Paul, "PDF-Photoshop-Master-Engineer" Pascal, Maartje, Gulfem, Ferry, Du Chang, Jiaping and Jurren kind and free as a bird.

I would like to mention also all the lab-workers for their assistance and their sympathy! And I would like to thank all the divers and skiers from IsoTis with whom I spent very nice time in the Alps, Maarsenveense Plassen and the Red Sea. Special thank to Sebastiaan for his buddy-patience, and to Esther, my funny snorkel buddy!

Finally, my Chinese colleagues and friends who introduced me in their rich eastern culture, especially Yanling, ShiHong, HongJun. *Cheche*! It has been always a sincere pleasure to share moments with you!

I would like also to acknowledge the international community of Utrecht, gathering in Jan Primus with Tony Hearn and all of the Macedonian, Italian, Kiwis, Taiwanese, Iranian, Spaniards, Finnish, German, English, Portuguese, Aussies, Swiss, Canadian, Bulgarian, Irish, Taiwanese, Scotish. I would like to thank specially: Stephanie and Erica for being present in nice and bad moments; Vincent my housemate in Wilhelminapark for making me share the Trois-Monts and Maroilles, my other Wilhelminapark housemate Alex for his Grole, Rieke for a weekly email to go to Jan Primus; Claire for being as you are; Laurence not only for the very few times we went to play badminton; Cyril and Philippe for their French hospitality.

Vita, my unique Dutch room mate, who introduced me to her family. Bedankt for your friendly hospitality and sorry for the fishes and mushrooms in the fridge…

Thank you Michel for very many things, especially for painting my study room dedicated for this thesis (you see, I made it short!).

I would like to thank all of my friends from the old time, although we did not have to much time to meet, you have been always present and supportive by phone, by letters, by emails and by visits. Thanks to Angélique, Anne, Argitxu, Isabelle, Thomas, Txomin and Valérie.

Je voudrais aussi remercier du plus profond de mon coeur maman, mes grand-parents maternels, Chantal, Patric, Fabien et Gilles qui m'ont toujours choyée et epaulée durant ces 29 années. Merci pour toute l'affection que j'ai reçue de vous et que, j'espère, je vous rends!

Finally, I would like to have a thought to the ones who have done the biggest sacrifice for my PhD: the rats, the rabbits and the goats.

CURRICULUM VITAE

Florence Barrère was born on June 25, 1973 in Saint-Gaudens, a small French city in the Pyrenees. After her graduation from the Theophile Gautier high school (Tarbes, France) in 1991, she joined the University Paul Sabatier (Toulouse, France), whereby she was awarded a Bachelor degree in Physical Chemistry, with honors, in February 1996. During her studies, she performed traineeships in the laboratory of archaeometry of Orleans, and in the laboratory of geology-geochemistry of Toulouse. Thereafter she graduated with honors from a Master's degree equivalent (Diplome d'Etude Approfondie) in Material Science in June 1997. From January to June 1997, she worked on the sol-gel synthesis of vanadyle phosphate in the Laboratory of Phosphates, a department of the Ecole Nationale Superieure de Chimie, Toulouse. In February 1998, she joined IsoTis NV as PhD student under the supervision of Prof. C.A. van Blitterswijk and Prof. K. de Groot.